

**GPS SATELLITE SKY
DISTRIBUTION: IMPACT ON
THE PROPAGATION OF SOME
IMPORTANT ERRORS IN
PRECISE RELATIVE
POSITIONING**

R. SANTERRE

October 1989



**TECHNICAL REPORT
NO. 145**

PREFACE

In order to make our extensive series of technical reports more readily available, we have scanned the old master copies and produced electronic versions in Portable Document Format. The quality of the images varies depending on the quality of the originals. The images have not been converted to searchable text.

**GPS SATELLITE SKY DISTRIBUTION:
IMPACT ON THE PROPAGATION OF SOME
IMPORTANT ERRORS IN PRECISE RELATIVE
POSITIONING**

Rock Santerre

Department of Surveying Engineering
University of New Brunswick
P.O. Box 4400
Fredericton, N.B.
Canada
E3B 5A3

October 1989
Latest Reprinting December 1994

© R. Santerre, 1989

PREFACE

This technical report is a reproduction of a dissertation submitted in partial fulfillment of the requirements for the degree of Doctor of Philosophy in the Department of Surveying Engineering, September 1989. The research was co-supervised by Dr. David E. Wells and Dr. Richard B. Langley., and funding was provided partially by the Natural Sciences and Engineering Research Council of Canada, and by the National Research Council of Canada's Industrial Research Assistance Program agreement with Usher Canada Ltd.

As with any copyrighted material, permission to reprint or quote extensively from this report must be received from the author. The citation to this work should appear as follows:

Santerre, R. (1989). *GPS Satellite Sky Distribution: Impact on the Propagation of Some Important Errors in Precise Relative Positioning*. Ph.D. dissertation, Department of Surveying Engineering Technical Report No. 145, University of New Brunswick, Fredericton, New Brunswick, Canada, 220 pp.

Abstract

This research is a study of the impact of the Global Positioning System (GPS) satellite sky distribution on the propagation of some important errors in precise static relative positioning, for baselines shorter than about 100 km.

Even the full operational GPS constellation of 24 satellites will not provide a uniform distribution of the visible satellites in the observer's sky. The satellite sky distribution is a function of site latitude, because GPS satellite orbits have inclinations different than 90° .

Covariance matrix behaviour and the effects of some important systematic errors on precise relative positioning are studied as a function of GPS satellite sky distribution, using an improved and expanded simulation technique originally suggested by Geiger of ETH Zürich. Unknowns considered are the station coordinates, the relative receiver clock parameter and the relative tropospheric zenith delay parameter. Biases analysed are: relative tropospheric refraction, absolute ionospheric refraction, offset in the horizontal coordinates of the fixed station and offset in the height of the fixed station. The simulation results agree with those obtained from real GPS data processing with an associated error of about $\pm 25\%$.

Orientation and shape of the confidence ellipsoid, and correlation among the selected unknowns, are used to monitor the behaviour of the covariance matrix. Systematic errors introduced in the station network by the biases are represented as station coordinate discrepancies and affine transformation parameters. Numerical values of these parameters are presented for satellite configurations produced by both the prototype and the full GPS constellations.

The study has yielded an appreciation of the behaviour of the covariance matrix and the variations in the effects of systematic errors as a function of the satellite sky distribution and the elevation mask angle selection. The magnitudes of the effects of the studied biases on relative positioning are up to 10 cm for baseline length independent errors and up to 10 ppm for baseline length dependent errors. Applications of this technique are suggested for planning (pre-analysis) and assessment (post-analysis) in GPS production surveys.

Résumé

Cette recherche est une étude de l'impact de la distribution des satellites du système de positionnement global GPS (Global Positioning System) dans le ciel de l'observateur sur la propagation de quelques erreurs importantes dans les résultats du positionnement relatif de précision en mode statique, pour des lignes de base d'une centaine de kilomètres ou moins.

Même le déploiement complet de la constellation GPS, composée de 24 satellites, ne produira une distribution uniforme des satellites dans le ciel de l'observateur. La distribution est fonction de la latitude du site d'observations, parce que les orbites des satellites GPS ont des inclinaisons différentes de 90° .

Le comportement de la matrice de variances-covariances et les effets de quelques erreurs systématiques importantes sur les résultats du positionnement relatif de précision sont étudiés en fonction de la distribution des satellites GPS dans le ciel de l'observateur, en utilisant une version améliorée d'une technique de simulations initialement suggérée par Geiger de l'institut ETH de Zürich. Les inconnues considérées sont les coordonnées des stations, la synchronisation relative des horloges des récepteurs et le délai troposphérique zénithal relatif. Les biais analysés sont: la réfraction troposphérique relative, la réfraction ionosphérique absolue, le biais dans les coordonnées horizontales de la station fixe et le biais dans la coordonnée verticale de la station fixe. Les résultats des simulations sont en accord avec ceux obtenus du traitement d'observations GPS réelles avec une marge d'erreur d'environ $\pm 25\%$.

L'orientation et la forme de l'ellipsoïde de confiance, et les coefficients de corrélation entre

les inconnues sélectionnées, sont utilisés pour étudier le comportement de la matrice de variances-covariances. Les erreurs systématiques introduites par les biais dans un réseau de stations sont représentées par les changements dans les coordonnées des stations et les paramètres des transformations affines. Les valeurs numériques de ces paramètres sont présentées pour des configurations de satellites produites par la constellation prototype et la constellation complète GPS.

L'étude a permis d'apprécier le comportement de la matrice de variances-covariances et les variations dans les effets des erreurs systématiques en fonction de la distribution des satellites dans le ciel de l'observateur et de la sélection de l'angle d'élévation minimal d'observations. Les magnitudes des effets des biais étudiés sur les résultats du positionnement relatif peuvent atteindre 10 cm pour les erreurs indépendantes de la longueur des lignes de base et 10 ppm pour les erreurs dépendantes de la longueur des lignes de base. Les applications suggérées de cette technique sont la planification (pré-analyse) et l'évaluation des résultats (post-analyse) des campagnes GPS.

Table of Contents

	page
Abstract	ii
Résumé	iv
Table of Contents	vi
List of Tables	ix
List of Figures	xii
Acknowledgments	xiv
Chapter 1: Introduction	1
1.1 Motivation	1
1.2 Previous studies	3
1.3 Methodology	4
1.4 Outline of the dissertation	5
1.5 Novelities of the work	7
Chapter 2: GPS satellite visibility at observer sites	9
2.1 Introduction	9
2.2 Satellite visibility algorithm	10
2.3 Satellite visibility representation	13
2.3.1 Future GPS constellation	13
2.3.2 Prototype GPS constellation	17
Chapter 3: Least squares adjustments and simulation techniques	19
3.1 Introduction	19
3.2 Observation equations	19
3.3 Equivalence of observation differencing methods	22
3.4 Simulation techniques	23
3.5 Details of Geiger's simulation technique	25
Chapter 4: Mathematical formulation of the simulation technique	33
4.1 Introduction	33
4.2 Covariance matrix	36
4.3 Relative tropospheric refraction	41
4.4 Absolute ionospheric refraction	44
4.5 Offset in the horizontal coordinates of the fixed station	47
4.5.1 Offset in the latitude of the fixed station	50

4.5.2	Offset in the longitude of the fixed station	51
4.6	Offset in the height of the fixed station	54
Chapter 5:	Comparison of predictions with results from real GPS data	57
5.1	Introduction	57
5.2	Covariance matrix	60
5.2.1	Juan de Fuca 1986 campaign	60
5.2.2	Ottawa 1983 campaign	61
5.2.3	CERN 1984 campaign	62
5.2.4	Port Alberni 1986 campaign	63
5.3	Relative tropospheric refraction	64
5.3.1	Juan de Fuca 1986 campaign	64
5.3.2	Ottawa 1983 campaign	65
5.3.3	CERN 1984 campaign	65
5.4	Absolute ionospheric refraction	67
5.4.1	Juan de Fuca 1986 campaign	67
5.4.2	CERN 1984 campaign	69
5.5	Offset in the latitude of the fixed station	72
5.5.1	Juan de Fuca 1986 campaign	72
5.5.2	Ottawa 1983 campaign	74
5.6	Offset in the longitude of the fixed station	75
5.6.1	Juan de Fuca 1986 campaign	75
5.6.2	Ottawa 1983 campaign	77
5.7	Offset in the height of the fixed station	78
5.7.1	Juan de Fuca 1986 campaign	78
5.7.2	Ottawa 1983 campaign	80
5.8	Summary of the comparison	81
Chapter 6:	Predictions for generic GPS satellite configurations	84
6.1	Introduction	84
6.2	Covariance matrix	87
6.2.1	Station coordinates and clock parameter	87
6.2.2	Station coordinates, clock parameter and relative tropospheric zenith delay parameter	98
6.3	Relative tropospheric refraction	103
6.4	Absolute ionospheric refraction	107
6.5	Offset in the latitude of the fixed station	111
6.6	Offset in the longitude of the fixed station	115
6.7	Offset in the height of the fixed station	120
Chapter 7:	Summary and conclusions	125
7.1	Summary of results	125
7.2	Implications for interpretation of GPS results	132
7.3	Suggestions for further work	134
References		136

Appendix I: Magnitude of the systematic error sources	140
I.1 Relative tropospheric refraction	140
I.2 Total electron content	141
I.3 Absolute station coordinates	143
Appendix II: Biases in single difference observations	145
II.1 Relative tropospheric zenith delay error	145
II.2 Absolute ionospheric refraction error	150
II.3 Offset in the horizontal coordinates of the fixed station	158
II.3.1 Offset in the latitude of the fixed station	164
II.3.2 Offset in the longitude of the fixed station	164
II.4 Offset in the height of the fixed station	165
II.5 Zenith angle functional relationships of biases	168
Appendix III: Integration terms	172
III.1 Integration over the azimuth sector	172
III.2 Integration over the zenith angle sector	173
III.3 Numerical values of matrices and vectors of normal equations	176
III.3.1 Normal equation matrices	176
III.3.2 Normal equation vectors	178
Appendix IV: Program DIPOPSIM description	181
IV.1 Outline of program DIPOPSIM	181
IV.2 Main program and subprogram documentation	183
Appendix V: Generic GPS satellite configurations and campaign descriptions ---	184
V.1 Generic GPS satellite configurations of the future GPS constellation ---	184
V.1.1 Equatorial site	184
V.1.2 Mid-latitude site	184
V.1.3 Polar site	184
V.2 GPS campaign descriptions	186
V.2.1 CERN 1984 campaign	186
V.2.2 Juan de Fuca 1986 campaign	188
V.2.3 Ottawa 1983 campaign	190
V.2.4 Port Alberni 1986 campaign	192
Appendix VI: Affine transformations	194
VI.1 Transformation definition and notation	194
VI.2 Affine and similarity transformations	197
VI.3 Design matrix and misclosure vector of the transformation	198
VI.4 Combination of the effects of latitude and longitude offsets of the fixed station	199

List of Tables

	page
5.1: Juan de Fuca covariance matrix behaviour from DIPOP processing. -----	60
5.2: Juan de Fuca covariance matrix behaviour from DIPOPSIM prediction. --	61
5.3: Ottawa covariance matrix behaviour from DIPOP processing. -----	61
5.4: Ottawa covariance matrix behaviour from DIPOPSIM prediction. -----	62
5.5: CERN covariance matrix behaviour from DIPOPSIM prediction. -----	62
5.6: Port Alberni ratio of the height standard deviation for solutions with and without a relative tropospheric zenith delay parameter. -----	63
5.7: Juan de Fuca baseline component errors due to relative tropospheric zenith delay error. -----	64
5.8: Ottawa baseline component errors due to relative tropospheric zenith delay error. -----	65
5.9: CERN magnification factor on station coordinates due to relative tropospheric zenith delay error. -----	66
5.10: Juan de Fuca baseline component errors due to absolute ionospheric refraction. -----	67
5.11a: Affine transformation parameters introduced in the Juan de Fuca network by absolute ionospheric refraction. -----	68
5.11b: Prediction of affine transformation parameters introduced in the Juan de Fuca network by absolute ionospheric refraction. -----	69
5.12: CERN baseline component errors due to absolute ionospheric refraction. -	70
5.13a: Affine transformation parameters introduced in the CERN network by absolute ionospheric refraction. -----	70
5.13b: Prediction of affine transformation parameters introduced in the CERN network by absolute ionospheric refraction. -----	71
5.14: Juan de Fuca baseline component errors due a 1" (30.9 m) offset in the latitude of the fixed station. -----	72
5.15a: Affine transformation parameters introduced in the Juan de Fuca network by a 1" (30.9 m) offset in the latitude of the fixed station. -----	73
5.15b: Prediction of affine transformation parameters introduced in the Juan de Fuca network by a 1" (30.9 m) offset in the latitude of the fixed station. --	73
5.16: Ottawa baseline component errors due a 1" (30.9 m) offset in the latitude of the fixed station. -----	74
5.17a: Affine transformation parameters introduced in the Ottawa network by a 1" (30.9 m) offset in the latitude of the fixed station. -----	74
5.17b: Prediction of affine transformation parameters introduced in the Ottawa network by a 1" (30.9 m) offset in the latitude of the fixed station. -----	75
5.18: Juan de Fuca baseline component errors due a 1" (20.5 m) offset in the longitude of the fixed station. -----	76
5.19a: Affine transformation parameters introduced in the Juan de Fuca network by a 1" (20.5 m) offset in the longitude of the fixed station. -----	76
5.19b: Prediction of affine transformation parameters introduced in the Juan de Fuca network by a 1" (20.5 m) offset in the longitude of the fixed station.	77
5.20: Ottawa baseline component errors due a 1" (21.7 m) offset in the longitude of the fixed station. -----	77
5.21a: Affine transformation parameters introduced in the Ottawa network by a 1" (21.7 m) offset in the longitude of the fixed station. -----	78
5.21b: Prediction of affine transformation parameters introduced in the Ottawa network by a 1" (21.7 m) offset in the longitude of the fixed station. -----	78

5.22:	Juan de Fuca baseline component errors due a 30 m offset in the height of the fixed station. -----	79
5.23a:	Affine transformation parameters introduced in the Juan de Fuca network by a 30 m offset in the height of the fixed station. -----	79
5.23b:	Prediction of affine transformation parameters introduced in the Juan de Fuca network by a 30 m offset in the height of the fixed station. -----	80
5.24:	Ottawa baseline component errors due a 30 m offset in the height of the fixed station. -----	80
5.25a:	Affine transformation parameters introduced in the Ottawa network by a 30 m offset in the height of the fixed station. -----	81
5.25b:	Prediction of affine transformation parameters introduced in the Ottawa network by a 30 m offset in the height of the fixed station. -----	81
6.1a:	DIOPPSIM prediction of the behaviour of matrix $(A^T A)^{-1}$ for equatorial site. -----	87
6.2a:	DIOPPSIM prediction of the behaviour of matrix $(A^T A)^{-1}$ for polar site. --	88
6.3a:	DIOPPSIM prediction of the behaviour of matrix $(A^T A)^{-1}$ for mid-latitude site. -----	89
6.4a:	DIOPPSIM prediction of the behaviour of matrix $(A^T A)^{-1}$ for CERN satellite configuration. -----	90
6.1b:	DIOPPSIM prediction of the behaviour of matrix $(A^T A)^{-1}$ where a relative tropospheric zenith delay parameter is estimated for equatorial site. -----	98
6.2b:	DIOPPSIM prediction of the behaviour of matrix $(A^T A)^{-1}$ where a relative tropospheric zenith delay parameter is estimated for polar site. -----	99
6.3b:	DIOPPSIM prediction of the behaviour of matrix $(A^T A)^{-1}$ where a relative tropospheric zenith delay parameter is estimated for mid-latitude site. ----	100
6.4b:	DIOPPSIM prediction of the behaviour of matrix $(A^T A)^{-1}$ where a relative tropospheric zenith delay parameter is estimated for CERN satellite configuration. -----	101
6.5:	Ratio of the station height standard deviation for solutions with and without a relative tropospheric zenith delay parameter. -----	102
6.6a:	DIOPPSIM prediction of the effects on station coordinates due to each 1 mm of relative tropospheric zenith delay error for equatorial site. -----	103
6.6b:	DIOPPSIM prediction of the effects on station coordinates due to each 1 mm of relative tropospheric zenith delay error for polar site. -----	103
6.6c:	DIOPPSIM prediction of the effects on station coordinates due to each 1 mm of relative tropospheric zenith delay error for mid-latitude site. ----	104
6.6d:	DIOPPSIM prediction of the effects on station coordinates due to each 1 mm of relative tropospheric zenith delay error for CERN satellite configuration. -----	104
6.7a:	DIOPPSIM prediction of the effects on station coordinates due to absolute ionospheric refraction error (per 1×10^{17} el/m ² of TEC) for equatorial site. 107	107
6.7b:	DIOPPSIM prediction of the effects on station coordinates due to absolute ionospheric refraction error (per 1×10^{17} el/m ² of TEC) for polar site. ----	108
6.7c:	DIOPPSIM prediction of the effects on station coordinates due to absolute ionospheric refraction error (per 1×10^{17} el/m ² of TEC) for mid-latitude site. 108	108
6.7d:	DIOPPSIM prediction of the effects on station coordinates due to absolute ionospheric refraction error (per 1×10^{17} el/m ² of TEC) for CERN satellite configuration. -----	109
6.8a:	DIOPPSIM prediction of the effects on station coordinates due to each 10 m of latitude offset of the fixed station for equatorial site. -----	112

6.8b:	DIOPPSIM prediction of the effects on station coordinates due to each 10 m of latitude offset of the fixed station for polar site. -----	112
6.8c:	DIOPPSIM prediction of the effects on station coordinates due to each 10 m of latitude offset of the fixed station for mid-latitude site. -----	112
6.8d:	DIOPPSIM prediction of the effects on station coordinates due to each 10 m of latitude offset of the fixed station for CERN satellite configuration. -----	112
6.9a:	DIOPPSIM prediction of the effects on station coordinates due to each 10 m of longitude offset of the fixed station for equatorial site. -----	115
6.9b:	DIOPPSIM prediction of the effects on station coordinates due to each 10 m of longitude offset of the fixed station for polar site. -----	115
6.9c:	DIOPPSIM prediction of the effects on station coordinates due to each 10 m of longitude offset of the fixed station for mid-latitude site. -----	116
6.9d:	DIOPPSIM prediction of the effects on station coordinates due to each 10 m of longitude offset of the fixed station for CERN satellite configuration. -----	117
6.10a:	DIOPPSIM prediction of the effects on station coordinates due to each 10 m of height offset of the fixed station for equatorial site. -----	120
6.10b:	DIOPPSIM prediction of the effects on station coordinates due to each 10 m of height offset of the fixed station for polar site. -----	120
6.10c:	DIOPPSIM prediction of the effects on station coordinates due to each 10 m of height offset of the fixed station for mid-latitude site. -----	121
6.10d:	DIOPPSIM prediction of the effects on station coordinates due to each 10 m of height offset of the fixed station for CERN satellite configuration. -----	121
7.1a:	Summary of the behaviour of the covariance matrix for different satellite configurations; ζ^{\max} : 70°. -----	129
7.1b:	Summary of the behaviour of the covariance matrix for different satellite configurations; ζ^{\max} : 80°. -----	129
7.2a:	Summary of the effects of some important systematic errors in precise relative positioning for different satellite configurations; ζ^{\max} : 70°. -----	130
7.2b:	Summary of the effects of some important systematic errors in precise relative positioning for different satellite configurations; ζ^{\max} : 80°. -----	130
I.1:	Variation of the Hopfield's tropospheric zenith delay due to pressure, temperature and relative humidity errors. -----	140
I.2:	Summary of some GPS static absolute positioning results. -----	143
II.1:	Tropospheric refraction mapping function values as a function of zenith angle. -----	148
II.2:	Zenith angle at the ionospheric layer height (ζ') as a function of the zenith angle at the Earth's surface (ζ) and values of $\sec\zeta$ and $\sec\zeta'$; h^{ion} : 350 km. -----	153
II.3:	Maximum absolute values for the ℓ/R_e term and the ℓ/ρ_1 term. -----	157

List of Figures

	page
2.1: Truncated sphere generated by a satellite constellation with inclination different than 90° . -----	10
2.2: Coordinate systems and satellite observation geometry. -----	12
2.3: Shadow areas where GPS satellites cannot be observed as a function of site latitude (satellite orbital inclination: 55°). -----	14
2.4: Ground tracks generated by GPS satellites with an orbital inclination of 55° over a period of 12 hours. -----	16
2.5: Examples of satellite sky distributions generated by GPS satellites with an orbital inclination of 55° over a period of 3 hours. -----	16
2.6: Ground tracks generated by the prototype GPS satellites. -----	18
2.7: Satellite sky distribution for Vancouver Island. -----	18
3.1: Local geodetic system and integration boundaries. -----	29
6.1a: Ratio of the semi-axes of the confidence ellipsoid where station coordinates and clock parameter are estimated. -----	91
6.1b: Ratio of the semi-axes of the confidence ellipsoid where station coordinates, clock and tropospheric zenith delay parameters are estimated. -----	91
6.2a: Orientation of the confidence ellipsoid where station coordinates and clock parameter are estimated. -----	92
6.2b: Orientation of the confidence ellipsoid where station coordinates, clock and tropospheric zenith delay parameters are estimated. -----	92
6.3a: Correlation coefficient among unknowns where station coordinates and clock parameter are estimated. Equatorial site. -----	93
6.3b: Correlation coefficient among unknowns where station coordinates, clock and tropospheric zenith delay parameters are estimated. Equatorial site. --	93
6.4a: Correlation coefficient among unknowns where station coordinates and clock parameter are estimated. Polar site. -----	94
6.4b: Correlation coefficient among unknowns where station coordinates, clock and tropospheric zenith delay parameters are estimated. Polar site. -----	94
6.5a: Correlation coefficient among unknowns where station coordinates and clock parameter are estimated. Mid-latitude site. -----	95
6.5b: Correlation coefficient among unknowns where station coordinates, clock and tropospheric zenith delay parameters are estimated. Mid-latitude site. -	95
6.6a: Correlation coefficient among unknowns where station coordinates and clock parameter are estimated. CERN satellite configuration. -----	96
6.6b: Correlation coefficient among unknowns where station coordinates, clock and tropospheric zenith delay parameters are estimated. CERN satellite configuration. -----	96
6.7a: Translation effect due to relative tropospheric zenith delay error. Equatorial and mid-latitude sites. -----	105
6.7b: Translation effect due to relative tropospheric zenith delay error. Polar site. -----	105
6.7c: Translation effect due to relative tropospheric zenith delay error. CERN satellite configuration. -----	106
6.8a: Affine transformation parameters due to absolute ionospheric refraction error. Equatorial and polar sites. -----	108
6.8b: Affine transformation parameters due to absolute ionospheric refraction error. Mid-latitude site. -----	109

6.8c:	Affine transformation parameters due to absolute ionospheric refraction error. CERN satellite configuration. -----	110
6.9a:	Affine transformation parameters due to a latitude offset in the fixed station. Equatorial and polar sites. -----	113
6.9b:	Affine transformation parameters due to a latitude offset in the fixed station. Mid-latitude site. -----	113
6.9c:	Affine transformation parameters due to a latitude offset in the fixed station. CERN satellite configuration. -----	114
6.10a:	Affine transformation parameters due to a longitude offset in the fixed station. Equatorial and polar sites. -----	116
6.10b:	Affine transformation parameters due to a longitude offset in the fixed station. Mid-latitude site. -----	117
6.10c:	Affine transformation parameters due to a longitude offset in the fixed station. CERN satellite configuration. -----	118
6.11a:	Affine transformation parameters due to a height offset in the fixed station. Equatorial and polar sites. -----	121
6.11b:	Affine transformation parameters due to a height offset in the fixed station. Mid-latitude site. -----	122
6.11c:	Affine transformation parameters due to a height offset in the fixed station. CERN satellite configuration. -----	122
II.1:	Bias in single difference observation due to relative tropospheric zenith delay error. -----	147
II.2:	Zenith angles at 2 different stations and at the infinitesimally thick ionospheric layer. -----	150
II.3a:	Bias in single difference observation due to an offset in the horizontal coordinates of the fixed station (first projection). -----	160
II.3b:	Bias in single difference observation due to an offset in the horizontal coordinates of the fixed station (second projection). -----	160
II.4:	Coordinate systems representation for the study of an offset in the horizontal coordinates of the fixed station. -----	161
II.5:	Bias in single difference observation due to an offset in the height of the fixed station. -----	166
II.6:	Coordinate systems representation for the study of an offset in the height of the fixed station. -----	166
II.7a:	Zenith angle functions related to tropospheric zenith delay. -----	169
II.7b:	Zenith angle functions related to absolute ionospheric refraction error. ---	170
II.7c:	Zenith angle functions related to offsets in the coordinates of the fixed station. -----	170
V.1:	Example of satellite configurations of the future GPS constellation. -----	185
V.2a:	Satellite visibility CERN 1984 campaign. -----	187
V.2b:	Station network CERN 1984 campaign. -----	187
V.3a:	Satellite visibility Juan de Fuca 1986 campaign. -----	189
V.3b:	Station network Juan de Fuca 1986 campaign. -----	189
V.4a:	Satellite visibility Ottawa 1983 campaign. -----	191
V.4b:	Station network Ottawa 1983 campaign. -----	191
V.5a:	Satellite visibility Port Alberni 1986 campaign. -----	193
V.5b:	Station network Port Alberni 1986 campaign. -----	193
VI.1	Interpretation of affine transformation parameters in a left-handed coordinate system. -----	195

Acknowledgments

Part of this research was funded by the Natural Sciences and Engineering Research Council of Canada Strategic Research Grants: "Geodetic and Geodynamic Applications of Space-Based Positioning Systems" held by Dr. R.B. Langley, Dr. D.E. Wells and Dr. J.M. Tranquilla (Electrical Engineering) and "Application of Differential GPS Positioning" held by Dr. J.M. Tranquilla, Dr. R.B. Langley, Dr. D.E. Wells, Dr. P. Vaníček and Dr. A. Kleusberg. This research was also partially funded by the National Research Council of Canada and Usher Canada Ltd. through an Industrial Research Assistance Program agreement "High Precision Engineering Surveys - GPS Software Development for Precise Engineering Surveys" held by Dr. R.B. Langley. The financial support provided by the University of New Brunswick through a Magee Postgraduate Merit Award and by "Le Fonds Joncas de l'Ordre des arpenteurs-géomètres du Québec" has been appreciated.

Many thanks go to the Pacific Geoscience Centre of the Geological Survey of Canada, Department of Energy, Mines and Resources for access to the data of the Juan de Fuca and Port Alberni 1986 GPS campaigns. The Earth Physics Branch (now the Geophysics Division of the Geological Survey of Canada), Department of Energy, Mines and Resources is also acknowledged for their permission to use the data of the Ottawa 1983 GPS campaign.

I would particularly like to express my appreciation to my co-supervisors Dr. David E. Wells and Dr. Richard B. Langley for giving me the opportunity to dedicate all my time to research. The quality and quantity of work they perform, as well as the team spirit which exists amongst the geodesy group have been a source of motivation. This example I hope to follow throughout my professional career. I also want to acknowledge Dr. Alfred

Kleusberg for his technical and scientific support and his availability.

The constructive recommendations of the Examining Board have been appreciated and have helped to improve the final version of this thesis. The members of the Board consisted of: Dr. David E. Wells (co-supervisor), Dr. Richard B. Langley (co-supervisor), Dr. Alfred Kleusberg (Surveying Engineering), Dr. Bradford G. Nickerson (Computer Science), Dr. Joseph C. White (Geology) and Dr. Gerhard Beutler (Astronomical Institute, University of Berne, Switzerland).

Finally, I would like to dedicate this thesis to some very special people. Because the following words come from the deepest part of my heart I want to express them in my mother tongue.

"Cette thèse de doctorat est dédiée à mes parents Louis-Philippe et Rachel et à mes grands-parents Georges, Claire, Omer et Yvonne. Sans avoir eu l'opportunité de recevoir des diplômes d'études vous avez réussi, par votre ingéniosité, votre tenacité, votre sens du travail bien fait et votre fierté, à laisser des traces que les générations futures de notre pays tenteront de suivre."

Chapter 1

Introduction

1.1 Motivation

The main goal of this work is to study the impact of the Global Positioning System (GPS) satellite sky distribution on the propagation of some important errors in precise static relative positioning.

The Global Positioning System is now used for different applications from positioning, velocity and acceleration determination to time synchronization. Absolute positioning as well as relative (differential) positioning are possible, either in static or kinematic modes. Pseudoranges and carrier beat phases can be observed from the Navstar satellites. For precise surveying, geodetic and geodynamics applications requiring a high level of positioning accuracy, the observations of carrier phase in static (few hours) and relative mode is the best combination to potentially achieve these positioning needs. GPS has the potential to compete, in terms of production costs and positioning accuracy, with conventional terrestrial methods as well as with other precise extra-terrestrial techniques like satellite laser ranging and very long baseline interferometry.

Naturally, like any other experimental works, the GPS positioning potential is limited by the amount of random and systematic error contaminating the observations. Even in relative GPS positioning the following errors can still have adverse consequences: the wave propagation delays due to the troposphere and the ionosphere, the satellite position errors, the offset in the coordinates of the fixed station, the multipath effect and the antenna phase centre variation, to name a few. Knowledge of the nature and the magnitude of these errors is the basis for the analysis of their effects in positioning results. The reader is

referred to Appendix I for a brief survey of the nature and the magnitude of some important biases studied in this thesis. The second step of the analysis is to monitor the effect of these biases in the GPS observations. As it is shown in Appendix II, the effect of the (studied) biases in the observations are a function of the direction of the observed satellite (i.e., they are dependent on the azimuth and the zenith angle of the observed satellite). However what is of primary interest is to know how these biases are propagated in the estimated station coordinates throughout the least squares adjustment process. For positioning purposes the station coordinates are the desired parameters and the others are considered as nuisance parameters.

Recognizing that the design matrix, i.e., the partial derivative of the observation equation with respect to the estimated parameters, needed to construct the normal equation of the least squares adjustments, as well as the effect of the biases in the observations, are a function of the satellite observation direction, it is obvious that the GPS satellite sky distribution will have an impact on the propagation of errors in the positioning results. The satellite sky distribution (or satellite configuration) can be defined as the portion of the observer's sky hemisphere covered by satellite observations during the observing session. Central to this thesis is the study of the impact of the observer's satellite sky distribution. This is particularly important for positioning with GPS because the orbit inclination of the GPS constellation, as it will be shown in detail, produces satellite sky distribution dependent on the latitude of the observer's site.

More specifically we want to answer the following basic questions: What is the behaviour of the estimated parameter covariance matrix as a function of satellite configurations? How are systematic errors propagated into the station coordinates as a function of satellite configurations? What is the tolerance value a systematic error should not exceed in order to achieve a predetermined positioning accuracy level?

1.2 Previous studies

Geiger [1987; 1988] has investigated the effects of the tropospheric refraction error and the antenna phase centre variation on the station coordinate results. The satellite configuration was assumed quasi-hemispherical (observations in all azimuths and elevation angles, but with a 20° elevation mask angle). The parameters considered in the solutions were the station coordinates and a clock parameter.

Beutler et al. [1988] have studied the effects of numerous biases (troposphere, ionosphere, GM-value, fixed station height, fixed station horizontal coordinates, along track orbit error) for a quasi-hemispherical satellite configuration. Without underestimating their work, which has been a tremendous source of inspiration, we should note that their approach is purely geometric (i.e., clock parameters are not and cannot be taken into account) and may lead to erroneous results, in some circumstances.

Herring [1986] has investigated the effect of systematic and random errors of the tropospheric zenith delay in the station height results for very long baseline interferometry (VLBI) experiments. His study is also applicable for GPS because the tropospheric refraction affects similarly the observations of both systems. In this experiment the observations were assumed uniformly spaced in elevation angle between 90° and a selectable elevation mask angle. A clock parameter and optionally a tropospheric zenith delay parameter were considered in the simulations.

Davis [1986] has followed Herring's approach to study the effect of the tropospheric refraction mapping function error and the behaviour of the estimated parameter covariance matrix. He has also studied the effect of refractivity azimuthal asymmetry (horizontal gradient) using a real VLBI observing schedule.

Interpretation of the estimated parameter standard deviations, the shape and the orientation of the confidence ellipsoid, the station coordinate discrepancies with respect to other precise and independent positioning systems, and the trend in the observation residuals, as a function of the satellite configurations have been often reported by GPS processing groups on a case by case basis. However, neither a complete and systematic analysis of the impact of satellite sky distribution on the propagation of errors in the positioning results, nor the study of the dependence of the satellite sky distribution on the latitude site have been done so far.

1.3 Methodology

Due to the extent of the investigation, considering the number of estimated parameters, the number of systematic errors and the number of satellite configurations (typical of the prototype and future GPS constellations) we want to study, we have to use a simulation technique which allows easy, fast but yet correct generalized studies of the impact of the satellite sky distribution on the propagation of errors in relative positioning. One technique having these attributes is the one developed by Geiger [1987, 1988].

We have improved and used Geiger's simulation technique to monitor the behaviour of the covariance matrix, as a function of satellite configuration, in terms of standard deviations, shape and orientation of the confidence ellipsoid and the correlation among the different estimated parameters (station coordinates, relative receiver clock offset and optionally relative tropospheric zenith delay parameter). Efforts have been made to take into account the maximum number of the most important systematic errors (relative tropospheric zenith delay, absolute ionospheric refraction, offset in the horizontal coordinates of the fixed station and offset in the height of the fixed station). The effects of these biases on positioning results are monitored by looking at the station coordinate discrepancies and at

the station network deformation parameters introduced by such systematic errors as a function of satellite sky distribution.

However, we have to note that the technique has some weakness. For example, parameters or errors which are satellite dependent, like the carrier phase ambiguity parameters and the satellite orbit errors, cannot be monitored.

The technique requires proper analytical modelling of the studied systematic errors on the relative observations. To do so, we have been inspired by the work of Beutler et al. [1988]. Substantial improvement in the mathematical formulation has been done to this earlier work: a better tropospheric refraction mapping function is used, a different and more accurate absolute ionospheric delay modelling has been developed and a complete formulation of the offset in the horizontal coordinates of the fixed station has been derived.

The results of this investigation are applicable to relative static positioning with maximum inter-station distances of about 100 km. Note that some of the investigation can also be used directly to study the effect in absolute positioning results.

1.4 Outline of the dissertation

Chapter 2 contains the description of an algorithm which allows the visualization of the GPS satellite configurations as a function of the latitude of the observer sites. Illustrations of the observer's sky satellite visibility for the future and the prototype GPS constellations are presented.

The least squares adjustments principles and the simulation technique options are introduced in Chapter 3. The chapter starts with a review of the observation equations for the undifferenced and differenced carrier phase observables. A description of the

advantages and the disadvantages of these observation modes is given. Documentation of the equivalence of the observation differencing methods is presented. Different simulation techniques are suggested and the rationale for the selection of Geiger's technique, the most appropriate technique for reaching the dissertation objectives, is outlined. The chapter ends with the mathematical equations and a summary of the assumptions and limitations of Geiger's simulation technique.

Chapter 4 contains the mathematical formulation of each of the elements of the normal equation matrix (N) and the normal equation vectors (U) of the least squares adjustments process in the form required by Geiger's simulation technique. The combination of unknowns can be selected from among the station coordinates, the relative receiver clock parameter and optionally the tropospheric zenith delay parameter. The systematic biases studied are the relative tropospheric zenith delay error, the absolute ionospheric refraction error, the horizontal coordinate (latitude and longitude) offsets of the fixed station and the height offset of the fixed station. The matrix N and vectors U are developed for the general case, i.e., for any kind of satellite sky distribution, and for two particular satellite sky distribution cases. The analysis of the matrix and vectors of the normal equations allows us to see some important trends in the behaviour of the covariance matrix and the signature of the studied systematic errors in the station coordinates.

The assessment of the simulation technique is performed by comparing the results of the technique with those obtained from the processing of real GPS data. The results of the comparisons are presented in Chapter 5. Four different GPS campaigns having 3 different satellite configurations are used. Two of the satellite sky distributions are rather poor and the third one is one of the best distributions which can be obtained with the prototype GPS satellite constellation. Comparisons of the orientation and the shape of the station coordinate confidence ellipsoids are presented. The propagation of the systematic errors

into the estimated parameters is studied in terms of station coordinate discrepancies and station network deformation.

Chapter 6 contains the results of a generalized study of the behaviour of the covariance matrix and of the effects of the systematic errors for 4 different satellite configurations. The first 3 configurations are representative of the expected satellite sky distributions for equatorial, mid-latitude and polar sites when the complete GPS constellation will be in place. The fourth configuration is representative of a poor distribution produced by the prototype GPS constellation. The behaviour of the covariance matrix is monitored in terms of: orientation of the confidence ellipsoids; ratio of the semi-axes of the confidence ellipsoid; and the correlation coefficient among the unknowns. These parameters are tabulated and plotted for different elevation mask angles for the 4 satellite configurations. Also tabulated and plotted in this manner are the station network deformation parameters which illustrate the biases introduced in the station coordinates due to the studied systematic errors.

Chapter 7 summarizes the results of the research, mentions the implications for interpretation of GPS results and gives suggestions for further work.

1.5 Novelties of the work

To conclude this chapter we highlight, in this section, the novelties and the contributions of this work. They can be summarized (in a chronological way) as follows:

- 1) The proper conception of GPS satellite sky distribution as a function of the latitude of the observer sites;
- 2) The improved formulation of many important biases in the single difference observations;
- 3) The introduction of a tropospheric zenith delay parameter in Geiger's simulation

technique (any combination among the following unknowns are possible in the least squares solution: station coordinates, clock parameter and tropospheric zenith delay parameter);

- 4) The automation of the simulation technique achieved by the coding of a software program called DIPOPSIM (Differential POsitioning Program SIMulator);
- 5) The assessment of the improved version of Geiger's simulation technique;
- 6) The detailed study of the behaviour of the covariance matrix (confidence ellipsoid);
- 7) The detailed study of the effects of some important biases (systematic errors) on the positioning results;
- 8) The study of the impact of GPS satellite sky distribution (including elevation mask angle selection) on the behaviour of the covariance matrix and the propagation of important systematic errors in precise relative positioning;
- 9) The production of a guide to know the tolerance values which some important systematic errors should not exceed in order to achieve a predetermined positioning accuracy level.

Chapter 2

GPS satellite visibility at observer sites

2.1 Introduction

Some people have the misconception that with the deployment of the full GPS constellation of 24 satellites the distribution of satellites in the observer's sky will be uniform, i.e., the satellite observations will cover the sky in all azimuths and zenith angles. However this will not be the case.

The future GPS constellation will have 6 orbital planes evenly spaced along the equatorial plane. Each of the orbital planes will contain 4 satellites. The orbit will be almost circular with semi-axes of about 26,560 km. The altitude change planned to increase the semi-major axis from 26,560 km to 26,609 km is currently being reconsidered [Green et al., 1989]. The inclination of the orbital plane will be 55° . From the space point of view, we can illustrate (refer to Figure 2.1) the constellation by a truncated sphere of radius equal to the semi-axis of the satellite orbit. The truncation is due to the inclination of the orbital planes. In other words, a truncated sphere generated by a satellite constellation can be defined as the loci of all possible satellite orbital paths of a given inclination. Clearly, the observer's sky satellite coverage will be a function of the site latitude.

The following sections are presented to illustrate that the uniform GPS constellation, in space, does not equate to uniform satellite sky coverage at different observing sites. Section 2.2 presents the development of the algorithm used to evaluate the sky's shadow area as a function of the site latitude. Section 2.3 shows illustrations of observer's sky satellite visibility for the future and the prototype GPS constellations.

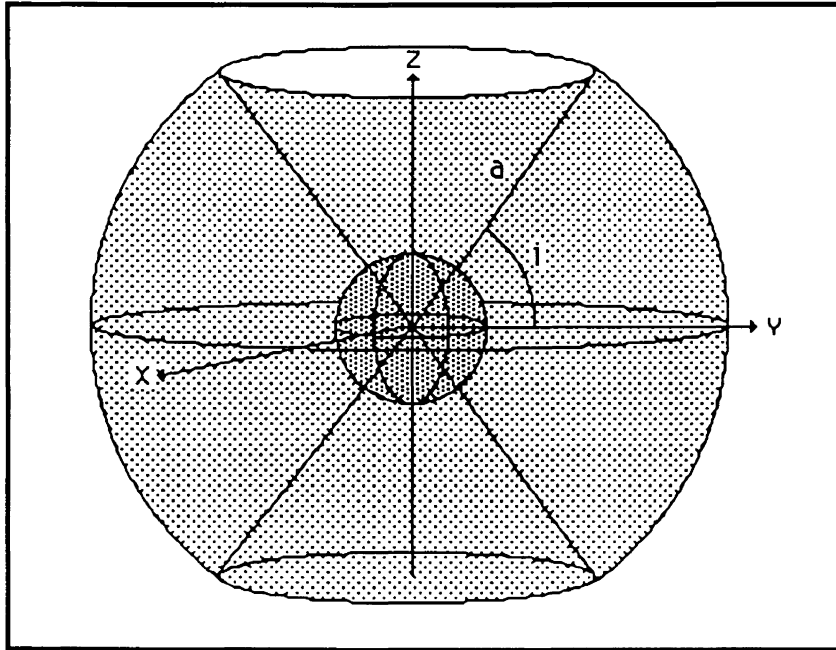


Figure 2.1: Truncated sphere generated by a satellite constellation with inclination different than 90° .

2.2 Satellite visibility algorithm

Given the Earth radius (R_e), the spherical latitude (ϕ) and the spherical longitude (λ) of an observer, the inclination (i) and the period (T) or the semi-axis (a) of a satellite constellation with circular orbits; find whether or not an observation with a zenith angle (ζ) and an azimuth (α) made at the observer site on the Earth's surface might be possible. In other words, will a ray originating from the observer's site in the direction defined by α and ζ intersect the truncated sphere generated by the GPS satellite trajectories around the Earth?

To answer this question, we have to evaluate: 1) the distance (ρ) from the observer to the sphere; 2) the Z-coordinate (Z^S) of the intersection of the observation ray with the sphere. If the the following condition is satisfied:

$$|Z^S| > a \sin i, \quad (2.1)$$

then it will never be possible to make an observation in this direction at this location.

To evaluate the distance (ρ), we start with the following relation:

$$(X^S)^2 + (Y^S)^2 + (Z^S)^2 = a^2 \quad (2.2)$$

where X^S , Y^S and Z^S (\vec{X}^S) are the coordinates of a theoretical satellite in the right-handed Earth-Centered and Earth-Fixed (ECEF) system. Do not confuse X^S with the norm of vector \vec{X}^S . The norm of \vec{X}^S is equal to the semi-major axis (a), see eqn. (2.2), and X^S is the X-coordinate of the satellite position.

The satellite coordinates (\vec{x}^S) in the left-handed local geodetic (LG) system defined at the observer site are:

$$\vec{x}^S = \begin{pmatrix} \rho \sin\zeta \cos\alpha \\ \rho \sin\zeta \sin\alpha \\ \rho \cos\zeta \end{pmatrix} \quad (2.3)$$

Figure 2.2 illustrates the coordinate systems and the satellite observation geometry.

The transformation from the LG-system to the ECEF-system is given by:

$$\vec{X}^S = \mathbb{P}_x \mathbb{R}_z(\lambda) \mathbb{R}_y(90^\circ - \phi) \vec{x}^S + \mathbb{T} \quad (2.4)$$

where \mathbb{R}_y and \mathbb{R}_z are rotation matrices, \mathbb{P}_x is a reflection matrix and \mathbb{T} is a translation matrix given by:

$$\mathbb{T} = \begin{pmatrix} R_e \cos\phi \cos\lambda \\ R_e \cos\phi \sin\lambda \\ R_e \sin\phi \end{pmatrix} \quad (2.5)$$

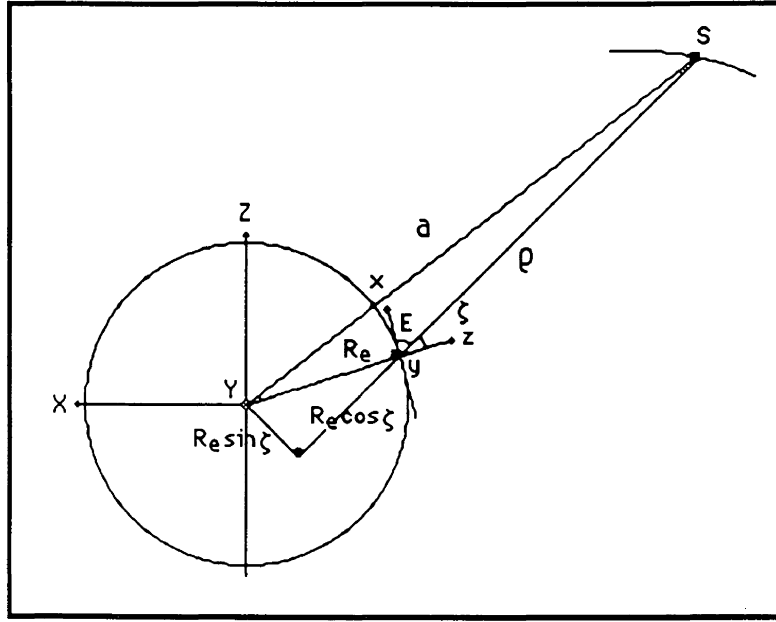


Figure 2.2: Coordinate systems and satellite observation geometry.

The evaluation of eqn. (2.4), with the use of equations (2.3) and (2.5), gives:

$$\vec{X}^S = \begin{pmatrix} -\rho \sin \zeta \cos \alpha \sin \phi \cos \lambda & -\rho \sin \zeta \sin \alpha \sin \lambda & +\rho \cos \zeta \cos \phi \cos \lambda & +R_e \cos \phi \cos \lambda \\ -\rho \sin \zeta \cos \alpha \sin \phi \sin \lambda & +\rho \sin \zeta \sin \alpha \cos \lambda & +\rho \cos \zeta \cos \phi \sin \lambda & +R_e \cos \phi \sin \lambda \\ \rho \sin \zeta \cos \alpha \cos \phi & & +\rho \cos \zeta \sin \phi & +R_e \sin \phi \end{pmatrix} \quad (2.6)$$

The introduction of the above results in eqn. (2.2) gives this very simple quadratic equation:

$$a^2 = \rho^2 + R_e^2 + 2 R_e \rho \cos \zeta \quad (2.7)$$

Geometrically, the relation is obvious with the help of Figure 2.2.

Equation (2.7) can be solved by the quadratic formula, we then get:

$$\rho = (a^2 - R_e^2 \sin^2 \zeta)^{1/2} - R_e \cos \zeta \quad (2.8)$$

This can also be obtained geometrically, again with the help of Figure 2.2.

This relation is independent of the observer site and the observation azimuth; we only need to know the radius of the Earth (R_e), the semi-axis of the satellite constellation (a) and the zenith angle (ζ) of the observation.

With the distance from the observer to the sphere (ρ), the latitude of the observer (ϕ), the Earth radius (R_e), and the azimuth (α) and the zenith angle (ζ) of the observation, we are able to evaluate Z^S (eqn. 2.6). Note that the above relations are applicable for sites at any longitude (functionally independent of λ).

Then if the relation in eqn. (2.1) is satisfied, we will never be able to make an observation in the ray direction defined by α and ζ , at latitude ϕ .

2.3 Satellite visibility representation

2.3.1 Future GPS constellation

With the algorithm presented in equations (2.1), (2.6) and (2.8), it is quite easy to calculate the portion of the sky where it will be impossible to observe GPS satellites.

In Figures 2.3, we have projected on polar plots (azimuth vs. zenith angle), for north latitudes: 0° , 15° , 30° , 45° , 55° , 60° , 75° and 90° , the area of the observer's sky (shadow area) where it will be not possible to make observations. Note that for a given latitude, the plot will be the same for any longitude. The plots for south latitudes are similar to those for north latitudes except for the reflection along the east-west axis, i.e., a shadow area in the north for north latitudes will be present in the south for south latitudes.

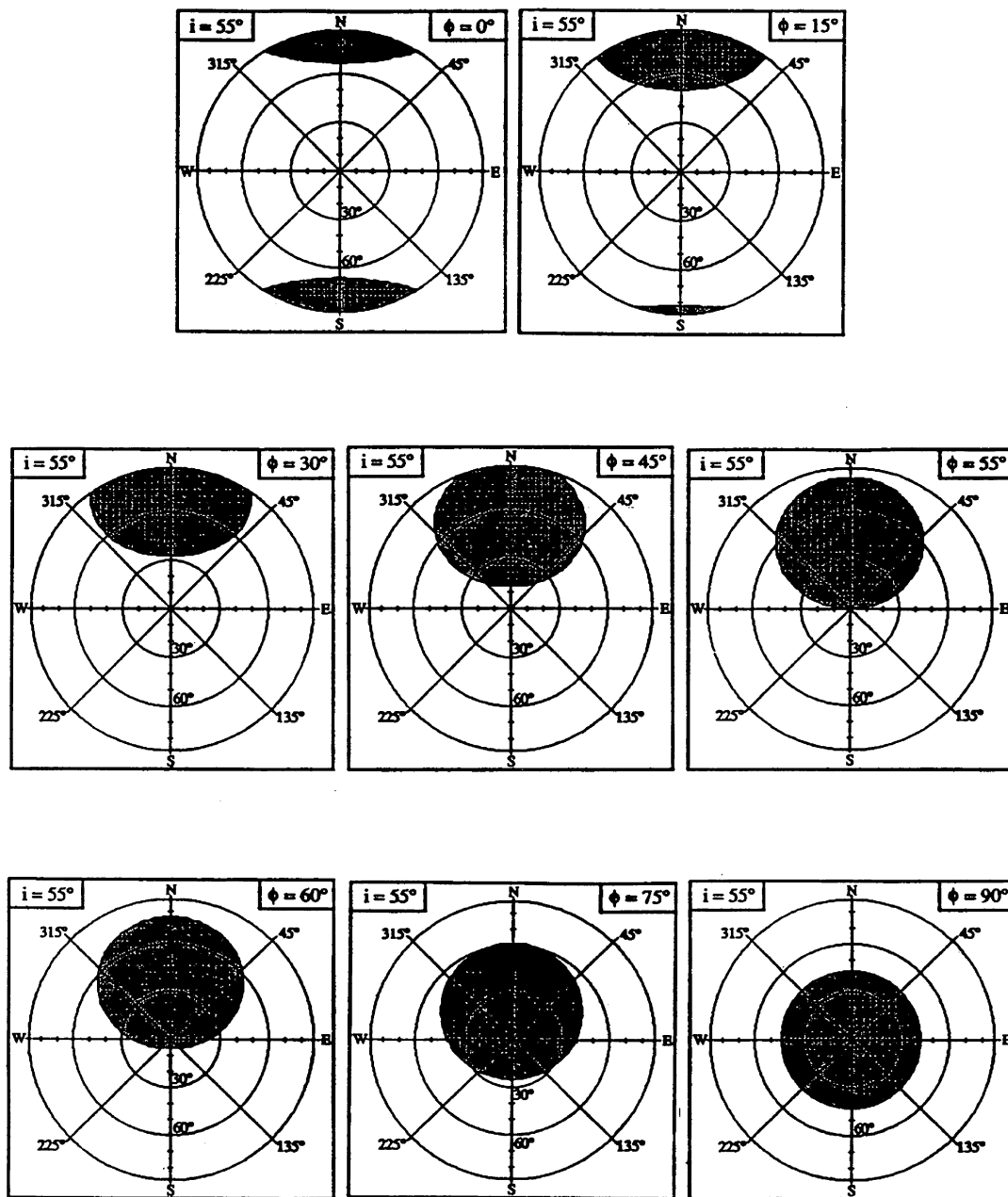


Figure 2.3: Shadow areas where GPS satellites cannot be observed as a function of site latitude (satellite orbital inclination: 55°).

As a general trend, the shadow area moves from the horizon to the zenith as the latitude increases from 0° to 90° . The most uniform satellite sky distribution occurs at the equator. Two sectors between azimuths 330° and 30° , and 150° and 210° define the shadow area with unattainable observations. In the north and south directions, no observation is possible below an elevation angle of 23° , the restriction vanishing as the azimuth reaches the edges of the sectors. At latitude 45° , observations in the north direction (between 315° and 45°) will be possible only close to the zenith, and close to the horizon for azimuths around 45° and 315° . This represents a clear lack of symmetry along the east-west axis. The only advantage of the sky distribution of GPS satellites at mid-latitude sites is that the clearance in the northern direction (southern direction for south latitude sites) is not required. At latitude 55° , the shadow area becomes tangent to the zenith because the satellite inclination is 55° . Observations in the northern sector are only possible at low elevations. At the pole, we have potential observations in all azimuths but only observations at elevation angles below 45° will be possible.

Figure 2.4 shows the ground tracks defined by the satellites on the surface of the Earth to better conceptualize the situation from the space point of view. The inclination of the satellite orbits is particularly well illustrated in such a plot.

Figures 2.5 show examples of satellite sky distributions within the "unshadowed" area. This illustration permits an appreciation of the degree of uniformity (density distribution) of the satellite sky coverage. These are for a particular 3 hour observation period at latitudes 0° , 45° and 90° , respectively.

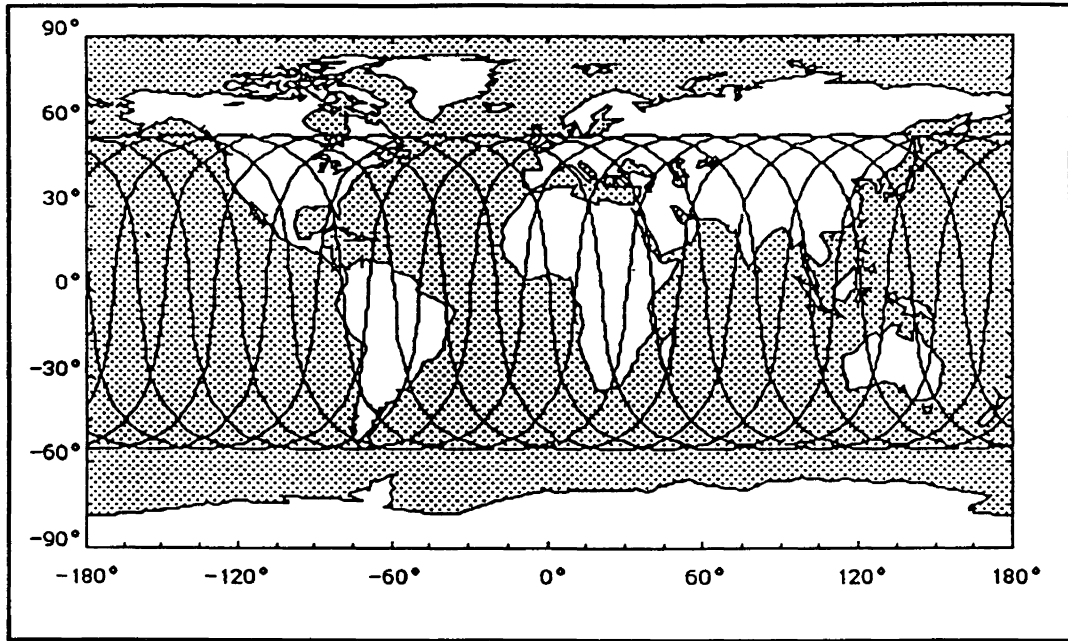


Figure 2.4: Ground tracks generated by GPS satellites with an orbital inclination of 55° over a period of 12 hours.

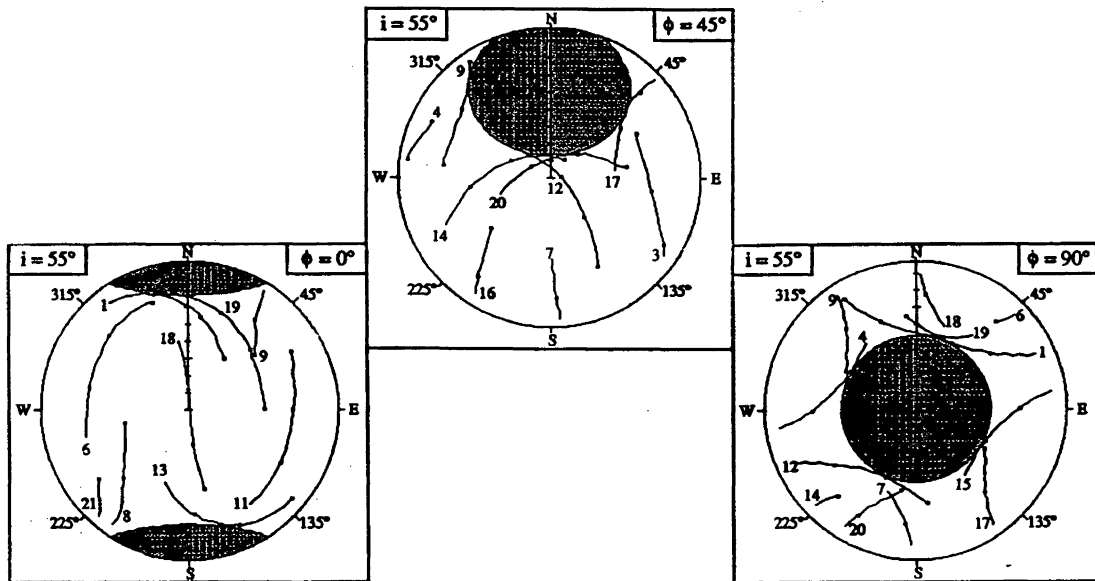


Figure 2.5: Examples of satellite sky distributions generated by GPS satellites with an orbital inclination of 55° over a period of 3 hours.

2.3.2 Prototype GPS constellation

Figure 2.6 shows the ground tracks defined by the prototype satellite constellation on the surface of the Earth for a 5 hour observation period. Compare these ground tracks with those of Figure 2.4 for the visualization of the different satellite orbit inclinations.

Figure 2.7 is the polar plot of an actual (3 September 1986) satellite sky distribution for Vancouver Island ($\phi: 49^\circ$) from 17:00 to 21:45 UT. The values of the satellite orbit inclinations ranged between 62.6° and 64.2° .

The hole towards the north as we have seen is not a coincidence. It is not a cause of the incomplete GPS constellation; it is simply due to the satellite orbit inclination. If we compare Figure 2.7 and Figure 2.5 ($\phi: 45^\circ$), we remark that the sky's shadow area is greater for an inclination of 55° than for an inclination of 64° . It is obvious that a constellation of polar satellites ($i: 90^\circ$) does not give rise to such a shadow area.

In section V.2, we present other satellite configurations produced by the prototype satellite constellation from different GPS campaigns.

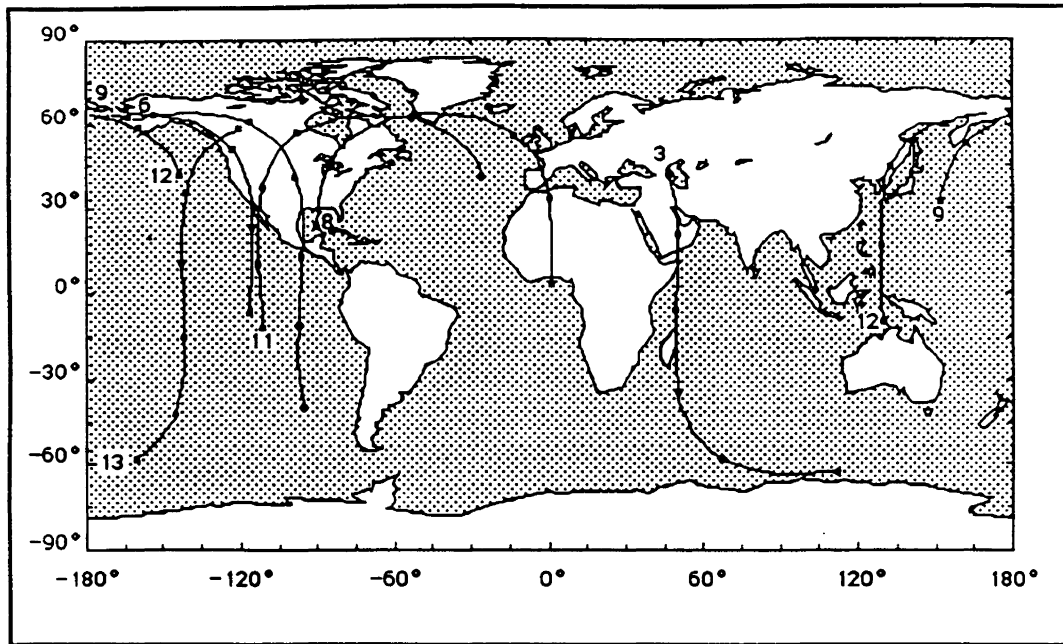


Figure 2.6: Ground tracks generated by the prototype GPS satellites (3 September 1986, 17 - 22 hr UT).

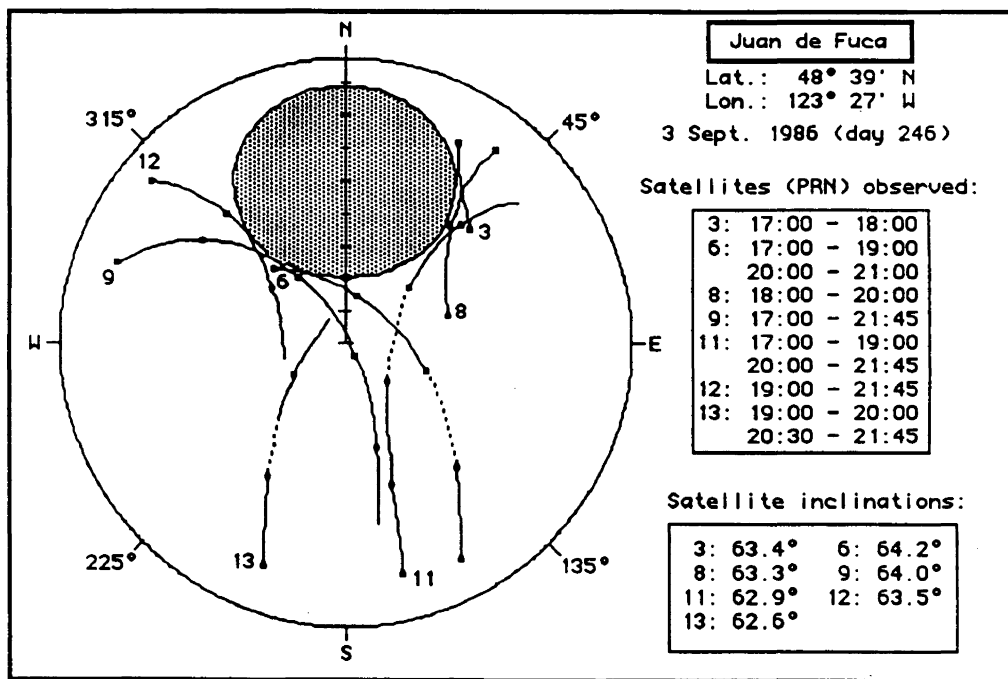


Figure 2.7: Satellite sky distribution for Vancouver Island (3 September 1986, 17:00 - 21:45 UT).

Chapter 3

Least squares adjustments and simulation techniques

3.1 Introduction

In this chapter, we present the basic mathematical tools and techniques needed to study the behaviour of the covariance matrix and the effects of systematic errors on station coordinates as a function of the satellite sky distribution. In section 3.2, we describe the observation equations for the undifferenced, single difference, double difference and triple difference carrier phase observables. The equivalence of observation differencing methods is demonstrated in section 3.3. An overview of different simulation techniques is given in section 3.4. More details about Geiger's simulation technique are presented in section 3.5.

3.2 Observation equations

The observation equation gives the relation existing between the observations and the parameters (both desired and nuisance parameters). The observation equation is the starting point for any analysis or processing of observed data. The observations of interest for our investigation are: the undifferenced carrier phase, the (between-receiver) single difference carrier phase, the (receiver-satellite) double difference carrier phase and the (receiver-satellite-epoch) triple difference carrier phase. The reader is referred to [Wells et al., 1986; chapter 8] for more detail concerning the linear combinations of observations.

The undifferenced carrier phase observation equation can be written as follows:

$$\begin{aligned}\overline{\Phi} &= \rho + c \cdot (dt_R - dt^S) + \lambda \cdot N + \text{dion} + \text{dtrop} + v \\ \rho &= \|\vec{r} - \vec{R}\| \end{aligned} \quad (3.1)$$

where:

$\overline{\Phi}$: carrier phase observable (in length units)
 ρ : geometric range between satellite and receiver (containing implicitly the receiver

\vec{R} : position vector \vec{R} at the receiving time and the satellite position vector \vec{r} at the transmitting time in the GPS time frame)
 c : vacuum speed of light
 dt_R : receiver clock error
 dt^S : satellite clock error
 λ : carrier wavelength
 N : integer carrier phase ambiguity
 $dion$: range error due to ionospheric refraction (a negative value for the phase advance)
 $dtrop$: range error due to tropospheric refraction
 v : carrier phase observation noise and remaining unmodelled effects

This is the fundamental GPS carrier phase equation of observation from which any other linear combinations of observations can be derived.

The (between-receiver) single difference carrier phase observation equation is:

$$\Delta\bar{\Phi} = \Delta\rho + c \cdot \Delta dt_R + \lambda \cdot \Delta N + \Delta dion + \Delta dtrop + \Delta v \quad (3.2)$$

where:

$\Delta\bar{\Phi}$: single difference carrier phase observable (in length units)
 $\Delta\rho$: geometric single difference range
 Δdt_R : relative receiver clock error
 ΔN : integer single difference carrier phase ambiguity
 $\Delta dion$: single difference range error due to ionospheric refraction
 $\Delta dtrop$: single difference range error due to tropospheric refraction
 Δv : single difference carrier phase observation noise and remaining unmodelled effects

The sense of the single difference operator (Δ) is as follows: $\Delta(*)_{ij} = (*)_j - (*)_i$.

The advantages of the (between-receiver) single differences are the removal or the great reduction of the effects of satellite clock errors and the reduction of the effects of orbit errors and propagation (ionospheric and tropospheric) errors. These are the main reasons for the high accuracy of the relative positioning obtained with GPS.

The (receiver-satellite) double difference carrier phase observation equation is:

$$\nabla\Delta\bar{\Phi} = \nabla\Delta\rho + \lambda \cdot \nabla\Delta N + \nabla\Delta dion + \nabla\Delta dtrop + \nabla\Delta v \quad (3.3)$$

where:

$\nabla\Delta\bar{\Phi}$: double difference carrier phase observable (in length units)

$\nabla\Delta\rho$: geometric double difference range
 $\nabla\Delta N$: integer double difference carrier phase ambiguity
 $\nabla\Delta\text{dion}$: double difference range error due to ionospheric refraction
 $\nabla\Delta\text{dtrop}$: double difference range error due to tropospheric refraction
 $\nabla\Delta v$: double difference carrier phase observation noise and remaining unmodelled effects

The sense of the double difference operator ($\nabla\Delta$) is as follows:

$$\nabla\Delta(*)_{ij}^{rs} = [(*)_{j^s} - (*)_{i^s}] - [(*)_{j^r} - (*)_{i^r}].$$

The advantage of the (receiver-satellite) double differences over the (between-receiver) single differences is the removal or the great reduction of the effects of receiver clock errors. The double difference observation processing mode is one of the most used techniques of operational software (e.g. UNB DIPOP software [Santerre, 1988; Vaníček et al., 1985] and the Bernese software [Gurtner et al., 1985]).

The (receiver-satellite-epoch) triple difference carrier phase observation equation is:

$$\delta\nabla\Delta\bar{\Phi} = \delta\nabla\Delta\rho + \delta\nabla\Delta\text{dion} + \delta\nabla\Delta\text{dtrop} + \delta\nabla\Delta v \quad (3.4)$$

where:

$\delta\nabla\Delta\bar{\Phi}$: triple difference carrier phase observable (in length units)
 $\delta\nabla\Delta\rho$: geometric triple difference range
 $\delta\nabla\Delta\text{dion}$: triple difference range error due to ionospheric refraction
 $\delta\nabla\Delta\text{dtrop}$: triple difference range error due to tropospheric refraction
 $\delta\nabla\Delta v$: triple difference carrier phase observation noise and remaining unmodelled effects

The sense of the triple difference operator ($\delta\nabla\Delta$) is as follows:

$$\delta\nabla\Delta(*)_{ij}^{rs} = \{[(*)_{j^s} - (*)_{i^s}] - [(*)_{j^r} - (*)_{i^r}]\}_{\text{epoch } n+1} - \{[(*)_{j^s} - (*)_{i^s}] - [(*)_{j^r} - (*)_{i^r}]\}_{\text{epoch } n}$$

The additive feature of the (receiver-satellite-epoch) triple differences over the (receiver-satellite) double differences is the cancellation of the carrier phase ambiguity. Unfortunately, with this kind of observable, we will not be able to exploit the integer nature of the phase ambiguity parameters in the least squares adjustments. The ability to fix carrier phase ambiguity parameters (to integer values) in the least squares adjustment process is primordial to achieve a high level of positioning accuracy.

In the sequel, assuming that the phase ambiguities have been fixed, we will replace the carrier phase observables $(\bar{\Phi}, \Delta\bar{\Phi}, \nabla\Delta\bar{\Phi})$ by unambiguous carrier phase observables denoted by: $\Phi, \Delta\Phi$ and $\nabla\Delta\Phi$.

3.3 Equivalence of observation differencing methods

The following paragraphs contain documentation, extracted from independent investigators' works, which demonstrates the equivalence between the observation differencing processing modes. The equivalence of the observation differencing methods is important to realize and will be advantageously exploited in Chapter 5. This latter chapter contains the comparison of prediction results based on single difference observations with results from real GPS data processed in double difference mode.

Lindlohr and Wells [1985] have demonstrated the equivalence of undifferenced, differenced, and orthogonalization modes:

"Undifferenced and differenced GPS carrier beat phase observations result in the same normal equations for the estimates of the desired parameters, as long as the models chosen for the undifferenced observation biases satisfy the fundamental differencing theorem."

The fundamental differencing theorem was stated as follows:

"Linear biases can be accounted for either by reducing the number of observations so that the biases cancel, or by adding an equal number of unknowns to model the biases. Both approaches give identical results."

The four sufficient conditions for the validity of the fundamental differencing theorem were given and explicitly demonstrated. The reader is referred to the original paper for more details.

The above demonstration assumed that the carrier beat phases were equally weighted and uncorrelated. Schaffrin and Grafarend [1986] made a generalization by considering a full

weight matrix for the carrier beat phase observations. They arrived at the same conclusion: the differencing methods are equivalent.

Bock et al. [1985] have reported:

"The baseline-vector estimate obtained from a biases-free fit to double differences is identical with the estimate obtained with the so-called "uncorrelated triple difference" algorithm (...) when there are no gaps in the observations. (...)"

Milbert and Kass [1985] wrote that:

"(...) The receiver data were processed by a triple difference model, which used a covariance decorrelation algorithm (...). This algorithm is equivalent to a single difference model [with clock parameters solved for] over a baseline where cycle biases were not held fixed at integer values. (...)"

The above two statements indicate the equivalence of the single difference processing mode (with clock parameters solved for) and the double difference processing mode.

One of the conclusions reached by Ashkenazi and Yau [1986] was:

"As expected from theoretical considerations, "double difference" observables would also lead to identical answers with "single difference" processing, provided the former are accompanied by appropriate correlation (or weight) matrices. (...)"

Finally, Lichten and Border [1987] stated that:

"(...) clocks modeled as white noise [in single difference processing mode]; at each measurement time the clocks are considered to be independent of their values at other times. The effect is equivalent to clock elimination through double differencing (...)"

3.4 Simulation techniques

To investigate the behaviour of the covariance matrix and the effects of systematic errors on station coordinates as a function of the satellite sky distribution, simulation techniques can be used. Different simulation techniques exist, each of them having their own advantages and disadvantages.

Real observations and controlled additive errors: This technique consists of processing the data with the best information available and using the results as reference values against which the other results may be compared. The other results are obtained by processing data contaminated by controlled (voluntarily introduced) errors. It is this technique which has been used, in Chapter 5, to assess the prediction results obtained from the improved version of Geiger's simulation technique, described below.

Simulated observations (perfect data with controlled additive errors): When no observations are available for a specific network and satellite configuration, e.g., pre-analysis study, it is then necessary to create simulated observations on which we will superpose controlled errors. This technique is identical to the first one except that the real observations are replaced by theoretical and errorless observations.

The advantages of the above techniques are: 1) the theoretical investigation is minimized (in comparison with the two techniques described below); 2) they give specific answers to specific questions for specific satellite and network configurations; 3) any kind of errors can be investigated. The disadvantages are: 1) the need to create and store simulated data (or modified collected data); 2) the processing time is appreciable; 3) generalization is difficult to achieve due to the large number of computer runs, representative of different satellite configurations and station networks, necessary to draw general conclusions about the effects of different errors.

Bernese geometrical technique [Beutler et al., 1988]: This is a geometrical approach which, under certain ideal assumptions, produces very simple and valuable formulae describing the influence of biases. The theoretical developments are reduced to a minimum by showing that many biases are members of two classes: Class 1 biases (on the observable) are identical for observations made at (ζ, α) and at $(\zeta, \alpha+180^\circ)$, where ζ is the zenith angle

and α is the azimuth. Class 2 biases are identical in the absolute value but of opposite sign for observations at (ζ, α) and at $(\zeta, \alpha+180^\circ)$. It is shown that class 1 biases introduce errors into estimated station heights. Class 2 biases give rise to length errors (scale effects). For more detail, refer to Beutler et al. [1988].

The advantages are: 1) no need to create or to modify observations; 2) the saving of processing time; 3) generalization is easy and quick to realize. The disadvantages are: 1) the requirement of considerable theoretical investigation (analytical modelling of the propagation of systematic errors in single difference observations and into the adjusted parameters); 2) the impossibility of considering satellite dependent biases or unknowns; 3) the impossibility of taking into account non-geometric parameters, like clock or tropospheric delay. The fact of not being able to take into account a clock parameter in the simulation may lead to erroneous results, particularly where the effect caused by the studied bias affects the station height. This is explained by the high correlation (as it will be shown in Chapters 5 and 6) existing between these two parameters.

Geiger's technique [Geiger, 1987; 1988]: This technique has basically the same attributes (advantages and disadvantages) as the Bernese technique except that it fortunately allows us to take into account non-geometric parameters and to study realistic satellite sky distributions. It is the technique that we have extensively used to make the studies and the analyses presented in the next chapters.

3.5 Details of Geiger's simulation technique

The starting point of the technique is the system of normal equation matrices of the least squares adjustment. The distinctive feature of Geiger's simulation technique resides in the way the accumulation (summation) of the normal equation matrix (N) and vector (U) are performed. The (between-receiver) single difference observables have to be used with this

technique.

The system of normal equation matrices is as usual:

$$\hat{\delta} = (A^T P_{\ell} A + P_x)^{-1} (A^T P_{\ell} \varepsilon \Delta \Phi) = (N + P_x)^{-1} U \quad (3.5)$$

where:

$\hat{\delta}$ is the vector of the estimated increment to the initial value of the least squares parameters (the description of the parameters is presented below);

A is the design matrix;

P_{ℓ} is the observation weight matrix;

P_x is the parameter a priori weight matrix; and

$\varepsilon \Delta \Phi$ is the bias in the single difference observation (which replaces the usual misclosure vector W).

The parameters are: the station coordinates (parameters 1, 2 and 3) expressed in the local geodetic system (x, y, z); the relative receiver clock synchronization (parameter 4) expressed in length units ($c \cdot \Delta t_R$), simply denoted (ct); and, optionally, the relative tropospheric zenith delay (parameter 5) expressed in length units ($\Delta t_{\text{trop}}(0)$, see section II.1), simply denoted (tr).

In practice, during the processing of real GPS data in single difference mode, one clock parameter is usually estimated at each epoch. Because Geiger's simulation technique cannot take into account time dependent parameter, only one clock parameter can be estimated. This is theoretically equivalent to assume that all observations were made simultaneously, i.e., considering one observation epoch only.

The elements of the design matrix (the derivative of the observation equation with respect to the estimated parameters), in the left-handed local geodetic system are (recall eqn. (3.2)):

$$\begin{aligned}
e_1 &= -\sin\zeta \cos\alpha & : \partial\Delta\Phi/\partial x \\
e_2 &= -\sin\zeta \sin\alpha & : \partial\Delta\Phi/\partial y \\
e_3 &= -\cos\zeta & : \partial\Delta\Phi/\partial z \\
e_4 &= 1 & : \partial\Delta\Phi/c\partial t \\
\text{and optionally,} \\
e_5 &= (1 - b \tan^2\zeta + 1.5b^2 \tan^4\zeta) \sec\zeta & : \partial\Delta\Phi/\partial \tau
\end{aligned} \tag{3.6}$$

The elements e_1 , e_2 , and e_3 are the derivatives of the single difference observation equation with respect to the station coordinates (x , y , z) of the free station. In relative positioning, for short baselines (small networks), we often fix one station, i.e., we assign to its coordinates large P_x values, which is equivalent to not solving for its coordinates. This explains why there are no elements of the design matrix assigned to the fixed station. The fourth element of the design matrix is related to the relative receiver clock synchronization. And optionally, we have introduced the term e_5 which is the derivative of the observation equation with respect to the relative tropospheric zenith delay.

The matrix (N) and the vector (U) can be expressed in generic form, as follows:

$$N = \begin{pmatrix} [e_1e_1] & [e_1e_2] & [e_1e_3] & [e_1e_4] & [e_1e_5] \\ [e_2e_1] & [e_2e_2] & [e_2e_3] & [e_2e_4] & [e_2e_5] \\ [e_3e_1] & [e_3e_2] & [e_3e_3] & [e_3e_4] & [e_3e_5] \\ [e_4e_1] & [e_4e_2] & [e_4e_3] & [e_4e_4] & [e_4e_5] \\ [e_5e_1] & [e_5e_2] & [e_5e_3] & [e_5e_4] & [e_5e_5] \end{pmatrix}; \quad U = \begin{pmatrix} [e_1\varepsilon\Delta\Phi] \\ [e_2\varepsilon\Delta\Phi] \\ [e_3\varepsilon\Delta\Phi] \\ [e_4\varepsilon\Delta\Phi] \\ [e_5\varepsilon\Delta\Phi] \end{pmatrix} \tag{3.7}$$

The brackets symbolize the summation over the total number of observations and the term $\varepsilon\Delta\Phi(\zeta,\alpha)$ is the misclosure vector:

$$\varepsilon\Delta\Phi = \Delta\Phi_{\text{observed}} - \Delta\Phi_{\text{theoretical}} \tag{3.8}$$

For a baseline (A , B), the sense of the (between-receiver) single difference is defined as:

$$\Delta\Phi = \Phi_B - \Phi_A \quad (3.9)$$

The central idea of the technique is to assume that the GPS satellite observation distribution is continuous. This assumption allows us to replace the summations over the total number of observations, implied in the normal equation matrices, by integrals. Moreover, we will assume that the distribution is homogeneous, i.e., the number of observations by area units (surface density) is constant over the observer's sky (excluding the shadow areas where observations are not made, e.g., refer to Figure 2.5). In other words, this is the homogeneous spreading of the observations taken along the satellite sky tracks, within the boundaries defining the area of the observer's sky covered by all the satellite sky tracks.

More explicitly, the summations over the total number of observations $[e_i e_j]$ are replaced by the following integral:

$$[e_i e_j] \approx \int_{\alpha_{\text{from}}}^{\alpha_{\text{to}}} \int_{\zeta_{\text{min}}}^{\zeta_{\text{max}}} \beta e_i e_j \sin\zeta \, d\zeta \, d\alpha \quad (3.10a)$$

and similarly the expressions $[e_i \varepsilon\Delta\rho]$ are replaced by:

$$[e_i \varepsilon\Delta\Phi] \approx \int_{\alpha_{\text{from}}}^{\alpha_{\text{to}}} \int_{\zeta_{\text{min}}}^{\zeta_{\text{max}}} \beta e_i \varepsilon\Delta\Phi \sin\zeta \, d\zeta \, d\alpha \quad (3.10b)$$

The integration is performed over an azimuth sector defined by α_{from} and α_{to} and over a zenith angle sector defined by ζ_{min} and ζ_{max} .

Refer to Figure 3.1 for the visualization of the situation and the description of the coordinate system used: the x-axis is directed towards north, the y-axis is directed towards the east direction and the z-axis is directed towards the zenith completing the left-handed

local geodetic system.

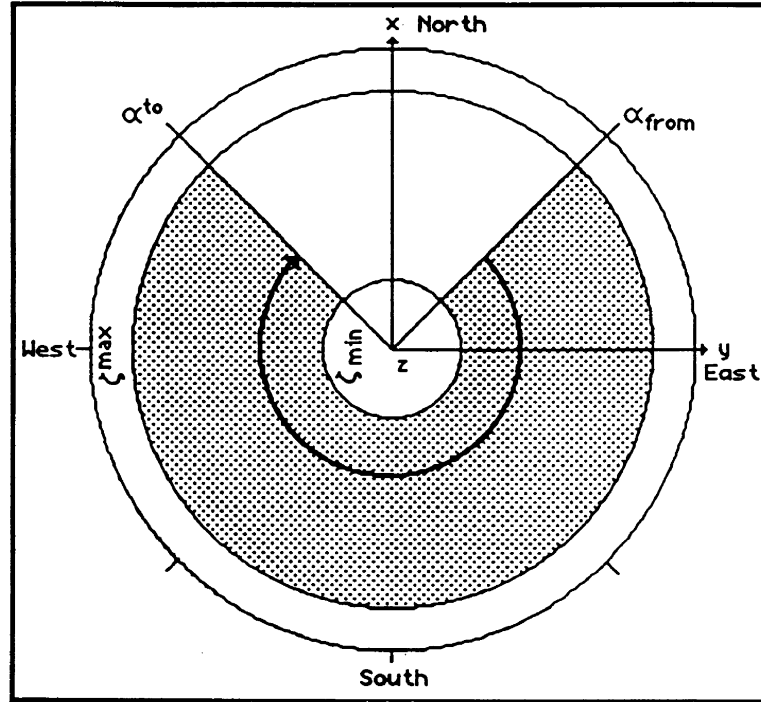


Figure 3.1: Local geodetic system and integration boundaries.

Naturally, the same process can be generalized for the definition of more than one integration sector.

The term " $\sin\zeta$ " in the integrals of equations (3.10) takes into account the homogeneity assumption of the density distribution, and β is equal to:

$$\beta = n / 2\pi \tag{3.11}$$

where "n" is defined as the total number of "fictitious" observations in the observer's sky hemisphere and " 2π " is the normalization factor of the integration over the azimuth sector.

Using the above definition, the number of observations in the selected sector (n_{sec}) is equal

to:

$$n_{\text{sec}} = \int_{\alpha_{\text{from}}}^{\alpha_{\text{to}}} \int_{\zeta_{\text{min}}}^{\zeta_{\text{max}}} \beta \sin \zeta \, d\zeta \, d\alpha$$

$$n_{\text{sec}} = \beta (\cos \zeta_{\text{min}} - \cos \zeta_{\text{max}}) (\alpha_{\text{to}} - \alpha_{\text{from}}) = \beta I_{100} J_{00} \quad (3.12)$$

The term I_{100} is a particular case ($i = 1, j = 0$ and $k = 0$) of the general form of the integrals over the zenith angle sector:

$$I_{ijk} = \int_{\zeta_{\text{min}}}^{\zeta_{\text{max}}} \sin^i \zeta \cos^j \zeta \zeta^k \, d\zeta \quad (3.13a)$$

The term J_{00} is a particular case ($i = 0, j = 0$) of the general form of the integrals over the azimuth sector:

$$J_{ij} = \int_{\alpha_{\text{from}}}^{\alpha_{\text{to}}} \sin^i \alpha \cos^j \alpha \, d\alpha \quad (3.13b)$$

The list and the analytical evaluation of the I_{ijk} and J_{ij} terms used in this thesis are presented in Appendix III.

The result of the integrations performed on each of the elements of the symmetric normal equations matrix $N (A^T P_{\rho} A)$ and the elements of vectors $U (A^T P_{\rho} \epsilon \Delta \Phi)$ for each of the analysed biases will be presented in Chapter 4.

In summary, we have: 1) to develop a mathematical expression for $\epsilon \Delta \Phi$ for each bias of

interest; 2) to evaluate the terms $[e_i e_j]$ and $[e_i \varepsilon \Delta \Phi]$ of eqn. (3.7) using the integral equations (3.10) (these integrals are evaluated at integration boundaries defining the selected satellite sky distribution); and 3) to solve for the unknowns with the use of eqn. (3.5).

The automation of the technique has been achieved by the coding of a program called DIPOPSIM (Differential POSitioning Program SIMulator). The description of this program is presented in Appendix IV.

Assumptions and decisions

This sub-section lists the assumptions inherent to the simulation technique and the decisions we have made to produce the results presented in the next chapters.

- 1) The baseline length is short (less than about 100 km) compared to the receiver-satellite range;
- 2) The baseline height component is small compared to the baseline length (baseline zenith angle $\sim 90^\circ$);
- 3) The time dependent errors and the time dependent parameters cannot be taken into account by the simulation technique;
- 4) Only one relative receiver clock parameter can be estimated. This is equivalent to assume that all observations were made simultaneously, i.e., considering one observation epoch only;
- 5) The satellite dependent errors and the satellite dependent parameters cannot be taken into account by the simulation technique;
- 6) The carrier phase ambiguities are assumed fixed (not introduced as unknowns).

Usually, for small baseline lengths, it is possible to fix them easily. Moreover, appropriate techniques and specifications can yield phase ambiguity resolution for baselines as long as 2,000 km [Blewitt, 1989; Dong and Bock, 1989];

- 7) The satellite orbits are assumed errorless and not estimated;
- 8) Only one baseline at a time is considered, i.e., the correlations among the stations of a network are not taken into account and/or cannot be monitored;
- 9) The satellite sky density distribution is assumed continuous and homogeneous within the selected integration boundaries. Homogeneity is certainly the most sensible assumption but yet the most realistic of the simplest distributions;
- 10) The observations are assumed uncorrelated and uniformly weighted. The observation weight matrix is defined as: $P_\ell = k I$, where I is the identity matrix;
- 11) The tests have been performed with all P_x set to zero.

The assessment and the pertinence of the assumptions used in Geiger's simulation technique are presented in Chapter 5.

Utility for absolute positioning analysis

Note that the technique can be used in the analysis of absolute positioning. Models for the bias on range ($\epsilon\Phi$) for different errors would have to be developed and substituted for ($\epsilon\Delta\Phi$).

In fact, except for the magnitude ($\epsilon\Phi > \epsilon\Delta\Phi$), the conclusions which will be reached in the analysis of the effects due to relative tropospheric zenith delay error on relative positioning, are also valid for the study of absolute tropospheric zenith delay error on absolute positioning. Similarly, the analysis of the covariance matrix behaviour is also valid for absolute positioning.

Chapter 4

Mathematical formulation of the simulation technique

4.1 Introduction

In section 3.5 we have described the process of Geiger's simulation technique. In this chapter we will explicitly present the mathematical expressions of each of the elements of the matrices and vectors of the normal equations of the least squares adjustments.

The unknown parameters that we will consider in the least squares adjustments are the x-, y- and z-coordinates (in the left-handed local geodetic system) of the free station, the relative receiver clock parameter expressed in length units (ct is the abbreviation for $c \cdot \Delta t_R$) and optionally, the relative tropospheric zenith delay parameter (tr is the abbreviation for $\Delta t_{\text{trop}}(0)$). The studied systematic errors are: 1) the relative tropospheric zenith delay; 2) the absolute ionospheric refraction; 3) the offset in horizontal coordinates (latitude and longitude) of the fixed station; and 4) the height offset of the fixed station. These (satellite independent) errors are some of the more important errors affecting precise relative positioning results which can be analysed with Geiger's simulation technique.

In order to construct the normal equation matrix we need the elements of the design matrix. These are the partial derivatives of the single difference observation with respect to the unknown parameters. The elements of the design matrix have been presented in section 3.5; for convenience we write them again, here:

$$\begin{aligned} e_1 &= -\sin\zeta \cos\alpha & : \partial\Delta\Phi/\partial x \\ e_2 &= -\sin\zeta \sin\alpha & : \partial\Delta\Phi/\partial y \\ e_3 &= -\cos\zeta & : \partial\Delta\Phi/\partial z \\ e_4 &= 1 & : \partial\Delta\Phi/c\partial t \end{aligned} \tag{4.1}$$

and optionally,

$$e_5 = (1 - b \tan^2 \zeta + 1.5b^2 \tan^4 \zeta) \sec \zeta \quad : \partial \Delta \Phi / \partial \tau$$

In section 4.2, we first present the elements of the normal equation matrix N for the general case and for two particular cases: i) where the upper azimuth integration boundary $\alpha_{to} = 360^\circ - \alpha_{from}$ (α_{from} is the lower azimuth integration boundary); and ii) where $\alpha_{from} = 0^\circ$ and $\alpha_{to} = 360^\circ$, i.e., an all-azimuth satellite distribution. Secondly, the structure of the inverse of the normal equation matrix (N^{-1}) is presented for the 2 particular satellite sky distribution cases.

These two particular azimuthal satellite distributions have been selected because they are representative of the generic satellite configurations that we will study in Chapter 6.

To construct the elements of the normal equation vectors we need, in addition to the above design matrix elements, to evaluate the misclosure vector ($\epsilon \Delta \Phi$), i.e., the bias in the single difference observation introduced by the studied systematic error. The biases in single difference observations for each of the systematic errors, mentioned above, have been developed in Appendix II. Documentation of the expected magnitude of the systematic error sources is given in Appendix I.

The analytical forms of the elements of the design matrix $e_i(\zeta, \alpha)$ and the bias in the single difference observation $\epsilon \Delta \Phi(\zeta, \alpha)$ allow us to evaluate the integrals of equations (3.10). In Geiger's simulation approach, equation (3.10a) is the formula to construct the $[e_i \ e_j]$ elements of matrix N , and equation (3.10b) is the formula to construct the $[e_i \ \epsilon \Delta \Phi]$ elements of vector U .

For each of the studied systematic errors, we present: 1) the bias in the single difference observation; 2) the general structure of the elements $[e_i \ \epsilon\Delta\Phi]$ of vector U ; 3) the functional dependence of the $[e_i \ \epsilon\Delta\Phi]$ terms; 4) the structure of the elements for the two particular satellite sky distribution cases described above; and 5) the trends of the interaction of vector U with the matrix N^{-1} , i.e., the way the systematic error will propagate into the station coordinates for the two particular satellite sky distribution cases.

The trends will be "qualitatively" obtained by analysing the internal structure and the components (I_{ijk} and J_{ij} terms) of matrix N^{-1} and vector U . The effects of the studied systematic errors into the coordinates of a station network will be described by similarity (or affine) transformation parameters. The reader is referred to Appendix VI for a definition of the similarity and affine transformation parameters used in this chapter.

Section 4.3 deals with the tropospheric refraction, section 4.4 with the absolute ionosphere refraction, section 4.5 contains the investigation of the effect of an offset in the horizontal coordinates (latitude and longitude) of the fixed station and finally section 4.6 deals with the offset in the height of the fixed station. Throughout this chapter (as well as in section 3.5 and Appendix II) we often mention the terms "short baseline length" and "small baseline height difference". These are the basic assumptions used, in Appendix II, to develop a simple analytical expression for the bias of the single difference observation $\epsilon\Delta\Phi$. A short baseline length, in this context, means a length less than about 100 km and a small baseline height difference means that the zenith angle of the baseline departs just a few degrees from 90° .

The number of formulae (elements $[e_i \ e_j]$ and $[e_i \ \epsilon\Delta\Phi]$) which have been analytically integrated is 15 for the normal equation matrix and 5 for each of the four normal equation

vectors for a total of 20 and a grand total of 35. The azimuth integration terms J_{ij} and the zenith angle integration terms I_{ijk} , used in the calculation of the elements of the matrix N and the different vectors U , are presented in section III.1 and III.2, respectively. To give an idea of the magnitude of the elements $[e_i e_j]$ and $[e_i \epsilon \Delta \Phi]$, we present in section III.3 some examples of numerical values of the elements of the matrices N and N^{-1} and the vector U for different satellite configurations, different combination of parameters and different systematic errors.

The content of this chapter will help us to better understand the inside of the least squares adjustment processes in terms of the covariance matrix and of the propagation of systematic errors and their functional dependence to the satellite sky distributions in a "qualitative" manner. This analysis will allow us to better interpret the "quantitative" results presented in Chapters 5 and 6.

4.2 Covariance matrix

In this section, we present the elements of matrices N and N^{-1} calculated with eqn. (3.10a) and the use of eqn. (4.1). Emphasis is put on the analysis of two particular satellite configurations representative of the generic satellite configurations that we will study in Chapter 6.

Normal equation matrix N : $(A^T P_\ell A)$

The terms $[e_i e_j]$ of the normal equation matrix $(A^T P_\ell A)$ are:

$$[e_1 e_1] = \beta P_\ell I_{300} J_{02}$$

$$[e_2 e_1] = \beta P_\ell I_{300} J_{11}$$

$$[e_2 e_2] = \beta P_\ell I_{300} J_{20}$$

$$[e_3 e_1] = \beta P_\ell I_{210} J_{01}$$

$$\begin{aligned}
[e_3 e_2] &= \beta P_\ell I_{210} J_{10} \\
[e_3 e_3] &= \beta P_\ell I_{120} J_{00} \\
[e_4 e_1] &= -\beta P_\ell I_{200} J_{01} \\
[e_4 e_2] &= -\beta P_\ell I_{200} J_{10} \\
[e_4 e_3] &= -\beta P_\ell I_{110} J_{00} \\
[e_4 e_4] &= \beta P_\ell I_{100} J_{00}
\end{aligned} \tag{4.2a}$$

and optionally,

$$\begin{aligned}
[e_5 e_1] &= -\beta P_\ell (I_{2-10} - b I_{4-30} + 1.5b^2 I_{6-50}) J_{01} \\
[e_5 e_2] &= -\beta P_\ell (I_{2-10} - b I_{4-30} + 1.5b^2 I_{6-50}) J_{10} \\
[e_5 e_3] &= -\beta P_\ell (I_{100} - b I_{3-20} + 1.5b^2 I_{5-40}) J_{00} \\
[e_5 e_4] &= \beta P_\ell (I_{1-10} - b I_{3-30} + 1.5b^2 I_{5-50}) J_{00} \\
[e_5 e_5] &= \beta P_\ell (I_{1-20} - 2b I_{3-40} + 4b^2 I_{5-60} - 3b^3 I_{7-80} + 2.25b^4 I_{9-100}) J_{00}
\end{aligned}$$

For convenience, we will write these terms in matrix form. Because of space restriction, we will only write the first and more important I_{ijk} term for the $[e_5 e_i]$ elements (the one related to tropospheric zenith delay parameter); this will not compromise the following "qualitative" investigation. For the calculation of the results presented in Chapters 5 and 6 and section III.3, the full mathematical expressions are used. The expressions on the right and bottom of the matrices are the elements of the design matrix, see eqn. (4.1).

$$N = \beta P_\ell \begin{pmatrix} I_{300} J_{02} & I_{300} J_{11} & I_{210} J_{01} & -I_{200} J_{01} & -I_{2-10} J_{01} \\ I_{300} J_{11} & I_{300} J_{20} & I_{210} J_{10} & -I_{200} J_{10} & -I_{2-10} J_{10} \\ I_{210} J_{01} & I_{210} J_{10} & I_{120} J_{00} & -I_{110} J_{00} & -I_{100} J_{00} \\ -I_{200} J_{01} & -I_{200} J_{10} & -I_{110} J_{00} & I_{100} J_{00} & I_{1-10} J_{00} \\ -I_{2-10} J_{01} & -I_{2-10} J_{10} & -I_{100} J_{00} & I_{1-10} J_{00} & I_{1-20} J_{00} \end{pmatrix} \begin{matrix} -\sin\zeta \cos\alpha \\ -\sin\zeta \sin\alpha \\ -\cos\zeta \\ 1 \\ \sec\zeta \end{matrix} \tag{4.2b}$$

$$\begin{matrix} -\sin\zeta \cos\alpha & -\sin\zeta \sin\alpha & -\cos\zeta & 1 & \sec\zeta \end{matrix}$$

Equation (4.2b) tells us that nearby stations, having similar satellite sky distribution, will have station coordinate confidence ellipsoids similar in shape and orientation.

A closer inspection of eqn. (4.2b) allows us to see that the I_{ijk} terms (the ones that are a function of zenith angle) of the first and second lines (rows) are identical, because the first and the second elements of the design matrix contain the same $\sin\zeta$ function. The J_{ij} terms (the ones that are a function of the azimuth sector) of the third, fourth and fifth lines (columns) are identical, because the third, fourth and fifth elements of the design matrix are all independent of azimuth (α). All the terms $[e_i e_j]$ are functions of both the azimuth and the zenith angle sectors.

Particular cases:

i) $\alpha^{to} = 360^\circ - \alpha_{from}$, ($J_{10} = J_{11} = 0$)

$$N = \beta P \ell \begin{pmatrix} I_{300} J_{02} & 0 & I_{210} J_{01} & -I_{200} J_{01} & -I_{2-10} J_{01} \\ 0 & I_{300} J_{20} & 0 & 0 & 0 \\ I_{210} J_{01} & 0 & I_{120} J_{00} & -I_{110} J_{00} & -I_{100} J_{00} \\ -I_{200} J_{01} & 0 & -I_{110} J_{00} & I_{100} J_{00} & I_{1-10} J_{00} \\ -I_{2-10} J_{01} & 0 & -I_{100} J_{00} & I_{1-10} J_{00} & I_{1-20} J_{00} \end{pmatrix} \begin{matrix} -\sin\zeta \cos\alpha \\ -\sin\zeta \sin\alpha \\ -\cos\zeta \\ 1 \\ \sec\zeta \end{matrix} \quad (4.2c)$$

$$\begin{matrix} -\sin\zeta \cos\alpha & -\sin\zeta \sin\alpha & -\cos\zeta & 1 & \sec\zeta \end{matrix}$$

For this kind of satellite sky distribution, the terms J_{10} and J_{11} equal zero. This means that there is no correlation between the y-coordinate (the coordinate perpendicular to the horizontal symmetry axis of the satellite sky distribution) and the 4 other unknowns. However, correlations exist among all the other parameters.

ii) $\alpha_{\text{from}} = 0^\circ$ and $\alpha^{\text{to}} = 360^\circ$, ($J_{01} = J_{10} = J_{11} = 0$, $J_{02} = J_{20} = \pi$ and $J_{00} = 2\pi$)

$$N = \beta P_\ell \begin{pmatrix} I_{300} \pi & 0 & 0 & 0 & 0 \\ 0 & I_{300} \pi & 0 & 0 & 0 \\ 0 & 0 & I_{120} 2\pi & -I_{110} 2\pi & -I_{100} 2\pi \\ 0 & 0 & -I_{110} 2\pi & I_{100} 2\pi & I_{1-10} 2\pi \\ 0 & 0 & -I_{100} 2\pi & I_{1-10} 2\pi & I_{1-20} 2\pi \end{pmatrix} \begin{matrix} -\sin\zeta \cos\alpha \\ -\sin\zeta \sin\alpha \\ -\cos\zeta \\ 1 \\ \sec\zeta \end{matrix} \quad (4.2d)$$

$$\begin{matrix} -\sin\zeta \cos\alpha & -\sin\zeta \sin\alpha & -\cos\zeta & 1 & \sec\zeta \end{matrix}$$

For an all-azimuth satellite distribution, the terms J_{01} , J_{10} and J_{11} equal zero. This means that there is no correlation between the horizontal coordinates and the 3 other unknowns.

However, whatever the azimuthal satellite distribution, the term J_{00} will never be zero and correlations will always exist among the station height, the clock and the tropospheric delay parameters. These correlations prevent us from making any attempt to geometrically interpret the behaviour of the covariance matrix. Note also the equality between the term J_{02} and J_{20} .

Inverse of the normal equation matrix N: $(A^T P_\ell A)^{-1}$

The shape of the matrix N^{-1} is similar to the shape of matrix N. For the general case the matrix N^{-1} is a full matrix making impossible the writing of its elements in a compact and understandable analytical form.

Even for the first particular case ($\alpha^{\text{to}} = 360^\circ - \alpha_{\text{from}}$), the elements of the matrix N^{-1} are still complicated. For this reason we have to use some generic IJ_{mn} expressions, where the subscripts "m" and "n" indicate the row and the column position in matrix N^{-1} ,

respectively. These IJ_{mn} expressions (coming from the analytical form of the adjoint method of matrix inversion) are mixtures of terms I_{ijk} and J_{ij} , too lengthy to be explicitly written in compact form. However, these abbreviations will not compromise the "qualitative" study presented in this chapter. For even more simplicity we will only consider the station coordinates and the clock parameter as unknowns.

Particular cases:

i) $\alpha^{to} = 360^\circ - \alpha_{from}$, ($J_{10} = J_{11} = 0$)

$$N^{-1} = B^{-1} \begin{pmatrix} I_{300}^{-1} J_{02}^{-1} + IJ_{11} & 0 & IJ_{13} & IJ_{14} \\ 0 & I_{300}^{-1} J_{20}^{-1} & 0 & 0 \\ IJ_{31} & 0 & I_{100} I^{-1} J_{00}^{-1} + IJ_{33} & I_{110} I^{-1} J_{00}^{-1} + IJ_{34} \\ IJ_{41} & 0 & I_{110} I^{-1} J_{00}^{-1} + IJ_{43} & I_{120} I^{-1} J_{00}^{-1} + IJ_{44} \\ -\sin\zeta \cos\alpha & -\sin\zeta \sin\alpha & -\cos\zeta & 1 \end{pmatrix} \quad (4.3a)$$

where: $I^{-1} = (I_{120} I_{100} - I_{110}^2)^{-1}$ and $B^{-1} = \beta^{-1} P_\ell^{-1}$

ii) $\alpha_{from} = 0^\circ$ and $\alpha^{to} = 360^\circ$, ($J_{01} = J_{10} = J_{11} = 0$, $J_{02} = J_{20} = \pi$ and $J_{00} = 2\pi$)

$$N^{-1} = B^{-1} \begin{pmatrix} I_{300}^{-1} \pi^{-1} & 0 & 0 & 0 \\ 0 & I_{300}^{-1} \pi^{-1} & 0 & 0 \\ 0 & 0 & I_{100} I^{-1} (2\pi)^{-1} & I_{110} I^{-1} (2\pi)^{-1} \\ 0 & 0 & I_{110} I^{-1} (2\pi)^{-1} & I_{120} I^{-1} (2\pi)^{-1} \\ -\sin\zeta \cos\alpha & -\sin\zeta \sin\alpha & -\cos\zeta & 1 \end{pmatrix} \begin{matrix} -\sin\zeta \cos\alpha \\ -\sin\zeta \sin\alpha \\ -\cos\zeta \\ 1 \end{matrix} \quad (4.3b)$$

where: $I^{-1} = (I_{120} I_{100} - I_{110}^2)^{-1}$ and $B^{-1} = \beta^{-1} P_\ell^{-1}$

In the second particular case, the IJ_{mn} expressions vanish, making the interpretation presented in the next sections much simpler.

In the next 4 sections, we present the elements of vector U calculated with eqn. (3.10b) and the use of eqn. (4.1) and the terms $\epsilon\Delta\Phi$ developed in Appendix II. Again the emphasis is put on the analysis of two particular satellite configurations representative of the generic satellite configurations that we will study in Chapter 6. The statements mentioned in sub-section "Interaction with matrix N^{-1} " have been reached by interacting (by multiplying symbolically) equation (4.3a) or (4.3b) with vector U presented in the following sections.

4.3 Relative tropospheric refraction

The bias introduced in the single difference observation due to this error is (section II.1):

$$\epsilon\Delta\Phi(\zeta) = (1 - b \tan^2\zeta + 1.5b^2 \tan^4\zeta) \sec\zeta \epsilon\Delta\text{trop}(0) = m(\zeta) \epsilon\Delta\text{trop}(0) \quad (4.4)$$

where:

$$b = 0.85 h^{\text{atm}}/R_e \approx 1.1 \times 10^{-3}$$

h^{atm} : height of the centre of gravity for a vertical column of air (8 km)

R_e : Earth's radius (6,378 km)

$\epsilon\Delta\text{trop}(0)$: relative tropospheric zenith delay error

$m(\zeta)$: tropospheric mapping function

Summary of assumptions and approximations:

- 1) For short baseline length ($\ell < 100$ km) and small station height difference ($\zeta_0 \approx 90^\circ$) we can assume that the zenith angles at both stations for the same satellite are identical ($\zeta_2 \approx \zeta_1 \approx \zeta$), i.e., $m(\zeta_2) \approx m(\zeta_1) \approx m(\zeta)$, see eqn. (II.6). This means that the local verticals at the stations are practically parallel and the parallactic angle at the satellite is small.
- 2) Hartmann and Leitinger's mapping function, eqn. (II.8b), is an approximation of the "true" tropospheric mapping function.
- 3) The use of the mapping function is restricted to zenith angles smaller than 85° , see Table II.1.
- 4) The relative tropospheric zenith delay error is constant during the observing session.

Normal equation vector U: $(A^T P_{\ell} \varepsilon \Delta \Phi)$

$$\begin{aligned}
 [e_1 \varepsilon \Delta \Phi] &= -\beta P_{\ell} (I_{2-10} - b I_{4-30} + 1.5b^2 I_{6-50}) J_{01} \varepsilon \Delta t_{\text{trop}}(0) \\
 [e_2 \varepsilon \Delta \Phi] &= -\beta P_{\ell} (I_{2-10} - b I_{4-30} + 1.5b^2 I_{6-50}) J_{10} \varepsilon \Delta t_{\text{trop}}(0) \\
 [e_3 \varepsilon \Delta \Phi] &= -\beta P_{\ell} (I_{100} - b I_{3-20} + 1.5b^2 I_{5-40}) J_{00} \varepsilon \Delta t_{\text{trop}}(0) \\
 [e_4 \varepsilon \Delta \Phi] &= \beta P_{\ell} (I_{1-10} - b I_{3-30} + 1.5b^2 I_{5-50}) J_{00} \varepsilon \Delta t_{\text{trop}}(0) \\
 \text{and optionally,} \\
 [e_5 \varepsilon \Delta \Phi] &= \beta P_{\ell} (I_{1-20} - 2b I_{3-40} + 4b^2 I_{5-60} - 3b^3 I_{7-80} + 2.25b^4 I_{9-100}) J_{00} \varepsilon \Delta t_{\text{trop}}(0)
 \end{aligned} \tag{4.5a}$$

Functional dependence of the $[e_i \varepsilon \Delta \Phi]$ terms:

- 1) All terms are proportional to relative tropospheric zenith delay bias $\varepsilon \Delta t_{\text{trop}}(0)$;
- 2) All terms are independent of baseline length and baseline azimuth;
- 3) The terms $[e_1 \varepsilon \Delta \Phi]$ and $[e_2 \varepsilon \Delta \Phi]$ have the same dependence on ζ (terms in I_{ijk});
- 4) The terms $[e_3 \varepsilon \Delta \Phi]$, $[e_4 \varepsilon \Delta \Phi]$ and $[e_5 \varepsilon \Delta \Phi]$ have the same dependence on α (terms in J_{ij});
- 5) The terms $[e_i \varepsilon \Delta \Phi]$ are equivalent to line $[e_5 e_i]$ (column $[e_i e_5]$) of matrix N. This means that constant relative tropospheric zenith delay mismodelling would be absorbed by the introduction of a relative tropospheric zenith delay parameter in the solution. We can also presume, because of the close relation between the tropospheric mapping function ($\sim \sec \zeta$) and the ionospheric mapping function $\sec \zeta'$ (where ζ' is the zenith angle at the height of the ionospheric layer, refer to section II.2), that some part of the relative ionospheric refraction will be absorbed by this parameter.

Particular cases:

i) $\alpha^{\text{to}} = 360^\circ - \alpha_{\text{from}}$, ($J_{10} = 0$)

$$\begin{aligned} [e_1 \varepsilon \Delta \Phi] &= -\beta P_\ell (I_{2-10} - b I_{4-30} + 1.5b^2 I_{6-50}) J_{01} \varepsilon \Delta t_{\text{trop}}(0) \\ [e_2 \varepsilon \Delta \Phi] &= 0 \\ [e_3 \varepsilon \Delta \Phi] &= -\beta P_\ell (I_{100} - b I_{3-20} + 1.5b^2 I_{5-40}) J_{00} \varepsilon \Delta t_{\text{trop}}(0) \\ [e_4 \varepsilon \Delta \Phi] &= \beta P_\ell (I_{1-10} - b I_{3-30} + 1.5b^2 I_{5-50}) J_{00} \varepsilon \Delta t_{\text{trop}}(0) \\ \text{and optionally,} \\ [e_5 \varepsilon \Delta \Phi] &= \beta P_\ell (I_{1-20} - 2b I_{3-40} + 4b^2 I_{5-60} - 3b^3 I_{7-80} + 2.25b^4 I_{9-100}) J_{00} \varepsilon \Delta t_{\text{trop}}(0) \end{aligned} \quad (4.5b)$$

ii) $\alpha_{\text{from}} = 0^\circ$ and $\alpha^{\text{to}} = 360^\circ$, ($J_{01} = J_{10} = 0$ and $J_{00} = 2\pi$)

$$\begin{aligned} [e_1 \varepsilon \Delta \Phi] &= 0 \\ [e_2 \varepsilon \Delta \Phi] &= 0 \\ [e_3 \varepsilon \Delta \Phi] &= -\beta P_\ell (I_{100} - b I_{3-20} + 1.5b^2 I_{5-40}) 2\pi \varepsilon \Delta t_{\text{trop}}(0) \\ [e_4 \varepsilon \Delta \Phi] &= \beta P_\ell (I_{1-10} - b I_{3-30} + 1.5b^2 I_{5-50}) 2\pi \varepsilon \Delta t_{\text{trop}}(0) \\ \text{and optionally,} \\ [e_5 \varepsilon \Delta \Phi] &= \beta P_\ell (I_{1-20} - 2b I_{3-40} + 4b^2 I_{5-60} - 3b^3 I_{7-80} + 2.25b^4 I_{9-100}) 2\pi \varepsilon \Delta t_{\text{trop}}(0) \end{aligned} \quad (4.5c)$$

Interaction with matrix N^{-1} :

- 1) The effects are independent of baseline length and baseline azimuth, however the relative tropospheric zenith delay might be dependent on baseline length;
- 2) The primary effect is a translation in the station height;
- 3) For an all-azimuth satellite distribution the horizontal coordinates are not affected;
- 4) The bulk of the primary effect is independent of the azimuth sector of the satellite distribution (the terms J_{00} vanish when multiplied by J_{00}^{-1});
- 5) The additive part of the effect in station height, present in a non-uniform azimuth satellite distribution, is sensitive to both the zenith and azimuth sectors of the satellite distribution;
- 6) The coordinate aligned with the horizontal symmetry axis is the only horizontal coordinate affected by a non-uniform azimuth satellite distribution;

- 7) The effect in the horizontal coordinate is sensitive to both the zenith and azimuth sectors of the satellite distribution;
- 8) Geometrical interpretation of the effects of this systematic error is misleading because of the correlation between the station height (the most affected coordinate) and the clock parameter;
- 9) If a relative tropospheric zenith delay parameter is included in the solution, constant relative tropospheric zenith delay mismodelling will be absorbed by this parameter (see item #5 of the functional dependence of the $[e_i \epsilon \Delta \Phi]$ terms, stated above).

4.4 Absolute ionospheric refraction

The bias introduced in the single difference observation due to this error is (section II.2):

$$\epsilon \Delta \Phi(\zeta, \alpha) = (B + 2C \zeta + 3D \zeta^2) (R_e^{-1} + \rho^{-1} \cos \zeta) \cos \Delta \alpha_0 \ell \text{ K TEC} \quad (4.6)$$

where:

$$B = 4 / (75 \pi) \approx 0.017$$

$$C = 16 / (10 \pi^2) \approx 0.16$$

$$D = 16 / \pi^3 \approx 0.52$$

$$K = 40.28 / f^2$$

f : carrier frequency (Hz)

TEC : total electron content (electrons/m²), the integrated electron density in the zenith direction

$$\Delta \alpha_0 = \alpha - \alpha_0$$

α_0 : baseline azimuth

ℓ : baseline length

R_e : Earth's radius (6,378 km)

ρ : station-satellite distance (~ 22,000 km)

Summary of assumptions and approximations:

- 1) The electrons are concentrated in a spherical layer of infinitesimal thickness at a height of 350 km;
- 2) TEC is uniform in the layer;
- 3) Equation (II.15a) is an approximation of the ionospheric mapping function;
- 4) Equation (II.19), (II.21b) and (II.24c) hold for short baseline length ($\ell < 100$ km);

- 5) Equation (II.23c) holds for small baseline height difference ($\zeta_0 \approx 90^\circ$);
- 6) Equation (II.28b) is not recommended for zenith angles greater than 80° ;
- 7) TEC is assumed constant during the session.

Normal equation vector U: ($A^T P_\ell \varepsilon \Delta \Phi$)

$$\begin{aligned}
 [e_1 \varepsilon \Delta \Phi] &= -\beta P_\ell \{ (B I_{200} + 2C I_{201} + 3D I_{202}) R_e^{-1} + (B I_{210} + 2C I_{211} + 3D I_{212}) \rho^{-1} \} \\
 &\quad (J_{02} \cos \alpha_0 + J_{11} \sin \alpha_0) \ell \text{ K TEC} \\
 [e_2 \varepsilon \Delta \Phi] &= -\beta P_\ell \{ (B I_{200} + 2C I_{201} + 3D I_{202}) R_e^{-1} + (B I_{210} + 2C I_{211} + 3D I_{212}) \rho^{-1} \} \\
 &\quad (J_{11} \cos \alpha_0 + J_{20} \sin \alpha_0) \ell \text{ K TEC} \\
 [e_3 \varepsilon \Delta \Phi] &= -\beta P_\ell \{ (B I_{110} + 2C I_{111} + 3D I_{112}) R_e^{-1} + (B I_{120} + 2C I_{121} + 3D I_{122}) \rho^{-1} \} \\
 &\quad (J_{01} \cos \alpha_0 + J_{10} \sin \alpha_0) \ell \text{ K TEC} \\
 [e_4 \varepsilon \Delta \Phi] &= \beta P_\ell \{ (B I_{100} + 2C I_{101} + 3D I_{102}) R_e^{-1} + (B I_{110} + 2C I_{111} + 3D I_{112}) \rho^{-1} \} \\
 &\quad (J_{01} \cos \alpha_0 + J_{10} \sin \alpha_0) \ell \text{ K TEC}
 \end{aligned} \tag{4.7a}$$

The term $[e_5 \varepsilon \Delta \Phi]$ has not been evaluated because the estimation of a relative (tropospheric zenith delay) parameter in the study of an absolute (ionospheric) bias is not relevant from a theoretical point of view.

Functional dependence of the $[e_i \varepsilon \Delta \Phi]$ terms:

- 1) All terms are proportional to baseline length;
- 2) All terms are proportional to TEC value;
- 3) All terms are inversely proportional to the square of the carrier frequency;
- 4) The terms R_e^{-1} take into account the Earth's curvature (non parallelism of the local verticals);
- 5) The terms ρ^{-1} take into account the parallactic angles at the satellite;
- 6) The terms $[e_1 \varepsilon \Delta \Phi]$ and $[e_2 \varepsilon \Delta \Phi]$ have the same dependence on ζ (terms in I_{ijk});

7) The terms $[e_3 \varepsilon \Delta \Phi]$ and $[e_4 \varepsilon \Delta \Phi]$ have the same dependence on α (terms in J_{ij}).

Particular cases:

i) $\alpha^{\text{to}} = 360^\circ - \alpha_{\text{from}}$, ($J_{10} = J_{11} = 0$)

$$\begin{aligned}
 [e_1 \varepsilon \Delta \Phi] &= -\beta P_\ell \{ (B I_{200} + 2C I_{201} + 3D I_{202}) R_e^{-1} + (B I_{210} + 2C I_{211} + 3D I_{212}) \rho^{-1} \} \\
 &\quad J_{02} \cos \alpha_0 \ell \text{ K TEC} \\
 [e_2 \varepsilon \Delta \Phi] &= -\beta P_\ell \{ (B I_{200} + 2C I_{201} + 3D I_{202}) R_e^{-1} + (B I_{210} + 2C I_{211} + 3D I_{212}) \rho^{-1} \} \\
 &\quad J_{20} \sin \alpha_0 \ell \text{ K TEC} \\
 [e_3 \varepsilon \Delta \Phi] &= -\beta P_\ell \{ (B I_{110} + 2C I_{111} + 3D I_{112}) R_e^{-1} + (B I_{120} + 2C I_{121} + 3D I_{122}) \rho^{-1} \} \\
 &\quad J_{01} \cos \alpha_0 \ell \text{ K TEC} \\
 [e_4 \varepsilon \Delta \Phi] &= \beta P_\ell \{ (B I_{100} + 2C I_{101} + 3D I_{102}) R_e^{-1} + (B I_{110} + 2C I_{111} + 3D I_{112}) \rho^{-1} \} \\
 &\quad J_{01} \cos \alpha_0 \ell \text{ K TEC}
 \end{aligned} \tag{4.7b}$$

ii) $\alpha_{\text{from}} = 0^\circ$ and $\alpha^{\text{to}} = 360^\circ$, ($J_{01} = J_{10} = J_{11} = 0$ and $J_{02} = J_{20} = \pi$)

$$\begin{aligned}
 [e_1 \varepsilon \Delta \Phi] &= -\beta P_\ell \{ (B I_{200} + 2C I_{201} + 3D I_{202}) R_e^{-1} + (B I_{210} + 2C I_{211} + 3D I_{212}) \rho^{-1} \} \\
 &\quad \pi \cos \alpha_0 \ell \text{ K TEC} \\
 [e_2 \varepsilon \Delta \Phi] &= -\beta P_\ell \{ (B I_{200} + 2C I_{201} + 3D I_{202}) R_e^{-1} + (B I_{210} + 2C I_{211} + 3D I_{212}) \rho^{-1} \} \\
 &\quad \pi \sin \alpha_0 \ell \text{ K TEC} \\
 [e_3 \varepsilon \Delta \Phi] &= 0 \\
 [e_4 \varepsilon \Delta \Phi] &= 0
 \end{aligned} \tag{4.7c}$$

Interaction with matrix N^{-1} :

1) For an all-azimuth satellite distribution, only the horizontal coordinates are affected;

2) The proportionality to ℓ , the dependence on α_0 ($\cos \alpha_0$ and $\sin \alpha_0$ associated with

$[e_1 \varepsilon \Delta \Phi]$ and $[e_2 \varepsilon \Delta \Phi]$, respectively), and the equality of terms J_{02} and J_{20} (for an all-azimuth satellite configuration), indicates the presence of a horizontal scale effect;

- 3) The effect in the horizontal coordinates is not sensitive to the azimuth sector of the satellite distribution (the terms J_{02} and J_{20} vanish when multiplied by J_{02}^{-1} and J_{20}^{-1} , respectively);
- 4) A non-uniform azimuth satellite distribution creates an additive effect in the horizontal coordinate aligned with the horizontal symmetry axis of the satellite distribution (directional scale: $\cos\alpha_0$ dependent). This directional scale effect is both sensitive to azimuth and zenith sectors of the satellite distribution;
- 5) A non-uniform azimuth satellite distribution creates an effect (rotation: $\cos\alpha_0$ dependent) in the station height. These rotation effects are sensitive to both azimuth and zenith sectors of the satellite distribution.

4.5 Offset in the horizontal coordinates of the fixed station

The bias introduced in the single difference observation due to this error is (section II.3):

$$\varepsilon\Delta\Phi(\zeta, \alpha) = - (\sin\Delta\alpha_0 \sin\Delta\alpha_1 + \cos^2\zeta \cos\Delta\alpha_0 \cos\Delta\alpha_1) \ell \Delta O/\rho \quad (4.8)$$

where:

$$\Delta\alpha_0 = \alpha - \alpha_0$$

α_0 : baseline azimuth

ℓ : baseline length

$$\Delta\alpha_1 = \alpha - \alpha_1$$

α_1 : azimuth of the offset in the horizontal coordinates of the fixed station

ΔO : magnitude of the offset in the horizontal coordinates of the fixed station

ρ : station-satellite distance ($\sim 22,000$ km)

Summary of assumptions and approximations:

- 1) Baseline height component is small ($\zeta_0 = 90^\circ$) compared to the baseline length (eqn. (II.32c));
- 2) Baseline length is short ($\ell < 100$ km) compared to the station-satellite distance (eqn. (II.36a)).

Normal equation vector U: ($A^T P_\ell \varepsilon \Delta \Phi$)

$$[e_1 \varepsilon \Delta \Phi] = \beta P_\ell \{ I_{200} (J_{21} \cos \alpha_0 \cos \alpha_1 - J_{12} \sin(\alpha_0 + \alpha_1) + J_{03} \sin \alpha_0 \sin \alpha_1) \\ + I_{220} (J_{03} \cos \alpha_0 \cos \alpha_1 + J_{12} \sin(\alpha_0 + \alpha_1) + J_{21} \sin \alpha_0 \sin \alpha_1) \} \ell \Delta O / \rho$$

$$[e_2 \varepsilon \Delta \Phi] = \beta P_\ell \{ I_{200} (J_{30} \cos \alpha_0 \cos \alpha_1 - J_{21} \sin(\alpha_0 + \alpha_1) + J_{12} \sin \alpha_0 \sin \alpha_1) \\ + I_{220} (J_{12} \cos \alpha_0 \cos \alpha_1 + J_{21} \sin(\alpha_0 + \alpha_1) + J_{30} \sin \alpha_0 \sin \alpha_1) \} \ell \Delta O / \rho$$

$$[e_3 \varepsilon \Delta \Phi] = \beta P_\ell \{ I_{110} (J_{20} \cos \alpha_0 \cos \alpha_1 - J_{11} \sin(\alpha_0 + \alpha_1) + J_{02} \sin \alpha_0 \sin \alpha_1) \\ + I_{130} (J_{02} \cos \alpha_0 \cos \alpha_1 + J_{11} \sin(\alpha_0 + \alpha_1) + J_{20} \sin \alpha_0 \sin \alpha_1) \} \ell \Delta O / \rho$$

$$[e_4 \varepsilon \Delta \Phi] = -\beta P_\ell \{ I_{100} (J_{20} \cos \alpha_0 \cos \alpha_1 - J_{11} \sin(\alpha_0 + \alpha_1) + J_{02} \sin \alpha_0 \sin \alpha_1) \\ + I_{120} (J_{02} \cos \alpha_0 \cos \alpha_1 + J_{11} \sin(\alpha_0 + \alpha_1) + J_{20} \sin \alpha_0 \sin \alpha_1) \} \ell \Delta O / \rho$$

and optionally,

$$[e_5 \varepsilon \Delta \Phi] = -\beta P_\ell \{ (I_{1-10} - b I_{3-30} + 1.5b^2 I_{5-50}) \\ (J_{20} \cos \alpha_0 \cos \alpha_1 - J_{11} \sin(\alpha_0 + \alpha_1) + J_{02} \sin \alpha_0 \sin \alpha_1) \\ + (I_{110} - b I_{3-10} + 1.5b^2 I_{5-30}) \\ (J_{02} \cos \alpha_0 \cos \alpha_1 + J_{11} \sin(\alpha_0 + \alpha_1) + J_{20} \sin \alpha_0 \sin \alpha_1) \} \ell \Delta O / \rho$$

(4.9a)

Functional dependence of the $[e_i \varepsilon \Delta \Phi]$ terms:

- 1) All terms are proportional to baseline length (ℓ);
- 2) All terms are proportional to horizontal offset of the fixed station (ΔO);
- 3) All terms are inversely proportional to the station-satellite distance (ρ);
- 4) The $[e_1 \varepsilon \Delta \Phi]$ and $[e_2 \varepsilon \Delta \Phi]$ terms have the same dependence on ζ (terms in I_{ijk});
- 5) The $[e_3 \varepsilon \Delta \Phi]$, $[e_4 \varepsilon \Delta \Phi]$ and $[e_5 \varepsilon \Delta \Phi]$ terms have the same dependence on α (terms in J_{ij}).

Particular cases:

i) $\alpha^{to} = 360^\circ - \alpha_{from}$, ($J_{11} = J_{12} = J_{30} = 0$)

$$\begin{aligned}
 [e_1 \varepsilon \Delta \Phi] &= \beta P_\ell \{ I_{200} (J_{21} \cos \alpha_0 \cos \alpha_1 + J_{03} \sin \alpha_0 \sin \alpha_1) \\
 &\quad + I_{220} (J_{03} \cos \alpha_0 \cos \alpha_1 + J_{21} \sin \alpha_0 \sin \alpha_1) \} \ell \Delta O / \rho \\
 [e_2 \varepsilon \Delta \Phi] &= \beta P_\ell \{ (I_{220} - I_{200}) J_{21} \sin(\alpha_0 + \alpha_1) \} \ell \Delta O / \rho \\
 [e_3 \varepsilon \Delta \Phi] &= \beta P_\ell \{ I_{110} (J_{20} \cos \alpha_0 \cos \alpha_1 + J_{02} \sin \alpha_0 \sin \alpha_1) \\
 &\quad + I_{130} (J_{02} \cos \alpha_0 \cos \alpha_1 + J_{20} \sin \alpha_0 \sin \alpha_1) \} \ell \Delta O / \rho \\
 [e_4 \varepsilon \Delta \Phi] &= -\beta P_\ell \{ I_{100} (J_{20} \cos \alpha_0 \cos \alpha_1 + J_{02} \sin \alpha_0 \sin \alpha_1) \\
 &\quad + I_{120} (J_{02} \cos \alpha_0 \cos \alpha_1 + J_{20} \sin \alpha_0 \sin \alpha_1) \} \ell \Delta O / \rho
 \end{aligned} \tag{4.9b}$$

and optionally,

$$\begin{aligned}
 [e_5 \varepsilon \Delta \Phi] &= -\beta P_\ell \{ (I_{1-10} - b I_{3-30} + 1.5b^2 I_{5-50}) (J_{20} \cos \alpha_0 \cos \alpha_1 + J_{02} \sin \alpha_0 \sin \alpha_1) \\
 &\quad + (I_{110} - b I_{3-10} + 1.5b^2 I_{5-30}) (J_{02} \cos \alpha_0 \cos \alpha_1 + J_{20} \sin \alpha_0 \sin \alpha_1) \} \ell \Delta O / \rho
 \end{aligned}$$

ii) $\alpha_{from} = 0^\circ$ and $\alpha^{to} = 360^\circ$, ($J_{03} = J_{11} = J_{12} = J_{21} = J_{30} = 0$ and $J_{02} = J_{20} = \pi$)

$$\begin{aligned}
 [e_1 \varepsilon \Delta \Phi] &= 0 \\
 [e_2 \varepsilon \Delta \Phi] &= 0 \\
 [e_3 \varepsilon \Delta \Phi] &= \beta P_\ell \{ I_{110} (\pi \cos \alpha_0 \cos \alpha_1 + \pi \sin \alpha_0 \sin \alpha_1) \\
 &\quad + I_{130} (\pi \cos \alpha_0 \cos \alpha_1 + \pi \sin \alpha_0 \sin \alpha_1) \} \ell \Delta O / \rho \\
 [e_4 \varepsilon \Delta \Phi] &= -\beta P_\ell \{ I_{100} (\pi \cos \alpha_0 \cos \alpha_1 + \pi \sin \alpha_0 \sin \alpha_1) \\
 &\quad + I_{120} (\pi \cos \alpha_0 \cos \alpha_1 + \pi \sin \alpha_0 \sin \alpha_1) \} \ell \Delta O / \rho
 \end{aligned} \tag{4.9c}$$

and optionally,

$$\begin{aligned}
 [e_5 \varepsilon \Delta \Phi] &= -\beta P_\ell \{ (I_{1-10} - b I_{3-30} + 1.5b^2 I_{5-50}) (\pi \cos \alpha_0 \cos \alpha_1 + \pi \sin \alpha_0 \sin \alpha_1) \\
 &\quad + (I_{110} - b I_{3-10} + 1.5b^2 I_{5-30}) (\pi \cos \alpha_0 \cos \alpha_1 + \pi \sin \alpha_0 \sin \alpha_1) \} \ell \Delta O / \rho
 \end{aligned}$$

The only conclusion easily drawn from the above equations is that for an all-azimuth satellite distribution, the horizontal coordinates are unaffected.

The previous equations were written for any horizontal offset of a fixed station (ΔO). To simplify these equations and make generalization easier, we will split the horizontal offset into a latitude offset ($\Delta \phi$) and a longitude offset ($\Delta \lambda$).

4.5.1 Offset in the latitude of the fixed station

This is a special case of the offset in the horizontal coordinates of the fixed station where:

$$\alpha_1 = 0^\circ, \quad \Delta\alpha_1 = \alpha, \quad \sin\alpha_1 = 0, \quad \cos\alpha_1 = 1.$$

The bias introduced in the single difference observation due to this error is (section II.3.1):

$$\varepsilon\Delta\Phi(\zeta, \alpha) = - (\sin\Delta\alpha_0 \sin\alpha + \cos^2\zeta \cos\Delta\alpha_0 \cos\alpha) \ell \Delta\phi/\rho \quad (4.10)$$

Normal equation vector U: ($A^T P_\ell \varepsilon\Delta\Phi$)

$$\begin{aligned} [e_1 \varepsilon\Delta\Phi] &= \beta P_\ell \{ I_{200} (J_{21} \cos\alpha_0 - J_{12} \sin\alpha_0) + I_{220} (J_{03} \cos\alpha_0 + J_{12} \sin\alpha_0) \} \ell \Delta\phi/\rho \\ [e_2 \varepsilon\Delta\Phi] &= \beta P_\ell \{ I_{200} (J_{30} \cos\alpha_0 - J_{21} \sin\alpha_0) + I_{220} (J_{12} \cos\alpha_0 + J_{21} \sin\alpha_0) \} \ell \Delta\phi/\rho \\ [e_3 \varepsilon\Delta\Phi] &= \beta P_\ell \{ I_{110} (J_{20} \cos\alpha_0 - J_{11} \sin\alpha_0) + I_{130} (J_{02} \cos\alpha_0 + J_{11} \sin\alpha_0) \} \ell \Delta\phi/\rho \\ [e_4 \varepsilon\Delta\Phi] &= - \beta P_\ell \{ I_{100} (J_{20} \cos\alpha_0 - J_{11} \sin\alpha_0) + I_{120} (J_{02} \cos\alpha_0 + J_{11} \sin\alpha_0) \} \ell \Delta\phi/\rho \\ \text{and optionally,} \\ [e_5 \varepsilon\Delta\Phi] &= - \beta P_\ell \{ (I_{1-10} - b I_{3-30} + 1.5b^2 I_{5-50}) (J_{20} \cos\alpha_0 - J_{11} \sin\alpha_0) \\ &\quad + (I_{110} - b I_{3-10} + 1.5b^2 I_{5-30}) (J_{02} \cos\alpha_0 + J_{11} \sin\alpha_0) \} \ell \Delta\phi/\rho \end{aligned} \quad (4.11a)$$

Particular cases:

i) $\alpha^{to} = 360^\circ - \alpha_{from}$, ($J_{11} = J_{12} = J_{30} = 0$)

$$\begin{aligned} [e_1 \varepsilon\Delta\Phi] &= \beta P_\ell \{ I_{200} J_{21} \cos\alpha_0 + I_{220} J_{03} \cos\alpha_0 \} \ell \Delta\phi/\rho \\ [e_2 \varepsilon\Delta\Phi] &= \beta P_\ell \{ (I_{220} - I_{200}) J_{21} \sin\alpha_0 \} \ell \Delta\phi/\rho \\ [e_3 \varepsilon\Delta\Phi] &= \beta P_\ell \{ I_{110} J_{20} \cos\alpha_0 + I_{130} J_{02} \cos\alpha_0 \} \ell \Delta\phi/\rho \\ [e_4 \varepsilon\Delta\Phi] &= - \beta P_\ell \{ I_{100} J_{20} \cos\alpha_0 + I_{120} J_{02} \cos\alpha_0 \} \ell \Delta\phi/\rho \\ \text{and optionally,} \\ [e_5 \varepsilon\Delta\Phi] &= - \beta P_\ell \{ (I_{1-10} - b I_{3-30} + 1.5b^2 I_{5-50}) J_{20} \cos\alpha_0 \\ &\quad + (I_{110} - b I_{3-10} + 1.5b^2 I_{5-30}) J_{02} \cos\alpha_0 \} \ell \Delta\phi/\rho \end{aligned} \quad (4.11b)$$

ii) $\alpha_{\text{from}} = 0^\circ$ and $\alpha^{\text{to}} = 360^\circ$, ($J_{03} = J_{11} = J_{12} = J_{21} = J_{30} = 0$ and $J_{02} = J_{20} = \pi$)

$$\begin{aligned}
[e_1 \varepsilon\Delta\Phi] &= 0 \\
[e_2 \varepsilon\Delta\Phi] &= 0 \\
[e_3 \varepsilon\Delta\Phi] &= \beta P_\ell \{I_{110} \pi \cos\alpha_0 + I_{130} \pi \cos\alpha_0\} \ell \Delta\phi/\rho \\
[e_4 \varepsilon\Delta\Phi] &= -\beta P_\ell \{I_{100} \pi \cos\alpha_0 + I_{120} \pi \cos\alpha_0\} \ell \Delta\phi/\rho \\
\text{and optionally,} \\
[e_5 \varepsilon\Delta\Phi] &= -\beta P_\ell \{(I_{1-10} - b I_{3-30} + 1.5b^2 I_{5-50}) \pi \cos\alpha_0 \\
&\quad + (I_{110} - b I_{3-10} + 1.5b^2 I_{5-30}) \pi \cos\alpha_0\} \ell \Delta\phi/\rho
\end{aligned} \tag{4.11c}$$

The interaction with matrix N^{-1} for the vector U of the latitude offset of the fixed station is presented in the next sub-section with the analysis of the longitude offset.

4.5.2 Offset in the longitude of the fixed station

This is a special case of the offset in the horizontal coordinates of the fixed station where:

$$\begin{aligned}
\alpha_1 &= 90^\circ, & \Delta\alpha_1 &= \alpha - 90^\circ, & \sin\Delta\alpha_1 &= -\cos\alpha, & \cos\Delta\alpha_1 &= \sin\alpha, \\
\sin\alpha_1 &= 1, & \cos\alpha_1 &= 0, & \sin(\alpha_0 + \alpha_1) &= \cos\alpha_0.
\end{aligned}$$

The bias introduced in the single difference observation due to this error is (section II.3.2):

$$\varepsilon\Delta\Phi(\zeta, \alpha) = (\sin\Delta\alpha_0 \cos\alpha - \cos^2\zeta \cos\Delta\alpha_0 \sin\alpha) \ell \Delta\lambda/\rho \tag{4.12}$$

Normal equation vector U: ($A^T P_\ell \varepsilon\Delta\Phi$)

$$\begin{aligned}
[e_1 \varepsilon\Delta\Phi] &= \beta P_\ell \{I_{200} (-J_{12} \cos\alpha_0 + J_{03} \sin\alpha_0) + I_{220} (J_{12} \cos\alpha_0 + J_{21} \sin\alpha_0)\} \ell \Delta\lambda/\rho \\
[e_2 \varepsilon\Delta\Phi] &= \beta P_\ell \{I_{200} (-J_{21} \cos\alpha_0 + J_{12} \sin\alpha_0) + I_{220} (J_{21} \cos\alpha_0 + J_{30} \sin\alpha_0)\} \ell \Delta\lambda/\rho \\
[e_3 \varepsilon\Delta\Phi] &= \beta P_\ell \{I_{110} (-J_{11} \cos\alpha_0 + J_{02} \sin\alpha_0) + I_{130} (J_{11} \cos\alpha_0 + J_{20} \sin\alpha_0)\} \ell \Delta\lambda/\rho \\
[e_4 \varepsilon\Delta\Phi] &= -\beta P_\ell \{I_{100} (-J_{11} \cos\alpha_0 + J_{02} \sin\alpha_0) + I_{120} (J_{11} \cos\alpha_0 + J_{20} \sin\alpha_0)\} \ell \Delta\lambda/\rho \\
\text{and optionally,} \\
[e_5 \varepsilon\Delta\Phi] &= -\beta P_\ell \{(I_{1-10} - b I_{3-30} + 1.5b^2 I_{5-50}) (-J_{11} \cos\alpha_0 + J_{02} \sin\alpha_0) \\
&\quad + (I_{110} - b I_{3-10} + 1.5b^2 I_{5-30}) (J_{11} \cos\alpha_0 + J_{20} \sin\alpha_0)\} \ell \Delta\lambda/\rho
\end{aligned} \tag{4.13a}$$

Particular cases:

i) $\alpha^{to} = 360^\circ - \alpha_{from}$, ($J_{11} = J_{12} = J_{30} = 0$)

$$\begin{aligned}
 [e_1 \varepsilon \Delta \Phi] &= \beta P_\ell \{ I_{200} J_{03} \sin \alpha_0 + I_{220} J_{21} \sin \alpha_0 \} \ell \Delta \lambda / \rho \\
 [e_2 \varepsilon \Delta \Phi] &= \beta P_\ell \{ (I_{220} - I_{200}) J_{21} \cos \alpha_0 \} \ell \Delta \lambda / \rho \\
 [e_3 \varepsilon \Delta \Phi] &= \beta P_\ell \{ I_{110} J_{02} \sin \alpha_0 + I_{130} J_{20} \sin \alpha_0 \} \ell \Delta \lambda / \rho \\
 [e_4 \varepsilon \Delta \Phi] &= -\beta P_\ell \{ I_{100} J_{02} \sin \alpha_0 + I_{120} J_{20} \sin \alpha_0 \} \ell \Delta \lambda / \rho \\
 \text{and optionally,} \\
 [e_5 \varepsilon \Delta \Phi] &= -\beta P_\ell \{ (I_{1-10} - b I_{3-30} + 1.5b^2 I_{5-50}) J_{02} \sin \alpha_0 \\
 &\quad + (I_{110} - b I_{3-10} + 1.5b^2 I_{5-30}) J_{20} \sin \alpha_0 \} \ell \Delta \lambda / \rho
 \end{aligned} \tag{4.13b}$$

ii) $\alpha_{from} = 0^\circ$ and $\alpha^{to} = 360^\circ$, ($J_{03} = J_{11} = J_{12} = J_{21} = J_{30} = 0$ and $J_{02} = J_{20} = \pi$)

$$\begin{aligned}
 [e_1 \varepsilon \Delta \Phi] &= 0 \\
 [e_2 \varepsilon \Delta \Phi] &= 0 \\
 [e_3 \varepsilon \Delta \Phi] &= \beta P_\ell \{ I_{110} \pi \sin \alpha_0 + I_{130} \pi \sin \alpha_0 \} \ell \Delta \lambda / \rho \\
 [e_4 \varepsilon \Delta \Phi] &= -\beta P_\ell \{ I_{100} \pi \sin \alpha_0 + I_{120} \pi \sin \alpha_0 \} \ell \Delta \lambda / \rho \\
 \text{and optionally,} \\
 [e_5 \varepsilon \Delta \Phi] &= -\beta P_\ell \{ (I_{1-10} - b I_{3-30} + 1.5b^2 I_{5-50}) \pi \sin \alpha_0 \\
 &\quad + (I_{110} - b I_{3-10} + 1.5b^2 I_{5-30}) \pi \sin \alpha_0 \} \ell \Delta \lambda / \rho
 \end{aligned} \tag{4.13c}$$

Interaction with matrix N^{-1} (applicable for both horizontal coordinate offsets):

- 1) For an all-azimuth satellite distribution, the horizontal coordinates are unaffected;
- 2) The effect in station height is a rotation around a horizontal axis (due to the dependence on α_0 and ℓ);
- 3) The rotation is around a horizontal axis perpendicular to the horizontal offset direction ($\cos \alpha_0$ associated with $\Delta \phi$ and $\sin \alpha_0$ associated with $\Delta \lambda$);
- 4) Because J_{02} equals J_{20} for an all-azimuth satellite distribution, for this distribution, the magnitude of the rotation will be equal for latitude and longitude offsets;
- 5) This primary effect is sensitive to both the azimuth and the zenith sectors of the satellite distribution (none of the J_{ij} and I_{ijk} terms vanish when multiplied by N^{-1});

- 6) Among the systematic errors studied in this document, the horizontal offset of the fixed station is the only one for which the primary effect (or the bulk of the primary effect) is sensitive to the azimuth sector of the satellite distribution (the secondary effects of all the studied systematic errors are always sensible to both the azimuth and the zenith sectors of the satellite distribution);
- 7) Non-uniform azimuth satellite distribution causes also an effect in the horizontal coordinates. This secondary effect is sensitive to both the azimuth and the zenith sectors of the satellite distribution;
- 8) The inequality of the I_{ijk} and J_{ij} terms in $[e_1 \ \epsilon\Delta\Phi]$ and $[e_2 \ \epsilon\Delta\Phi]$ means that the effect in the horizontal coordinates cannot be explained by introducing a horizontal scale factor (other affine parameters like directional scales and shears have to be introduced);
- 9) The complementarity of $\cos\alpha_0$ and $\sin\alpha_0$ between the two offsets explains why we will have directional scale factors (K_i) for a latitude offset and horizontal shears (S_i) for a longitude offset;
- 10) Moreover, the fact that there is no correlation between the y-coordinate (the coordinate aligned perpendicular to the horizontal symmetry axis of the satellite sky distribution) and the other unknowns in the covariance matrix, we will have the value of K_y equal to S_y ;
- 11) Geometrical interpretation of the effects of this systematic error is misleading because of the correlation between the station height (the most affected coordinate) and the clock parameter.

4.6 Offset in the height of the fixed station

The bias introduced in the single difference observation due to this error is (section II.4):

$$\varepsilon\Delta\Phi(\zeta,\alpha) = \sin\zeta \cos\zeta \cos\Delta\alpha_0 \ell \Delta h/\rho \quad (4.14)$$

where:

$$\Delta\alpha_0 = \alpha - \alpha_0$$

α_0 : baseline azimuth

ℓ : baseline length

Δh : offset in the height of the fixed station

ρ : station-satellite distance ($\sim 22,000$ km)

Summary of assumptions and approximations:

- 1) Baseline height component is small ($\zeta_0 = 90^\circ$) compared to the baseline length (eqn. (II.38c));
- 2) Baseline length is short ($\ell < 100$ km) compared to the station-satellite distance (eqn. (II.42a)).

Normal equation vector U: ($A^T P_\ell \varepsilon\Delta\Phi$)

$$\begin{aligned} [e_1 \varepsilon\Delta\Phi] &= -\beta P_\ell I_{310} (J_{02} \cos\alpha_0 + J_{11} \sin\alpha_0) \ell \Delta h/\rho \\ [e_2 \varepsilon\Delta\Phi] &= -\beta P_\ell I_{310} (J_{11} \cos\alpha_0 + J_{20} \sin\alpha_0) \ell \Delta h/\rho \\ [e_3 \varepsilon\Delta\Phi] &= -\beta P_\ell I_{220} (J_{01} \cos\alpha_0 + J_{10} \sin\alpha_0) \ell \Delta h/\rho \\ [e_4 \varepsilon\Delta\Phi] &= \beta P_\ell I_{210} (J_{01} \cos\alpha_0 + J_{10} \sin\alpha_0) \ell \Delta h/\rho \\ \text{and optionally,} \\ [e_5 \varepsilon\Delta\Phi] &= \beta P_\ell (I_{200} - b I_{4-20} + 1.5b^2 I_{6-40}) (J_{01} \cos\alpha_0 + J_{10} \sin\alpha_0) \ell \Delta h/\rho \end{aligned} \quad (4.15a)$$

Functional dependence of the $[e_i \varepsilon\Delta\Phi]$ terms:

- 1) All terms are proportional to baseline length (ℓ);
- 2) All terms are proportional to the height offset of the fixed station (Δh);
- 3) All terms are inversely proportional to the station-satellite distance (ρ);

- 4) The $[e_1 \varepsilon \Delta \Phi]$ and $[e_2 \varepsilon \Delta \Phi]$ terms have the same dependence on ζ (terms in I_{ijk});
- 5) The $[e_3 \varepsilon \Delta \Phi]$, $[e_4 \varepsilon \Delta \Phi]$ and $[e_5 \varepsilon \Delta \Phi]$ terms have the same dependence on α (terms in J_{ij}).

Particular cases:

i) $\alpha^{to} = 360^\circ - \alpha_{from}$, ($J_{10} = J_{11} = 0$)

$$\begin{aligned}
[e_1 \varepsilon \Delta \Phi] &= -\beta P_\ell I_{310} J_{02} \cos \alpha_0 \ell \Delta h / \rho \\
[e_2 \varepsilon \Delta \Phi] &= -\beta P_\ell I_{310} J_{20} \sin \alpha_0 \ell \Delta h / \rho \\
[e_3 \varepsilon \Delta \Phi] &= -\beta P_\ell I_{220} J_{01} \cos \alpha_0 \ell \Delta h / \rho \\
[e_4 \varepsilon \Delta \Phi] &= \beta P_\ell I_{210} J_{01} \cos \alpha_0 \ell \Delta h / \rho \\
\text{and optionally,} \\
[e_5 \varepsilon \Delta \Phi] &= \beta P_\ell (I_{200} - b I_{4-20} + 1.5b^2 I_{6-40}) J_{01} \cos \alpha_0 \ell \Delta h / \rho
\end{aligned} \tag{4.15b}$$

ii) $\alpha_{from} = 0^\circ$ and $\alpha^{to} = 360^\circ$, ($J_{01} = J_{10} = J_{11} = 0$ and $J_{02} = J_{20} = \pi$)

$$\begin{aligned}
[e_1 \varepsilon \Delta \Phi] &= -\beta P_\ell I_{310} \pi \cos \alpha_0 \ell \Delta h / \rho \\
[e_2 \varepsilon \Delta \Phi] &= -\beta P_\ell I_{310} \pi \sin \alpha_0 \ell \Delta h / \rho \\
[e_3 \varepsilon \Delta \Phi] &= 0 \\
[e_4 \varepsilon \Delta \Phi] &= 0 \\
\text{and optionally,} \\
[e_5 \varepsilon \Delta \Phi] &= 0
\end{aligned} \tag{4.15c}$$

Interaction with matrix N^{-1} :

- 1) For an all-azimuth satellite distribution, only the horizontal coordinates are affected;
- 2) The proportionality to ℓ , the dependence on α_0 ($\cos \alpha_0$ and $\sin \alpha_0$ associated with $[e_1 \varepsilon \Delta \Phi]$ and $[e_2 \varepsilon \Delta \Phi]$, respectively), and the equality of terms J_{02} and J_{20} (for an all-azimuth satellite configuration), indicates the presence of a horizontal scale effect;
- 3) The effect in the horizontal coordinates is not sensitive to the azimuth sector of the satellite distribution (the terms J_{02} and J_{20} vanish when multiplied by J_{02}^{-1} and J_{20}^{-1} ,

respectively);

- 4) A non-uniform azimuth satellite distribution creates an additive effect in the horizontal coordinate aligned with the horizontal symmetry axis of the satellite distribution (directional scale: $\cos\alpha_0$ dependent). This directional scale effect is both sensitive to azimuth and zenith sectors of the satellite distribution;
- 5) A non-uniform azimuth satellite distribution creates an effect (rotation: $\cos\alpha_0$ dependent) in the station height. These rotation effects are sensitive to both azimuth and zenith sectors of the satellite distribution;
- 6) The affine transformation effects are the same as the effect of absolute ionospheric refraction. However, their values are different due to the different zenith angle functions. The reader is referred to section II.5 for the illustration of this last statement.

Chapter 5

Comparison of predictions with results from real GPS data

5.1 Introduction

The primary goal of this chapter is to assess the DIPOPSIM program prediction results. To reach this goal, we have compared the DIPOPSIM prediction results with those obtained from real GPS data processing (e.g., DIPOP and Bernese software). The latter approach required, for the study of systematic errors, processing the real GPS data twice without and with controlled additive errors as explained in section 3.4. Remember that the DIPOPSIM simulations are based on single difference observations and that the GPS data campaigns have been processed in the double difference mode. This fact will also allow us to demonstrate, once more, the equivalence of the observation differencing methods, as shown in section 3.3. If not otherwise mentioned, the processing of the real GPS data has been done with fixed carrier phase ambiguities.

The results presented in this chapter will allow us to associate numbers with the "qualitative" investigation of Chapter 4. However, keep in mind that the general trends presented in Chapter 4 have been obtained by analysing simple satellite sky distributions. The satellite sky distributions associated with the GPS campaigns, used in the present chapter, are much more complicated.

The behaviour of the covariance matrix is monitored by looking at: 1) the ratio of the semi-axes of the confidence ellipsoid; 2) the orientation of the semi-axes of the confidence ellipsoid; and 3) the correlation coefficient values. The semi-major, the semi-medium and the semi-minor axes are denoted by a , b and c , respectively. The notation for the correlation coefficient, e.g., x,z , means the correlation value between the station

coordinates x and z. The reason that we will compare only the ratio of the semi-axes of the confidence ellipsoid rather than the semi-axis magnitudes themselves is that the formal accuracy of the GPS solutions is overestimated and considered unrealistic. It is believed that this unrealistic formal accuracy is due to mismodelling and by ignoring the physical correlation among the observations in the present day GPS data processing.

The monitoring of the effects of systematic errors is done in two ways: 1) the station coordinate (baseline component) discrepancies; and 2) the affine (similarity) transformation parameters needed to recover the discrepancies introduced into the station coordinates. The similarity transformation parameters (3 translations, 3 rotations and 1 scale factor) only form a subset of the whole family of affine transformation parameters. The affine transformation mathematics and terminology are presented in Appendix VI. Many combinations of affine (similarity) transformation parameter solutions will be presented to stress the need of additional affine transformation parameters over the usual similarity transformation parameters. The selection of the best combination of affine parameters is based on the value of the root mean square (rms) of the transformation. In fact, the comparison of the "real" and the "predicted" values of affine transformation parameters is done for the affine (or similarity) parameter combination which gives the smallest rms value. If only (constant) systematic errors are present, the rms of the transformation should be zero. Also note that the formal accuracy of the affine transformation parameters are presented at the 1σ level.

The sense of baseline "A,B" component discrepancies is as follows:

$$(\vec{x}_B - \vec{x}_A)_{\text{biased}} - (\vec{x}_B - \vec{x}_A)_{\text{true}}$$

This means that the results should be interpreted as the effects on the station coordinates

caused by the studied bias.

The interpretation of the affine transformation parameters is in this sense: the transformations are to be performed on the "true" coordinates to get the station coordinates affected by the studied bias. In other words, these are the transformation parameters necessary to recover the systematic effects introduced into the station network by the studied bias.

The description of the "real" satellite sky distribution and the station network configuration of the four GPS campaigns, used to make the comparison, are presented in section V.2. Also presented in section V.2, are the definition of the integration boundaries, representing the "real" satellite sky distribution of the selected GPS campaigns, used in DIPOPSIM. Three different satellite configurations have been studied. The Juan de Fuca (Port Alberni) satellite configuration is one of the most uniform that the actual GPS satellite constellation can permit. On the other hand, the Ottawa and CERN campaigns had poor satellite sky distributions.

The data of the Juan de Fuca is used in all the tests. The Ottawa campaign is not used for the absolute ionospheric refraction test because we did not have the tool to apply ionospheric corrections to the ionospherically contaminated L1 observations. The CERN campaign is only used for the testing of the covariance matrix behaviour, the relative tropospheric refraction and the absolute ionospheric refraction, because it is the only information which was available to us through the intermediary of the University of Berne GPS group's publication. The Port Alberni campaign is used to illustrate the behaviour of the standard deviation of station height, where a relative tropospheric zenith delay parameter is optionally introduced in the least squares adjustment solution.

The results of the different tests are grouped into 6 sections. Section 5.2 is the comparison of the covariance matrix; section 5.3 is related to the relative tropospheric refraction error; section 5.4 deals with the absolute ionospheric error; section 5.5 contains the comparison of the effects of an offset in the latitude of the fixed station; section 5.6 deals with the effects of an offset in the longitude of the fixed station and section 5.7 contains the results of the analysis of an offset in the height of the fixed station. Finally, section 5.8 gives a summary of all the comparisons performed throughout this chapter.

5.2 Covariance matrix

5.2.1 Juan de Fuca 1986 campaign

Table 5.1 contains the information related to the monitoring of the behaviour of the covariance matrix of the Juan de Fuca campaign from DIPOP processing in double difference mode.

Table 5.1: Juan de Fuca covariance matrix behaviour from DIPOP processing in double difference mode. Semi-axis and standard deviation units are in mm.

Station	a	az.	el.	b	az.	el.	c	az.	el.	σ_x	σ_y	σ_z
DU	4	235°	85°	2	58°	5°	2	148°	0°	2	2	4
DI	3	234°	85°	2	59°	5°	1	149°	0°	1	2	3
DO	3	231°	85°	2	59°	5°	1	149°	-1°	1	1	3
SM	4	238°	85°	2	60°	5°	2	150°	0°	2	2	4
WO	5	240°	85°	3	60°	5°	2	150°	0°	2	2	5
IC	4	236°	85°	2	60°	5°	1	150°	0°	2	2	4
BE	3	231°	85°	2	59°	5°	1	149°	-1°	2	2	3
Ave:	3.7	235°	85°	2.1	59°	5°	1.4	149°	0°	1.7	1.9	3.7
Ave:	a/c			b/c			c/c			σ_x/c	σ_y/c	σ_z/c
	2.6			1.5			1			1.2	1.4	2.6

All correlation coefficients among station coordinates of each station smaller than 0.50

It is interesting to note the similarity of the confidence ellipsoid of all the stations of the network, as theoretically expected from section 4.2.

The covariance matrix behaviour from DIPOPSIM prediction in single difference mode is reported in Table 5.2.

Table 5.2: Juan de Fuca covariance matrix behaviour from DIPOPSIM prediction in single difference mode.

a/c	az.	el.	b/c	az.	el.	c/c	az.	el.	σ_x/c	σ_y/c	σ_z/c
2.5	195°	88°	1.3	61°	1°	1	151°	-1°	1.1	1.2	2.5
z,t: 0.97; x,y: 0.22; x,t: -0.07; x,z: -0.06; y,z: -0.01; y,t: -0.01											

The values of the ratio a/c and b/c have been recovered at 96% and 87%, respectively. The ratios σ_x/c , σ_y/c and σ_z/c have been recovered at 92%, 86% and 96%, respectively. The orientation of the confidence ellipsoid is within $\pm 5^\circ$, but the azimuth of the semi-major axis is different by 40° . But this is not that significant because at the large elevation angle of the semi-major axis ($\sim 85^\circ$) a large change in azimuth results in only a small directional change in the sky.

5.2.2 Ottawa 1983 campaign

Table 5.3 contains the information related to the monitoring of the behaviour of the covariance matrix of the Ottawa campaign from DIPOP processing in double difference mode.

Table 5.3: Ottawa covariance matrix behaviour from DIPOP processing in double difference mode. Semi-axis and standard deviation units are in mm.

Station	a	az.	el.	b	az.	el.	c	az.	el.	σ_x	σ_y	σ_z
MO	7	301°	84°	3	326°	-5°	2	56°	2°	3	2	7
6A	10	240°	87°	4	330°	0°	3	60°	3°	4	3	10
Ave:	8.5	271°	86°	3.5	328°	-3°	2.5	58°	3°	3.5	2.5	8.5
Ave:	a/c			b/c			c/c			σ_x/c	σ_y/c	σ_z/c
	3.4			1.4			1			1.4	1.0	3.4
Station MO correlation coefficients: x,y: -0.45, y,z: -0.21, x,z < 0.10												
Station 6A correlation coefficients: x,y: -0.39, y,z: -0.13, x,z < 0.10												

The covariance matrix behaviour from DIPOPSIM prediction in single difference mode is reported in Table 5.4.

Table 5.4: Ottawa covariance matrix behaviour from DIPOPSIM prediction in single difference mode.

a/c	az.	el.	b/c	az.	el.	c/c	az.	el.	σ_x/c	σ_y/c	σ_z/c
2.5	264°	76°	1.6	318°	-8°	1	47°	11°	1.4	1.4	2.5
z,t: 0.93; y,t: -0.56; x,y: -0.37; y,z: -0.33; x,z: -0.09; x,t: 0.04											

The values of the ratio a/c and b/c have been recovered at 74% and 114%, respectively. The ratio σ_x/c , σ_y/c and σ_z/c have been recovered at 100%, 140% and 74%, respectively. The orientation of the confidence ellipsoid is within $\pm 10^\circ$. The correlation coefficient x,y is well recovered and the y,z prediction value error is not larger than the difference between the values associated to the two stations.

5.2.3 CERN 1984 campaign

The following information has been extracted from Gervaise et al., [1985]. In their Table 3b: "RMS of ellipsoidal coordinates and coordinate differences", they mentioned that latitude is best estimated, followed by longitude and height. The average values of the estimated standard deviations of all the stations of the network adjustment are: ± 1.0 mm in latitude, ± 2.2 mm in longitude and ± 3.1 mm in height. The ratio σ_y/σ_x is equal to 2.2 and the ratio σ_z/σ_x is equal to 3.1.

Table 5.5 contains the results of the covariance matrix behaviour from DIPOPSIM prediction in single difference mode.

Table 5.5: CERN covariance matrix behaviour from DIPOPSIM prediction in single difference mode.

a/c	az.	el.	b/c	az.	el.	c/c	az.	el.	σ_x/c	σ_y/c	σ_z/c
3.8	87°	55°	1.6	81°	-34°	1	353°	2°	1.0	2.5	3.2
z,t: 0.92; y,t: 0.89; y,z: 0.67; x,y: 0.16; x,t: 0.14; x,z: 0.08											

The ratio σ_y/σ_x and σ_z/σ_x have been recovered at 114% and 103%, respectively. Unfortunately, no information was reported by the Bernese GPS group about the confidence ellipsoid.

From the above examples, we can note that the correlation between the station height and the clock parameter (DIPOPSIM results) is very high and that the semi-major axis is always pointing towards the satellite sky coverage. However, other tests (not reported here) have shown that it is the semi-minor axis which points towards the satellite sky coverage, if a clock parameter is not introduced in the DIPOPSIM predictions based on single difference mode. This last point will be further discussed in section 5.8.

5.2.4 Port Alberni 1986 campaign

Table 5.6 presents the Port Alberni ratio of the station height standard deviation for solutions with and without a relative tropospheric zenith delay parameter. Solutions from real GPS data processed with DIPOP in double difference mode and DIPOPSIM predictions in single difference mode are compared.

Table 5.6: Port Alberni ratio of the station height standard deviation for solutions with and without a relative tropospheric zenith delay parameter.

ζ^{\max} :	70°	80°
DIPOP processing in double difference mode:	3.4	2.2
DIPOPSIM prediction in single difference mode:	3.9	2.5

The ratio of the height standard deviation for ζ^{\max} : 70° has been recovered at 115% and for ζ^{\max} : 80° the value has been recovered at 114%.

These high ratios are indicative of a high degree of correlation between the station height

and the relative tropospheric zenith delay parameter.

5.3 Relative tropospheric refraction

5.3.1 Juan de Fuca 1986 campaign

Table 5.7 contains the results of the effects on the station coordinates caused by a relative tropospheric zenith delay error for the Juan de Fuca campaign. Results from real data processed with DIPOP in double difference mode as well as prediction from DIPOPSIM based on single difference mode are presented.

Table 5.7: Juan de Fuca baseline component errors due to relative tropospheric zenith delay error of 10 cm. Top part is from DIPOP processing in double difference mode, last line is from DIPOPSIM prediction in single difference mode. In parentheses are the corresponding magnification factors.

Baseline	ℓ	Δh	α_0	dx (mm)	dy (mm)	dz (mm)
PG, DO*	19 km	204 m	156°	-5	-3	222
BE, DO*	29 km	22 m	128°	-3	-2	222
DI, DO*	12 km	194 m	310°	-4	-3	221
DI, DU*	28 km	-29 m	18°	-5	-6	217
DI, IC*	25 km	10 m	91°	-3	-2	221
SM, IC*	12 km	25 m	345°	-3	-2	222
SM, WO*	21 km	64 m	164°	-3	-2	223
Average:				-4 (-0.04)	-3 (-0.03)	221 (2.21)
DIPOPSIM:				0 (0.00)	1 (0.01)	239 (2.39)

*Station with underestimated wet tropospheric zenith delay correction.

The results clearly show the independence of the magnification factors on the baseline length and azimuth (translation parameters). The average height magnification factor is 2.21 and the maximum effect on the horizontal coordinates is -6 mm for a 10 cm error in the relative tropospheric zenith delay modelling. If the zenith error is 1 cm the effect on the horizontal coordinates will be below 1 mm, but still the height effect will be important and will be equal to 2.2 cm. Discrepancies for baseline DI,DU are explained by the fact that 10% fewer observations were available for the processing of this baseline.

The height magnification factor due to the tropospheric zenith delay modelling has been recovered at 108%. The height magnification factor is simply obtained by dividing the value of the translation along the z axis (Tz) by the relative tropospheric zenith delay error expressed in length units.

5.3.2 Ottawa 1983 campaign

Table 5.8 contains the results of the effects on the station coordinates caused by a relative tropospheric zenith delay error for the Ottawa campaign. Results from real data processed with DIPOP in double difference mode as well as prediction from DIPOPSIM based on single difference are presented.

Table 5.8: Ottawa baseline component errors due to relative tropospheric zenith delay error of 10 cm. Top part is from DIPOP processing in double difference mode, last line is from DIPOPSIM prediction in single difference mode. In parentheses are the corresponding magnification factors.

Baseline	ℓ	Δh	α_0	dx (mm)	dy (mm)	dz (mm)
PA, MO*	13 km	-65 m	335°	6	-8	221
PA, 6A*	22 km	-77 m	72°	9	-6	214
Average:				8 (0.08)	-7 (-0.07)	218 (2.18)
DIPOPSIM:				1 (0.01)	0 (0.00)	293 (2.93)

*Station with underestimated wet tropospheric zenith delay correction.

The height magnification factor is recovered at 134%. The other effects are not significant.

5.3.3 CERN 1984 campaign

Beutler and Gurtner [1987a] have reported an analysis made with two baselines (3.5 km and 8.1 km) of the CERN 1984 campaign, processed with the Bernese software (double difference observations mode). They have found that:

"The dominating error actually was in height -- the height amplification factor being 3.2 for both baselines. The errors in longitude were of the order of one tenth of the errors in height (showing that the distribution with respect to the azimuth was not ideal), the errors in latitude were negligible."

Table 5.9 presents those results along with the DIPOPSIM predictions.

Table 5.9: CERN magnification factor on station coordinates due to relative tropospheric zenith delay error.

	Mag x	Mag y	Mag z
Bernese processing in double difference mode:	0.0	0.3	3.2
DIPOPSIM prediction in single difference mode:	0.01	0.46	3.99

The height magnification factor has been recovered at 125%, the magnification effect in longitude (9 times smaller) has been recovered at 153%, and no significant effect in latitude has been predicted either.

Additional DIPOPSIM tests, with the CERN satellite configuration, have shown that the non-introduction of a clock parameter in the simulated single difference observations mode leads to erroneous interpretation, e.g., the height magnification changes of sign and the y-coordinate becomes the most affected coordinate!

The sign change in the height magnification factor, if a clock parameter is not included in the solution, has been noticed by Geiger [1987; 1988]:

"(...) Note that the height will increase with errors greater than 0 (distance measurement too long)! This is due to the fourth unknown (clock parameter), which absorbs in a certain sense a part of the error effects. If we consider only three unknowns the height will decrease if the measurements are too long. This corresponds better to the geometrical idea of positioning."

The above examples indicate that the predictions with single difference observables without taking into account a clock parameter in the solution or the geometrical interpretation of the effect of the relative tropospheric correction mismodelling lead to a wrong conclusion in the interpretation of the station coordinate effects, both in magnitude and sign!

5.4 Absolute ionospheric refraction

5.4.1 Juan de Fuca 1986 campaign

Based on the dual frequency data of the TI 4100 receivers, the estimation of the total electron content varied between 0.92×10^{17} el/m² and 1.23×10^{17} el/m² (rather low TEC values), during that day [Georgiadou and Kleusberg, 1988]. For program DIPOPSIM purposes, we assumed an average TEC value equal to 1×10^{17} el/m².

Table 5.10 contains the (real and predicted) results of the effects on the Juan de Fuca station coordinates caused by absolute ionospheric refraction.

Table 5.10: Juan de Fuca baseline component errors due to absolute ionospheric refraction (TEC $\approx 1 \times 10^{17}$ el/m²). Lines: 1) DIPOP processing in double difference mode; 2) DIPOPSIM prediction in single difference mode.

Baseline	ℓ	Δh	α_0	dx (mm)	dy (mm)	dz (mm)
PG, DO	19 km	204 m	156°	10	-5	-2
				11	-5	0
DU, DI	28 km	29 m	342°	-11	4	15
				-17	5	0
DI, DO	12 km	194 m	310°	-2	8	-7
				-5	5	0
DI, IC	25 km	10 m	91°	-1	-15	-17
				1	-15	0
DO, BE	29 km	-22 m	232°	8	14	-1
				11	13	0
SM, WO	21 km	64 m	164°	10	-2	-10
				12	-4	0
SM, IC	12 km	25 m	345°	-5	1	0
				-7	2	0

Table 5.11a presents the affine transformation parameters introduced by the absolute ionospheric refraction. Table 5.11b contains the predicted affine transformation parameters. The last line of these tables (and for the other similar tables of this chapter) is

the rms of the coordinate differences where affine transformations are not applied.

Table 5.11a: Affine transformation parameters introduced in the Juan de Fuca network by absolute ionospheric refraction ($TEC = 1 \times 10^{17} \text{ el/m}^2$), (from lines 1 of Table 5.10).

Parameters	rms (mm)	Tx (mm)	Ty (mm)	Tz (mm)	Rx (10^{-6} rad)	Ry (10^{-6} rad)	Rz (10^{-6} rad)	K (ppm)
3T, 3R, 1K	3	-2 ± 2	0 ± 2	8 ± 4	$-.22 \pm .06$	$-.30 \pm .10$	$.05 \pm .05$	$-.56 \pm .05$
3R, 1K	4				$-.22 \pm .07$	$-.10 \pm .06$	$.08 \pm .03$	$-.53 \pm .03$
1K	7							$-.53 \pm .06$
		Rx (10^{-6} rad)	Ry (10^{-6} rad)	Sx (ppm)	Sy (ppm)	K (ppm)		
2R, 2S, 1K	4	$-.22 \pm .07$	$-.10 \pm .06$	$-.10 \pm .06$	$.06 \pm .05$	$-.54 \pm .05$		
		Rx (10^{-6} rad)	Ry (10^{-6} rad)	Sx (ppm)	Sy (ppm)	Kx (ppm)	Ky (ppm)	
2R, 2S, 2K	4	$-.21 \pm .07$	$-.10 \pm .06$	$-.05 \pm .07$	$.01 \pm .06$	$-.48 \pm .06$	$-.63 \pm .07$	
0 (Coord. diff.)	17							

None of the affine transformations have been able to bring the rms of the transformation to zero millimetres, which is the goal if we only deal with (constant) systematic error. This shows that the observables (station coordinates) are also affected by random errors affecting both L1 and L3 observables. The L3 observable is the so-called ionospheric free linear combination, see below. It is worthwhile to note that even if the L3 solution is practically unaffected by the ionospheric refraction, the noise level of the L3 observations is larger than the noise level of the L1 observations. This is a consequence of the linear combination of L1 and L2 observations to form the ionospheric free linear combination (L3). A closer look at the residuals has shown them to be randomly distributed among the station coordinates; the larger residuals being associated with the height coordinate of stations DI and WO. Another explanation for this "non-zero" rms resides in the fact that the total electron content was not constant during the observing session.

If we take into account the 3σ accuracy associated with the estimated parameters (the accuracy results in Tables 5.11 are at the 1σ level), we realise that the Rx rotation as well as the differential between the Kx and Ky parameters are not significant. It appears from

this analysis that only the scale factor K is significant.

Table 5.11b: Prediction of affine transformation parameters introduced in the Juan de Fuca network by absolute ionospheric refraction (TEC: 1×10^{17} el/m²), (from lines 2 of Table 5.10).

Parameters	rms (mm)	Tx (mm)	Ty (mm)	Tz (mm)	Rx (10 ⁻⁶ rad)	Ry (10 ⁻⁶ rad)	Rz (10 ⁻⁶ rad)	K (ppm)
3T, 3R, 1K	0	1 ±0	-1 ±0	0 ±0	-01 ±.01	.01 ±.01	-02 ±.01	-59 ±.01
3R, 1K	0				-01 ±.01	.02 ±.01	-01 ±.00	-61 ±.00
1K	1							-61 ±.00
		Rx (10 ⁻⁶ rad)	Ry (10 ⁻⁶ rad)	Sx (ppm)	Sy (ppm)	K (ppm)		
2R, 2S, 1K	0	-01 ±.01	.02 ±.01	.03 ±.01	.00 ±.00	-60 ±.00		
		Rx (10 ⁻⁶ rad)	Ry (10 ⁻⁶ rad)	Sx (ppm)	Sy (ppm)	Kx (ppm)	Ky (ppm)	
2R, 2S, 2K	0	.00 ±.00	.02 ±.00	.02 ±.00	.02 ±.00	-61 ±.00	-58 ±.00	
0 (Coord. diff.)	18							

The prediction shows that indeed the rotation effect as well as the differential between the parameters Kx and Ky are very small. The prediction of the main effect K is recovered at 111%.

5.4.2 CERN 1984 campaign

In order to study the influence of the ionosphere, the Bernese GPS group have introduced the simple layer model to the single frequency Macrometer observations. Their model allows the TEC value to vary for daytime observations as a function of the hour angle of the Sun and the latitude of the observation piercing point at the ionosphere layer height. For nighttime observation, as in the CERN campaign, TEC is assumed constant. The height of the infinitesimal ionospheric layer used was 300 km. With the DIPOPSIM simulations, the height of the ionospheric layer is assumed equal to 350 km.

Table 5.12 contains the (real and predicted) results of the effects on the CERN station coordinates caused by absolute ionospheric refraction.

Table 5.12: CERN baseline component errors due to absolute ionospheric refraction (TEC: 3×10^{17} el/m²). Lines: 1) Bernese processing in double difference mode; 2) DIPOPSIM prediction in single difference mode.

Baseline	ℓ	Δh	α_0	dx (mm)	dy (mm)	dz (mm)
31,26	7.3 km	70 m	195°	15	2	-7
				14	4	-3
31,30	3.6 km	319 m	273°	0	4	-12
				0	5	-6
31,32	4.6 km	65 m	102°	2	-9	11
				2	-6	7
31,33	6.5 km	312 m	34°	-12	-4	8
				-11	-6	6
31,34	8.1 km	28 m	134°	12	-6	14
				12	-8	9
31,36	7.0 km	175 m	237°	8	6	-17
				8	9	-9

Table 5.13a presents the affine transformation parameters associated with the absolute ionospheric refraction. Table 5.13b contains the predicted affine transformation parameters. In these tables, the numbers between parentheses of the second last line are the values of the affine transformation parameters for a TEC of 1×10^{17} el/m².

Table 5.13a: Affine transformation parameters introduced in the CERN network by absolute ionospheric refraction (TEC: 3×10^{17} el/m²), (from lines 1 of Table 5.12).

Parameters	rms (mm)	Tx (mm)	Ty (mm)	Tz (mm)	Rx (10 ⁻⁶ rad)	Ry (10 ⁻⁶ rad)	Rz (10 ⁻⁶ rad)	K (ppm)
3T, 3R, 1K	2	1 ± 1	0 ± 1	-1 ± 1	2.70 ± .21	-.03 ± .22	.10 ± .15	-1.67 ± .15
3R, 1K	2				2.65 ± .20	-.15 ± .20	.09 ± .14	-1.71 ± .14
1R	7				2.67 ± .63			
1K	7							-1.71 ± .47
		Rx (10 ⁻⁶ rad)	Ry (10 ⁻⁶ rad)	Sx (ppm)	Sy (ppm)	K (ppm)		
2R, 2S, 1K	2	2.65 ± .21	-.15 ± .20	-.07 ± .21	.10 ± .20	-1.72 ± .15		
		Rx (10 ⁻⁶ rad)	Ry (10 ⁻⁶ rad)	Sx (ppm)	Sy (ppm)	Kx (ppm)	Ky (ppm)	
2R, 2S, 2K	2	2.66 ± .15	-.14 ± .15	-.01 ± .15	.04 ± .15	-2.11 ± .15	-1.28 ± .15	
(TEC: 1×10^{17}):		(.89)	(-.05)	(.00)	(.01)	(-.70)	(-.43)	
0 (Coord. diff.)	10							

The rms does not vanish for different affine parameter combinations. This cannot be explained by the noise of the ionosphere free solution because a deterministic ionospheric model has been used. The explanation may reside in the fact that each station of the network has been observed twice during two different nights and each 3 night window has been split in two observing sessions. This means that if different ionospheric conditions prevail during different observing sessions the difference will go into the affine transformation residuals which in turn increase the rms. Despite this situation, we can conclude that the Rx parameter as well as the differential between the parameters Kx and Ky are significant.

Table 5.13b: Prediction of affine transformation parameters introduced in the CERN network by absolute ionospheric refraction (TEC: 3×10^{17} el/m²), (from lines 2 of Table 5.12).

Parameters	rms (mm)	Tx (mm)	Ty (mm)	Tz (mm)	Rx (10 ⁻⁶ rad)	Ry (10 ⁻⁶ rad)	Rz (10 ⁻⁶ rad)	K (ppm)
3T, 3R, 1K	1	1 ± 1	1 ± 1	0 ± 1	1.54 ± .12	-.10 ± .12	.00 ± .08	-1.76 ± .08
3R, 1K	1				1.55 ± .12	-.05 ± .11	-.04 ± .08	-1.78 ± .08
1R	7				1.56 ± .63			
1K	4							-1.78 ± .27
		Rx (10 ⁻⁶ rad)	Ry (10 ⁻⁶ rad)	Sx (ppm)	Sy (ppm)	K (ppm)		
2R, 2S, 1K	1	1.55 ± .12	-.05 ± .11	-.04 ± .12	-.11 ± .11	-1.77 ± .08		
		Rx (10 ⁻⁶ rad)	Ry (10 ⁻⁶ rad)	Sx (ppm)	Sy (ppm)	Kx (ppm)	Ky (ppm)	
2R, 2S, 2K	0	1.56 ± .02	-.05 ± .02	.00 ± .02	-.15 ± .02	-2.04 ± .02	-1.48 ± .02	
(TEC: 1×10^{17}):		(.52)	(-.02)	(.00)	(-.05)	(-.68)	(-.49)	
0 (Coord. diff.)	8							

The predictions prove that the parameters Rx, Kx and Ky are significant. For the "2R, 2S, 2K" transformation the value of the uncertainties of ±0.02 ppm (or 10⁻⁶ rad) represents ±0.1 mm on a 5 km baseline. This is not assumed significant and it is attributed to round-off errors, because the input station coordinates are given at the 0.1 mm level. The prediction of the primary effects Rx and Kx are recovered at 59% and 97%, respectively. The parameter Ky (2 times smaller than Rx) is recovered at 116%. The other parameters are 10 times smaller than the primary effects and are considered negligible. Let us mention

that 3 ambiguities out of 36 had to be estimated in the real data processing and that the predictions are based on the assumption that the solution is free of ambiguity parameters.

5.5 Offset in the latitude of the fixed station

5.5.1 Juan de Fuca 1986 campaign

Table 5.14 contains the (real and predicted) results of the effects on the Juan de Fuca station coordinates caused by an offset in the latitude of the fixed station.

Table 5.14: Juan de Fuca baseline component errors due to a 1" (30.9 m) offset in the latitude of the fixed station. Lines: 1) DIPOP processing in double difference mode; 2) DIPOPSIM prediction in single difference mode.

Baseline	ℓ	Δh	α_0	dx (mm)	dy (mm)	dz (mm)
PG, DO	19 km	204 m	156°	-6	-3	-28
				-5	0	-23
DU, DI	28 km	29 m	342°	8	4	46
				7	-1	36
DI, DO	12 km	194 m	310°	4	4	13
				3	2	12
DI, IC	25 km	10 m	91°	-6	-13	-3
				-5	-7	-9
DO, BE	29 km	-22 m	232°	1	13	-26
				0	8	-15
SM, WO	21 km	64 m	164°	-6	-2	-31
				-5	1	-26
SM, IC	12 km	25 m	345°	3	1	18
				3	-1	15

Table 5.15a presents the affine transformation parameters introduced by an offset in the latitude of the fixed station. Table 5.15b contains the predicted affine transformation parameters. In these tables (and the other similar tables presented in the following sub-sections), the numbers between parentheses of the second last line are the values of the affine transformation parameters for a coordinate offset in the fixed station of 10 m.

Table 5.15a: Affine transformation parameters introduced in the Juan de Fuca network by a 1" (30.9 m) offset in the latitude of the fixed station, (from lines 1 of Table 5.14).

Parameters	rms (mm)	Tx (mm)	Ty (mm)	Tz (mm)	Rx (10 ⁻⁶ rad)	Ry (10 ⁻⁶ rad)	Rz (10 ⁻⁶ rad)	K (ppm)
3T, 3R, 1K	6	-17 ±5	6 ±5	1 ±7	-09 ±.11	-1.60 ±.19	.28 ±.09	-.26 ±.09
3R, 1K	8				-09 ±.15	-1.58 ±.13	.36 ±.06	.03 ±.06
1R	13					-1.64 ±.13		
		Rx (10 ⁻⁶ rad)	Ry (10 ⁻⁶ rad)	Sx (ppm)	Sy (ppm)	Kx (ppm)	Ky (ppm)	
2R, 2S, 2K (offset: 10 m)	1	-.09 ±.01 (-.03)	-1.59 ±.01 (-.51)	-.22 ±.01 (-.07)	-.07 ±.01 (-.02)	.25 ±.01 (.08)	-.52 ±.01 (-.17)	
0 (Coord. diff.)	38							

Theoretically the 6 parameter affine transformation should recover all the effects caused by the latitude offset in the fixed station. However, the rms of the transformation is ±1 mm. In fact, a look at the residuals has shown small residual outliers associated with station DU. The explanation is that for the determination of these station coordinates (baseline DI, DU) 10% fewer observations were available. This implies that the distribution of satellite observations on the sky for this station (baseline) was not exactly identical to that of the other stations.

Table 5.15b: Prediction of affine transformation parameters introduced in the Juan de Fuca network by a 1" (30.9 m) offset in the latitude of the fixed station, (from lines 2 of Table 5.14).

Parameters	rms (mm)	Tx (mm)	Ty (mm)	Tz (mm)	Rx (10 ⁻⁶ rad)	Ry (10 ⁻⁶ rad)	Rz (10 ⁻⁶ rad)	K (ppm)
3T, 3R, 1K	4	-10 ±3	6 ±3	0 ±5	-.31 ±.08	-1.21 ±.13	.18 ±.06	-.08 ±.06
3R, 1K	5				-.31 ±.10	-1.21 ±.09	.19 ±.04	.12 ±.04
1R	9					-1.42 ±.09		
		Rx (10 ⁻⁶ rad)	Ry (10 ⁻⁶ rad)	Sx (ppm)	Sy (ppm)	Kx (ppm)	Ky (ppm)	
2R, 2S, 2K (offset: 10 m)	0	-.31 ±.00 (-.10)	-1.21 ±.00 (-.39)	-.19 ±.00 (-.06)	-.12 ±.00 (-.04)	.20 ±.00 (.06)	-.27 ±.00 (-.09)	
0 (Coord. diff.)	32							

The more important parameter Ry has been recovered at 76% and the second largest parameter Ky (3 times smaller than Ry) has been recovered at 52%. The parameters Kx and Sx (6 times smaller than Ry) have been recovered at 80% and 86%, respectively. The

other parameters are 10 times smaller than R_y and are considered negligible.

5.5.2 Ottawa 1983 campaign

Table 5.16 contains the (real and predicted) results of the effects on the Ottawa station coordinates caused by an offset in the latitude of the fixed station.

Table 5.16: Ottawa baseline component errors due to a 1" (30.9 m) offset in the latitude of the fixed station. Lines: 1) DIPOP processing in double difference mode; 2) DIPOPSIM prediction in single difference mode.

Baseline	ℓ	Δh	α_0	dx (mm)	dy (mm)	dz (mm)
PA, MO	13 km	-65 m	335°	-2	3	10
				-4	1	5
PA, 6A	22 km	-77 m	72°	13	-12	17
				14	-10	13

Table 5.17a presents the affine transformation parameters introduced by an offset in the latitude of the fixed station. Table 5.17b contains the predicted affine transformation parameters. The coordinates of fixed station PA were used in the transformation adjustment solutions in order to have more observations than unknowns (the same procedure is used in sub-sections 5.6.2 and 5.7.2).

Table 5.17a: Affine transformation parameters introduced in the Ottawa network by a 1" (30.9 m) offset in the latitude of the fixed station, (from lines 1 of Table 5.16).

Parameters	rms (mm)	Tx (mm)	Ty (mm)	Tz (mm)	Rx (10^{-6} rad)	Ry (10^{-6} rad)	Rz (10^{-6} rad)	K (ppm)
3T, 3R, 1K	5	4 ±3	2 ±3	0 ±5	.46 ±.24	-1.12 ±.56	-.50 ±.22	-.48 ±.22
3R, 1K	4				.46 ±.21	-1.12 ±.33	-.53 ±.17	-.31 ±.17
1R	7					-1.31 ±.54		
		Rx (10^{-6} rad)	Ry (10^{-6} rad)	Sx (ppm)	Sy (ppm)	Kx (ppm)	Ky (ppm)	
2R, 2S, 2K (offset: 10 m)	0	.46 ±.00 (.15)	-1.11 ±.00 (-.36)	.61 ±.00 (.20)	-.06 ±.00 (-.02)	.10 ±.00 (.03)	-.56 ±.00 (-.18)	
0 (Coord. diff.)	9							

Table 5.17b: Prediction of affine transformation parameters introduced in the Ottawa network by a 1" (30.9 m) offset in the latitude of the fixed station, (from lines 2 of Table 5.16).

Parameters	rms (mm)	Tx (mm)	Ty (mm)	Tz (mm)	Rx (10^{-6} rad)	Ry (10^{-6} rad)	Rz (10^{-6} rad)	K (ppm)
3T, 3R, 1K	4	3 ±3	3 ±3	0 ±4	.41 ±.19	-.61 ±.46	-.59 ±.18	-.38 ±.18
3R, 1K	3				.41 ±.17	-.61 ±.26	-.58 ±.14	-.24 ±.14
1R	7					-.78 ±.51		
		Rx (10^{-6} rad)	Ry (10^{-6} rad)	Sx (ppm)	Sy (ppm)	Kx (ppm)	Ky (ppm)	
2R, 2S, 2K (offset: 10 m)	0	.41 ±.00 (.13)	-.61 ±.00 (-.20)	.70 ±.00 (.23)	-.13 ±.00 (-.04)	-.01 ±.00 (-.00)	-.42 ±.00 (-.14)	
0 (Coord. diff.)	7							

The more important parameter Ry has been recovered at 55%. The 2 seconds larger parameters Sx and Ky (2 times smaller than Ry) have been recovered at 115% and 75%, respectively. The third largest parameter Rx (about 3 times smaller than Ry) has been recovered at 89%. The magnitude of the other parameters are negligible being 10 times smaller than Ry.

5.6 Offset in the longitude of the fixed station

5.6.1 Juan de Fuca 1986 campaign

Table 5.18 contains the (real and predicted) results of the effects on the Juan de Fuca station coordinates caused by an offset in the latitude of the fixed station.

Table 5.19a presents the affine transformation parameters introduced by an offset in the longitude of the fixed station. Table 5.19b contains the predicted affine transformation parameters.

Table 5.18: Juan de Fuca baseline component errors due to a 1" (20.5 m) offset in the longitude of the fixed station. Lines: 1) DIPOP processing in double difference mode; 2) DIPOPSIM prediction in single difference mode.

Baseline	ℓ	Δh	α_0	dx (mm)	dy (mm)	dz (mm)
PG, DO	19 km	204 m	156°	1	6	7
				1	4	7
DU, DI	28 km	29 m	342°	-2	-10	-7
				-2	-6	-10
DI, DO	12 km	194 m	310°	0	-3	-7
				0	-2	-6
DI, IC	25 km	10 m	91°	-4	2	18
				-3	2	13
DO, BE	29 km	-22 m	232°	6	5	-15
				5	1	-8
SM, WO	21 km	64 m	164°	2	7	5
				2	4	7
SM, IC	12 km	25 m	345°	-1	-4	-3
				-1	-2	-4

Table 5.19a: Affine transformation parameters introduced in the Juan de Fuca network by a 1" (20.5 m) offset in the longitude of the fixed station, (from lines 1 of Table 5.18).

Parameters	rms (mm)	Tx (mm)	Ty (mm)	Tz (mm)	Rx (10^{-6} rad)	Ry (10^{-6} rad)	Rz (10^{-6} rad)	K (ppm)
3T, 3R, 1K	4	4 ±3	11 ±3	0 ±4	.70 ±.07	.06 ±.12	-.02 ±.06	.10 ±.06
3R, 1K	5				.70 ±.10	.07 ±.08	-.21 ±.04	.14 ±.04
1R	9				.76 ±.10			
		Rx (10^{-6} rad)	Ry (10^{-6} rad)	Sx (ppm)	Sy (ppm)	Kx (ppm)	Ky (ppm)	
2R, 2S, 2K (offset: 10 m)	0	.69 ±.00 (.34)	.07 ±.00 (.03)	-.14 ±.00 (-.08)	-.34 ±.00 (-.17)	-.14 ±.00 (-.07)	.07 ±.00 (.03)	
0 (Coord. diff.)	17							

Table 5.19b: Prediction of affine transformation parameters introduced in the Juan de Fuca network by a 1" (20.5 m) offset in the longitude of the fixed station, (from lines 2 of Table 5.18).

Parameters	rms (mm)	Tx (mm)	Ty (mm)	Tz (mm)	Rx (10^{-6} rad)	Ry (10^{-6} rad)	Rz (10^{-6} rad)	K (ppm)
3T, 3R, 1K	3	4 ±2	7 ±2	0 ±3	.50 ±.05	.21 ±.08	.01 ±.04	.08 ±.04
3R, 1K	4				.50 ±.07	.21 ±.06	-.12 ±.03	.09 ±.03
1R	6				.69 ±.07			
		Rx (10^{-6} rad)	Ry (10^{-6} rad)	Sx (ppm)	Sy (ppm)	Kx (ppm)	Ky (ppm)	
2R, 2S, 2K (offset: 10 m)	0	.50 ±.00 (.24)	.21 ±.00 (.10)	-.13 ±.00 (-.06)	-.18 ±.00 (-.09)	-.12 ±.00 (-.06)	.08 ±.00 (.04)	
0 (Coord. diff.)	14							

The more important parameter Rx has been recovered at 72% and the second largest parameter Sy (2 times smaller than Rx) has been recovered at 53%. The parameters Kx and Sx (5 times smaller than Rx) have been recovered at 86% and 93%, respectively. The two other parameters are 10 times smaller than Rx and are considered negligible.

5.6.2 Ottawa 1983 campaign

Table 5.20 contains the (real and predicted) results of the effects on the Ottawa station coordinates caused by an offset in the longitude of the fixed station.

Table 5.20: Ottawa baseline component errors due to a 1" (21.7 m) offset in the longitude of the fixed station. Lines: 1) DIPOP processing in double difference mode; 2) DIPOPSIM prediction in single difference mode.

Baseline	ℓ	Δh	α_0	dx (mm)	dy (mm)	dz (mm)
PA, MO	13 km	-65 m	335°	6	-4	-2
				6	-4	-1
PA, 6A	22 km	-77 m	72°	1	-1	25
				3	0	20

Table 5.21a presents the affine transformation parameters introduced by an offset in the longitude of the fixed station. Table 5.21b contains the predicted affine transformation parameters.

Table 5.21a: Affine transformation parameters introduced in the Ottawa network by a 1" (21.7 m) offset in the longitude of the fixed station, (from lines 1 of Table 5.20).

Parameters	rms (mm)	Tx (mm)	Ty (mm)	Tz (mm)	Rx (10^{-6} rad)	Ry (10^{-6} rad)	Rz (10^{-6} rad)	K (ppm)
3T, 3R, 1K	3	1 ±2	-3 ±2	0 ±3	1.11 ±.16	-.36 ±.38	.06 ±.15	.15 ±.15
3R, 1K	3				1.11 ±.14	-.36 ±.22	-.06 ±.11	.12 ±.11
1R	3				1.16 ±.14			
		Rx (10^{-6} rad)	Ry (10^{-6} rad)	Sx (ppm)	Sy (ppm)	Kx (ppm)	Ky (ppm)	
2R, 2S, 2K (offset: 10 m)	0	1.11 ±.00 (.51)	-.36 ±.00 (-.17)	-.12 ±.00 (-.06)	-.35 ±.00 (-.16)	.42 ±.00 (.19)	.08 ±.00 (.04)	
0 (Coord. diff.)	9							

Table 5.21b: Prediction of affine transformation parameters introduced in the Ottawa network by a 1" (21.7 m) offset in the longitude of the fixed station, (from lines 2 of Table 5.20).

Parameters	rms (mm)	Tx (mm)	Ty (mm)	Tz (mm)	Rx (10^{-6} rad)	Ry (10^{-6} rad)	Rz (10^{-6} rad)	K (ppm)
3T, 3R, 1K	3	2 ±2	-2 ±2	0 ±3	.88 ±.14	-.30 ±.32	-.03 ±.12	.17 ±.12
3R, 1K	2				.88 ±.12	-.30 ±.19	-.13 ±.10	.17 ±.10
1R	3				.93 ±.14			
		Rx (10^{-6} rad)	Ry (10^{-6} rad)	Sx (ppm)	Sy (ppm)	Kx (ppm)	Ky (ppm)	
2R, 2S, 2K (offset: 10 m)	0	.88 ±.00 (.41)	-.30 ±.00 (-.14)	.00 ±.00 (.00)	-.30 ±.00 (-.14)	.49 ±.00 (.23)	.10 ±.00 (.05)	
0 (Coord. diff.)	7							

The more important parameter Rx has been recovered at 79%. The 3 seconds larger parameters Kx and Ry and Sy (3 times smaller than Rx) have been recovered at 117%, 83% and 86%, respectively. The magnitude of the other parameters are negligible being 10 times smaller than Rx.

5.7 Offset in the height of the fixed station

5.7.1 Juan de Fuca 1986 campaign

Table 5.22 contains the (real and predicted) results of the effects on the Juan de Fuca station coordinates caused by an offset in the height of the fixed station.

Table 5.22: Juan de Fuca baseline component errors due to a 30 m offset in the height of the fixed station. Lines: 1) DIPOP processing in double difference mode; 2) DIPOPSIM prediction in single difference mode.

Baseline	ℓ	Δh	α_0	dx (mm)	dy (mm)	dz (mm)
PG, DO	19 km	204 m	156°	14	-7	1
				14	-6	0
DU, DI	28 km	29 m	342°	-24	9	0
				-22	7	1
DI, DO	12 km	194 m	310°	-7	8	-1
				-6	8	0
DI, IC	25 km	10 m	91°	2	-22	2
				0	-22	0
DO, BE	29 km	-22 m	232°	13	19	-1
				16	20	-1
SM, WO	21 km	64 m	164°	16	-6	1
				16	-5	-1
SM, IC	12 km	25 m	345°	-9	3	-1
				-9	2	0

Table 5.23a presents the affine transformation parameters introduced by an offset in the height of the fixed station. Table 5.23b contains the predicted affine transformation parameters.

Table 5.23a: Affine transformation parameters introduced in the Juan de Fuca network by a 30 m offset in the height of the fixed station, (from lines 1 of Table 5.22).

Parameters	rms (mm)	Tx (mm)	Ty (mm)	Tz (mm)	Rx (10^{-6} rad)	Ry (10^{-6} rad)	Rz (10^{-6} rad)	K (ppm)
3T, 3R, 1K	1	-1 ± 1	-2 ± 1	1 ± 1	.09 ± .02	.00 ± .03	-.02 ± .01	-.87 ± .01
3R, 1K	1				.09 ± .02	.02 ± .02	.03 ± .01	-.87 ± .01
1K	2							-.87 ± .02
		Rx (10^{-6} rad)	Ry (10^{-6} rad)	Sx (ppm)	Sy (ppm)	Kx (ppm)	Ky (ppm)	
2R, 2S, 2K (offset: 10 m)	1	.09 ± .01 (.03)	.02 ± .01 (.01)	.05 ± .01 (.02)	.05 ± .01 (.02)	-.81 ± .01 (-.27)	-.85 ± .01 (-.28)	
0 (Coord. diff.)	25							

Theoretically the 6 parameter affine transformation should recover all the effects caused by

the height offset in the fixed station. However, the rms of the transformation is ± 1 mm. The explanation for this fact has been given in section 5.5.1.

Table 5.23b: Prediction of affine transformation parameters introduced in the Juan de Fuca network by a 30 m offset in the height of the fixed station, (from lines 2 of Table 5.22).

Parameters	rms (mm)	Tx (mm)	Ty (mm)	Tz (mm)	Rx (10^{-6} rad)	Ry (10^{-6} rad)	Rz (10^{-6} rad)	K (ppm)
3T, 3R, 1K	1	-1 \pm 0	1 \pm 0	0 \pm 1	.00 \pm .01	-.03 \pm .02	.02 \pm .01	-.84 \pm .01
3R, 1K	1				.00 \pm .01	-.03 \pm .01	.02 \pm .01	-.81 \pm .01
1K	1							-.81 \pm .01
		Rx (10^{-6} rad)	Ry (10^{-6} rad)	Sx (ppm)	Sy (ppm)	Kx (ppm)	Ky (ppm)	
2R, 2S, 2K	0	.00 \pm .00	-.03 \pm .00	-.03 \pm .00	-.02 \pm .00	-.81 \pm .00	-.86 \pm .00	
(offset: 10 m)		(.00)	(-.01)	(-.01)	(-.01)	(-.27)	(-.29)	
0 (Coord. diff.)	24							

The prediction of the main effects Kx and Ky have recovered at 100% and 102%, respectively. If we solve only for one scale parameter K, this value is recovered at 93%. The other effects are 10 times less important than the main effects and are considered negligible.

5.7.2 Ottawa 1983 campaign

Table 5.24 contains the (real and predicted) results of the effects on the Ottawa station coordinates caused by an offset in the height of the fixed station.

Table 5.24: Ottawa baseline component errors due to a 30 m offset in the height of the fixed station.
Lines: 1) DIPOP processing in double difference mode; 2) DIPOPSIM prediction in single difference mode.

Baseline	ℓ	Δh	α_0	dx (mm)	dy (mm)	dz (mm)
PA, MO	13 km	-65 m	335°	-11 -9	5 4	-3 -3
PA, 6A	22 km	-77 m	72°	-5 -6	-19 -16	10 10

Table 5.25a presents the affine transformation parameters introduced by an offset in the

height of the fixed station. Table 5.25b contains the predicted affine transformation parameters.

Table 5.25a: Affine transformation parameters introduced in the Ottawa network by a 30 m offset in the height of the fixed station, (from lines 1 of Table 5.24).

Parameters	rms (mm)	Tx (mm)	Ty (mm)	Tz (mm)	Rx (10^{-6} rad)	Ry (10^{-6} rad)	Rz (10^{-6} rad)	K (ppm)
3T, 3R, 1K	0	0 ±0	0 ±0	0 ±0	.49 ±.02	.01 ±.04	-.06 ±.02	-.91 ±.02
3R, 1K	0				.49 ±.01	.01 ±.02	-.06 ±.01	-.90 ±.01
1K	4							-.90 ±.15
		Rx (10^{-6} rad)	Ry (10^{-6} rad)	Sx (ppm)	Sy (ppm)	Kx (ppm)	Ky (ppm)	
2R, 2S, 2K	0	.49 ±.00	.00 ±.00	.07 ±.00	-.02 ±.00	-.88 ±.00	-.91 ±.00	
(offset: 10 m)		(.16)	(.00)	(.02)	(-.01)	(-.29)	(-.30)	
0 (Coord. diff.)	8							

Table 5.25b: Prediction of affine transformation parameters introduced in the Ottawa network by a 30 m offset in the height of the fixed station, (from lines 2 of Table 5.24).

Parameters	rms (mm)	Tx (mm)	Ty (mm)	Tz (mm)	Rx (10^{-6} rad)	Ry (10^{-6} rad)	Rz (10^{-6} rad)	K (ppm)
3T, 3R, 1K	0	0 ±0	0 ±0	0 ±0	.47 ±.01	.03 ±.02	.00 ±.01	-.78 ±.01
3R, 1K	0				.47 ±.01	.03 ±.01	.00 ±.01	-.79 ±.01
1K	3							-.79 ±.14
		Rx (10^{-6} rad)	Ry (10^{-6} rad)	Sx (ppm)	Sy (ppm)	Kx (ppm)	Ky (ppm)	
2R, 2S, 2K	0	.47 ±.00	.02 ±.00	.00 ±.00	-.02 ±.00	-.80 ±.00	-.78 ±.00	
(offset: 10 m)		(.16)	(.01)	(.00)	(-.01)	(-.27)	(-.26)	
0 (Coord. diff.)	7							

The more important parameters Kx and Ky have been recovered at 91% and 86%, respectively. The third largest parameter Rx (2 times smaller than Kx and Ky) has been recovered at 96%. If we solve only for one scale parameter K, this value is recovered at 88%. The magnitude of the other parameters are negligible being 10 times smaller than Kx and Ky.

5.8 Summary of the comparison

Four different GPS campaigns having three different satellite sky distributions have been used to assess the quality of program DIPOPSIM predictions. The behaviour of the

covariance matrix and the effects caused by 5 different systematic errors have been studied. A total of 14 tests have been performed in this investigation.

The comparison of the predictions of program DIPOPSIM and the results of real GPS data has shown that the orientation of the confidence ellipsoid can be obtained at better than $\pm 10^\circ$ and that the shape of the confidence ellipsoid (semi-axes ratio) can be recovered with an error less than $\pm 15\%$.

The study of the prediction of the systematic errors allows us to state the following points. The effects which are not dependent on the satellite azimuthal distribution (refer to chapter 4) like the horizontal scale introduced by the absolute ionospheric refraction and the height offset of the fixed station are the best predicted parameters. The 2 worst prediction cases out of 12 primary effects reach errors of -41% and -45%. The 3 worst prediction cases out of 15 secondary effects (from 2 to 9 times smaller than the primary effects) reach errors of -47%, -48% and +53%. All the effects being 10 times smaller than the primary effects were considered negligible and not taken into account in the study. Using all the 27 affine parameter prediction results (expressed in percentage) we have estimated that the prediction error is about $\pm 25\%$. This statistic has been evaluated with the following equation:

$$[(\text{average error})^2 + (\text{sample standard deviation about the mean})^2]^{1/2}.$$

This prediction error can be attributed to: 1) the assumptions used in the development of the analytical expressions of the biases in single difference observations, Appendix II; 2) the assumptions of continuity and homogeneity of the satellite sky distribution used in DIPOPSIM, section 3.5; and 3) the definition of the integration boundaries representing the real satellite sky distribution of the selected GPS campaigns, section V.2.

The overall performance of the DIPOPSIM predictions is encouraging and considered

satisfactory. Remember that the real strength of the technique is that it does not require any observations and consequently the generalized studies of the behaviour of the covariance matrix and of the effects of systematic errors can be achieved.

The use of the data of the Juan de Fuca network (~ 40 km x 50 km) and the Port Alberni sub-network (~ 50 km x 80 km) proves that the developed simulation technique (DIPOPSIM) is applicable to baselines as long as 100 km. The practical usefulness of the technique for longer baseline length has to be tested using real GPS data collected from networks of larger size.

The above statistic can also be interpreted as another proof (refer to section 3.3) of the equivalence (within the limitation of the assumptions used in DIPOPSIM) between single difference observations modelled with clock parameters and the double difference mode used in the processing of real GPS data (DIPOP and Bernese software).

Single difference prediction results where a clock parameter is not estimated generally lead to erroneous results. The most spectacular proofs being the experiments of the studies of the covariance matrix and the relative tropospheric zenith delay error. This means that the geometrical interpretation of the behaviour of the covariance matrix and the geometrical interpretation of the effect of some systematic errors (the ones affecting primarily the station height) lead to wrong conclusions. This fact is explained by the high correlation existing between the clock parameter and the station height.

It has also been demonstrated that some of the effects of the studied systematic errors cannot be explained only by similarity transformation parameters (see also Chapter 4). In those cases the use of additional affine transformation parameters is necessary to recover the systematic effects introduced into the station coordinates by the model errors.

Chapter 6

Predictions for generic GPS satellite configurations

6.1 Introduction

In Chapter 5 we have assessed the quality of the prediction results obtained from program DIPOPSIM. In this chapter we will exploit the capability of the simulation technique to produce generalized studies of the behaviour of the covariance matrix as well as the effects of systematic errors on the station coordinates as a function of the satellite sky distribution. This will also permit us to confirm and to quantify the expectation of the investigation made in Chapter 4.

The studied satellite configurations correspond to generic satellite configurations that one can expect when observing the future GPS constellation for a few hours in equatorial, mid-latitude and polar sites.

The reader is referred to section V.1 for the visualization of the satellite sky distributions typical of these sites.

The integration boundaries used in DIPOPSIM to define the selected generic GPS satellite configurations are as follows:

Equatorial site (Eq.): $\alpha_{\text{from}}: 0^\circ$, $\alpha^{\text{to}}: 360^\circ$ and $\zeta_{\text{min}}: 0^\circ$, $\zeta^{\text{max}} < 90^\circ$;

Mid-latitude site (Mid.): $\alpha_{\text{from}}: 45^\circ$, $\alpha^{\text{to}}: 315^\circ$ and $\zeta_{\text{min}}: 0^\circ$, $\zeta^{\text{max}} < 90^\circ$;

Polar site (Pol.): $\alpha_{\text{from}}: 0^\circ$, $\alpha^{\text{to}}: 360^\circ$ and $\zeta_{\text{min}}: 45^\circ$, $\zeta^{\text{max}} < 90^\circ$.

In addition to these 3 generic satellite configurations we have added to this study another

configuration which is representative of an extremely non-uniform satellite sky distribution produced by the prototype GPS constellation. An example of such satellite configuration occurred during the CERN 1984 campaign (refer to section V.2). To simplify the analysis we have considered that the satellite configuration can be simply described by the following integration boundaries:

CERN satellite configuration: $\alpha_{\text{from}}: 25^\circ$, $\alpha_{\text{to}}: 155^\circ$ and $\zeta_{\text{min}}: 20^\circ$, $\zeta^{\text{max}} < 90^\circ$.

Throughout this chapter, we will call this configuration the CERN satellite configuration to distinguish it from the CERN 1984 campaign satellite configuration used in the analysis of Chapter 5.

The results are presented in tabular form, for maximum zenith angle values of 65° to 90° (where allowed) in steps of 5° . They are also presented in graphical form, for maximum zenith angle values a few degrees larger than the minimum zenith angle to 90° (where allowed) in steps of 1° .

The behaviour of the covariance matrix is monitored by looking at: 1) the magnitude and the ratio of the semi-axes of the confidence ellipsoid; 2) the orientation of the semi-axes of the confidence ellipsoid; and 3) the correlation coefficient values. The semi-major, the semi-medium and the semi-minor axes are denoted by a , b and c , respectively. The orientation of the semi-major axis, for example, is described by the azimuth of the axis α_a and the elevation angle of the axis E_a . The notation for the correlation coefficient, e.g., x,z , means the correlation value between the station coordinates x and z .

In fact it is the behaviour of the matrix $(A^T A)^{-1}$ that we have monitored. To scale the semi-axes of the confidence ellipsoid and the standard deviation of the station coordinates

in "units of length" we have to multiply those values by σ_{SD} (the a posteriori standard deviation of the single difference observations).

The semi-axes of the confidence ellipsoid and the standard deviation of the station coordinates are also a function of the number of single difference observations in the selected sky sector (n_{sec}). The equation for n_{sec} has been given in Chapter 3 (eqn. 3.12), we rewrite it here for convenience:

$$n_{sec} = n (\cos\zeta_{min} - \cos\zeta^{max}) (\alpha^{to} - \alpha_{from}) / 2\pi$$

where "n" is defined as the total number of "fictitious" single difference observations in the observer's sky hemisphere and 2π is the normalization factor of the integration over the azimuth sector.

The value of 500 has been arbitrarily assigned to "n" in the prediction runs presented in this chapter. This means that different satellite sky distributions will have a different number of single difference observations, n_{sec} , and in turn the magnitudes of the semi-axes and the standard deviations will be affected. Keep this point in mind when comparing simulation results from different satellite sky distributions (and different maximum zenith angles).

The monitoring of the effects of systematic errors is done by looking at the affine transformation parameters associated with the station network. The affine transformation mathematics and terminology is presented in Appendix VI.

As was the case in Chapter 5, the interpretation of the affine transformation parameters is in this sense: the transformations are to be performed on the true coordinates to get the

station coordinates affected by the studied bias. In other words, these are the transformation parameters necessary to recover the systematic effects introduced into the station network by the studied bias.

The predictions are grouped into 6 sections. Section 6.2 contains the study of the covariance matrix behaviour (without and with a relative tropospheric zenith delay parameter); section 6.3 is related to the relative tropospheric refraction error; section 6.4 deals with the absolute ionospheric refraction error; section 6.5 contains the study of the effects of an offset in the latitude of the fixed station; section 6.6 deals with the effects of an offset in the longitude of the fixed station and section 6.7 contains the results of the analysis of an offset in the height of the fixed station. Each section ends with a summary of general trends which are the conclusions we reach in the analysis of the prediction results.

6.2 Covariance matrix

6.2.1 Station coordinates and clock parameter

Tables 6.1a, 6.2a, 6.3a and 6.4a contain the predictions of the behaviour of matrix $(A^T A)^{-1}$ for the equatorial, polar, mid-latitude and CERN satellite configurations, respectively. The associated Tables 6.1b, 6.2b, 6.3b and 6.4b are presented in the next sub-section where a relative tropospheric zenith delay parameter is optionally estimated.

Table 6.1a: DIPOPSIM prediction of the behaviour of matrix $(A^T A)^{-1}$ for equatorial site. The semi-major axis (a) points towards the zenith direction.

ζ^{\max} :	65°	70°	75°	80°	85°	90°
n_{sec} :	289	329	371	413	456	500
a :	0.353	0.290	0.243	0.206	0.178	0.155
a/c :	2.9	2.7	2.5	2.3	2.1	2.0
b = c :	0.122	0.109	0.098	0.090	0.083	0.077
z,t :	0.97	0.96	0.95	0.93	0.90	0.87

Results of Table 6.1a are also presented in Figures 6.1a and 6.3a.

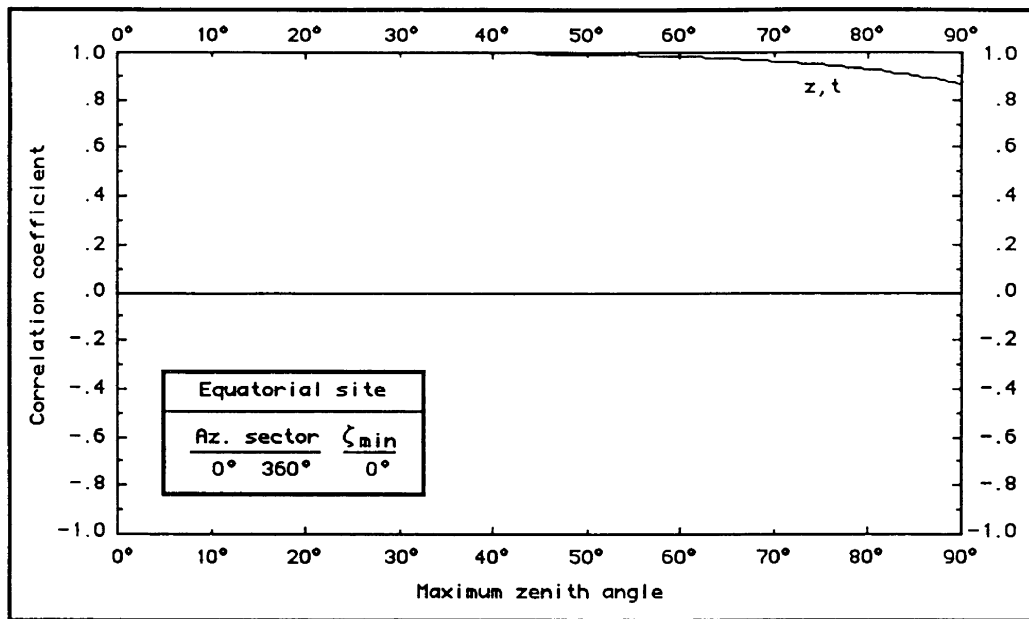


Figure 6.3a: Correlation coefficient among unknowns where station coordinates and clock parameter are estimated. Equatorial site.

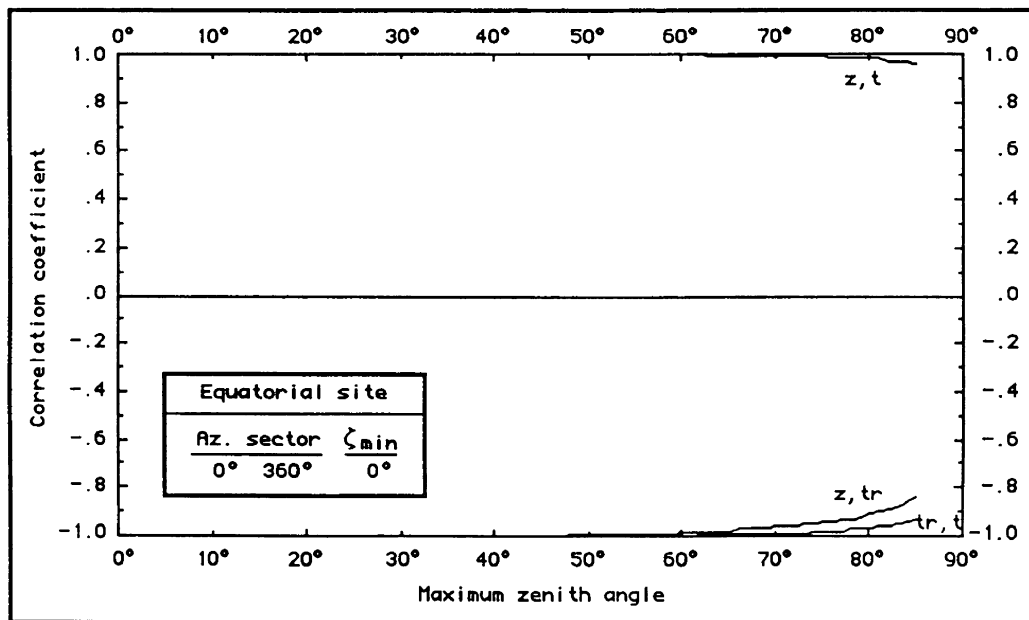


Figure 6.3b: Correlation coefficient among unknowns where station coordinates, clock and tropospheric zenith delay parameters are estimated. Equatorial site.

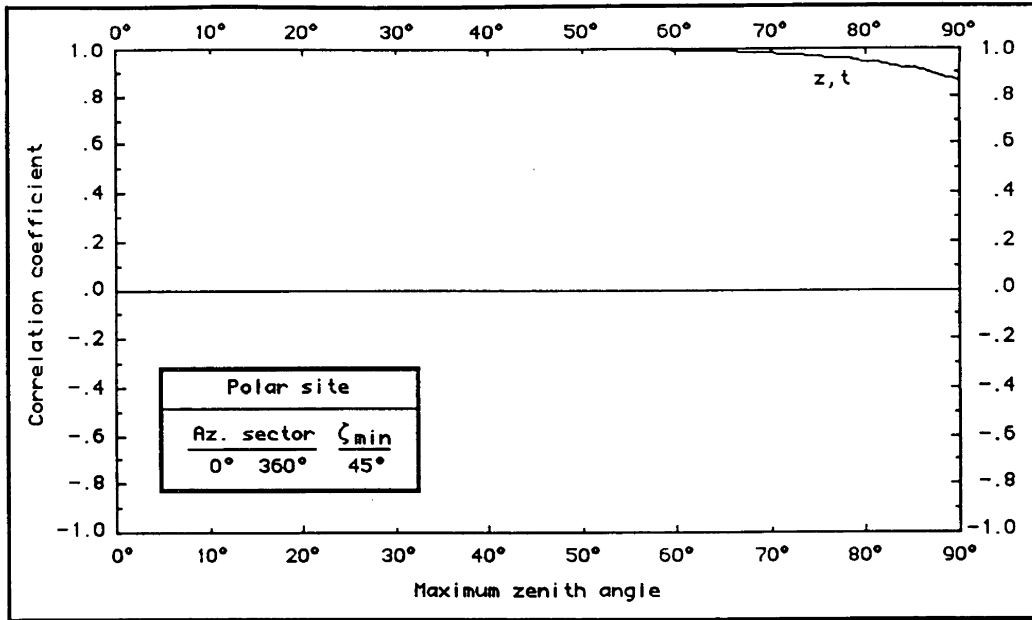


Figure 6.4a: Correlation coefficient among unknowns where station coordinates and clock parameter are estimated. Polar site.

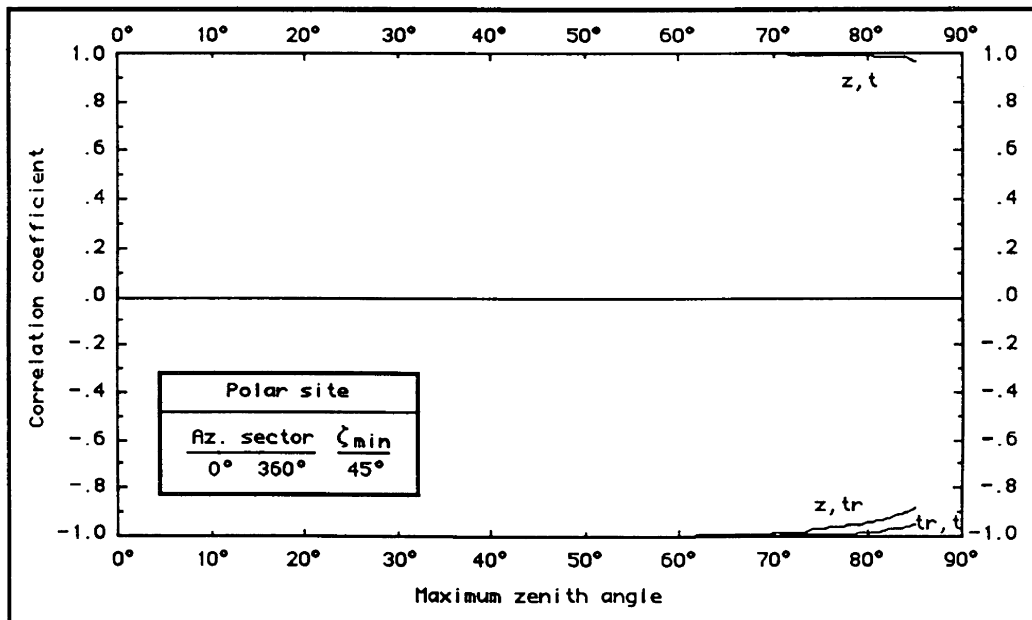


Figure 6.4b: Correlation coefficient among unknowns where station coordinates, clock and tropospheric zenith delay parameters are estimated. Polar site.

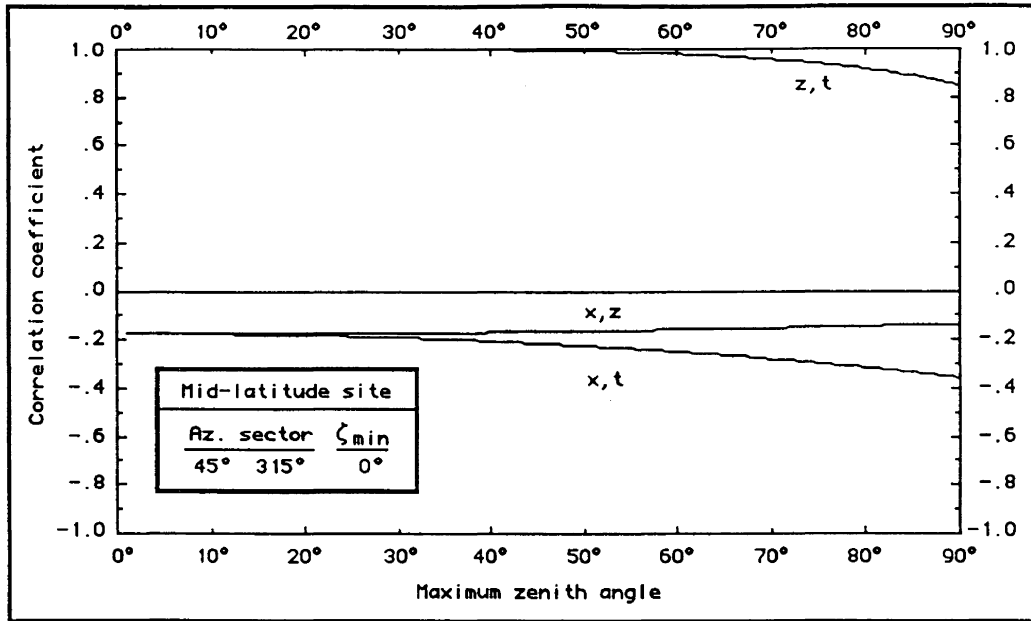


Figure 6.5a: Correlation coefficient among unknowns where station coordinates and clock parameter are estimated. Mid-latitude site.

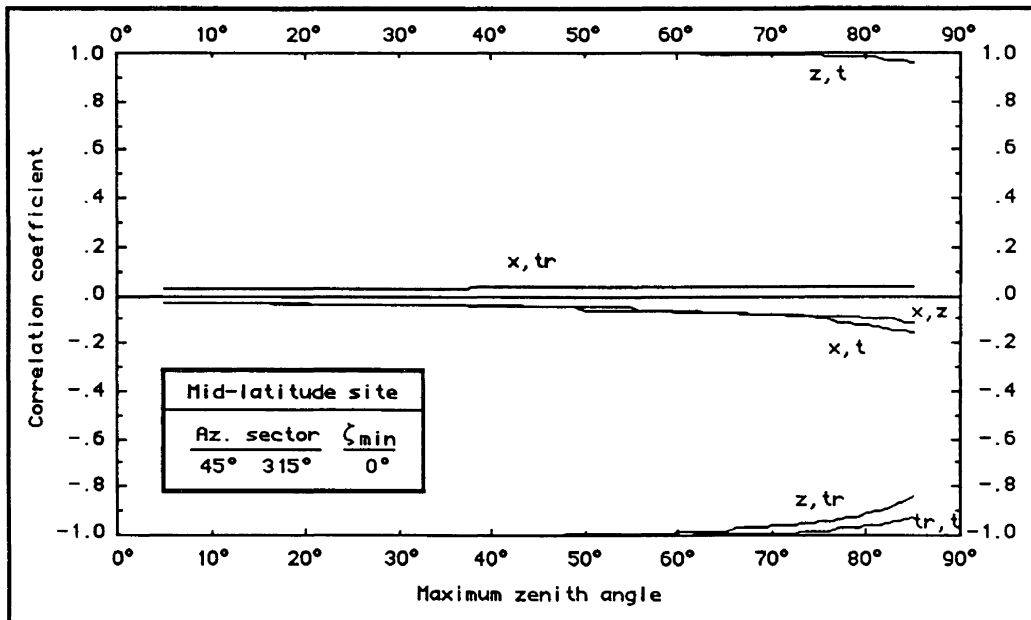


Figure 6.5b: Correlation coefficient among unknowns where station coordinates, clock and tropospheric zenith delay parameters are estimated. Mid-latitude site.

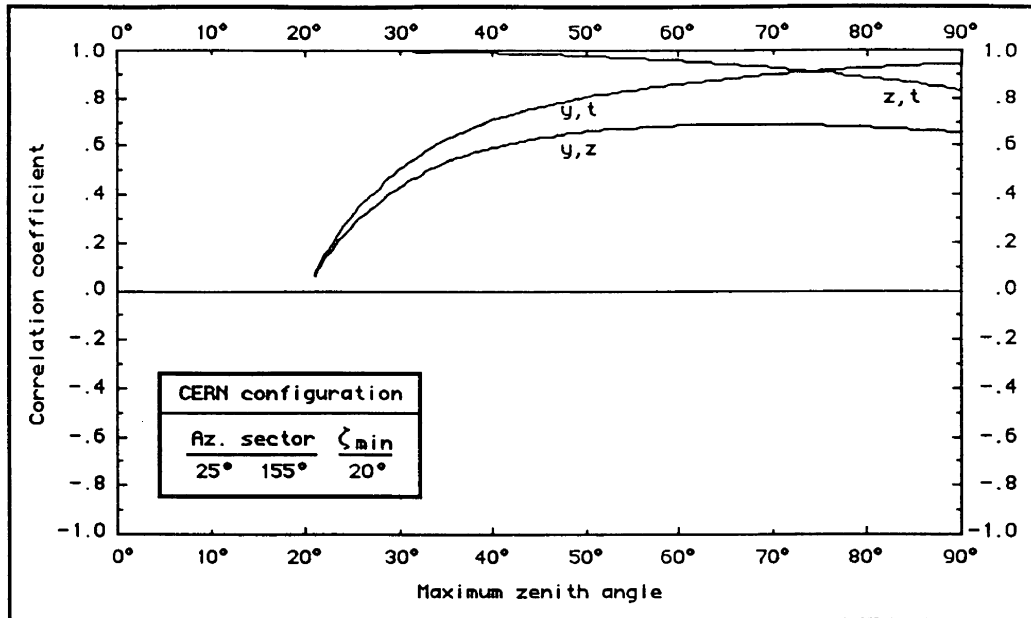


Figure 6.6a: Correlation coefficient among unknowns where station coordinates and clock parameter are estimated. CERN satellite configuration.

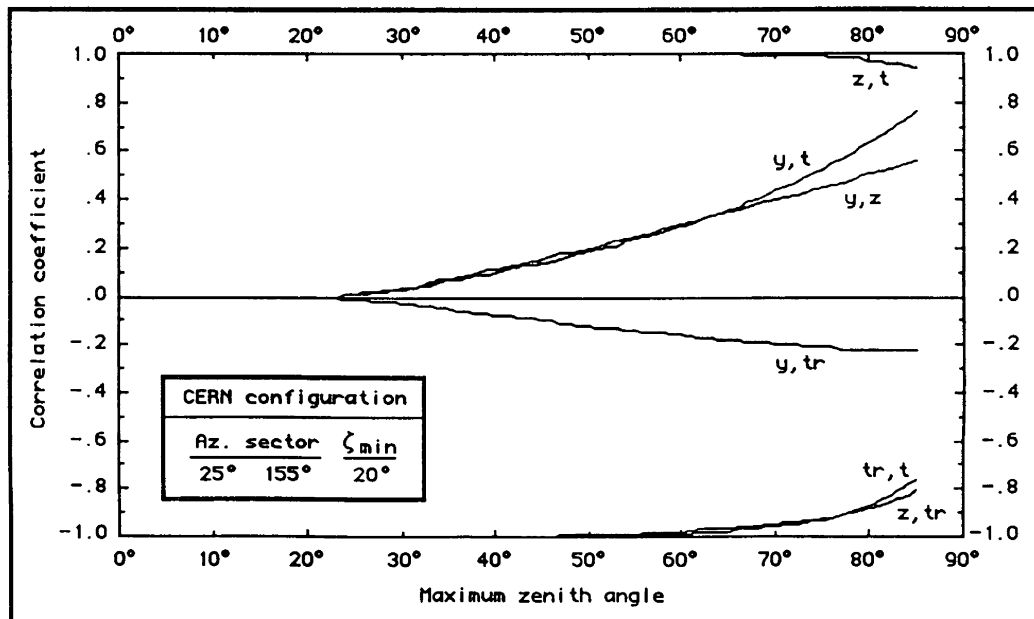


Figure 6.6b: Correlation coefficient among unknowns where station coordinates, clock and tropospheric zenith delay parameters are estimated. CERN satellite configuration.

From the results presented in Tables 6.1a to 6.4a and Figures 6.1a to 6.6a, we can highlight the following conclusions related to the behaviour of the covariance matrix where station coordinates and clock parameter are estimated.

General trends

- 1) The covariance matrix is a function of the unknowns in the solution; of the satellite sky distribution (geometry strength); of the number of observations; and of the observation weight;
- 2) The covariance matrix is not a function of baseline orientation;
- 3) The semi-major axis of the confidence ellipsoid (a) points towards the satellite sky coverage;
- 4) The azimuth of this semi-major axis equals the azimuth of the horizontal symmetry axis of the satellite sky distribution (at equatorial and polar sites, the azimuth is undefined because the semi-major axis points towards the zenith direction);
- 5) The elevation angle of this semi-major axis increases as the maximum zenith angle decreases for non-uniform azimuth satellite distributions (at equatorial and polar sites, the elevation angle of the semi-major axis is invariant and equal 90°);
- 6) Because the semi-minor axis (c) always lies in the horizontal plane its azimuth is perpendicular to the azimuth of the semi-major axis (a) (the direction of the semi-medium axis (b) is perpendicular to the 2 other axes);
- 7) For a full hemisphere of observations, the standard deviation of the height is twice the standard deviation of the horizontal coordinates (this is a consequence of the high correlation between the height coordinate and the clock parameter);
- 8) A larger ratio (a/c) occurs at the polar site because high zenith angle observations do not contain strong information about the station height component;
- 9) The ratio (a/c) decreases as the maximum zenith angle increases (the correlation (z,t) decreases);

- 10) The standard deviation of the height decreases as the maximum zenith angle increases;
- 11) For an all-azimuth satellite distribution, the semi-medium axis is equal to the semi-minor axis;
- 12) High correlation exists between the clock parameter and the station height component (z,t);
- 13) The polar site shows slightly larger values for the correlation coefficient (z,t) than the other satellite configurations;
- 14) Correlation (z,t) decreases as the maximum zenith angle increases;
- 15) Non-uniform azimuth satellite distribution creates correlation among other unknowns as well.

6.2.2 Station coordinates, clock parameter and relative tropospheric zenith delay parameter

Tables 6.1b, 6.2b, 6.3b and 6.4b contain the predictions of the behaviour of matrix $(A^T A)^{-1}$ for the equatorial, polar, mid-latitude and CERN satellite configurations, respectively, where a relative tropospheric zenith delay parameter is added to the solution along with the station coordinates and the clock parameter.

Table 6.1b: DIPOPSIM prediction of the behaviour of matrix $(A^T A)^{-1}$ where a relative tropospheric zenith delay parameter is estimated for equatorial site. The semi-major axis (a) points towards the zenith direction.

ζ^{\max} :	65°	70°	75°	80°	85°
n_{sec} :	289	329	371	413	456
a :	1.624	1.083	0.731	0.495	0.330
a/c :	13.5	9.8	7.3	5.6	4.1
b = c :	0.122	0.109	0.098	0.090	0.083
z,t :	0.99	0.99	0.99	0.98	0.96
tr,t :	-0.99	-0.99	-0.98	-0.97	-0.93
z,tr :	-0.98	-0.96	-0.94	-0.91	-0.84

Results of Table 6.1b are illustrated in Figures 6.1b and 6.3b.

The high correlation between the relative tropospheric zenith delay parameter, the clock

parameter and the station height is obvious. This fact conducts directly to an enhancement of the ratio a/c compared to the case where a relative tropospheric zenith delay parameter is not estimated (Table 6.1a).

Table 6.2b: DIPOPSIM prediction of the behaviour of matrix $(A^T A)^{-1}$ where a relative tropospheric zenith delay parameter is estimated for polar site. The semi-major axis (a) points towards the zenith direction.

ζ^{\max} :	65°	70°	75°	80°	85°
n_{sec} :	142	183	224	267	310
a :	7.808	3.837	2.067	1.174	0.678
a/c :	55.8	32.0	18.8	11.7	7.6
$b = c$:	0.144	0.124	0.109	0.098	0.089
z, t :	1.00	1.00	0.99	0.99	0.97
tr, t :	-1.00	-1.00	-0.99	-0.98	-0.95
z, tr :	-0.99	-0.98	-0.97	-0.94	-0.88

Results presented in Table 6.2b are plotted in Figures 6.1b and 6.4b. Note that the scale of the vertical axis of Figure 6.1b is twice the scale of the vertical axis of Figure 6.1a.

The least squares adjustment conditions encountered in this situation (high correlation between the relative tropospheric zenith delay parameter, the clock parameter and the station height; and the high zenith angle observations) lead naturally to an extremely high ratio between the semi-major axis and the semi-minor axis of the confidence ellipsoid (a/c).

Table 6.3b: DIPOPSIM prediction of the behaviour of matrix $(A^T A)^{-1}$ where a relative tropospheric zenith delay parameter is estimated for mid-latitude site.

ζ^{\max} :	65°	70°	75°	80°	85°
n_{sec} :	217	247	278	310	342
a :	1.881	1.254	0.848	0.574	0.384
a/c :	14.7	11.0	8.2	6.1	4.4
Ea :	90°	89°	89°	89°	88°
α_a :	180°	180°	180°	180°	180°
b :	0.180	0.161	0.145	0.132	0.122
b/c :	1.4	1.4	1.4	1.4	1.4
Eb :	0°	-1°	-1°	-1°	-2°
α_b :	180°	180°	180°	180°	180°
c :	0.128	0.114	0.103	0.094	0.087
Ec :	0°	0°	0°	0°	0°
α_c :	90°	90°	90°	90°	90°
σ_x :	0.181	0.161	0.146	0.133	0.123
σ_x/c :	1.4	1.4	1.4	1.4	1.4
σ_y :	0.128	0.114	0.103	0.094	0.087
σ_y/c :	1.0	1.0	1.0	1.0	1.0
σ_z :	1.881	1.254	0.848	0.574	0.384
σ_z/c :	14.7	11.0	8.2	6.1	4.4
z,t :	0.99	0.99	0.99	0.99	0.96
x,t :	-0.07	-0.08	-0.10	-0.12	-0.16
x,z :	-0.07	-0.08	-0.09	-0.10	-0.11
tr,t :	-0.99	-0.99	-0.98	-0.96	-0.92
z,tr :	-0.98	-0.96	-0.94	-0.91	-0.84
x,tr :	0.04	0.04	0.04	0.04	0.04

Results of Table 6.3b are presented in Figures 6.1b, 6.2b and 6.5b.

The additional characteristic of this situation is found in the increase of the elevation angle of the semi-major axis of the confidence ellipsoid compared to the elevation angle values reported for the mid-latitude site for solutions without a relative tropospheric zenith delay parameter (Table 6.3a).

Table 6.4b: DIPOPSIM prediction of the behaviour of matrix $(A^T A)^{-1}$ where a relative tropospheric zenith delay parameter is estimated for CERN satellite configuration.

ζ^{\max} :	65°	70°	75°	80°	85°
n_{sec} :	93	108	123	138	154
a :	3.677	2.427	1.652	1.157	0.836
a/c :	14.6	10.8	8.2	6.3	4.9
Ea :	85°	82°	78°	71°	60°
α_a :	90°	90°	90°	90°	90°
b :	0.768	0.665	0.577	0.495	0.410
b/c :	3.1	3.0	2.9	2.7	2.4
Eb :	-5°	-8°	-12°	-19°	-30°
α_b :	90°	90°	90°	90°	90°
c :	0.251	0.224	0.202	0.185	0.170
Ec :	0°	0°	0°	0°	0°
α_c :	0°	0°	0°	0°	0°
σ_x :	0.251	0.224	0.202	0.185	0.170
σ_x/c :	1.0	1.0	1.0	1.0	1.0
σ_y :	0.823	0.732	0.660	0.600	0.550
σ_y/c :	3.3	3.3	3.3	3.2	3.2
σ_z :	3.665	2.408	1.621	1.106	0.751
σ_z/c :	14.6	10.8	8.0	6.0	4.4
z,t :	1.00	0.99	0.99	0.97	0.94
y,t :	0.36	0.44	0.53	0.64	0.76
y,z :	0.35	0.40	0.45	0.51	0.56
tr,t :	-0.98	-0.96	-0.93	-0.87	-0.76
z,tr :	-0.97	-0.95	-0.92	-0.88	-0.81
y,tr :	-0.18	-0.20	-0.21	-0.22	-0.22

Results of Table 6.4b are graphically presented in Figures 6.1b, 6.2b and 6.6b.

The comment given, above, for the mid-latitude site is also applicable for the CERN satellite configuration. Moreover, we should note the exceptional change in the behaviour of the correlation coefficients y,t and y,z as a function of the maximum zenith angle between the solution without (Figure 6.6a) and the solution with a relative tropospheric zenith delay parameter (Figure 6.6b).

It is also interesting to look at the ratio of the station height standard deviation for solutions

with and without a relative tropospheric zenith delay parameter for different satellite sky distribution. Table 6.5 presents this ratio for different maximum zenith angles.

Table 6.5: Ratio of the station height standard deviation for solutions with and without a relative tropospheric zenith delay parameter.

ζ^{\max} :	65°	70°	75°	80°	85°
Equatorial:	4.6	3.7	3.0	2.4	1.9
Polar:	7.6	5.5	4.0	2.9	2.1
Mid-latitude:	4.6	3.7	3.0	2.4	1.9
CERN:	3.8	3.1	2.6	2.1	1.7

These high ratio are indicative of a high degree of correlation between the station height and the relative tropospheric zenith delay parameter.

The general trends in the behaviour of the covariance matrix given in sub-section 6.2.1 are also applicable to this sub-section, except for item #7. Moreover, from the results presented in Tables 6.1b to 6.4b and Figures 6.1b to 6.6b, we can highlight the following additional conclusions related to the behaviour of the covariance matrix where a relative tropospheric zenith delay parameter is added in the least squares solution.

General trends

- 1) For non-uniform azimuth satellite distributions, the elevation angle of the semi-major axis is higher compared to the case where no relative tropospheric zenith delay parameter is estimated;
- 2) The ratio semi-major/semi-minor axes (a/c) is enhanced by the introduction of a relative tropospheric zenith delay parameter;
- 3) For equatorial, mid-latitude and polar sites, the value of the semi-minor axis (c) does not change, whether a relative tropospheric zenith delay parameter is estimated or not. The same statement holds for the semi-medium axis (b), except for the mid-latitude sites where we can see a slightly higher value where a relative tropospheric zenith delay

parameter is estimated. For the CERN satellite configuration the ratio (b/c) is higher compared to the case where no relative tropospheric zenith delay parameter is estimated;

- 4) Relative tropospheric zenith delay parameter, clock parameter and station height coordinate are highly correlated;
- 5) Correlation coefficients (z,t), (z,tr) and (tr,t) decrease (in absolute value) as the maximum zenith angle increases;
- 6) The correlation coefficient (z,t) is the largest one (in absolute value), even larger than the (z,tr) and (tr,t) correlation coefficients;
- 7) The correlation coefficient (z,t) is higher compared to the case where no relative tropospheric zenith delay parameter is estimated.

6.3 Relative tropospheric refraction

Tables 6.6a, 6.6b, 6.6c and 6.6d contain the predictions of effects of relative tropospheric zenith delay error for the equatorial, polar, mid-latitude and CERN satellite configurations, respectively.

Table 6.6a: DIPOPSIM prediction of the effects on station coordinates due to each 1 mm of relative tropospheric zenith delay error for equatorial site.

ζ^{\max} :	65°	70°	75°	80°	85°	
Tz :	2.18	2.59	3.19	4.18	6.16	(mm)

In Figure 6.7a are presented the affine transformation parameter values for different maximum zenith angles, for the equatorial site.

Table 6.6b: DIPOPSIM prediction of the effects on station coordinates due to each 1 mm of relative tropospheric zenith delay error for polar site.

ζ^{\max} :	65°	70°	75°	80°	85°	
Tz :	3.23	3.87	4.86	6.51	9.92	(mm)

In Figure 6.7b are presented the affine transformation parameter values for different maximum zenith angles, for the polar site.

Table 6.6c: DIPOPSIM prediction of the effects on station coordinates due to each 1 mm of relative tropospheric zenith delay error for mid-latitude site.

ζ^{\max} :	65°	70°	75°	80°	85°	
Tz :	2.19	2.59	3.19	4.19	6.18	(mm)
Tx :	-0.01	-0.01	-0.02	-0.04	-0.09	(mm)

In Figure 6.7a are presented the affine transformation parameter values for different maximum zenith angles, for the mid-latitude site.

Table 6.6d: DIPOPSIM prediction of the effects on station coordinates due to each 1 mm of relative tropospheric zenith delay error for CERN satellite configuration.

ζ^{\max} :	65°	70°	75°	80°	85°	
Tz :	2.43	2.92	3.67	4.93	7.54	(mm)
Ty :	0.10	0.18	0.34	0.67	1.50	(mm)

In Figure 6.7c are presented the affine transformation parameter values for different maximum zenith angles, for the CERN satellite configuration.

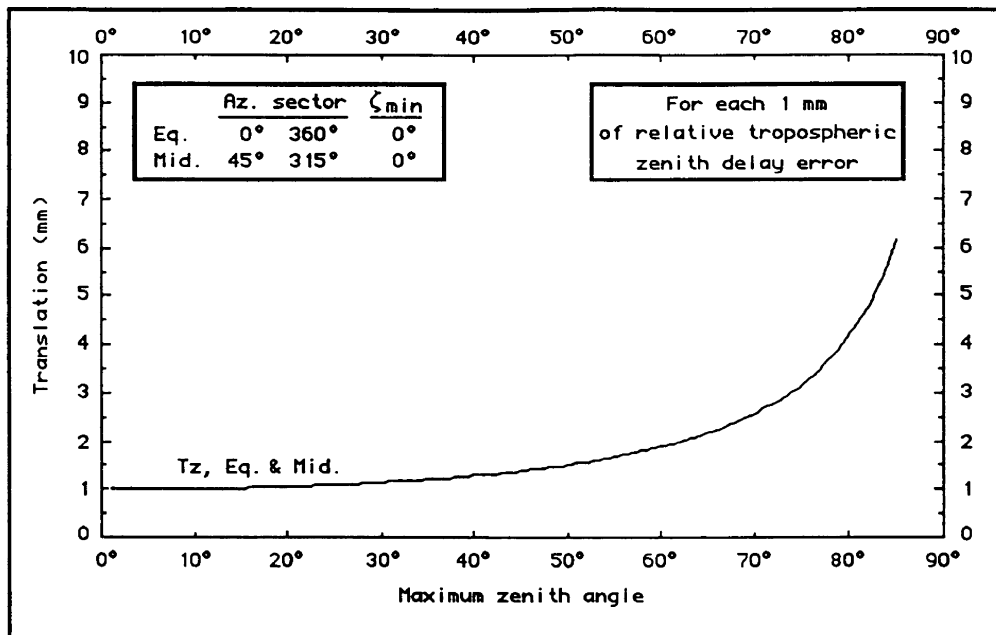


Figure 6.7a: Translation effect due to relative tropospheric zenith delay error. Equatorial and mid-latitude sites.

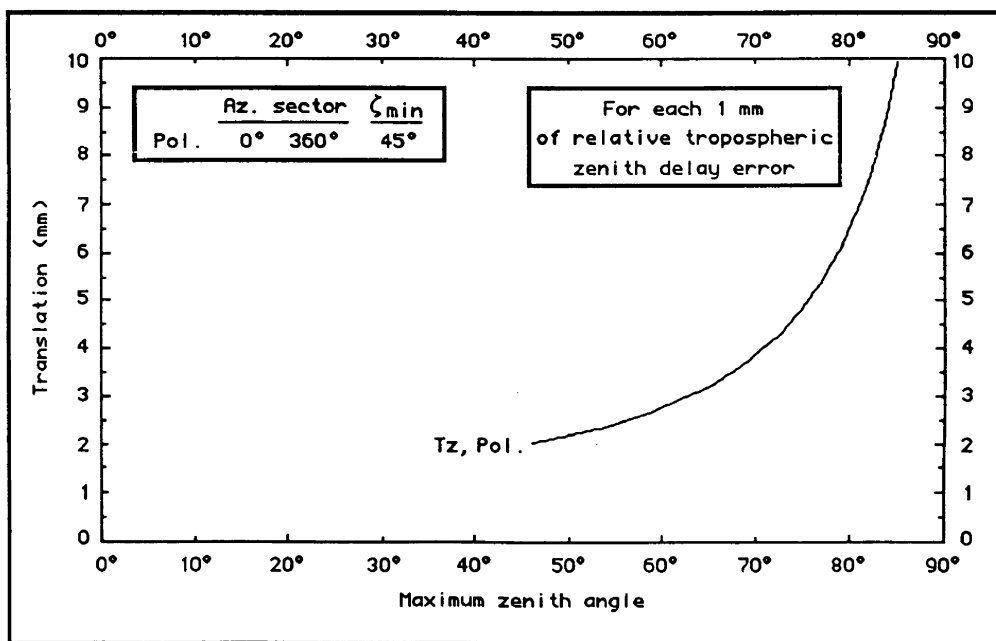


Figure 6.7b: Translation effect due to relative tropospheric zenith delay error. Polar site.

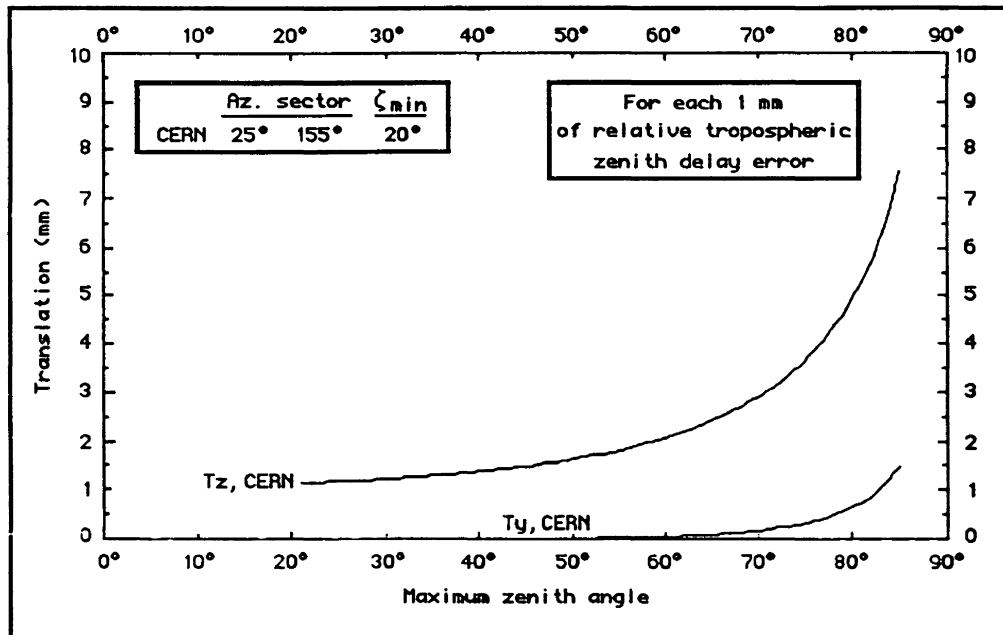


Figure 6.7c: Translation effect due to relative tropospheric zenith delay error. CERN satellite configuration.

From the results presented in Tables 6.6 and Figures 6.7, we can highlight the following conclusions related to the effects of relative tropospheric refraction.

General trends

- 1) Effect is proportional to the relative tropospheric zenith delay error;
- 2) Main effect is a translation affecting the station height;
- 3) If corrected observations are still too long (tropospheric correction too small) the baseline height component increases;
- 4) Magnification factor (translation divided by relative tropospheric zenith delay error) is independent of baseline length and azimuth;
- 5) Effect is a function of the selection of the maximum zenith angle ζ^{\max} ;
- 6) Absolute value of the effect increases with an increase of ζ^{\max} (paradox with item #10, section 6.2.1, where the standard deviation of the height decreases with an increase of

ζ^{\max});

- 7) Polar situation is the worst one; all observations are at high zenith angles;
- 8) Mid-latitude case results show essentially the same height effect as the equatorial situation and show a negligible horizontal effect;
- 9) Observer's satellite sky distribution must be very bad to show significant horizontal coordinate effects;
- 10) Effect on horizontal coordinates is along the horizontal symmetry axis of the satellite sky distribution (independently of the baseline azimuth or length).

Note that if a relative tropospheric zenith delay parameter is added to the solution all the effect is absorbed by this parameter and the other parameters are unaffected by the relative tropospheric zenith delay mismodelling. This is a valid statement if we only consider the systematic (constant) part of the tropospheric refraction effect. The study of the behaviour of the random part (the varying part within an observing session) of the tropospheric refraction error has been done by Herring [1986] for an all-azimuth satellite sky distribution. The study of the impact of satellite sky distribution on the propagation of the random part of the tropospheric refraction error is a suggestion for further work.

6.4 Absolute ionospheric refraction

Tables 6.7a, 6.7b, 6.7c and 6.7d contain the predictions of the effects of absolute ionospheric refraction error for the equatorial, polar, mid-latitude and CERN satellite configurations, respectively.

Table 6.7a: DIPOPSIM prediction of the effects on station coordinates due to absolute ionospheric refraction error (per 1×10^{17} el/m² of TEC, L1 carrier phase) for equatorial site.

ζ^{\max} :	65°	70°	75°	80°	
K :	-0.590	-0.629	-0.668	-0.708	(ppm)

Table 6.7b: DIPOPSIM prediction of the effects on station coordinates due to absolute ionospheric refraction error (per 1×10^{17} el/m² of TEC, L1 carrier phase) for polar site.

ζ_{\max} :	65°	70°	75°	80°	
K :	-0.650	-0.685	-0.720	-0.757	(ppm)

In Figure 6.8a are presented the affine transformation parameter values for different maximum zenith angles, for the equatorial and polar sites.

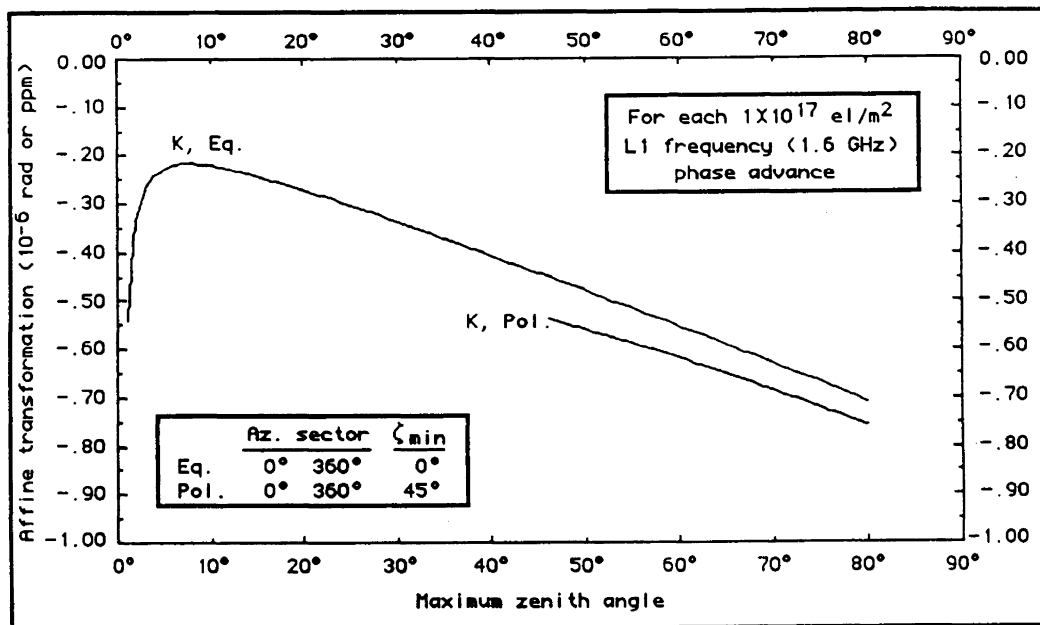


Figure 6.8a: Affine transformation parameters due to absolute ionospheric refraction error (phase advance). Equatorial and polar sites.

Table 6.7c: DIPOPSIM prediction of the effects on station coordinates due to absolute ionospheric refraction error (per 1×10^{17} el/m² of TEC, L1 carrier phase) for mid-latitude site.

ζ_{\max} :	65°	70°	75°	80°	
K :	-0.590	-0.629	-0.668	-0.708	(ppm)
ΔK_x :	0.001	0.001	0.001	0.002	(ppm)
R_y :	0.127	0.131	0.136	0.141	(10^{-6} rad)

In Figure 6.8b are presented the affine transformation parameter values for different maximum zenith angles, for the mid-latitude site.

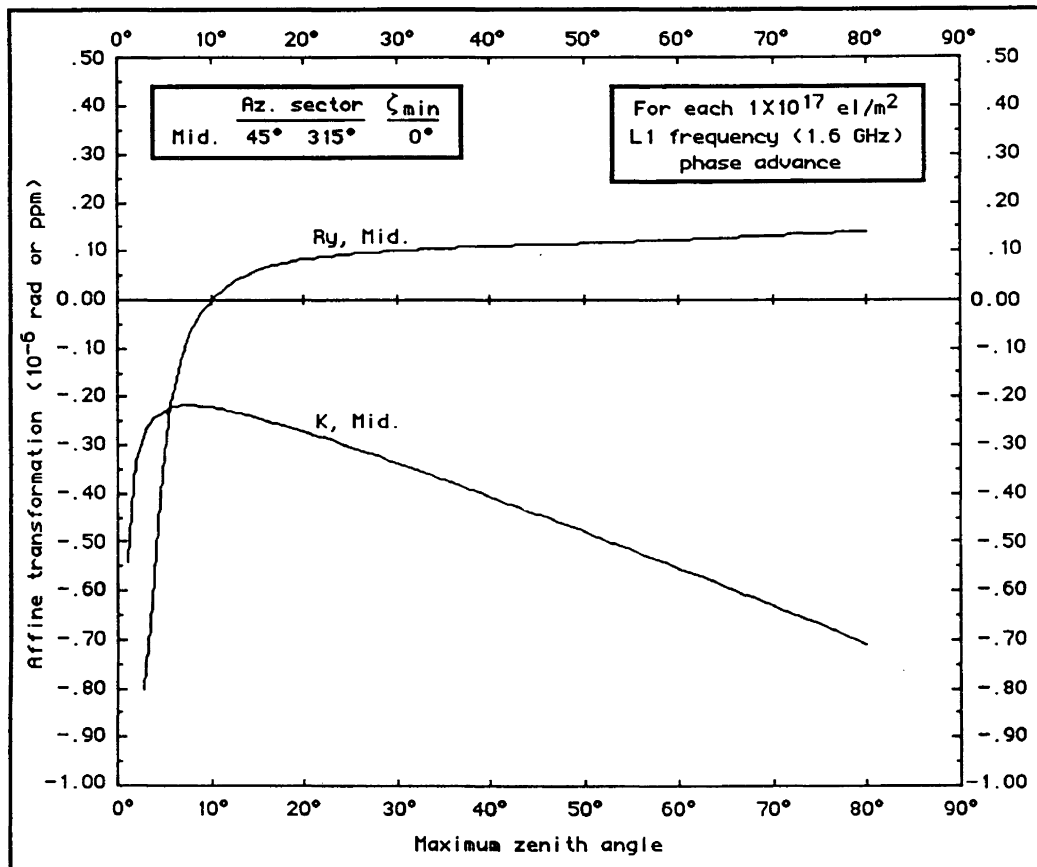


Figure 6.8b: Affine transformation parameters due to absolute ionospheric refraction error (phase advance).
Mid-latitude site.

Table 6.7d: DIPOPSIM prediction of the effects on station coordinates due to absolute ionospheric refraction error (per 1×10^{17} el/m^2 of TEC, L1 carrier phase) for CERN satellite configuration.

ζ_{max} :	65°	70°	75°	80°	
K :	-0.594	-0.633	-0.672	-0.711	(ppm)
ΔK_y :	0.018	0.025	0.032	0.041	(ppm)
Rx :	0.415	0.426	0.438	0.452	(10^{-6} rad)

In Figure 6.8c are presented the affine transformation parameter values for different maximum zenith angles, for the CERN satellite configuration.

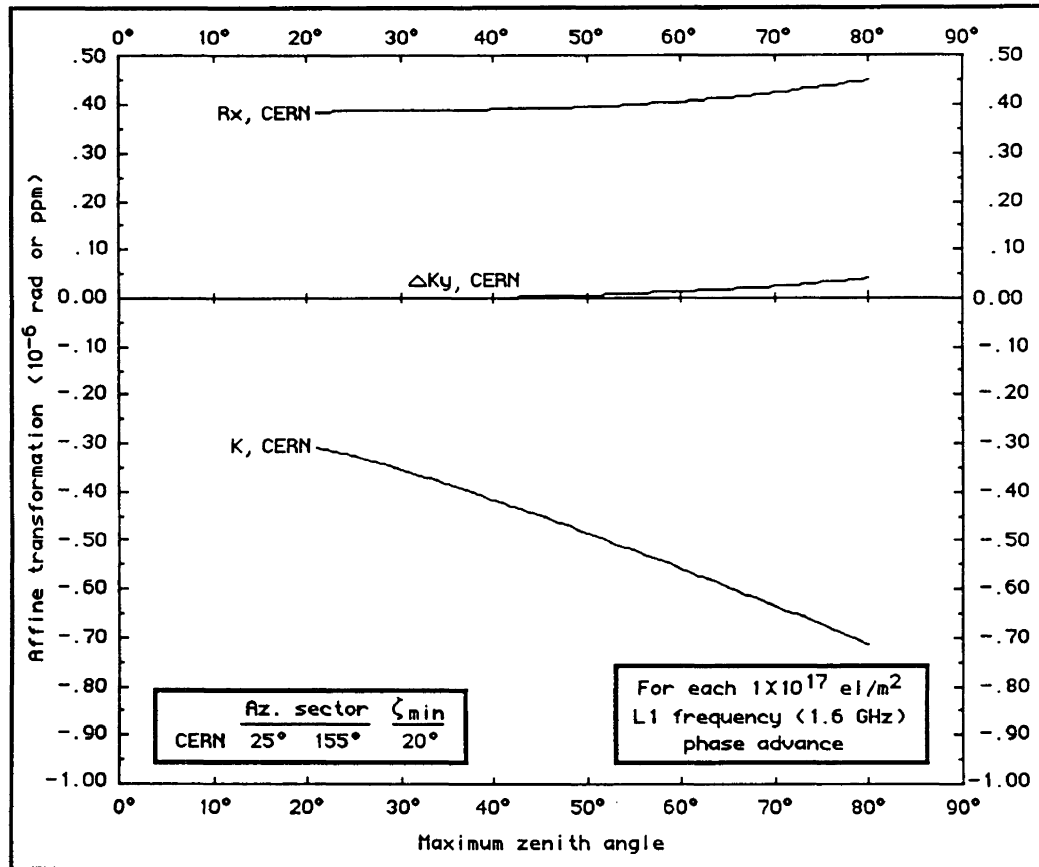


Figure 6.8c: Affine transformation parameters due to absolute ionospheric refraction error (phase advance).
CERN satellite configuration.

From the results presented in Tables 6.7 and Figures 6.8, we can highlight the following conclusions related to the effects of absolute ionospheric refraction.

General trends

- 1) Effect is proportional to TEC value and inversely proportional to the square of the carrier frequency;
- 2) Effect is proportional to baseline length (effect is non-negligible even on very short baseline);
- 3) Main effect is a horizontal scale effect affecting the horizontal coordinates;

- 4) If absolute ionospheric phase advance correction is neglected, the baseline (network) length is too short;
- 5) Horizontal scale effect is uniquely a function of zenith angle boundaries (equatorial and mid-latitude sites show the same horizontal scale effect);
- 6) Absolute value of the horizontal scale effect increases with an increase of the maximum zenith angle ζ^{\max} ;
- 7) Polar situation is the worst one; all observations are at high zenith angles;
- 8) Non-uniform azimuth satellite distribution causes the baseline (network) to rotate (effect on height);
- 9) Rotation is around the horizontal axis perpendicular to the horizontal symmetry axis of the satellite sky distribution. More precisely, the positive rotation (in the left-handed local geodetic system) is around a horizontal axis having an azimuth of: $\alpha_{\text{sym}} - 90^\circ$; where α_{sym} is the azimuth of the horizontal symmetry axis of the satellite sky distribution;
- 10) The larger the azimuth sector without satellite observations, the larger the rotation (for poor satellite geometry the rotation effect can be as large as the horizontal scale effect);
- 11) A small directional horizontal scale effect is also introduced by a non-uniform azimuth satellite distribution;
- 12) The directional horizontal scale effect is in the direction of the horizontal symmetry axis of the satellite sky distribution;
- 13) The directional horizontal scale has the opposite sign of the main horizontal scale effect.

6.5 Offset in the latitude of the fixed station

Tables 6.8a, 6.8b, 6.8c and 6.8d contain the predictions of the effects of a latitude offset of the fixed station for the equatorial, polar, mid-latitude and CERN satellite

configurations, respectively.

Table 6.8a: DIPOPSIM prediction of the effects on station coordinates due to each 10 m of latitude offset of the fixed station for equatorial site.

ζ^{\max} :	65°	70°	75°	80°	85°	90°
Ry :	-0.323	-0.305	-0.286	-0.267	-0.247	-0.227 (10 ⁻⁶ rad)

Table 6.8b: DIPOPSIM prediction of the effects on station coordinates due to each 10 m of latitude offset of the fixed station for polar site.

ζ^{\max} :	65°	70°	75°	80°	85°	90°
Ry :	-0.257	-0.238	-0.220	-0.200	-0.181	-0.161 (10 ⁻⁶ rad)

In Figure 6.9a are presented the affine transformation parameter values for different maximum zenith angles, for the equatorial and polar sites.

Table 6.8c: DIPOPSIM prediction of the effects on station coordinates due to each 10 m of latitude offset of the fixed station for mid-latitude site.

ζ^{\max} :	65°	70°	75°	80°	85°	90°
Ry :	-0.201	-0.190	-0.178	-0.166	-0.154	-0.142 (10 ⁻⁶ rad)
Kx :	0.149	0.156	0.162	0.167	0.172	0.175 (ppm)
Ky :	0.028	0.030	0.031	0.032	0.032	0.033 (ppm)

In Figure 6.9b are presented the affine transformation parameter values for different maximum zenith angles, for the mid-latitude site.

Table 6.8d: DIPOPSIM prediction of the effects on station coordinates due to each 10 m of latitude offset of the fixed station for CERN satellite configuration.

ζ^{\max} :	65°	70°	75°	80°	85°	90°
Ry :	-0.606	-0.567	-0.527	-0.485	-0.442	-0.400 (10 ⁻⁶ rad)
Sx :	-0.228	-0.239	-0.247	-0.255	-0.261	-0.266 (ppm)
Sy :	0.494	0.509	0.520	0.526	0.528	0.526 (ppm)

In Figure 6.9c are presented the affine transformation parameter values for different maximum zenith angles, for the CERN satellite configuration.

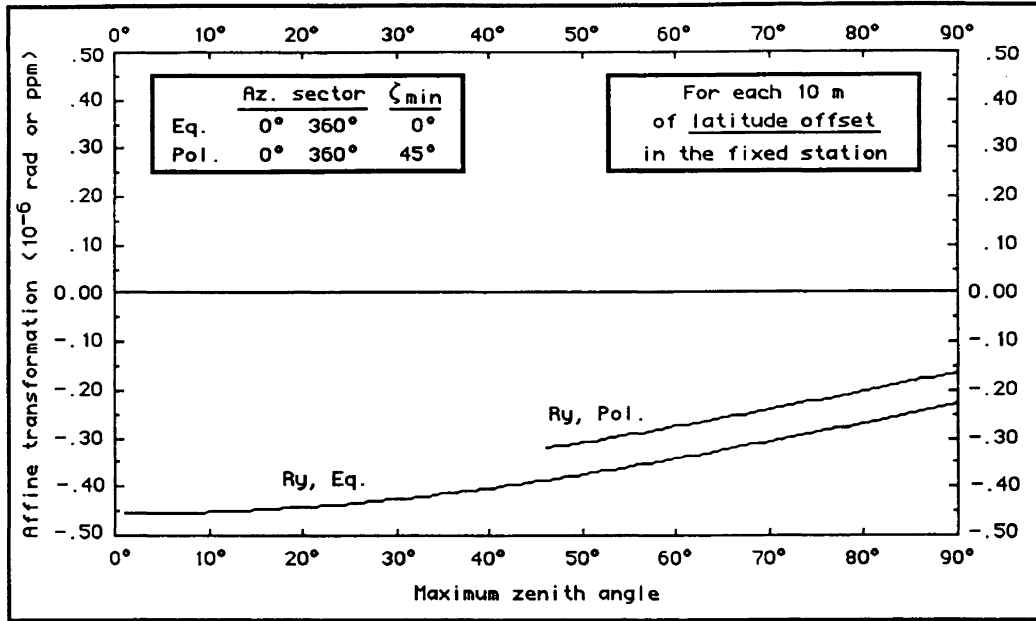


Figure 6.9a: Affine transformation parameters due to a latitude offset in the fixed station. Equatorial and polar sites.

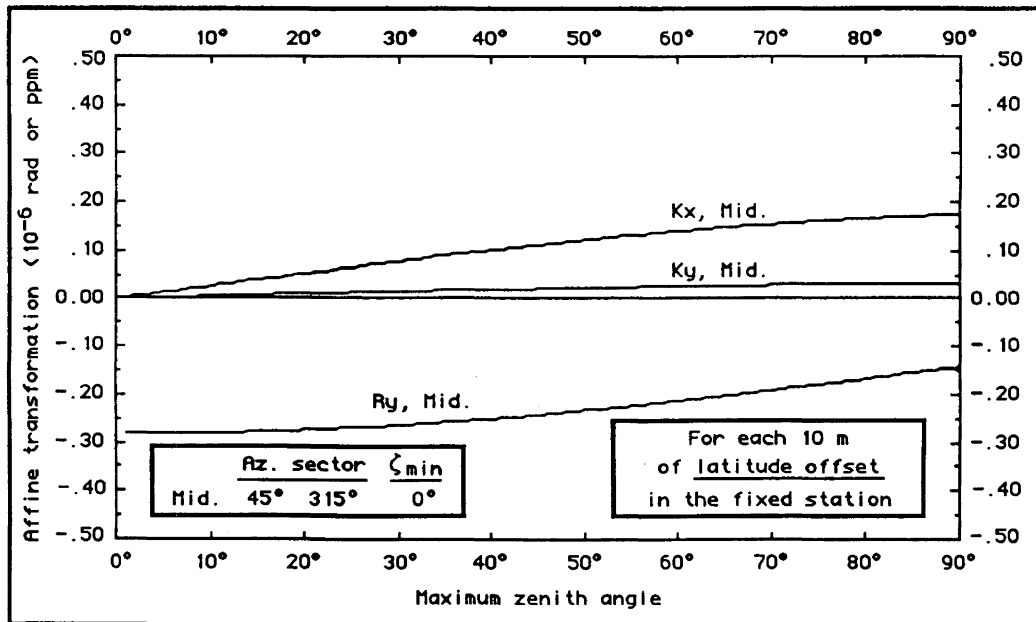


Figure 6.9b: Affine transformation parameters due to a latitude offset in the fixed station. Mid-latitude site.

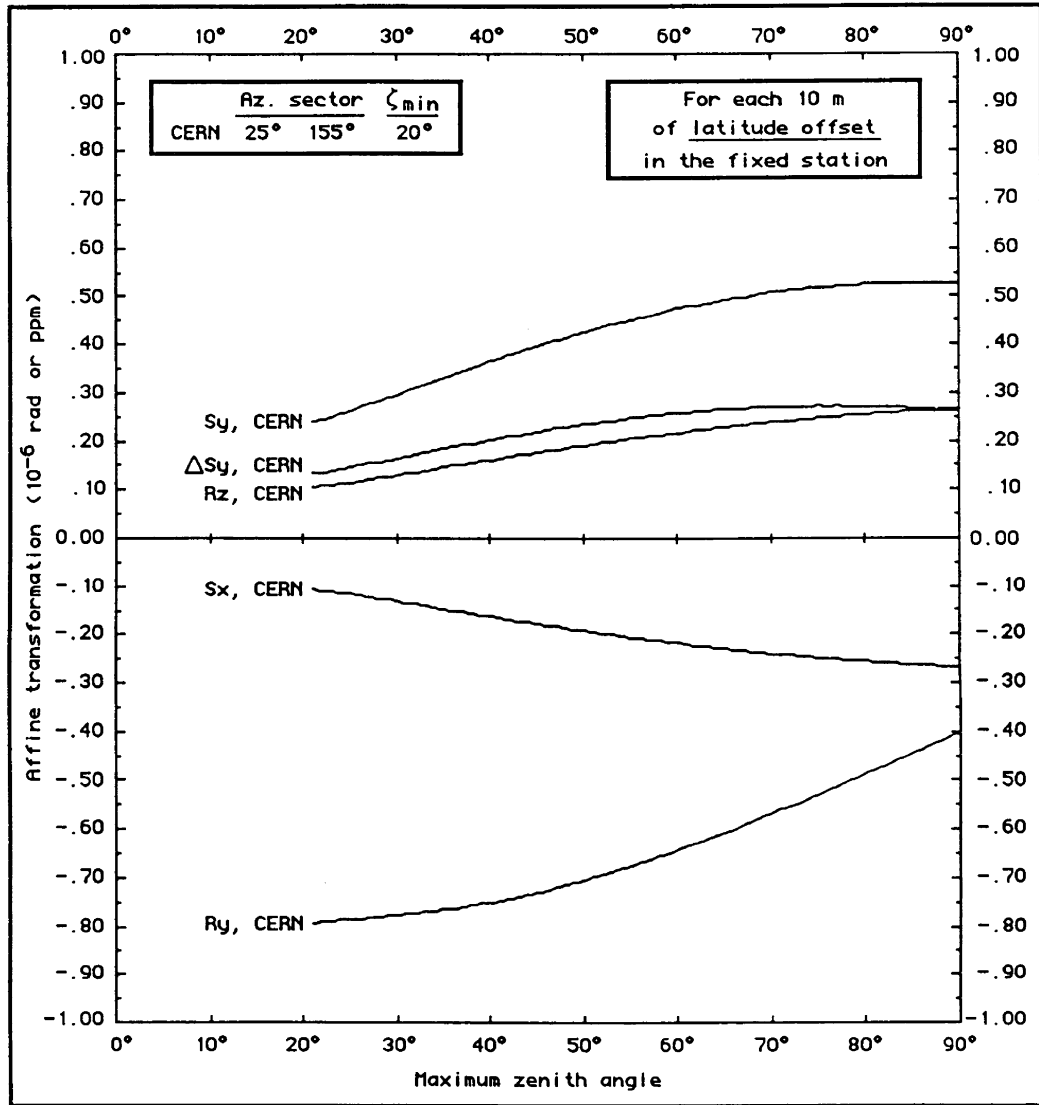


Figure 6.9c: Affine transformation parameters due to a latitude offset in the fixed station. CERN satellite configuration.

The general trends of the effects of a latitude offset of the fixed station will be presented in the next section along with the general trends of the effects of a longitude offset of the fixed station.

6.6 Offset in the longitude of the fixed station

Tables 6.9a, 6.9b, 6.9c and 6.9d contain the predictions of the effects of a longitude offset of the fixed station for the equatorial, polar, mid-latitude and CERN satellite configurations, respectively.

Table 6.9a: DIPOPSIM prediction of the effects on station coordinates due to each 10 m of longitude offset of the fixed station for equatorial site.

ζ^{\max} :	65°	70°	75°	80°	85°	90°
Rx :	0.323	0.305	0.286	0.267	0.247	0.227 (10 ⁻⁶ rad)

Table 6.9b: DIPOPSIM prediction of the effects on station coordinates due to each 10 m of longitude offset of the fixed station for polar site.

ζ^{\max} :	65°	70°	75°	80°	85°	90°
Rx :	0.257	0.238	0.220	0.200	0.181	0.161 (10 ⁻⁶ rad)

In Figure 6.10a are presented the affine transformation parameter values for different maximum zenith angles, for the equatorial and polar sites.

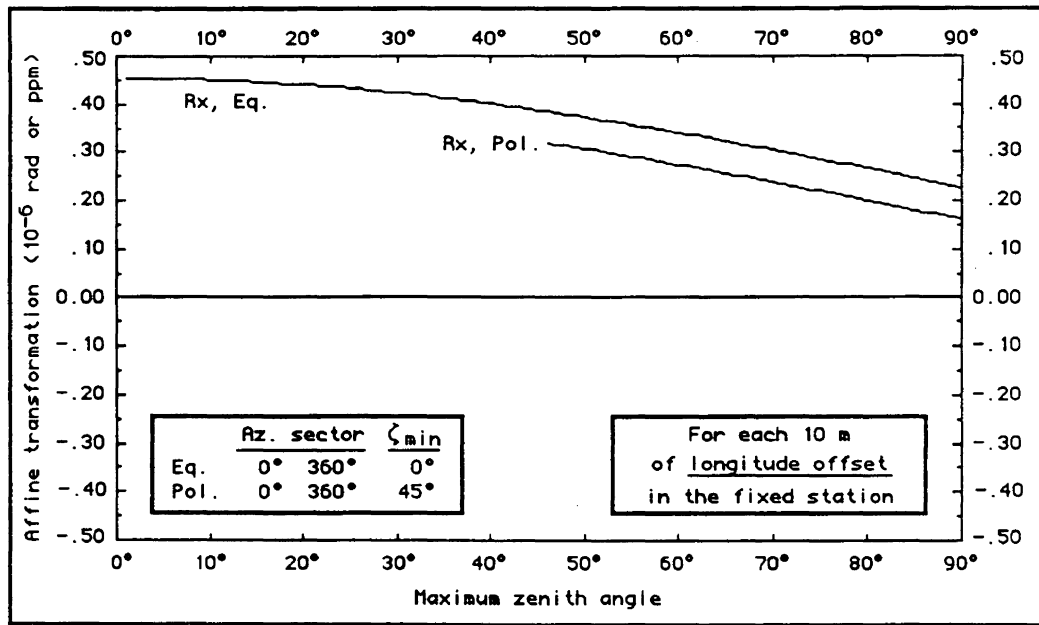


Figure 6.10a: Affine transformation parameters due to a longitude offset in the fixed station. Equatorial and polar sites.

Table 6.9c: DIPOPSIM prediction of the effects on station coordinates due to each 10 m of longitude offset of the fixed station for mid-latitude site.

ζ_{max} :	65°	70°	75°	80°	85°	90°	
Rx :	0.445	0.419	0.393	0.367	0.339	0.312	(10 ⁻⁶ rad)
Sx :	-0.148	-0.154	-0.160	-0.165	-0.168	-0.171	(ppm)
Sy :	0.028	0.030	0.031	0.032	0.032	0.033	(ppm)

In Figure 6.10b are presented the affine transformation parameter values for different maximum zenith angles, for the mid-latitude site.

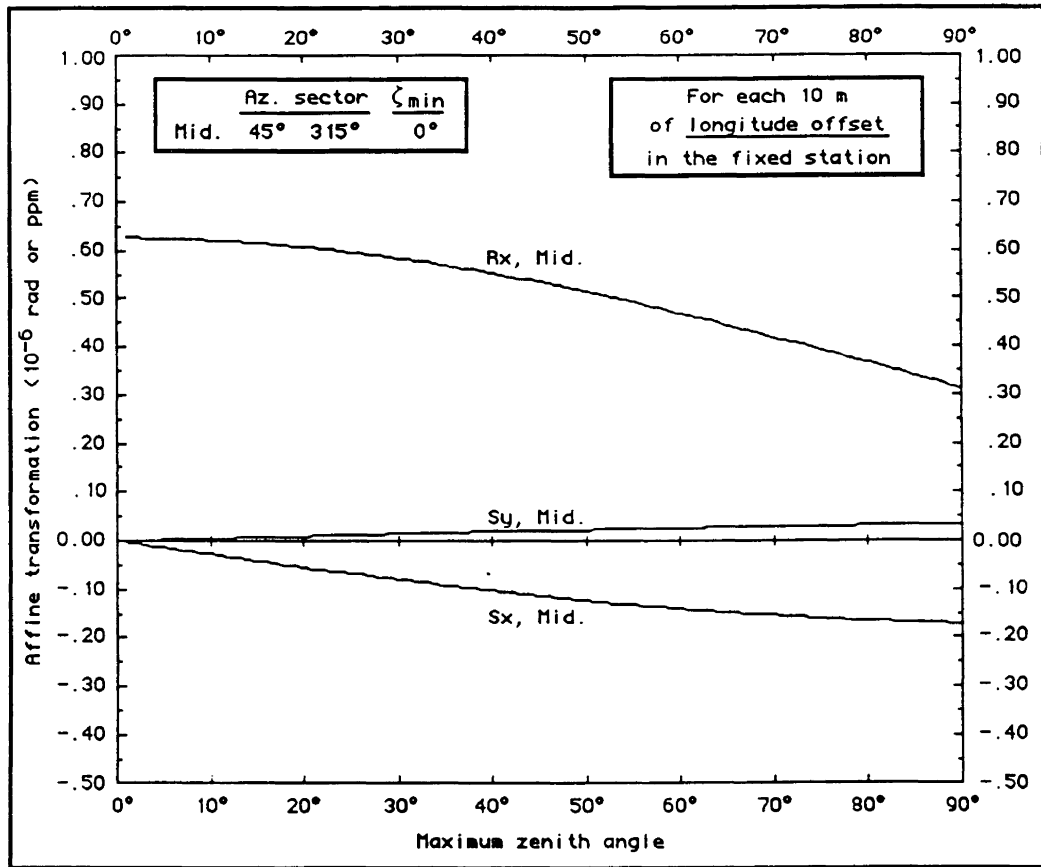


Figure 6.10b: Affine transformation parameters due to a longitude offset in the fixed station.
Mid-latitude site.

Table 6.9d: DIPOPSIM prediction of the effects on station coordinates due to each 10 m of longitude offset of the fixed station for CERN satellite configuration.

ζ_{max} :	65°	70°	75°	80°	85°	90°	
Rx :	0.003	0.001	0.000	0.000	-0.001	-0.001	(10^{-6} rad)
Kx :	-0.228	-0.239	-0.247	-0.255	-0.261	-0.266	(ppm)
Ky :	-0.508	-0.528	-0.546	-0.561	-0.574	-0.585	(ppm)

In Figure 6.10c are presented the affine transformation parameter values for different maximum zenith angles, for the CERN satellite configuration.

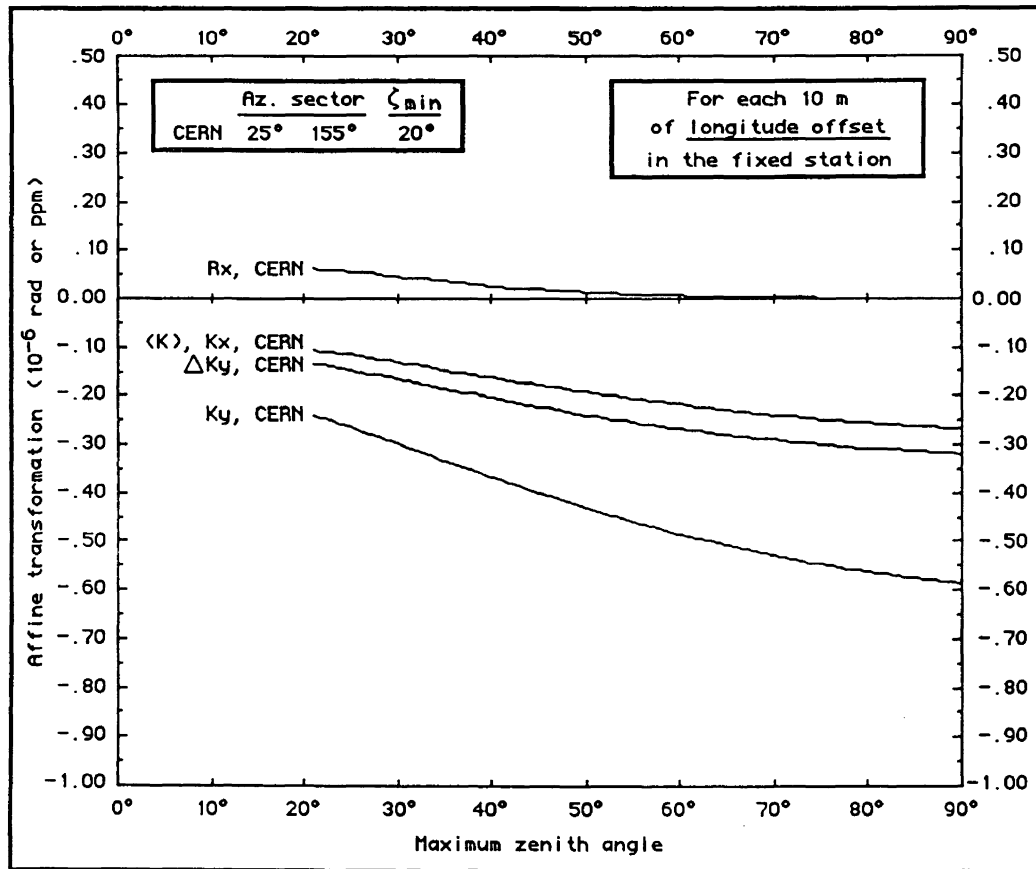


Figure 6.10c: Affine transformation parameters due to a longitude offset in the fixed station. CERN satellite configuration.

From the results presented in Tables 6.8 and 6.9 and Figures 6.9 and 6.10, we can highlight the following conclusions related to the effects of offset in the latitude and the longitude of the fixed station.

General trends (applicable for both horizontal coordinate offsets)

- 1) Effect is proportional to horizontal offset of the fixed station;
- 2) Effect is proportional to baseline length;
- 3) Magnitude of the affine parameters is sensitive to both zenith and particularly azimuth integration boundaries;

- 4) Main effect is a rotation effect affecting the station height;
- 5) Positive rotation (in the left-handed local geodetic system) is around a horizontal axis of azimuth $\alpha_1 - 90^\circ$, where α_1 is the azimuth of the horizontal offset;
- 6) The only case, where the (absolute) values of the effect of an offset in latitude and an offset in longitude are equal, is that for an all-azimuth observation sky;
- 7) Absolute value of the rotation decreases with an increase of the maximum zenith angle ζ^{\max} ;
- 8) Non-uniform azimuth satellite distribution causes effects on the horizontal coordinates;
- 9) The most affected horizontal coordinate is in the direction of the horizontal symmetry axis of the satellite sky distribution;
- 10) This effect on the horizontal coordinates can be illustrated by two directional scale factors or by two horizontal shear parameters;
- 11) The two directional scales have the same sign and the two horizontal shear parameters have opposite sign;
- 12) Directional scale factors appear when the horizontal symmetry axis of the satellite sky distribution is in the direction of the horizontal offset of the fixed station;
- 13) The directional scale factors are positive if α_1 is 180° away from the azimuth of the horizontal symmetry axis of the satellite sky distribution (α_{sym});
- 14) Horizontal shear parameters appear when the horizontal symmetry axis of the satellite sky distribution is perpendicular to the direction of the horizontal offset of the fixed station;
- 15) The shear along the y-axis is positive if $\alpha_{\text{sym}} - \alpha_1 = 90^\circ$ (or -270°), and negative if $\alpha_{\text{sym}} - \alpha_1 = 270^\circ$ (or -90°);
- 16) The absolute value of these parameters increases as ζ^{\max} increases;
- 17) For an extremely non-uniform satellite sky distribution these secondary effects can be as large as the main (rotation) effect.

The generalization of the effects on the station coordinates due to a horizontal offset of the fixed station of any direction can be constructed with the results presented for the latitude and longitude offset of the fixed station. The reader is referred to section VI.4 for the mathematical formulation.

6.7 Offset in the height of the fixed station

Tables 6.10a, 6.10b, 6.10c and 6.10d contain the predictions of the effects of a height offset of the fixed station for the equatorial, polar, mid-latitude and CERN satellite configurations, respectively.

Table 6.10a: DIPOPSIM prediction of the effects on station coordinates due to each 10 m of height offset of the fixed station for equatorial site.

ζ^{\max} :	65°	70°	75°	80°	85°	90°
K :	-0.285	-0.262	-0.239	-0.216	-0.193	-0.170 (ppm)

Table 6.10b: DIPOPSIM prediction of the effects on station coordinates due to each 10 m of height offset of the fixed station for polar site.

ζ^{\max} :	65°	70°	75°	80°	85°	90°
K :	-0.252	-0.231	-0.210	-0.188	-0.166	-0.145 (ppm)

In Figure 6.11a are presented the affine transformation parameter values for different maximum zenith angles, for the equatorial and polar sites.

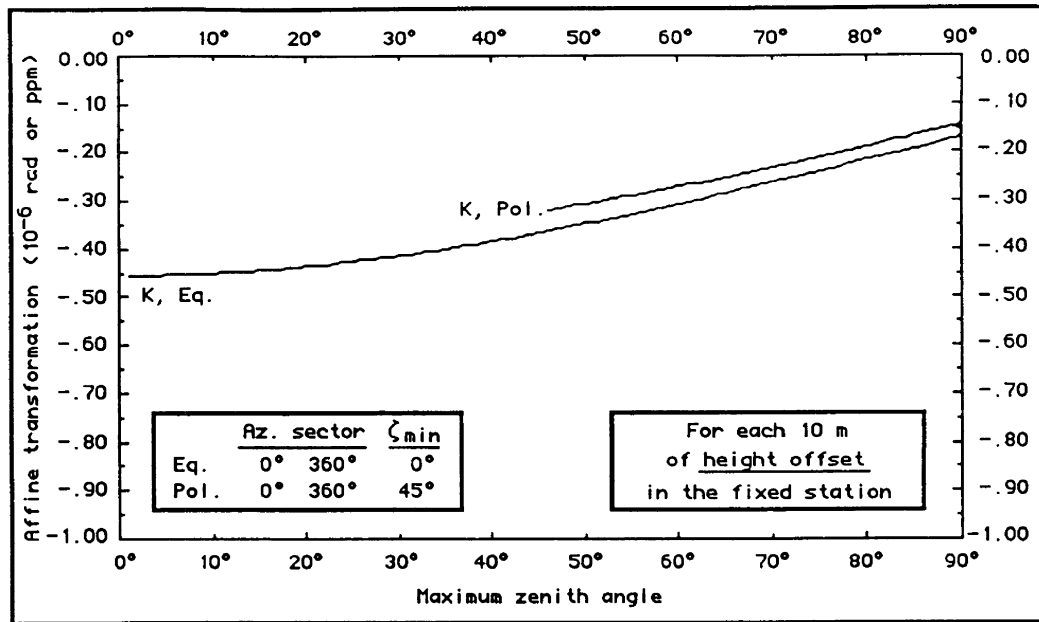


Figure 6.11a: Affine transformation parameters due to a height offset in the fixed station. Equatorial and polar sites.

Table 6.10c: DIPOPSIM prediction of the effects on station coordinates due to each 10 m of height offset of the fixed station for mid-latitude site.

ζ_{max} :	65°	70°	75°	80°	85°	90°	
K :	-0.285	-0.262	-0.239	-0.216	-0.193	-0.170	(ppm)
ΔK_x :	0.000	-0.001	-0.001	-0.001	-0.001	-0.002	(ppm)
R_y :	-0.069	-0.073	-0.076	-0.080	-0.083	-0.085	(10^{-6} rad)

In Figure 6.11b are presented the affine transformation parameter values for different maximum zenith angles, for the mid-latitude site.

Table 6.10d: DIPOPSIM prediction of the effects on station coordinates due to each 10 m of height offset of the fixed station for CERN satellite configuration.

ζ_{max} :	65°	70°	75°	80°	85°	90°	
K :	-0.283	-0.260	-0.237	-0.214	-0.192	-0.169	(ppm)
ΔK_y :	-0.013	-0.017	-0.022	-0.027	-0.032	-0.038	(ppm)
R_x :	-0.233	-0.243	-0.253	-0.261	-0.269	-0.276	(10^{-6} rad)

In Figure 6.11c are presented the affine transformation parameter values for different maximum zenith angles, for the CERN satellite configuration.

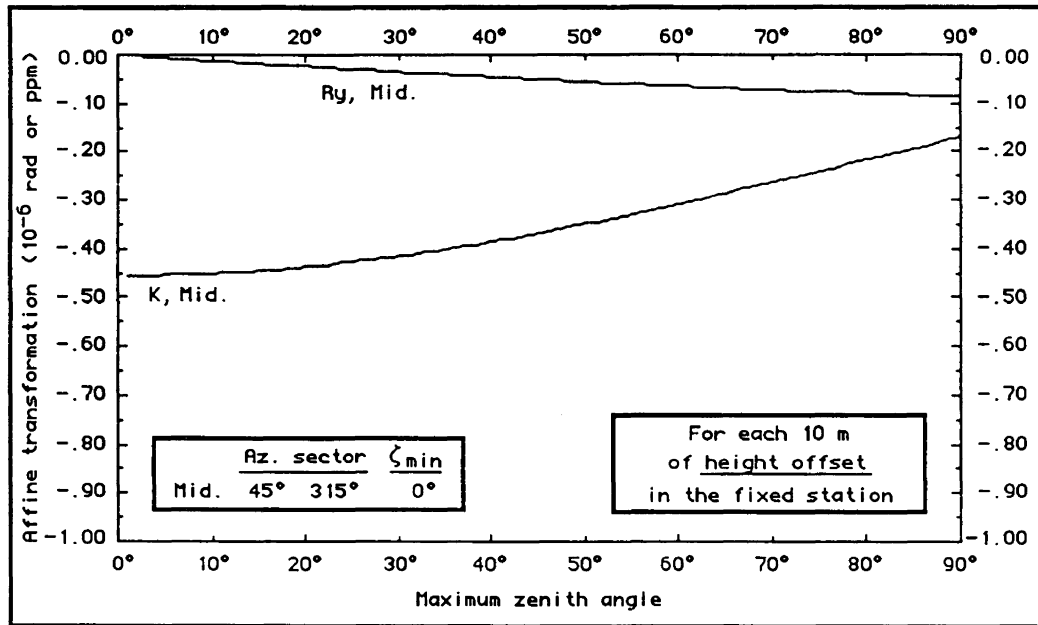


Figure 6.11b: Affine transformation parameters due to a height offset in the fixed station. Mid-latitude site.

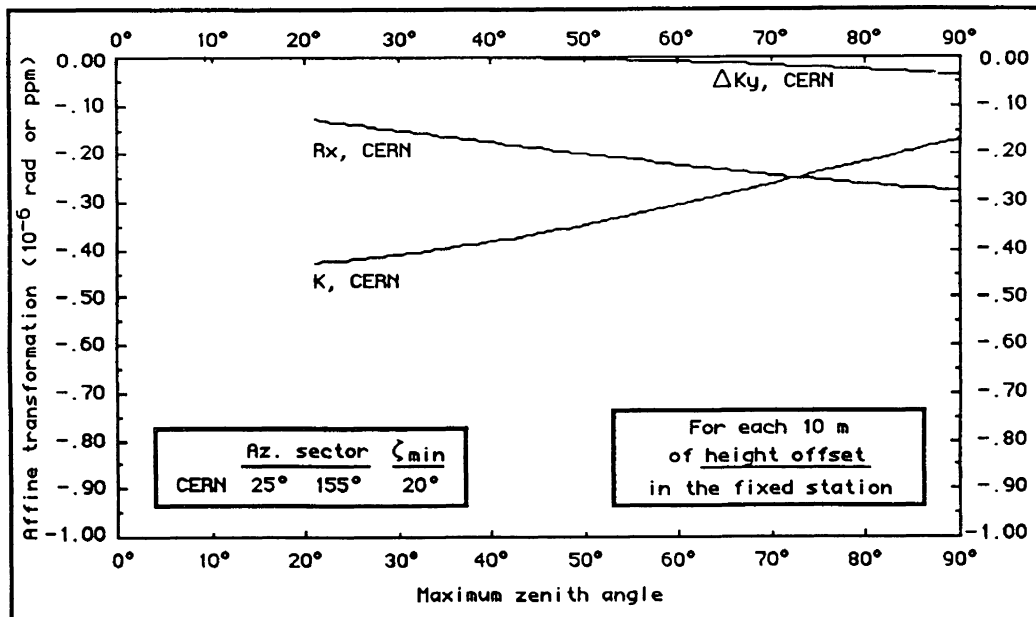


Figure 6.11c: Affine transformation parameters due to a height offset in the fixed station. CERN satellite configuration.

From the results presented in Tables 6.10 and Figures 6.11, we can highlight the following conclusions related to the effects of the offset in the height of the fixed station.

General trends

- 1) Effect is proportional to height offset of the fixed station;
- 2) Effect is proportional to baseline length;
- 3) Main effect is a horizontal scale effect affecting the horizontal coordinates;
- 4) If height of the fixed station is too high, the baseline (network) length is too short;
- 5) Horizontal scale effect is uniquely a function of zenith angle boundaries (equatorial and mid-latitude sites show the same horizontal scale effect);
- 6) Absolute value of the horizontal scale effect decreases with an increase of the maximum zenith angle ζ^{\max} ;
- 7) Absolute value of the horizontal scale effect decreases with an increase of the minimum zenith angle ζ_{\min} ;
- 8) Polar situation is the best one (larger ζ_{\min} , all observations are at high zenith angles);
- 9) Non-uniform azimuth satellite distribution causes the baseline (network) to rotate (effect on height);
- 10) Rotation is around the horizontal axis perpendicular to the horizontal symmetry axis of the satellite sky distribution. More precisely, the positive rotation (in the left-handed local geodetic system), for a positive height offset, is around a horizontal axis having an azimuth of: $\alpha_{\text{sym}} + 90^\circ$; where α_{sym} is the azimuth of the horizontal symmetry axis of the satellite sky distribution;
- 11) Absolute value of the rotation increases with an increase of ζ^{\max} ;
- 12) The larger the azimuth sector without satellite observations, the larger the rotation (for poor satellite geometry the rotation can be as large as the horizontal scale);
- 13) A small directional horizontal scale effect is also introduced by a non-uniform azimuth

satellite distribution;

- 14) The directional horizontal scale effect is in the direction of the horizontal symmetry axis of the satellite sky distribution;
- 15) The directional horizontal scale has the sign of the main horizontal scale effect.

Chapter 7

Summary and conclusions

7.1 Summary of results

It has been demonstrated that even with the deployment of the full GPS constellation of 24 satellites the distribution of the visible satellites in the observer's sky will not be uniform. Because of the inclination of 55° of all orbits the satellite coverage will be a function of the site latitude. For example, the satellite distribution over the sky at low latitudes will be almost uniform; at mid-latitudes practically no observations will be possible in the northern direction (roughly between azimuths 315° and 45°); and at high latitude sites, only observations between elevation angles 0° and 45° can be made.

The prototype satellite constellation can produce even worse satellite sky distributions because of its limited number of satellites and its non-uniform spatial distribution of satellites.

To study the impact of GPS satellite sky distribution on the propagation of errors in precise relative positioning (for baseline length less than about 100 km), we have improved and extended a simulation technique proposed by Geiger of ETH Zürich. The technique is powerful in the sense that neither real nor simulated observations are necessary. This is an efficient tool for making generalizations particularly where the behaviour of the covariance matrix and the effects of many kinds of systematic errors have to be investigated as a function of different satellite sky distributions.

The extensions to the technique that were made included: 1) adding a tropospheric zenith delay parameter to the basic station coordinates and clock parameter; 2) introducing in the

least squares adjustments process the single difference observation biases due to important systematic errors; 3) modification of the integration limit definition to be able to take into account different satellite sky distributions; 4) automating the technique by the coding of a computer program.

The behaviour of the covariance matrix, the confidence ellipsoid and the correlation coefficients, as functions of the unknown parameters selected in the least squares solution (station coordinates, clock and tropospheric zenith delay parameters) and as a function of the satellite sky distribution have been investigated. The propagation of some important systematic errors (relative tropospheric refraction error, absolute ionospheric refraction error, offset in the horizontal coordinates of the fixed station and offset in the height of the fixed station) on relative positioning results as a function of satellite sky distribution has been studied, as well.

A theoretical investigation of the elements of the normal equation matrix permitted the monitoring of the high correlation existing among the station height, the clock parameter and the tropospheric zenith delay parameter. The analysis of the interaction of the normal equation matrix with the element of the normal equation vectors allowed us to predict that similarity transformation parameters (3 translations, 3 rotations and 1 scale factor) will not be sufficient to represent the station coordinate discrepancies introduced by some of the studied systematic errors for non-uniform azimuth satellite distributions. Additional affine transformation parameters (directional horizontal scale factors and horizontal shear parameters) are then necessary.

The assessment of the prediction results has been carried out by comparing them to the results obtained by adding controlled systematic error to real GPS data originating from 4 different campaigns having 3 different satellite sky distributions. A total of 14 tests have

been performed and the comparisons reveal that the orientation of the confidence ellipsoid can be obtained with an accuracy better than $\pm 10^\circ$ and that the shape of the confidence ellipsoid can be recovered with an associated error of less than 15%. It has also been shown that the error in the predictions of the primary effects and the secondary effects (2 to 9 times smaller than the associated primary effects) of the studied systematic errors are about $\pm 25\%$ of the real values. Remember that the rationale for the selection of Geiger's technique was its capability to produce generalized studies of the behaviour of the covariance matrix as well as the effects of systematic errors on the station coordinates for different satellite sky distributions. To get a precise answer about the effects of a particular error for a particular satellite sky distribution standard simulation techniques ("real observations and controlled additive errors" or "simulated observations", see section 3.4) or the hybrid simulation technique suggested in section 7.3, should be used.

The comparison of the prediction results with those obtained from real GPS data processing has also permitted us to prove once more the equivalence of the single difference observation mode modelled with a clock parameter (as used in the predictions) and the double difference observation mode (as used in the processing of real GPS data).

Generalized study of the behaviour of the covariance matrix and of the effects of the systematic errors has been carried out for 4 different satellite configurations. The first 3 configurations are representative of the expected satellite configurations for the equatorial, mid-latitude and polar sites when the complete GPS constellation will be in place. The fourth configuration is representative of a poor satellite sky distribution produced by the prototype GPS constellation.

Illustrations of these satellite configurations are presented in the first column of Tables 7.1 and 7.2. Table 7.1a is a summary of the behaviour of the covariance matrix for the 4

satellite sky distributions with an elevation mask angle of 20° ($\zeta^{\max}: 70^\circ$). Table 7.1b is similar to Table 7.1a but the elevation mask angle is 10° ($\zeta^{\max}: 80^\circ$). In Tables 7.1, the term "und." means undefined. Tables 7.2a and 7.2b contain a summary of the effects of the studied systematic errors for the same 4 satellite configurations with an elevation mask angle of 20° ($\zeta^{\max}: 70^\circ$) and 10° ($\zeta^{\max}: 80^\circ$), respectively.

The following paragraphs are presented to outline the content of the summary tables. The numbers between parentheses are the minimum and the maximum values reached by the parameters presented in the corresponding table. This description will permit us to appreciate the magnitude of the effects as well as the change in the magnitude of the effects as a function of satellite configuration.

It is shown that the semi-major axis of the confidence ellipsoid points towards the satellite sky coverage. For a full hemisphere of observations ($\zeta^{\max}: 90^\circ$), the ratio semi-major/semi-minor axes (a/c) is 2 and gets larger as the satellite sky distribution degrades (2.3 to 5.7). A non-uniform azimuth satellite distribution makes the ratio of the semi-major and the semi-minor axes (b/c) greater than 1 (1.4 to 1.9) and creates correlations among the horizontal coordinates and the station height and the clock parameter (-0.32 to 0.93). Even with a uniform satellite sky distribution, high correlation exists between the station height and the clock parameter (0.89 to 0.98).

The introduction of a tropospheric zenith delay parameter increases the elevation angle of the semi-major axis of the confidence ellipsoid, enhances the ratio of the semi-axes of the confidence ellipsoid (a/c: 5.6 to 32.0, b/c: 1.4 to 3.0) and gives rise to a high correlation between this parameter and the station height, and the clock parameter (-0.87 to -1.00).

Table 7.1a: Summary of the behaviour of the covariance matrix for different satellite configurations; $\zeta^{\max}: 70^\circ$.

$\zeta^{\max}: 70^\circ$	Orientation		Ratio		Correlation	
		Hor.				
Parameters:	x, y, z, t	x, y, z, t, tr	x, y, z, t	x, y, z, t, tr	x, y, z, t	x, y, z, t, tr
 Equatorial	Ea: 90° α_a : und. Eb: 0° α_b : und. Ec: 0° α_c : und.	Ea: 90° α_a : und. Eb: 0° α_b : und. Ec: 0° α_c : und.	a/c: 2.7 b/c: 1.0	a/c: 9.8 b/c: 1.0	z,t: 0.96 z,tr: -0.99 z,tr: -0.96	z,t: 0.99 tr,t: -0.99 z,tr: -0.96
 Polar	Ea: 90° α_a : und. Eb: 0° α_b : und. Ec: 0° α_c : und.	Ea: 90° α_a : und. Eb: 0° α_b : und. Ec: 0° α_c : und.	a/c: 5.7 b/c: 1.0	a/c: 32.0 b/c: 1.0	z,t: 0.98 z,t: 1.00 tr,t: -1.00 z,tr: -0.98	z,t: 1.00 tr,t: -1.00 z,tr: -0.98
 Mid-latitude	Ea: 85° α_a : 180° Eb: -5° α_b : 180° Ec: 0° α_c : 90°	Ea: 89° α_a : 180° Eb: -1° α_b : 180° Ec: 0° α_c : 90°	a/c: 3.0 b/c: 1.4	a/c: 11.0 b/c: 1.4	z,t: 0.96 x,t: -0.28 x,z: -0.15 tr,t: -0.99 z,tr: -0.96 x,tr: 0.04	z,t: 0.99 x,t: -0.08 x,z: -0.08 tr,t: -0.99 z,tr: -0.96 x,tr: 0.04
 CERN	Ea: 48° α_a : 90° Eb: -42° α_b : 90° Ec: 0° α_c : 0°	Ea: 82° α_a : 90° Eb: -8° α_b : 90° Ec: 0° α_c : 0°	a/c: 4.3 b/c: 1.9	a/c: 10.8 b/c: 3.0	z,t: 0.93 y,t: 0.90 y,z: 0.69 z,t: 0.99 y,t: 0.44 y,z: 0.40 tr,t: -0.96 z,tr: -0.95 y,tr: -0.20	z,t: 0.99 y,t: 0.44 y,z: 0.40 tr,t: -0.96 z,tr: -0.95 y,tr: -0.20

Table 7.1b: Summary of the behaviour of the covariance matrix for different satellite configurations; $\zeta^{\max}: 80^\circ$.

$\zeta^{\max}: 80^\circ$	Orientation		Ratio		Correlation	
		Hor.				
Parameters:	x, y, z, t	x, y, z, t, tr	x, y, z, t	x, y, z, t, tr	x, y, z, t	x, y, z, t, tr
 Equatorial	Ea: 90° α_a : und. Eb: 0° α_b : und. Ec: 0° α_c : und.	Ea: 90° α_a : und. Eb: 0° α_b : und. Ec: 0° α_c : und.	a/c: 2.3 b/c: 1.0	a/c: 5.6 b/c: 1.0	z,t: 0.93 z,t: 0.98 tr,t: -0.97 z,tr: -0.91	z,t: 0.98 tr,t: -0.97 z,tr: -0.91
 Polar	Ea: 90° α_a : und. Eb: 0° α_b : und. Ec: 0° α_c : und.	Ea: 90° α_a : und. Eb: 0° α_b : und. Ec: 0° α_c : und.	a/c: 4.1 b/c: 1.0	a/c: 11.7 b/c: 1.0	z,t: 0.94 z,t: 0.99 tr,t: -0.98 z,tr: -0.94	z,t: 0.99 tr,t: -0.98 z,tr: -0.94
 Mid-latitude	Ea: 84° α_a : 180° Eb: -6° α_b : 180° Ec: 0° α_c : 90°	Ea: 89° α_a : 180° Eb: -1° α_b : 180° Ec: 0° α_c : 90°	a/c: 2.6 b/c: 1.4	a/c: 6.1 b/c: 1.4	z,t: 0.92 x,t: -0.32 x,z: -0.15 tr,t: -0.99 z,tr: -0.91 x,tr: 0.04	z,t: 0.99 x,t: -0.12 x,z: -0.10 tr,t: -0.96 z,tr: -0.91 x,tr: 0.04
 CERN	Ea: 40° α_a : 90° Eb: -50° α_b : 90° Ec: 0° α_c : 0°	Ea: 71° α_a : 90° Eb: -19° α_b : 90° Ec: 0° α_c : 0°	a/c: 3.9 b/c: 1.7	a/c: 6.3 b/c: 2.7	z,t: 0.89 y,t: 0.93 y,z: 0.68 z,t: 0.97 y,t: 0.64 y,z: 0.51 tr,t: -0.87 z,tr: -0.88 y,tr: -0.22	z,t: 0.97 y,t: 0.64 y,z: 0.51 tr,t: -0.87 z,tr: -0.88 y,tr: -0.22

Table 7.2a: Summary of the effects of some important systematic errors in precise relative positioning for different satellite configurations; $\zeta^{\max} : 70^\circ$.

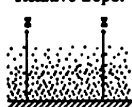
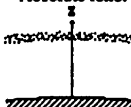


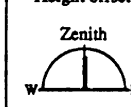
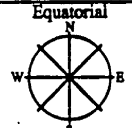
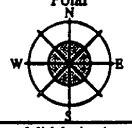
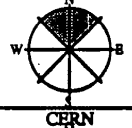
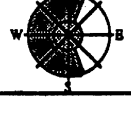

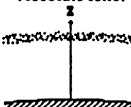
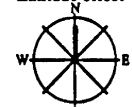
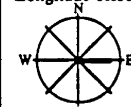
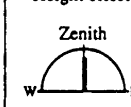
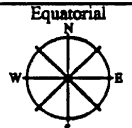
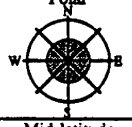
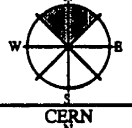
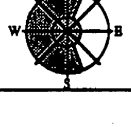
$\zeta^{\max} : 70^\circ$	Relative tropo. 	Absolute iono. 	Latitude offset 	Longitude offset 	Height offset 
Units:	mm per 1 mm of error	ppm or 10^{-6} rad per 1×10^{17} e/m ²	ppm or 10^{-6} rad per 10 m of offset	ppm or 10^{-6} rad per 10 m of offset	ppm or 10^{-6} rad per 10 m of offset
Equatorial 	Tz: 2.59	K: -0.629	Ry: -0.305	Rx: 0.305	K: -0.262
Polar 	Tz: 3.87	K: -0.685	Ry: -0.238	Rx: 0.238	K: -0.231
Mid-latitude 	Tz: 2.59 Tx: -0.01	K: -0.629 ΔKx : 0.001 Ry: 0.131	Ry: -0.190 Kx: 0.156 Ky: 0.030	Rx: 0.419 Sx: -0.154 Sy: 0.030	K: -0.262 ΔKx : -0.001 Ry: -0.073
CERN 	Tz: 2.92 Ty: 0.18	K: -0.633 ΔKy : 0.025 Rx: 0.426	Ry: -0.567 Sx: -0.239 Sy: 0.509	Rx: 0.001 Kx: -0.239 Ky: -0.528	K: -0.260 ΔKy : -0.017 Rx: -0.243

Table 7.2b: Summary of the effects of some important systematic errors in precise relative positioning for different satellite configurations; $\zeta^{\max} : 80^\circ$.

$\zeta^{\max} : 80^\circ$	Relative tropo. 	Absolute iono. 	Latitude offset 	Longitude offset 	Height offset 
Units:	mm per 1 mm of error	ppm or 10^{-6} rad per 1×10^{17} e/m ²	ppm or 10^{-6} rad per 10 m of offset	ppm or 10^{-6} rad per 10 m of offset	ppm or 10^{-6} rad per 10 m of offset
Equatorial 	Tz: 4.18	K: -0.708	Ry: -0.267	Rx: 0.267	K: -0.216
Polar 	Tz: 6.51	K: -0.757	Ry: -0.200	Rx: 0.200	K: -0.188
Mid-latitude 	Tz: 4.19 Tx: -0.04	K: -0.708 ΔKx : 0.002 Ry: 0.141	Ry: -0.166 Kx: 0.167 Ky: 0.032	Rx: 0.367 Sx: -0.165 Sy: 0.032	K: -0.216 ΔKx : -0.001 Ry: -0.080
CERN 	Tz: 4.93 Ty: 0.67	K: -0.711 ΔKy : 0.041 Rx: 0.452	Ry: -0.485 Sx: -0.255 Sy: 0.526	Rx: 0.000 Kx: -0.255 Ky: -0.561	K: -0.214 ΔKy : -0.027 Rx: -0.261

The effect of systematic errors on the station coordinates can be illustrated by simple similarity transformations for all azimuth satellite distributions, e.g., equatorial and polar site cases. However for a non-uniform azimuth satellite distribution, the recovery of the effects of some systematic errors on the station coordinates can only be illustrated by additional affine transformation parameters (directional horizontal scale factors and horizontal shear parameters).

The effect of relative tropospheric zenith delay mismodelling is manifested by translation along the z-axis (2.6 mm to 6.5 mm per 1 mm of error). A secondary effect explained by a translation along the horizontal symmetry axis of the satellite distribution is also present for non-uniform azimuth satellite distributions (-0.04 mm to 0.7 mm per 1 mm of error). The tropospheric magnification factor (translation value divided by relative tropospheric zenith delay error) is independent of the baseline length and azimuth.

The effect of absolute ionospheric refraction is manifested by a horizontal scale parameter (-0.63 to -0.76 ppm per 1×10^{17} el/m² of TEC). Secondary effects explained by a rotation (0.13 to 0.45×10^{-6} rad per 1×10^{17} el/m² of TEC) around the horizontal axis perpendicular to the horizontal symmetry axis of the satellite distribution and a directional differential scale effect (0.001 to 0.04 ppm per 1×10^{17} el/m² of TEC) along the horizontal symmetry axis of the satellite distribution are also present for non-uniform azimuth satellite distributions.

The effect of an offset in horizontal coordinates of the fixed station is manifested by a rotation (absolute values: 0.00 to 0.57×10^{-6} rad per 10 m of offset) around a horizontal axis perpendicular to the horizontal offset direction. Secondary effects explained by directional scales (absolute values: 0.03 to 0.56 ppm per 10 m of offset) along the x and y axes and shear parameters (absolute values: 0.03 to 0.53 ppm per 10 m of offset) affecting

both horizontal coordinate axes are also present for non-uniform azimuth satellite distributions.

The effect of a height offset of the fixed station is manifested by a horizontal scale parameter (-0.19 to -0.26 ppm per 10 m of offset). Secondary effects explained by a rotation (-0.07 to -0.26×10^{-6} rad per 10 m of offset) around the horizontal axis perpendicular to the horizontal symmetry axis of the satellite distribution and a directional differential scale effect (-0.001 to -0.03 ppm per 10 m of offset) along the horizontal symmetry axis of the satellite distribution are also present for non-uniform azimuth satellite distributions.

To end this section, let us mention that the study of the behaviour of the covariance matrix and the relative tropospheric zenith delay error effects, presented in this study for relative positioning, can directly be used for absolute positioning analysis.

7.2 Implications for interpretation of GPS results

The summary of our findings presented in the previous section contains the answers to the questions raised in Chapter 1. This study has allowed us to gain an appreciation of the impact of the satellite sky distribution on the behaviour of the covariance matrix and on the propagation of some important systematic errors in the positioning results. The study has also provided a guide to know the tolerance values which systematic errors should not exceed in order to achieve a predetermined positioning accuracy level.

The results of the study can also be used for the selection of the most appropriate elevation mask angle. This means finding the best compromise between the need of decorrelation between station height, clock parameter and tropospheric zenith delay parameter (giving a strengthening of the formal accuracy) provided by low elevation angle observations and the

effects of some systematic errors which get larger at low elevation angles.

The above example directly suggests that the developed simulation program can be used as a generalized planning tool, giving not only covariance information but also the influence of important systematic errors on positioning results. If a more detailed pre-analysis is required, rather than a generalized study, the use of the hybrid simulation technique, suggested in section 7.3, would be more appropriate to give precise answers for a particular satellite sky distribution. The developed method should be used in place of the GDOP (Geometric Dilution Of Precision) criteria to characterize the strength of a satellite sky distribution. The reasons to reject the use of a criteria based on GDOP value for static positioning analysis purposes are: 1) the GDOP parameter is uniquely based on one epoch of observations; this is not a good indicator of the satellite sky distribution for a complete session; and 2) this parameter only gives (partial) information-just that about the matrix $(A^T A)^{-1}$; in other words this does not give at all any indication about the way systematic errors propagate into the station coordinates.

For pre-analysis or post-analysis purposes, it is important to note that the effects on the station coordinates from the different systematic errors are cumulative. Moreover, one must keep in mind that: 1) the relative tropospheric zenith delay error is most likely to change from station to station and from session to session; 2) the TEC value which scales the absolute ionospheric refraction error assumed constant for all the stations during one session might change from session to session; and 3) the horizontal and vertical offset of a fixed station is common to the whole network of a GPS campaign. Also important to note once more is the fact that the tropospheric magnification factors are independent of baseline length and all the other effects of the studied systematic errors are baseline length dependent.

The comparison of the station coordinate differences between two different GPS campaigns (same network measured for example at two different times in the year) might not only contain real displacements but also systematic biases which have been propagated into the station coordinates differently. Such spurious displacements may be due to the change in magnitude of the systematic errors in the observations themselves but can also be due to satellite sky distributions being different during the two distinct GPS campaigns. The latter situation is a particular consequence when using the present changing satellite constellation as it builds up to the fully operational constellation. So, even constant systematic errors from campaign to campaign, like the offset in the coordinates of a fixed station, will be propagated differently into the station coordinates.

7.3 Suggestions for further work

This section contains some recommendations for future work which can be carried out as a continuation of the present study. We start with suggestions which do not require any (or minor) modifications to the present simulation program. Secondly, suggestions requiring substantial modifications related to the assumptions used in Geiger's simulation technique are provided and finally, suggestions for research requiring other simulations or mathematical tools are mentioned.

The following items belong to the first group of suggestions:

- The calculation of residuals to detect any possible error-specific signatures or trends in the residual shape as a function of satellite elevation angle and azimuth;
- The calculation of the a posteriori variance factor;
- The influence of a priori information of the standard deviation of unknowns as a function of the number of observations and the precision of the observations;
- The study of the ability of the tropospheric zenith delay parameter to absorb error other than the tropospheric error;

- The study of the propagation of errors where clock parameters alone are estimated in the least squares adjustments (clock synchronization).

In the second group of suggestions, we can mention:

- The study of the impact of satellite sky distribution on the propagation of random tropospheric refraction error;
- The consideration of a density distribution function other than one based on the assumption of homogeneity.

For the third group of suggestions, the use of the standard simulation technique could be used to study:

- The influence of satellite orbit errors on positioning results as a function of satellite sky distribution;
- The influence of carrier phase ambiguity free solution (additive parameters in the solution) as a function of satellite sky distribution;
- The phase ambiguity resolution performance (in terms of their standard deviations and their contamination by systematic errors) as a function of satellite sky distribution;
- The effects on longer baselines; recognizing that the observation geometry is different and that the local vertical and the satellite sky distribution of simultaneous observations at two very distant sites are significantly different.

To improve the execution time of the standard simulation technique it is suggested that in the calculation of the misclosure vector, the artificially contaminated observations be replaced by the formulae of biases in single difference observations as developed in Appendix II. This hybrid simulation technique would avoid the creation, the storage, the reading and the manipulation of a large number of observations required for the standard simulation technique.

References

- Ashkenazi, V. and J. Yau (1986). "Significance of discrepancies in the processing of GPS data with different algorithms." *Bulletin Géodésique*, 60, pp. 229-239.
- Beutler, G. and W. Gurtner (1987a). "The influence of atmospheric refraction on the evaluation of GPS phase observations." Astronomical Institute Report No. 16, University of Berne, Switzerland.
- Beutler, G. and W. Gurtner (1987b). "Influence of ionospheric refraction on the evaluation of GPS phase observations." Astronomical Institute Internal Report, University of Berne, Switzerland.
- Beutler, G., I Bauersima, W. Gurtner, M. Rothacher, T. Schildknecht and A. Geiger (1988). "Atmospheric refraction and other important biases in GPS carrier phase observations." *Atmospheric Effects on Geodetic Space Measurements*, School of Surveying Monograph No. 12, University of New South Wales, Kensington, Australia, pp. 15-43.
- Beutler, G., W. Gurtner, M. Rothacher, T. Schildknecht and I. Bauersima (1986). "Using the Global Positioning System (GPS) for high precision geodetic surveys: Highlights and problem areas." *Proceedings of IEEE PLANS '86*, Las Vegas, U.S.A., 4-7 November, pp. 243-250.
- Blewitt, G. (1989). "Carrier phase ambiguity resolution for the Global Positioning System applied to geodetic baselines up to 2000 km." *Journal of Geophysical Research*, 94(B8), pp. 10187-10203.
- Bock, Y., R.I. Abbot, C.C. Counselman, S.A. Gourevitch and R.W. King (1985). "Establishment of three-dimensional geodetic control by interferometry with the Global Positioning System." *Journal of Geophysical Research*, 90(B9), pp. 7689-7703.
- Bock, Y., R.I. Abbot, C.C. Counselman, S.A. Gourevitch, R.W. King and A.R. Paradis (1984). "Geodetic accuracy of the Macrometer model V-1000." *Bulletin Géodésique*, 58, pp. 211-221.
- Campbell, J., T. Maniatis, A. Müller, J. Vierbuchen and F.J. Lohmar (1986). "On the generation of ionospheric refraction corrections for single frequency GPS-measurements." *Proceedings of the Fourth International Geodetic Symposium on Satellite Positioning*, Austin, U.S.A., 28 April - 2 May, pp. 631-645.
- Coco, D.S. and J.R. Clynch (1982). "The variability of the tropospheric range correction due to water vapor fluctuations." *Proceedings of the Third International Geodetic Symposium on Satellite Doppler Positioning*, Las Cruces, U.S.A., 8-12 February, pp. 475-495.
- Davis, J.L. (1986). "Atmospheric effects on radio interferometry." Ph.D. Dissertation Harvard College Observatory, Cambridge, U.S.A. Air Force Geophysics Laboratory AFGL-TR-86-0243.

- Dong, D.-N. and Y. Bock (1989). "Global Positioning System network analysis with phase ambiguity resolution applied to crustal deformation studies in California." *Journal of Geophysical Research*, 94(B4), pp. 3949-3966.
- EOS News (1989) "Solar cycle 22 continues strong climb." EOS, Transactions of the American Geophysical Union, 70(26), 27 June, p. 674.
- Geiger, A. (1988). "Simulating disturbances in GPS by continuous satellite distribution." *Journal of Surveying Engineering*, 114(4), pp. 182-194.
- Geiger, A. (1987). "Simplified error estimation of satellite positioning." Paper presented at the GPS Technology Workshop, Jet Propulsion Laboratory, Pasadena, 23 March.
- Georgiadou, Y. (1987). "Results of the Port Alberni GPS survey 1986." Geophysics Division Internal Report, Geological Survey of Canada, Ottawa, Canada.
- Georgiadou, Y. and A. Kleusberg (1988). "On the effect of ionospheric delay on geodetic relative GPS positioning." *Manuscripta Geodaetica*, 13, pp. 1-8.
- Gervaise, J., M. Mayoud, G. Beutler and W. Gurtner (1985). "Test of GPS on the CERN-LEP control network." *Proceedings of Inertial, Doppler and GPS Measurements for National and Engineering Surveys*, München, FRG, 1-3 July, pp. 337-358.
- Goad, C.C. and L. Goodman (1974). "A modified Hopfield tropospheric refraction correction model." Paper presented at the Fall Annual Meeting of the American Geophysical Union, San Francisco, U.S.A., 12-17 December.
- Gough, R., E. Frei, J. Reiner and R. Scherrer (1987). "The WM101 and PoPs™: An investigation in the Swiss Alps." Wild Magnavox Satellite Survey Company.
- Gouldman, M.W., B.R. Hermann and E.R. Swift (1986). "Absolute station position solutions for sites involved in the Spring 1985 GPS precision baseline test." *Proceedings of the Fourth International Geodetic Symposium on Satellite Positioning*, Austin, U.S.A., 28 April - 2 May, pp. 1045-1057.
- Green, G.B., P.D. Massatt and N.W. Rhodus (1989). "The GPS 21 primary satellite constellation." *Navigation: Journal of the (U.S.) Institute of Navigation*, 36(1), pp. 9-24.
- Gurtner, W., G. Beutler, I. Bauersima and T. Schildknecht (1985). "Evaluation of GPS carrier difference observations: The Bernese second generation software package." *Proceedings of the First International Symposium on Precise Positioning with the Global Positioning System*, Rockville, U.S.A., 15-19 April, pp. 363-372.
- Hartmann, G.K. and R. Leitingner (1984). "Range errors due to ionospheric and tropospheric effects for signal frequencies above 100 MHz." *Bulletin Géodésique*, 58, pp. 109-136.

- Henson, D.J. and E.A. Collier (1986). "Effects of the ionosphere on GPS relative geodesy." *Proceedings of IEEE PLANS '86*, Las Vegas, U.S.A., 4-7 November, pp. 230-237.
- Herring, T.A. (1986). "Precision of vertical position estimates from very long baseline interferometry." *Journal of Geophysical Research*, 91(B9), pp. 9177-9182.
- Hopfield, H.S. (1972). "Tropospheric range error parameters: Further studies." Applied Physics Laboratory Technical Memorandum CP 015, The Johns Hopkins University, Silver Spring, U.S.A.
- Kleusberg, A. and L. Wanninger (1987). "Analysis of the Juan de Fuca GPS survey 1986." Department of Surveying Engineering Technical Report No. 127, University of New Brunswick, Fredericton, Canada.
- Klobuchar, J.A. (1975). "A first order, worldwide, ionospheric, time-delay algorithm." Air Force Cambridge Research Laboratories AFCRL-TR-75-0502, Air Force Surveys in Geophysics, No. 324, Hanscom AFB, U.S.A.
- Lachapelle, G., N. Beck and P. Héroux (1982). "NAVSTAR/GPS single point positioning using pseudo-range and Doppler observations." *Proceedings of the Third International Geodetic Symposium on Satellite Doppler Positioning*, Las Cruces, U.S.A., 8-12 February, pp. 1079-1091.
- Lichten, S.M. and J.S. Border (1987). "Strategies for high-precision Global Positioning System orbit determination." *Journal of Geophysical Research*, 92(B12), pp. 12,751-12,762.
- Lindlohr, W. and D.E. Wells (1985). "GPS design using undifferenced carrier beat phase observations." *Manuscripta Geodetica*, 10, pp. 255-295.
- Meyer, T.E., G.T. Tennis, J.A. Slater and B.J. DeNoyer (1986). "DMAHTC GPS point positioning software: Initial results." *Proceedings of the Fourth International Geodetic Symposium on Satellite Positioning*, Austin, U.S.A., 28 April - 2 May, pp. 1029-1043.
- Milbert, D.G. and W.G. Kass (1985). "Network adjustment of correlated coordinate difference observations." *Proceedings of the First International Symposium on Precise Positioning with the Global Positioning System*, Rockville, U.S.A., 15-19 April, pp. 657-665.
- Moffett, J.B. (1971). "Program requirements for two minute integrated Doppler satellite navigation solution." Applied Physics Laboratory Technical Memorandum TG-819-1, The Johns Hopkins University, Silver Spring, U.S.A.
- Rush, C.M. (1979). "Transionospheric radio propagation." *Aerospace Propagation Media Modelling and Prediction Schemes for Modern Communications, Navigation and Surveillance Systems*, AGARD Lecture Series No. 99, pp. 4.1- 4.28.
- Santerre, R. (1988). "DIPOP 2.0 (MPROC and PPROC): Structure, modifications and user guide." Department of Surveying Engineering Technical Memorandum No. 20, University of New Brunswick, Fredericton, Canada.

- Schaffrin, B. and E. Grafarend (1986). "Generating classes of equivalent linear models by nuisance parameter elimination - Applications to GPS observations." *Manuscripta Geodaetica*, 11, pp. 262-271.
- Vaníček, P., G. Beutler, A. Kleusberg, R.B. Langley, R. Santerre and D.E. Wells (1985). "DIPOP: Differential POsitioning Program package for the Global Positioning System." Department of Surveying Engineering Technical Memorandum No. 115, University of New Brunswick, Fredericton, Canada.
- Wells, D.E., N. Beck, D. Delikaraoglou, A. Kleusberg, E.J. Krakiwsky, G. Lachapelle, R.B. Langley, M. Nakiboglu, K.-P. Schwarz, J.M. Tranquilla, P. Vaníček (1986). "*Guide to GPS positioning*." Canadian GPS Associates, Fredericton, Canada.

Appendix I

Magnitude of the systematic error sources

I.1 Relative tropospheric refraction

Errors in the tropospheric refraction delay correction can be introduced by the zenith delay modelling, the weakness of the mapping function and the presence of horizontal refractivity gradient. The error in the zenith delay modelling has the largest detrimental effect on data refraction reduction. We will present 3 examples of error sources affecting the correct modelling of the tropospheric zenith delay in relative positioning mode.

Meteorological measurements:

Miscalibration or improper operational uses of meteorological instruments is one source of error. Table I.1 illustrates the variation of Hopfield's [1972] tropospheric zenith delay for a pressure error of 1 mbar, a temperature error of 1°C and a relative humidity error of 1%, for different surface meteorological conditions.

Table I.1: Variation of Hopfield's tropospheric zenith delay due to pressure (P), temperature (T) and relative humidity (RH) errors.

P (mbar)	T (°C)	RH (%)	$ \text{d}t_{\text{trop}}(0)/\Delta P $ (mm/1mbar)	$ \text{d}t_{\text{trop}}(0)/\Delta T $ (mm/1°C)	$ \text{d}t_{\text{trop}}(0)/\Delta RH $ (mm/1%)
1013.25	0	100	2	5	1
1013.25	15	100	2	11	1
1013.25	30	100	2	20	4
1013.25	0	50	2	3	0
1013.25	15	50	2	5	1
1013.25	30	50	2	10	4
1013.25	0	0	2	0	0
1013.25	15	0	2	0	1
1013.25	30	0	2	1	4

Decorrelation of wet tropospheric zenith delay:

Using a data base consisting of 22 summer days of meteorological measurements from 7 radiosonde stations and surface meteorological observations located in a semi-arid area of West Texas, Coco and Clynch [1982] have reported that: the standard deviation of the residuals of the Hopfield's zenith range correction model was about 4 cm and the standard deviation of the interstation residuals for interstation distances of 50-100 km had a value of about 3 cm. This implies that one would incur about the same error going from surface measurements to a wet tropospheric range correction value as from a wet tropospheric range correction value at one station to a wet tropospheric range correction value at another station about 50 to 100 km away.

Temperature inversion:

Geiger [1988] has reported that an error of about 4 cm was introduced in the calculated zenith delay from a layered tropospheric model due to temperature inversion condition occurring for a GPS test in a mountainous area near Turtmann (Swiss Alps). In this situation the higher station was installed above the inversion layer whose thickness was evaluated to be about 600 m from cablecar meteo-measurements.

I.2 Total electron content

The total electron content (TEC) is defined as the integrated electron density in the zenith direction expressed in electrons/m² (el/m²). The total electron content is a function of many variables; among them are local time, season, geographic (geomagnetic) location, and state of solar and the Earth's magnetic activity.

Diurnal variation: The TEC is highest in most regions of the world within a few hours of local noon. In fact, the phase of the diurnal maximum rarely changes more than ± 1 hour

from a mean of 14 hours local time [Klobuchar, 1975]. On the other hand ionospheric delay, which is proportional to TEC, reaches a minimum between midnight and 5 a.m. local time. During nighttime there is a residual ionospheric effect of about 10-20% of the daytime value [Campbell et al., 1986].

Seasonal variation: The range correction is greatest in winter and equinoctial months and minimum in summer months [Rush, 1979].

Geographic (geomagnetic) location: The equatorial anomaly region, located approximately $\pm 20^\circ$ away from the geomagnetic equator, is the region where the greatest TEC values are encountered [Klobuchar, 1975]. Ionospheric effects at the equator are about 2 times larger than the effects at mid-latitudes [Henson and Collier, 1986].

11-year solar activity cycle: During times of maximum solar activity the ionospheric delay is 5 times larger than during times of solar lowest activity [Campbell et al., 1986]. The current solar cycle (22) began with a minimum in sunspot activity in September 1986. The coming solar maximum should occur in late 1989 to early 1990 and the size should be comparable to the previous record holder, cycle 19, which peaked in 1958 [EOS News, 1989].

Hartmann and Leitinger [1984] have depicted the extreme conditions as follows: The region of the world and the conditions where a single-frequency GPS user will encounter the greatest errors are: in the geomagnetic latitude region 20° - 30° N or S around local noon, around the equinoxes and for periods of high solar activity. TEC values of up to 2×10^{18} el/m² are typical in such conditions. At the other extreme, TEC values as low as 10^{16} el/m² or even less could be encountered in the region of the so-called main trough in electron content, during winter nighttime for periods of low solar activity which are

geomagnetically quiet. Under these conditions the main trough in electron content is found in the geomagnetic latitude region 60° to 70°.

I.3 Absolute station coordinates

It is possible to get absolute station coordinates from GPS. Table I.2 summarizes some GPS static absolute positioning results obtained by different investigators using different approaches.

Table I.2: Summary of some GPS static absolute positioning results.

Investigator/ Year	receiver/ clock	observable/ differencing	time span/ # of sat.	satellite orbit source	accuracy/ comparison with
Gough et al. [1987]	WM 101 Crystal	L1 C/A-code range	3 hr 4-5 sat.	broadcast	about 15 m precise terrestrial
Gouldman et al. [1986]	TI 4100 Cs, Rb, H2	L1&L2 P-code range	7-8 hr 7 sat.	NSWC	1 to 4 m NNSS, VLBI, NAD
Meyer et al. [1986]	TI 4100 H2	L1&L2 carrier phase Doppler	7-8 hr 7 sat.	NSWC	1 to 8 m NAD
Bock et al. [1985]	V-1000 Crystal	L1 carrier phase S.D. between sat.	4-5 hr 4-5 sat.	NSWC and Aero Service	5 to 10 m (*)
Bock et al. [1984]	V-1000 Cs, H2	L1 carrier phase one way	7-10 hr 4-5 sat.	NSWC	2 to 5 m NNSS (1 m-level)
Bock et al. [1984]	V-1000 Crystal	L1 carrier phase S.D. between sat.	3-6 hr 4-5 sat.	NSWC	2 to 8 m NNSS (1 m-level)
Lachapelle et al. [1982]	STI 5010 Cesium	L1&L2 P-code range	10-18 hr 4 sat., seq.	broadcast	5 to 10 m NNSS
Lachapelle et al. [1982]	STI 5010 Cesium	L1&L2 carrier phase Doppler	10-18 hr 4 sat., seq.	broadcast	5 to 10 m NNSS

Abbreviation keys: Cs: Cesium, Rb: Rubidium, H2: Hydrogen Maser, NSWC: Naval Surface Weapons Center, NNSS: Navy Navigation Satellite System (Transit), VLBI: Very Long Baseline Interferometry, NAD: North American Datum, S.D.: single difference, seq.: sequencing channel receiver.

(*) Absolute point positioning of 3 stations and intercomparison between those coordinates by transferring the absolute coordinates of point 1 to the other stations using GPS relative-position vectors.

The main errors in these absolute positioning attempts come from the frequency stability (receiver and/or satellites) and the satellite orbit errors. The advantages of the technique are that it provides absolute coordinates in the satellite reference frame and the information is potentially available anytime and everywhere to all GPS users.

The selection of a fixed station whose absolute coordinates are already known in horizontal and vertical datum or determined by the Transit Doppler absolute positioning technique is another solution. However this a priori information is not always available (everywhere in the world) and care must be taken to transform those coordinates into the GPS satellite reference frame. If the a priori information about the height comes from a vertical datum, the orthometric height must be reduced to ellipsoid height with the knowledge of the geoid undulation. Geoid undulations, in some parts of the world, are not always precisely determined.

Appendix II

Biases in single difference observations

II.1 Relative tropospheric zenith delay error

We can express the range error due to tropospheric refraction ($dtrop(\zeta)$) as a function of the tropospheric zenith delay ($dtrop(0)$) and a mapping function ($m(\zeta)$).

$$dtrop(\zeta) = m(\zeta) dtrop(0) \quad (\text{II.1})$$

The (between-receiver) single difference tropospheric delay ($\Delta dtrop$) is:

$$\begin{aligned} \Delta dtrop_{12} &= dtrop(\zeta_2) - dtrop(\zeta_1) \\ \Delta dtrop_{12} &= m(\zeta_2) dtrop_2(0) - m(\zeta_1) dtrop_1(0) \end{aligned} \quad (\text{II.2})$$

Similarly, we can write the single difference tropospheric zenith delay, as follows:

$$\Delta dtrop(0)_{12} = dtrop_2(0) - dtrop_1(0) \quad (\text{II.3})$$

From eqn. (II.3), we can write:

$$dtrop_2(0) = \Delta dtrop(0)_{12} + dtrop_1(0) \quad (\text{II.4})$$

Introducing eqn. (II.4) in eqn. (II.2), we obtain:

$$\begin{aligned} \Delta dtrop_{12} &= m(\zeta_2) \Delta dtrop(0)_{12} + m(\zeta_2) dtrop_1(0) - m(\zeta_1) dtrop_1(0) \\ \Delta dtrop_{12} &= m(\zeta_2) \Delta dtrop(0)_{12} + [m(\zeta_2) - m(\zeta_1)] dtrop_1(0) \end{aligned} \quad (\text{II.5})$$

The first term of the right hand side of eqn. (II.5) is the relative tropospheric delay. It is the impact of the bias of the relative tropospheric delay correction that we will analyse in this section. The second term is the absolute tropospheric delay. In fact, $dtrop_1(0)$ can be

interpreted as the common (absolute) tropospheric zenith delay error affecting both stations. It will be shown that the effect of the (absolute) tropospheric delay is functionally close to the effect of the (absolute) ionospheric delay. We will come back to this analogy in section II.2.

Because our study is restricted to short baseline length (< 100 km), we can assume: $m(\zeta_2) \approx m(\zeta_1) \approx m(\zeta)$ and $\zeta_2 \approx \zeta_1 \approx \zeta$. Then the relative tropospheric delay can be expressed as follows (for convenience the subscripts of equation (II.5) have been dropped):

$$\Delta dtrop \approx m(\zeta) \Delta dtrop(0) \quad (II.6)$$

The bias in the single difference observation due to relative tropospheric zenith delay (correction) error is:

$$\varepsilon \Delta \Phi(\zeta) = \varepsilon \Delta dtrop \approx m(\zeta) \varepsilon \Delta dtrop(0) \quad (II.7a)$$

A documentation of the magnitude of potential error sources in the relative tropospheric zenith delay correction is presented in section I.1.

Figure II.1 is the graphical representation of the situation for an observation at zenith and an observation at some arbitrary zenith angle. Point P_1 represents the position of the station held fixed in the GPS relative positioning adjustment process. Point P_2 represents the real position of the free station.

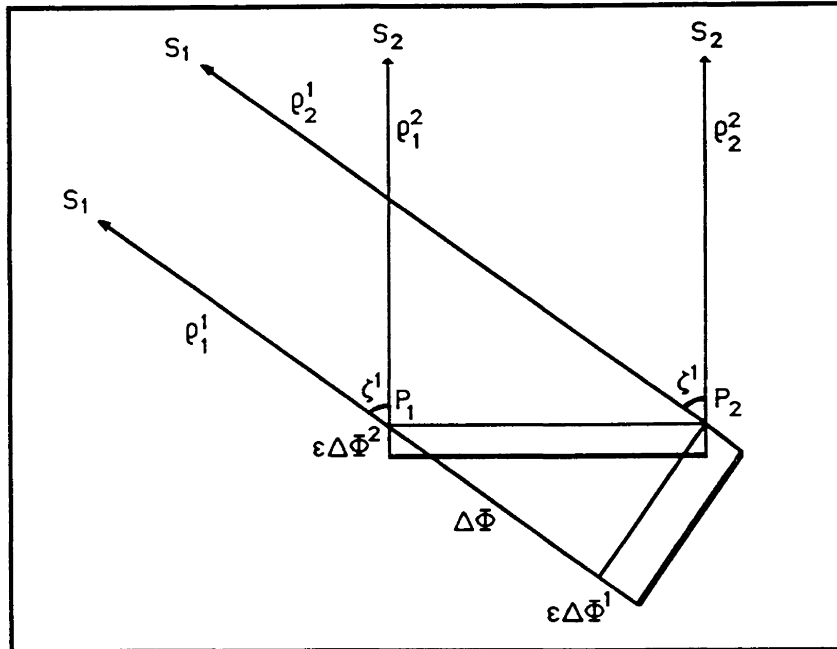


Figure II.1: Bias in single difference observation due to relative tropospheric zenith delay error.

The derivative of the single difference observation equation with respect to the relative tropospheric zenith error (noted as tr in the sequel) is (recall the observation equation (3.2) and eqn. (II.6)):

$$\partial \Delta \Phi / \partial tr \approx m(\zeta) \quad (\text{II.8a})$$

Tropospheric refraction mapping functions

Different mapping functions have been developed throughout the years. However, remember that we need an accurate mapping function which will allow an easy evaluation of the integration terms $[e_i \epsilon \Delta \Phi]$ and $[e_s e_i]$ (Chapter 4). We have compared, in Table II.1, four different mapping functions:

- 1) Flat Earth assumption: $\sec \zeta$

- 2) Hopfield (HOPF) prescribed form [Moffett, 1971]: $\text{cosec}[(E^2 + \theta^2)^{1/2}]$
 where:
 E is the elevation angle (degrees);
 θ equals 2.5° and 1.5° for the dry and the wet components, respectively.
- 3) Hartmann and Leitinger [1984] (H&L): $(1 - b \tan^2 \zeta + 1.5b^2 \tan^4 \zeta) \sec \zeta$
 where:
 $b = 0.85 h^{\text{atm}}/R_e \approx 1.1 \times 10^{-3}$;
 h^{atm} is the height of the centre of gravity for a vertical column of air (8 km);
 R_e is the Earth's radius (6,378 km).
- 4) The Modified Hopfield model mapping function (MHOPF) developed by Goad and Goodman [1974] is a rather complicated function expressed in series of coefficients obtained by a Taylor's series approximation relating the height, above the station, of a trajectory point in the atmosphere as a function of its range and elevation angle. Note that the coefficients are a function of the surface temperature and that a temperature of 15°C has been used in the calculation of Table II.1. This form will be obviously too complicated for our integration purpose, so we will not use it except for comparison values for the other mapping functions. This mapping function is not perfect but this is considered to be a fair approximation of the reality to assess the performance of the three other and simpler mapping functions.

Table II.1: Tropospheric refraction mapping function values as a function of zenith angle. MHOPF: [Goad and Goodman, 1974], HOPF: [Moffett, 1971], H&L: [Hartmann and Leitinger, 1984]. $\Delta(\%)$ is the difference with respect to MHOPF value.

ζ	E	MHOPF	$\sec \zeta$	$\Delta(\%)$	HOPF	$\Delta(\%)$	H&L	$\Delta(\%)$
0°	90°	1.000	1.000	(0.0)	1.000	(0.0)	1.000	(0.0)
10°	80°	1.016	1.016	(0.0)	1.016	(0.0)	1.016	(0.0)
20°	70°	1.064	1.064	(0.0)	1.064	(0.0)	1.064	(0.0)
30°	60°	1.154	1.155	(0.1)	1.154	(0.0)	1.154	(0.0)
40°	50°	1.304	1.305	(0.1)	1.304	(0.0)	1.304	(0.0)
50°	40°	1.553	1.556	(0.2)	1.553	(0.0)	1.553	(0.0)
60°	30°	1.994	2.000	(0.3)	1.994	(0.0)	1.994	(0.0)
70°	20°	2.900	2.924	(0.8)	2.902	(0.1)	2.901	(0.0)
75°	15°	3.807	3.864	(1.5)	3.813	(0.2)	3.808	(0.0)
80°	10°	5.571	5.759	(3.4)	5.589	(0.3)	5.571	(0.0)
85°	5°	10.227	11.474	(12.2)	10.266	(0.4)	10.208	(-0.2)

Only the "dry" mapping function is presented for MHOPF and HOPF.

The term $\sec\zeta$ starts to give large discrepancies for $\zeta > 70^\circ$. The discrepancy at $\zeta: 70^\circ$ is about 1% and at $\zeta: 85^\circ$ the discrepancy is about 12%. So, for zenith angles greater than 70° , this simple flat Earth mapping function is not recommended. The H&L mapping function is better (smaller Δ) and easier to integrate than the HOPF mapping function. The maximum discrepancy is -0.2% at $\zeta: 85^\circ$. However, this mapping function is not recommended for $\zeta > 85^\circ$, due to its inaccurate values produced at those zenith angles. Even if H&L function contains 3 terms dependent on ζ , each of them are easy to integrate.

Having selected Hartmann and Leitinger's mapping function, equations (II.7a) and (II.8a) will have the following form:

$$\varepsilon\Delta\Phi(\zeta) \approx (1 - b \tan^2\zeta + 1.5b^2 \tan^4\zeta) \sec\zeta \varepsilon\Delta\text{trop}(0) \quad (\text{II.7b})$$

$$\partial\Delta\Phi/\partial\tau \approx (1 - b \tan^2\zeta + 1.5b^2 \tan^4\zeta) \sec\zeta \quad (\text{II.8b})$$

Hartmann and Leitinger's mapping function and the "sec ζ " function are plotted in Figure II.7a.

Summary of assumptions and approximations:

- 1) For short baseline length ($\ell < 100$ km) and small station height difference ($\zeta_0 \approx 90^\circ$) we can assume that the zenith angles at both stations for the same satellite are identical ($\zeta_2 \approx \zeta_1 \approx \zeta$), i.e., $m(\zeta_2) \approx m(\zeta_1) \approx m(\zeta)$, see eqn. (II.6). This means that the local verticals at the stations are practically parallel and the parallactic angle at the satellite is small.
- 2) Hartmann and Leitinger's mapping function, eqn. (II.8b), is an approximation of the "true" tropospheric mapping function.
- 3) The use of the mapping function is restricted to zenith angles smaller than 85° , see Table II.1.

The effect of these assumptions and approximations are evaluated in Chapter 5 (Comparison of predictions with results from real GPS data) along with the other assumptions used in the simulation technique.

II.2 Absolute ionospheric refraction error

The single layer model is used to account for the ionospheric refraction error. This model assumes that all the free electrons in the atmosphere are concentrated in a spherical layer of infinitesimal thickness at height h^{ion} of about 350 km above the Earth's surface. Furthermore, the total electron content (TEC), defined as the integrated electron density in the zenith direction, is assumed uniform in the layer. Figure II.2 allows the visualization of the situation.

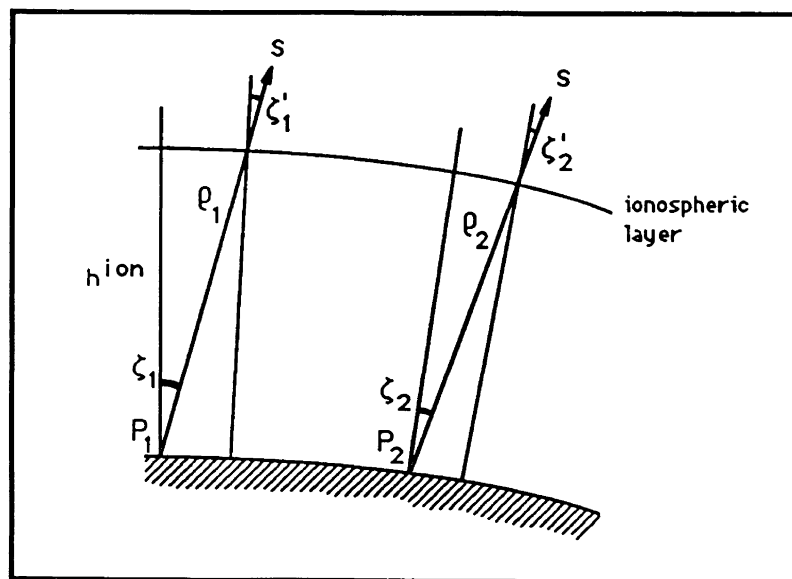


Figure II.2: Zenith angles at 2 different stations and at the infinitesimally thick ionospheric layer.

The ionospheric phase advance (dion), expressed in metres, is given by Hartmann and Leitinger [1984]:

$$\text{dion} = -(40.28/f^2) \text{ TEC sec}\zeta' \quad (\text{II.9})$$

where:

f: the carrier frequency (Hz)

TEC: total electron content (electrons/m² or el/m²)

ζ': zenith angle at the height of the ionospheric layer (h^{ion})

The expression for the ionospheric group delay is identical to the ionospheric phase advance, except for the sign. Typical TEC values may range from 0.5x10¹⁷ to 5x10¹⁷ el/m². Extreme values as low as 1x10¹⁶ el/m² and as large as 2x10¹⁸ el/m² can be reached (see section I.2 for more details). For the GPS L1 frequency (1.57542x10⁹ Hz) and a TEC equal to 1x10¹⁷ el/m², the ionospheric phase advance at the zenith is equal to -1.623 m; at zenith angle ζ: 70° (ζ': 63°) the phase advance is -3.575 m.

It is widely believed that the ionospheric refraction error will cancel once the (between-receiver) single difference is formed (relative positioning) especially for short baselines where we can assume TEC values identical above the two observing sites. This is not exactly true, because the ionospheric zenith angle at station P₁ (ζ'₁) is not exactly equal to the ionospheric zenith angle at station P₂ (ζ'₂) and because of the magnitude of the ionospheric zenith delay (or phase advance). If the ionospheric phase advance is not corrected the single difference observation will be biased by:

$$\varepsilon\Delta\Phi(\zeta'_1, \zeta'_2) = -(40.28/f^2) \text{ TEC} (\text{sec}\zeta'_2 - \text{sec}\zeta'_1) \quad (\text{II.10})$$

To express the above formula in term of zenith angle (ζ₁), we have: 1) to define ζ' as a function of ζ and h^{ion} or better yet express directly secζ' as a function of ζ and h^{ion}; and 2)

to formulate ζ_2 as a function of ζ_1 , ℓ and α_0 ; where ℓ and α_0 are the length and the azimuth of the baseline, respectively.

Before to go ahead with this mathematical development, we should notice the similarity between the last term of eqn. (II.5b) representing the absolute tropospheric refraction error and eqn. (II.10). The analogy between $m(\zeta)$ and $\sec\zeta'$, and $d_{\text{trop}}(0)$ and $[-(40.28/f^2) \text{TEC}]$ is obvious. However, because we usually apply a tropospheric refraction correction to the observations, based at least on standard meteorological values which can account for at least 90% of the total tropospheric effect, this leads us to a maximum absolute tropospheric zenith delay error of about 20 cm (10% of 2.3 m). This maximum value is about 8 times smaller than the absolute ionospheric zenith delay produced by the condition stated at the beginning of this section (L_1 frequency, TEC: 1×10^{17} el/m²). Because of the close functional relationship between the ionospheric mapping function $\sec\zeta'$ and the tropospheric mapping function ($\sim \sec\zeta$), we can expect that the impact of the absolute tropospheric refraction into the station coordinates will also be about 8 times smaller than the effect of the absolute ionospheric refraction presented in section 6.4. For this reason, the absolute tropospheric refraction effect is assumed negligible and will not be considered in our study.

Now, let us return to the development of equation (II.10).

The rigorous equation relating ζ' to ζ is given by:

$$\zeta' = \arcsin [R_e \sin\zeta / (R_e + h^{\text{ion}})] \quad (\text{II.11a})$$

where: R_e is the Earth's radius (6,378 km).

This equation has been obtained from the following sine rule:

$$\sin\zeta' = R_e \sin\zeta / (R_e + h^{\text{ion}}) \quad (\text{II.11b})$$

Klobuchar [1975] has introduced an approximate linear formula accurate to 0.2° for ζ smaller than 80°; to 0.4° at ζ : 85°; and to 0.3° at ζ : 90°. This formula has been fitted for h^{ion} equal to 350 km:

$$\zeta' \approx \zeta + 4 - [445 / (110 - \zeta)] \quad (\text{II.12})$$

where: ζ and ζ' are expressed in degrees.

Table II.2 gives the values of ζ' as a function of ζ , as well as the values of $\sec\zeta$ and $\sec\zeta'$, for h^{ion} equal to 350 km.

Table II.2: Zenith angle at the ionospheric layer height (ζ') as a function of the zenith angle at the Earth's surface (ζ) and values of $\sec\zeta$ and $\sec\zeta'$; h^{ion} : 350 km.

ζ :	0.0°	10.0°	20.0°	30.0°	40.0°	50.0°	60.0°	70.0°	80.0°	90.0°
ζ' :	0.0°	9.5°	18.9°	28.3°	37.5°	46.6°	55.2°	63.0°	69.0°	71.4°
$\sec\zeta$:	1.000	1.015	1.064	1.155	1.305	1.556	2.000	2.924	5.759	∞
$\sec\zeta'$:	1.000	1.014	1.057	1.136	1.261	1.455	1.751	2.201	2.790	3.141

However for this investigation, we are more interested in an expression giving directly $\sec\zeta'$ as a function of ζ . We can express $\sec\zeta'$ using the rigorous equation for ζ' :

$$\sec\zeta' = \sec \{ \arcsin [R_e \sin\zeta / (R_e + h^{\text{ion}})] \} \quad (\text{II.13a})$$

or

$$\sec\zeta' = [R_e + h^{\text{ion}}] / [(R_e \cos\zeta)^2 + 2 R_e h^{\text{ion}} + (h^{\text{ion}})^2]^{1/2} \quad (\text{II.13b})$$

Equation (II.13a) has been obtained by applying the function "sec" to eqn. (II.11a) and eqn. (II.13b) has been evaluated with eqn. (II.11b) and the relation " $\cos^2\zeta = 1 - \sin^2\zeta$ ". The disadvantage of these equations is that it becomes very difficult to evaluate the

integration terms $[e_j \epsilon \Delta \Phi]$ (Chapter 4). Klobuchar [1975] has also developed an approximate formula for the evaluation of $\sec \zeta'$ which will be much easier to use in the integration formulae.

$$\sec \zeta' \approx 1 + 2 [(\zeta + 6) / 90]^3 \quad (\text{II.14})$$

where: ζ is expressed in degrees.

The formula has also been fitted for h^{ion} equal to 350 km. The inaccuracy of this formula is never different by more than 2% from the true value, for ζ smaller than 85° . For our integration purposes it will be more convenient to express ζ in radians and to fully develop the cubic term, as follows:

$$\sec \zeta' \approx A + B \zeta + C \zeta^2 + D \zeta^3 \quad (\text{II.15a})$$

where: ζ is expressed in radians and

$$\begin{aligned} A &= 1 + (2 / 3375) \approx 1.0006 \\ B &= 4 / (75 \pi) \approx 0.017 \\ C &= 16 / (10 \pi^2) \approx 0.16 \\ D &= 16 / \pi^3 \approx 0.52 \end{aligned}$$

The second step consists in expressing ζ_2 as a function of ζ_1 , the baseline length (ℓ) and the baseline azimuth (α_0). To do this we have followed the route traced by Beutler and Gurtner [1987b]. We start with the scalar product definition for the vectors ρ and R :

$$\cos \zeta = \vec{\rho} \cdot \vec{R} / (\rho R) \quad (\text{II.16})$$

Using this definition we can write:

$$\cos \zeta_2 - \cos \zeta_1 = [\vec{\rho}_2 \cdot \vec{R}_2 / (\rho_2 R_2)] - [\vec{\rho}_1 \cdot \vec{R}_1 / (\rho_1 R_1)] \quad (\text{II.17})$$

The left-hand side term can be written as:

$$\cos\zeta_2 - \cos\zeta_1 = -2 \sin[(\zeta_1 + \zeta_2)/2] \sin[(\zeta_2 - \zeta_1)/2] \quad (\text{II.18})$$

Because of the small difference between zenith angles ζ_1 and ζ_2 , for relatively short baselines in comparison with the Earth's radius (see Table II.3), we can use the following approximations:

$$\begin{aligned} \sin[(\zeta_1 + \zeta_2)/2] &\approx \sin\zeta_1 \\ \sin[(\zeta_2 - \zeta_1)/2] &\approx (\zeta_2 - \zeta_1)/2 \end{aligned} \quad (\text{II.19})$$

Then the left-hand side of eqn. (II.17) becomes:

$$\cos\zeta_2 - \cos\zeta_1 \approx -(\zeta_2 - \zeta_1) \sin\zeta_1 \quad (\text{II.20})$$

To evaluate the right-hand side of eqn. (II.17) we furthermore define the following terms:

$$\begin{aligned} \vec{\rho}_2 &= \vec{\rho}_1 - \vec{\ell} \\ \rho_2^{-1} &\approx \rho_1^{-1} \left[1 + \frac{(\vec{\rho}_1 \cdot \vec{\ell})}{\rho_1^2} \right] \\ \vec{R}_2 &= \vec{R}_1 + \vec{\ell} \\ R_1 &\approx R_2 \approx R_e \end{aligned} \quad (\text{II.21})$$

Then we can write:

$$\frac{\vec{\rho}_2 \cdot \vec{R}_2}{\rho_2 R_2} - \frac{\vec{\rho}_1 \cdot \vec{R}_1}{\rho_1 R_1} \approx \frac{(\vec{\rho}_1 - \vec{\ell}) \cdot (\vec{R}_1 + \vec{\ell}) \left(1 + \frac{(\vec{\rho}_1 \cdot \vec{\ell})}{\rho_1^2} \right) - (\vec{\rho}_1 \cdot \vec{R}_1)}{\rho_1 R_e} \quad (\text{II.22})$$

The vectors \vec{R}_1 , $\vec{\rho}_1$ and $\vec{\ell}$ can be defined, in the local geodetic system of station P_1 , as:

$$\begin{aligned} \vec{R}_1 &\approx (0, 0, R_e) \\ \vec{\rho}_1 &= \rho_1 (\cos\alpha \sin\zeta_1, \sin\alpha \sin\zeta_1, \cos\zeta_1) \\ \vec{\ell} &= \ell (\cos\alpha_0 \sin\zeta_0, \sin\alpha_0 \sin\zeta_0, \cos\zeta_0) \approx \ell (\cos\alpha_0, \sin\alpha_0, 0) \end{aligned} \quad (\text{II.23})$$

For writing simplicity we have omitted in eqn. (II.23b) the subscript "1" associated with the azimuth of the satellite (α). We have to keep the subscript associated with ζ to

distinguish it from ζ_2 (the zenith angle at station P_2). The far right-hand side of eqn. (II.23c) is obtained, by assuming a small baseline height component, i.e., $\zeta_0 \approx 90^\circ$, $\sin\zeta_0 \approx 1$ and $\cos\zeta_0 \approx 0$.

This gives us:

$$\begin{aligned}\vec{R}_1 \cdot \vec{\rho}_1 &\approx R_e \rho_1 \cos\zeta_1 \\ \vec{\rho}_1 \cdot \vec{\ell} &\approx \rho_1 \ell \sin\zeta_1 \cos(\alpha - \alpha_0) \\ \vec{R}_1 \cdot \vec{\ell} &\approx 0\end{aligned}\tag{II.24}$$

Introducing these scalar products in eqn. (II.22) and neglecting the terms having denominators $\rho_1 R_e$ and $\rho_1^2 R_e$, we get:

$$\begin{aligned}\frac{\vec{\rho}_2 \cdot \vec{R}_2}{\rho_2 R_2} - \frac{\vec{\rho}_1 \cdot \vec{R}_1}{\rho_1 R_1} &= \cos\zeta_2 - \cos\zeta_1 \\ &\approx \frac{\ell}{R_e} \sin\zeta_1 \cos(\alpha - \alpha_0) + \frac{\ell}{\rho_1} \sin\zeta_1 \cos\zeta_1 \cos(\alpha - \alpha_0)\end{aligned}\tag{II.25}$$

Combining equation (II.20) with (II.25), we finally get the sought equation (ζ_1 and ζ_2 being expressed in radians):

$$\zeta_2 \approx \zeta_1 - \ell R_e^{-1} \cos(\alpha - \alpha_0) - \ell \rho_1^{-1} \cos\zeta_1 \cos(\alpha - \alpha_0)\tag{II.26}$$

To give an idea of the angle difference between ζ_1 and ζ_2 , we present in Table II.3, the maximum absolute values expected for the second and third terms of equation (II.26). An average value of 22,000 km is assumed for ρ_1 .

Table II.3: Maximum absolute values for the ℓ/R_e term and the ℓ/ρ_1 term (the second and third terms of equation (II.26)).

ℓ :	1 km	10 km	100 km
ℓ/R_e :	32."3 (1.57X10 ⁻⁴ rad)	5.'4 (1.57X10 ⁻³ rad)	53.'9 (1.57X10 ⁻² rad)
ℓ/ρ_1 :	9."4 (4.55X10 ⁻⁵ rad)	1.'6 (4.55X10 ⁻⁴ rad)	15.'6 (4.55X10 ⁻³ rad)

Now, we have the elements to express the difference ($\sec\zeta'_2 - \sec\zeta'_1$) as a function of ζ_1 , ℓ and α_0 . From eqn. (II.15a) we write:

$$\sec\zeta'_1 \approx A + B \zeta_1 + C \zeta_1^2 + D \zeta_1^3 \quad (\text{II.15b})$$

$$\sec\zeta'_2 \approx A + B \zeta_2 + C \zeta_2^2 + D \zeta_2^3 \quad (\text{II.15c})$$

Substituting eqn. (II.26) in eqn. (II.15c), developing the ζ_2^2 and the ζ_2^3 terms, rejecting the terms with denominators larger than ρ_1 , and setting $\Delta\alpha_0 = \alpha - \alpha_0$, we get:

$$\begin{aligned} \sec\zeta'_2 \approx & A \\ & + B [\zeta_1 - \ell R_e^{-1} \cos\Delta\alpha_0 - \ell \rho_1^{-1} \cos\zeta_1 \cos\Delta\alpha_0] \\ & + C [\zeta_1^2 - 2 \ell R_e^{-1} \zeta_1 \cos\Delta\alpha_0 - 2 \ell \rho_1^{-1} \zeta_1 \cos\zeta_1 \cos\Delta\alpha_0] \\ & + D [\zeta_1^3 - 3 \ell R_e^{-1} \zeta_1^2 \cos\Delta\alpha_0 - 3 \ell \rho_1^{-1} \zeta_1^2 \cos\zeta_1 \cos\Delta\alpha_0] \end{aligned} \quad (\text{II.27})$$

The subtraction of eqn. (II.15b) from eqn. (II.27) gives:

$$\begin{aligned} \sec\zeta'_2 - \sec\zeta'_1 \approx & B [- \ell R_e^{-1} \cos\Delta\alpha_0 - \ell \rho_1^{-1} \cos\zeta_1 \cos\Delta\alpha_0] \\ & + C [- 2 \ell R_e^{-1} \zeta_1 \cos\Delta\alpha_0 - 2 \ell \rho_1^{-1} \zeta_1 \cos\zeta_1 \cos\Delta\alpha_0] \\ & + D [- 3 \ell R_e^{-1} \zeta_1^2 \cos\Delta\alpha_0 - 3 \ell \rho_1^{-1} \zeta_1^2 \cos\zeta_1 \cos\Delta\alpha_0] \end{aligned} \quad (\text{II.28a})$$

More concisely, we can write eqn. (II.28a) in this form:

$$\sec\zeta'_2 - \sec\zeta'_1 \approx - \ell (B + 2C \zeta_1 + 3D \zeta_1^2) (R_e^{-1} + \rho_1^{-1} \cos\zeta_1) \cos\Delta\alpha_0 \quad (\text{II.28b})$$

Investigation has shown that eqn. (II.28b) is in the worst cases inaccurate by about 10% of the "true" value for zenith angles smaller than 80°. Figure II.7b illustrates the behaviour of the zenith angle functions of equation (II.28b) as a function of the zenith angle.

The substitution of eqn. (II.28b) into eqn. (II.10) gives the bias in the single difference observation due to the absolute ionospheric refraction.

$$\varepsilon\Delta\Phi(\zeta_1, \alpha) \approx (B + 2C \zeta_1 + 3D \zeta_1^2) (R_e^{-1} + \rho_1^{-1} \cos \zeta_1) \cos \Delta\alpha_0 \ell \text{ K TEC} \quad (\text{II.29a})$$

For writing simplicity, and keeping in mind that the quantities ρ , ζ and α and those associated with station P_1 we will omit the subscript "1" associated with station P_1 .

$$\varepsilon\Delta\Phi(\zeta, \alpha) \approx (B + 2C \zeta + 3D \zeta^2) (R_e^{-1} + \rho^{-1} \cos \zeta) \cos \Delta\alpha_0 \ell \text{ K TEC} \quad (\text{II.29b})$$

where: $K = 40.28/f^2$

Summary of assumptions and approximations:

- 1) The electrons are concentrated in a spherical layer of infinitesimal thickness at a height of 350 km;
- 2) TEC is uniform in the layer;
- 3) Equation (II.15a) is an approximation of the ionospheric mapping function;
- 4) Equations (II.19), (II.21b) and (II.24c) hold for short baseline length ($\ell < 100$ km);
- 5) Equation (II.23c) holds for small baseline height difference ($\zeta_0 \approx 90^\circ$);
- 6) Equation (II.28b) is not recommended for zenith angles greater than 80° .

As noticed in the previous section, the effect of these assumptions and approximations are evaluated in Chapter 5 (Comparison of predictions with results from real GPS data) along with the other assumptions used in the simulation technique.

II.3 Offset in the horizontal coordinates of the fixed station

When a coordinate offset is present in the fixed station, there are two effects: 1) the geometry of the theoretical (computed) single difference observation is distorted; and 2) the change of datum (the fixed point is moved in space) causes the baseline vector to translate

in space, as a consequence the same spatial vector does not subtend the same ellipsoidal arc ($\Delta\phi$, $\Delta\lambda$, Δh). The direct comparison of ellipsoidal baseline components from solutions with and without an offset in coordinates of the fixed station entangles the two effects. The second effect is just an artifact of the ellipsoidal coordinate system. The goal of this section is to isolate the first effect. The reader is referred to section I.3 for details concerning the order of magnitude of point positioning error.

To avoid any geometrical misinterpretation, we will use matrix algebra to calculate the mathematical expression for the bias in the single difference observation due to an offset in the horizontal coordinates of the fixed station.

Figures II.3 show the geometrical representation of the situation. The horizontal coordinate offset is represented by a magnitude ΔO and an azimuth α_1 . To simplify the construction of these figures, we regard the offset ΔO affecting the fixed station P_1 like an offset $-\Delta O$ affecting the satellite position S . The free station is represented by the point P_2 . The \sim symbol represents the position of a point affected by the horizontal coordinate offset. The symbols ' and " represent the projections of the three-dimensional geometry into the plane of Figures II.3a and II.3b, respectively. The symbol $\Delta\Phi_{\text{obs}}$ means the observed single difference and the symbol $\Delta\Phi_{\text{th}}$ means the theoretical single difference calculated with the biased coordinates of the fixed station.

In the local geodetic system of station P_1 , the coordinates of points S , \tilde{S} , \tilde{P}_1 and P_2 can be written as follows:

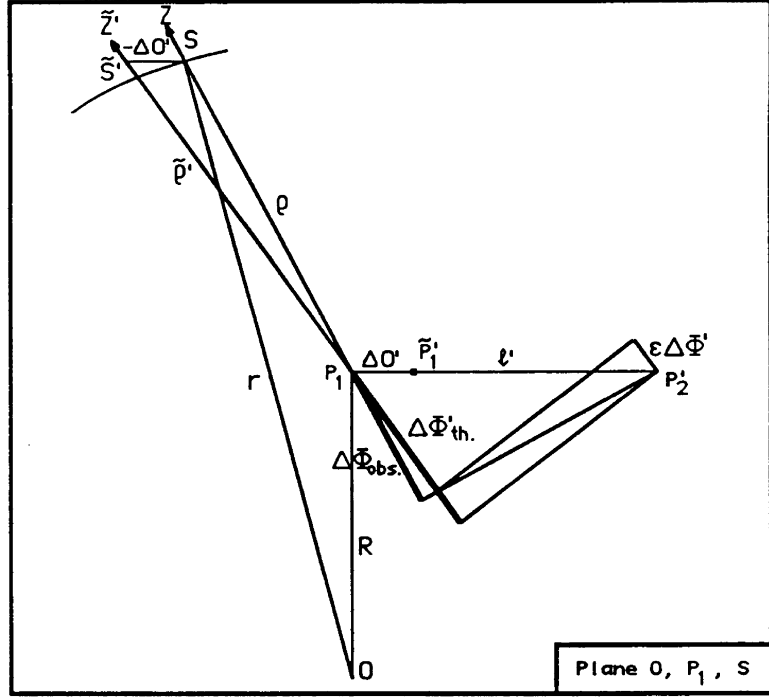


Figure II.3a: Bias in single difference observation due to an offset in the horizontal coordinates of the fixed station (first projection). After Beutler et al. [1988].

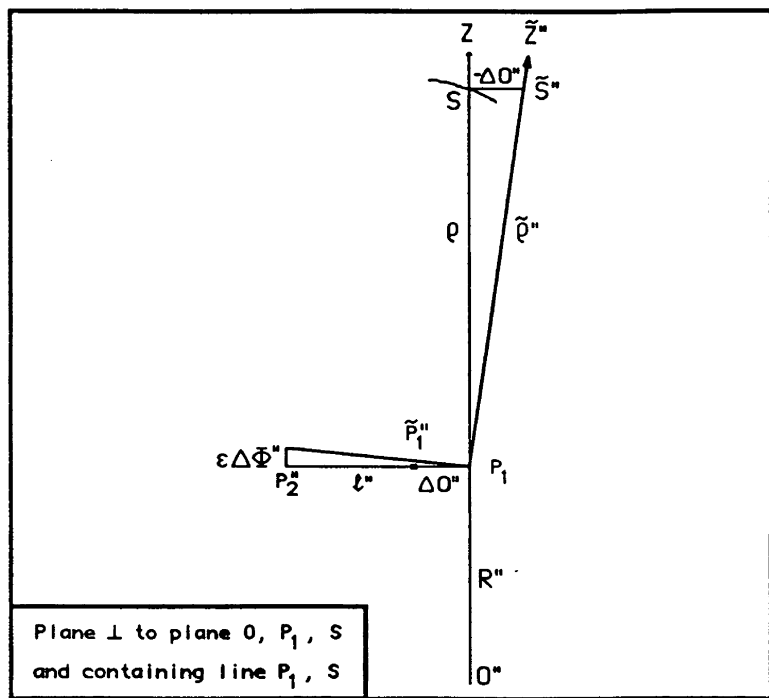


Figure II.3b: Bias in single difference observation due to an offset in the horizontal coordinates of the fixed station (second projection).

$$\begin{aligned}
x^S &= \rho \cos\alpha \sin\zeta & x_{P_1}^{\sim} &= \Delta O \cos\alpha_1 \\
y^S &= \rho \sin\alpha \sin\zeta & y_{P_1}^{\sim} &= \Delta O \sin\alpha_1 \\
z^S &= \rho \cos\zeta & z_{P_1}^{\sim} &= 0 \\
x_{\tilde{S}} &= \rho \cos\alpha \sin\zeta - \Delta O \cos\alpha_1 & x_{P_2} &= \ell \cos\alpha_0 \sin\zeta_0 \\
y_{\tilde{S}} &= \rho \sin\alpha \sin\zeta - \Delta O \sin\alpha_1 & y_{P_2} &= \ell \sin\alpha_0 \sin\zeta_0 \\
z_{\tilde{S}} &= \rho \cos\zeta & z_{P_2} &= \ell \cos\zeta_0
\end{aligned}
\tag{II.30}$$

To get a better interpretation of the observable $\Delta\Phi$ it is convenient to work in the X-system (not to be confused with the CT-system). The origin of the X-system is at point P_1 ; the Z-axis points towards satellite S; the X-axis is defined by the intersection of the perpendicular plane to the Z-axis and the horizontal plane; and the Y-axis points above the horizon completing the left-handed system. Refer to Figure II.4 for the visualization of the two coordinate systems. The link between the X-system and the x-system is:

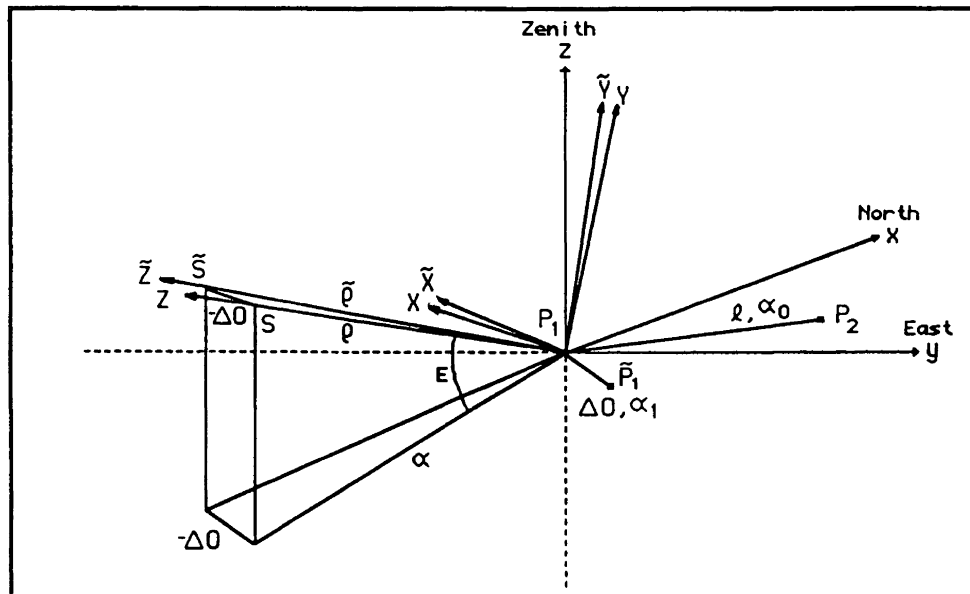


Figure II.4: Coordinate systems representation for the study of an offset in the horizontal coordinates of the fixed station.

$$\vec{X} = R_x(\zeta) R_z(\alpha + 90^\circ) \vec{x} \quad (\text{II.31})$$

$$\vec{X} = \begin{pmatrix} -\sin\alpha & \cos\alpha & 0 \\ -\cos\alpha \cos\zeta & -\sin\alpha \cos\zeta & \sin\zeta \\ \cos\alpha \sin\zeta & \sin\alpha \sin\zeta & \cos\zeta \end{pmatrix} \vec{x}$$

Let express the coordinates of points S, \tilde{S} and P₂ in this new system.

$$\begin{aligned} X^S &= 0 \\ Y^S &= 0 \\ Z^S &= \rho \end{aligned} \quad (\text{II.32a})$$

$$\begin{aligned} X^{\tilde{S}} &= \Delta O \sin\Delta\alpha_1 \\ Y^{\tilde{S}} &= \Delta O \cos\Delta\alpha_1 \cos\zeta \\ Z^{\tilde{S}} &= \rho - \Delta O \cos\Delta\alpha_1 \sin\zeta \end{aligned} \quad (\text{II.32b})$$

$$\begin{aligned} X_{P_2} &= -\ell \sin\zeta_0 \sin\Delta\alpha_0 && \approx -\ell \sin\Delta\alpha_0 \\ Y_{P_2} &= -\ell \sin\zeta_0 \cos\Delta\alpha_0 \cos\zeta + \ell \cos\zeta_0 \sin\zeta && \approx -\ell \cos\Delta\alpha_0 \cos\zeta \\ Z_{P_2} &= \ell \sin\zeta_0 \cos\Delta\alpha_0 \sin\zeta + \ell \cos\zeta_0 \cos\zeta && \approx \ell \cos\Delta\alpha_0 \sin\zeta \end{aligned} \quad (\text{II.32c})$$

where:

$$\Delta\alpha_0 = \alpha - \alpha_0$$

$$\Delta\alpha_1 = \alpha - \alpha_1$$

The far right-hand side of eqn. (II.32c) is obtained, by assuming a small baseline height component, i.e., $\zeta_0 \approx 90^\circ$, $\sin\zeta_0 \approx 1$ and $\cos\zeta_0 \approx 0$.

With the coordinates of points S and \tilde{S} in the X-system, we can define the following rotation angles to be used to define the \tilde{X} -system. The \tilde{X} -system can be defined like the X-system, but with its \tilde{Z} -axis pointing towards the satellite position \tilde{S} (see Figure (II.4)).

$$\Delta\tilde{\alpha} = \sin\Delta\alpha_1 \Delta O/\tilde{\rho} \approx \sin\Delta\alpha_1 \Delta O/\rho \quad (\text{II.33})$$

$$\Delta\tilde{\zeta} = \cos\Delta\alpha_1 \cos\zeta \Delta O/\tilde{\rho} \approx \cos\Delta\alpha_1 \cos\zeta \Delta O/\rho$$

The transformation between the X-system and the \tilde{X} -system is given by:

$$\begin{aligned} \vec{\tilde{X}} &= R_X(-\Delta\tilde{\zeta}) R_Y(\Delta\tilde{\alpha}) \vec{X} \\ \vec{\tilde{X}} &= \begin{pmatrix} 1 & 0 & -\Delta\tilde{\alpha} \\ 0 & 1 & -\Delta\tilde{\zeta} \\ \Delta\tilde{\alpha} & \Delta\tilde{\zeta} & 1 \end{pmatrix} \vec{X} \end{aligned} \quad (\text{II.34})$$

The calculation of the coordinates of point \tilde{S} in the \tilde{X} -system gives (as expected):

$$\tilde{X}^{\tilde{S}} = 0; \quad \tilde{Y}^{\tilde{S}} = 0; \quad \tilde{Z}^{\tilde{S}} = Z^{\tilde{S}}$$

The coordinate \tilde{Z}_{P_2} can also be calculated using eqn. (II.34), as follows:

$$\tilde{Z}_{P_2} = \Delta\tilde{\alpha} X_{P_2} + \Delta\tilde{\zeta} Y_{P_2} + Z_{P_2} \quad (\text{II.35a})$$

Introducing eqn. (II.32c) and (II.33) into eqn. (II.35a) gives:

$$\tilde{Z}_{P_2} = -\sin\Delta\alpha_0 \sin\Delta\alpha_1 \ell \Delta O/\rho - \cos^2\zeta \cos\Delta\alpha_0 \cos\Delta\alpha_1 \ell \Delta O/\rho + \sin\zeta \cos\Delta\alpha_0 \ell \quad (\text{II.35b})$$

From Figures II.3 and assuming that the curvature of the surface of position is negligible, which is a correct statement for short baseline length in comparison with the station-satellite distance, the interpretation of the misclosure of the single difference observation (observed minus theoretical values) can be interpreted as:

$$\varepsilon\Delta\Phi(\zeta, \alpha) \approx - (Z_{P_2} - \tilde{Z}_{P_2}) = \tilde{Z}_{P_2} - Z_{P_2} \quad (\text{II.36a})$$

We then get the sought after equation:

$$\varepsilon\Delta\Phi(\zeta, \alpha) \approx - (\sin\Delta\alpha_0 \sin\Delta\alpha_1 + \cos^2\zeta \cos\Delta\alpha_0 \cos\Delta\alpha_1) \ell \Delta O/\rho \quad (\text{II.36b})$$

Figure II.7c illustrates the behaviour of the zenith angle function of equation (II.36b) as a function of the zenith angle.

Summary of assumptions and approximations:

- 1) Baseline height component is small ($\zeta_0 \approx 90^\circ$) compared to the baseline length (eqn. (II.32c));
- 2) Baseline length is short ($\ell < 100$ km) compared to the station-satellite distance (eqn. (II.36a)).

The effect of these assumptions and approximations are evaluated in Chapter 5 (Comparison of predictions with results from real GPS data) along with the other assumptions used in the simulation technique.

II.3.1 Offset in the latitude of the fixed station

The bias due to a latitude offset of the fixed station ($\Delta\phi$) is a particular case of eqn. (II.36b), where, $\alpha_1 = 0^\circ$, $\Delta\alpha_1 = \alpha$, $\sin\alpha_1 = 0$ and $\cos\alpha_1 = 1$. Under this condition eqn. (II.36b) can written as follows:

$$\epsilon\Delta\Phi(\zeta,\alpha) \approx - (\sin\Delta\alpha_0 \sin\alpha + \cos^2\zeta \cos\Delta\alpha_0 \cos\alpha) \ell \Delta\phi/\rho \quad (\text{II.36c})$$

II.3.2 Offset in the longitude of the fixed station

The bias due to a longitude offset of the fixed station ($\Delta\lambda$) is also a particular case of eqn. (II.36b), where, $\alpha_1 = 90^\circ$, $\Delta\alpha_1 = \alpha - 90^\circ$, $\sin\Delta\alpha_1 = -\cos\alpha$, $\cos\Delta\alpha_1 = \sin\alpha$, $\sin\alpha_1 = 1$, $\cos\alpha_1 = 0$ and $\sin(\alpha_0+\alpha_1) = \cos\alpha_0$. Under this condition eqn. (II.36b) can written as follows:

$$\epsilon\Delta\Phi(\zeta,\alpha) \approx (\sin\Delta\alpha_0 \cos\alpha - \cos^2\zeta \cos\Delta\alpha_0 \sin\alpha) \ell \Delta\lambda/\rho \quad (\text{II.36d})$$

II.4 Offset in the height of the fixed station

In this section we follow the path taken in section II.3, except that the offset in the horizontal coordinates of the fixed station (ΔO) is replaced by the offset in the height of the fixed station (Δh). The reader is then referred to this previous section to know the definition of the symbols used here. Figure II.5 is equivalent to Figures II.3a and Figure II.6 is equivalent to Figure II.4.

In the local geodetic system of station P_1 , the coordinates of points S , \tilde{S} , \tilde{P}_1 and P_2 can be written as follows:

$$\begin{aligned}
 x^S &= \rho \cos\alpha \sin\zeta & x_{\tilde{P}_1} &= 0 \\
 y^S &= \rho \sin\alpha \sin\zeta & y_{\tilde{P}_1} &= 0 \\
 z^S &= \rho \cos\zeta & z_{\tilde{P}_1} &= \Delta h \\
 \\
 x_{\tilde{S}} &= \rho \cos\alpha \sin\zeta & x_{P_2} &= \ell \cos\alpha_0 \sin\zeta_0 \\
 y_{\tilde{S}} &= \rho \sin\alpha \sin\zeta & y_{P_2} &= \ell \sin\alpha_0 \sin\zeta_0 \\
 z_{\tilde{S}} &= \rho \cos\zeta - \Delta h & z_{P_2} &= \ell \cos\zeta_0
 \end{aligned} \tag{II.37}$$

The coordinate of points S , \tilde{S} and P_2 in the X-system are:

$$\begin{aligned}
 X^S &= 0 \\
 Y^S &= 0 \\
 Z^S &= \rho
 \end{aligned} \tag{II.38a}$$

$$\begin{aligned}
 X_{\tilde{S}} &= 0 \\
 Y_{\tilde{S}} &= -\Delta h \sin\zeta \\
 Z_{\tilde{S}} &= \rho - \Delta h \cos\zeta
 \end{aligned} \tag{II.38b}$$

$$\begin{aligned}
 X_{P_2} &= -\ell \sin\zeta_0 \sin\Delta\alpha_0 & & \approx -\ell \sin\Delta\alpha_0 \\
 Y_{P_2} &= -\ell \sin\zeta_0 \cos\Delta\alpha_0 \cos\zeta + \ell \cos\zeta_0 \sin\zeta & & \approx -\ell \cos\Delta\alpha_0 \cos\zeta \\
 Z_{P_2} &= \ell \sin\zeta_0 \cos\Delta\alpha_0 \sin\zeta + \ell \cos\zeta_0 \cos\zeta & & \approx \ell \cos\Delta\alpha_0 \sin\zeta
 \end{aligned} \tag{II.38c}$$

where: $\Delta\alpha_0 = \alpha - \alpha_0$

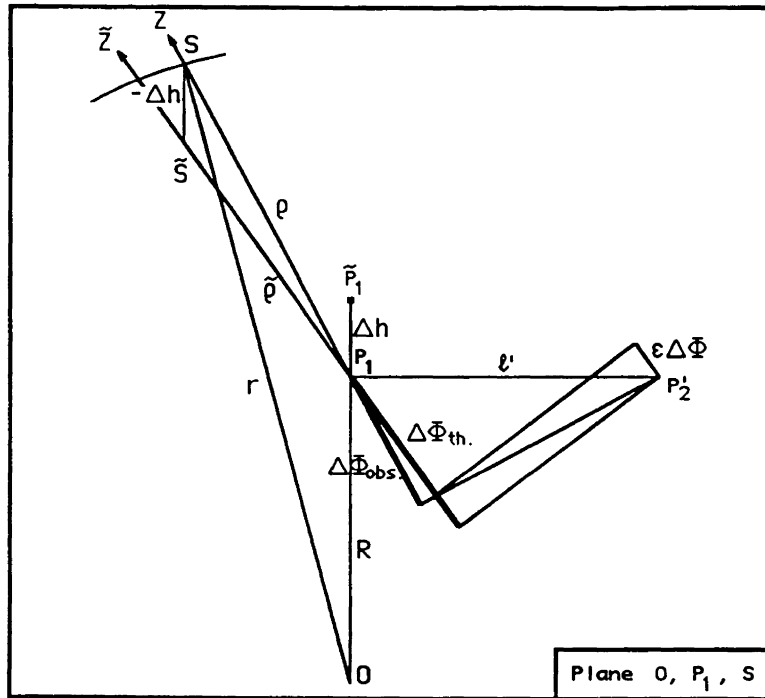


Figure II.5: Bias in single difference observation due to an offset in the height of the fixed station. After Beutler et al. [1988].

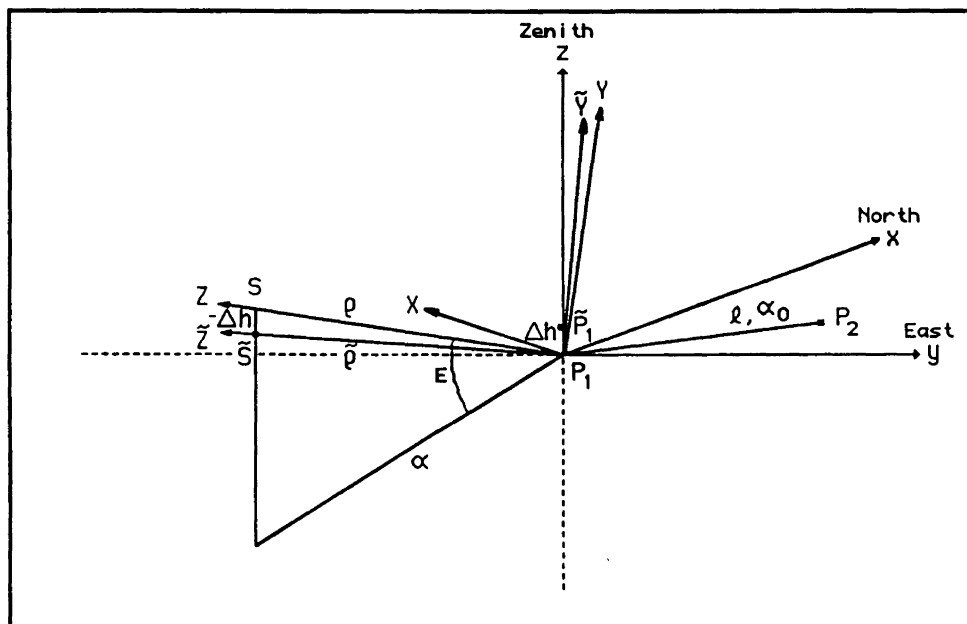


Figure II.6: Coordinate systems representation for the study of an offset in the height of the fixed station.

The far right-hand side of eqn. (II.38c) is obtained, by assuming a small baseline height component, i.e., $\zeta_0 \approx 90^\circ$, $\sin\zeta_0 \approx 1$ and $\cos\zeta_0 \approx 0$.

With the coordinates of points S and \tilde{S} in the X-system, we can define the following rotation angle to be used to define the \tilde{X} -system.

$$\Delta\tilde{\zeta} = -\sin\zeta \Delta h/\rho \approx -\sin\zeta \Delta h/\rho \quad (\text{II.39})$$

The transformation between the X-system and the \tilde{X} -system is given by:

$$\begin{aligned} \vec{\tilde{X}} &= R_X(-\Delta\tilde{\zeta}) \vec{X} \\ \vec{\tilde{X}} &= \begin{pmatrix} 1 & 0 & 0 \\ 0 & 1 & -\Delta\tilde{\zeta} \\ 0 & \Delta\tilde{\zeta} & 1 \end{pmatrix} \vec{X} \end{aligned} \quad (\text{II.40})$$

The calculation of the coordinates of point \tilde{S} in the \tilde{X} -system gives (as expected):

$$\tilde{X}^{\tilde{S}} = 0; \quad \tilde{Y}^{\tilde{S}} = 0; \quad \tilde{Z}^{\tilde{S}} = Z^{\tilde{S}}$$

The coordinate \tilde{Z}_{P_2} can also be calculated using eqn. (II.40), as follows:

$$\tilde{Z}_{P_2} = \Delta\tilde{\zeta} Y_{P_2} + Z_{P_2} \quad (\text{II.41a})$$

Introducing eqn. (II.38c) and (II.39) in the above equation gives:

$$\tilde{Z}_{P_2} \approx \sin\zeta \cos\zeta \cos\Delta\alpha_0 \ell \Delta h/\rho + \sin\zeta \cos\Delta\alpha_0 \ell \quad (\text{II.41b})$$

From Figures II.5 and assuming that the curvature of the surface of position is negligible, which is a correct statement for short baseline length in comparison with the

station-satellite distance, the interpretation of the misclosure of the single difference observation (observed minus theoretical values) can be interpreted as:

$$\varepsilon\Delta\Phi(\zeta,\alpha) \approx - (Z_{P_2} - \tilde{Z}_{P_2}) = \tilde{Z}_{P_2} - Z_{P_2} \quad (\text{II.42a})$$

We then get the sought after equation:

$$\varepsilon\Delta\Phi(\zeta,\alpha) \approx \sin\zeta \cos\zeta \cos\Delta\alpha_0 \ell \Delta h/\rho \quad (\text{II.42b})$$

Figure II.7c illustrates the behaviour of the zenith angle function of equation (II.42b) as a function of the zenith angle.

Summary of assumptions and approximations:

- 1) Baseline height component is small ($\zeta_0 \approx 90^\circ$) compared to the baseline length (eqn. (II.38c));
- 2) Baseline length is short ($\ell < 100$ km) compared to the station-satellite distance (eqn. (II.42a)).

As mentioned in section II.3, the effect of these assumptions and approximations are evaluated in Chapter 5 (Comparison of predictions with results from real GPS data) along with the other assumptions used in the simulation technique.

II.5 Zenith angle functional relationships of biases

It is remarkable that each of the studied biases has a completely different zenith angle function. For this reason we have plotted in Figures II.7 the values of these zenith angle functions against the zenith angle of the observations. The relationships of the biases to the azimuth of an observation is rather simple being sine or cosine functions.

In Figure II.7a we recognize the mapping function $m(\zeta)$ related to tropospheric zenith delay and its approximation $\sec\zeta$ valid for ζ smaller than 70° .

In Figure II.7b are presented the two zenith angle functions related to absolute ionospheric refraction. The function $F(\zeta)$ accounts for the non-parallelism of the two local verticals and $G(\zeta)$ accounts for the parallactic angle subtended by the observed satellite.

Finally in Figure II.7c we recognize the zenith angle function $(\cos^2\zeta)$ related to an offset in the horizontal coordinates of the fixed station and the zenith angle function $(\sin\zeta \cos\zeta)$ related to an offset in the height of the fixed station. For completeness we have added to this plot the functions $\sin\zeta$ and $\cos\zeta$.

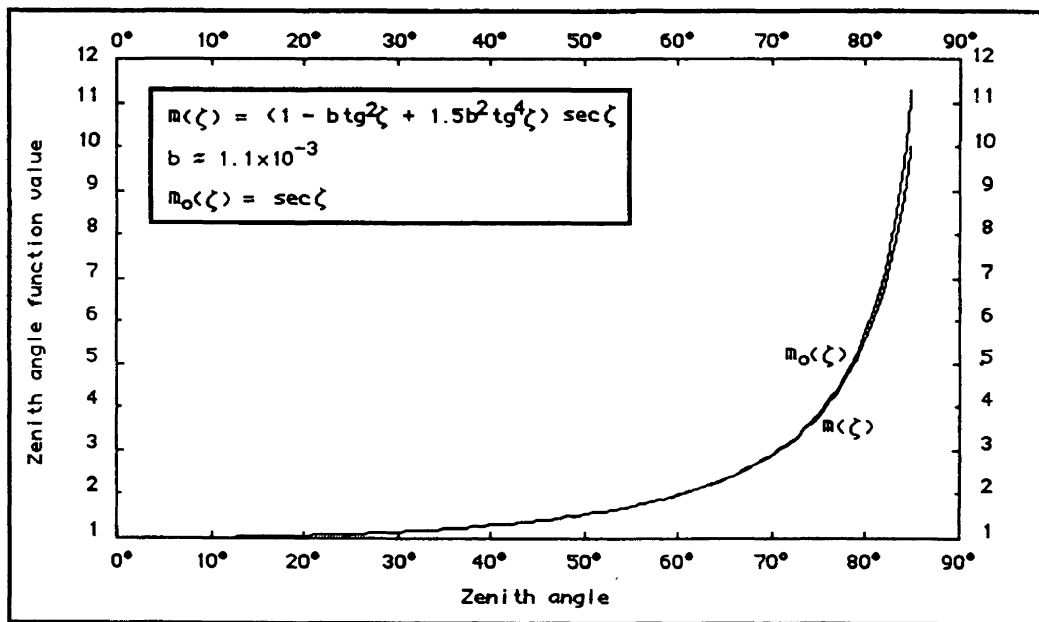


Figure II.7a: Zenith angle functions related to tropospheric zenith delay.

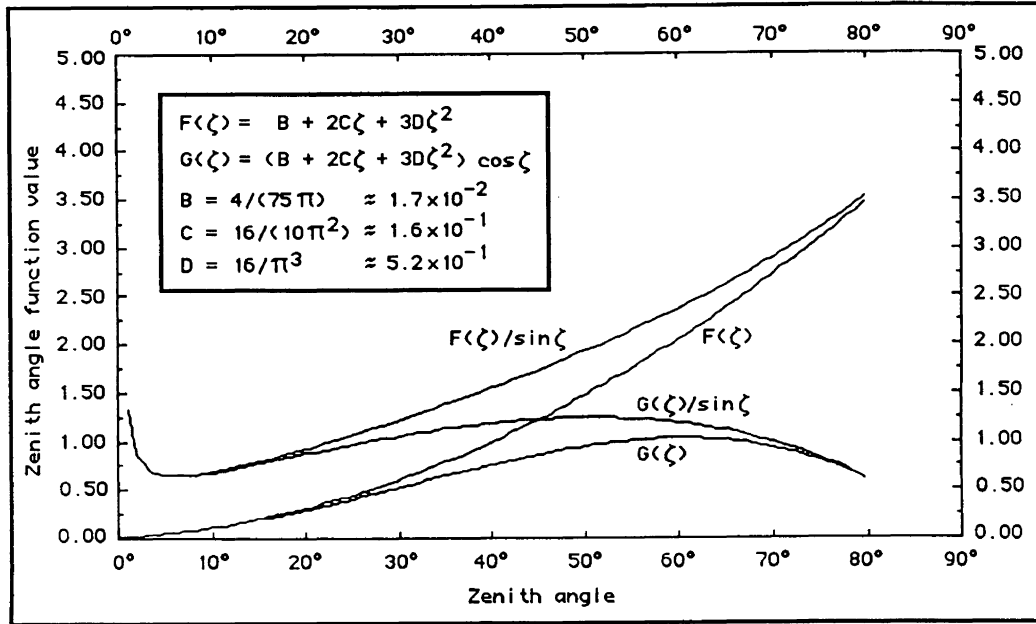


Figure II.7b: Zenith angle functions related to absolute ionospheric refraction error.

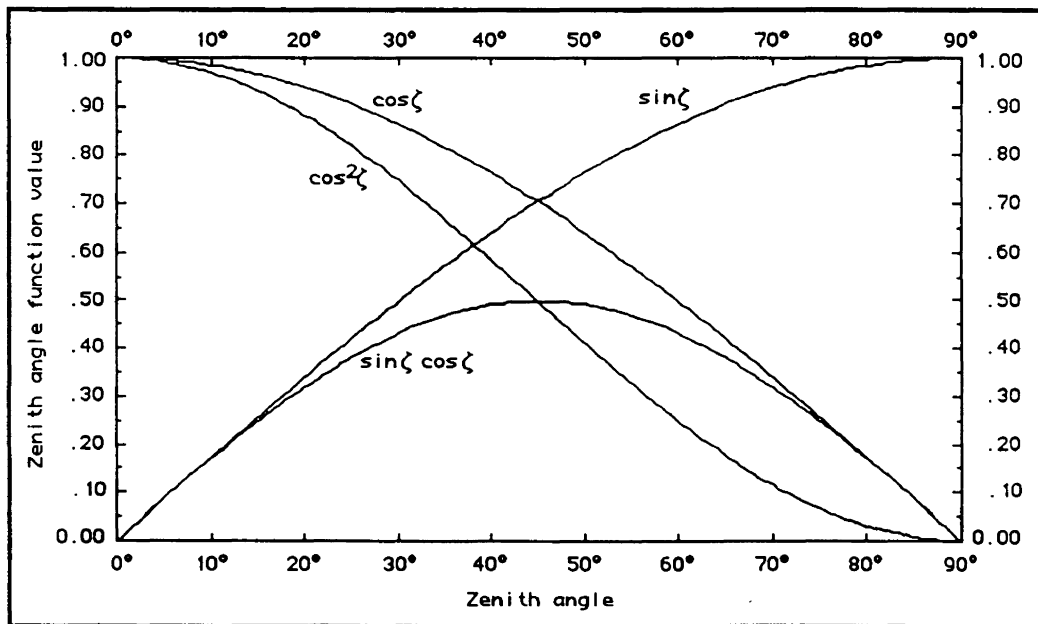


Figure II.7c: Zenith angle functions related to offsets in the coordinates of the fixed station.

To give a crude idea of the way these errors propagate themselves, as functions of the zenith angle, into the station coordinates estimated during the least squares adjustments we can interpret the situation as follows:

Knowing that a systematic error primarily causes a horizontal scale effect we can geometrically visualize that the error in the single difference observation, e.g., $F(\zeta)$, will be propagated in the horizontal station coordinates with magnitude: $F(\zeta)/\sin\zeta$. And knowing that a systematic error primarily causes a height effect we can geometrically visualize that the error in the single difference observation, e.g., $m(\zeta)$, will be propagated into the station height with magnitude: $m(\zeta)/\cos\zeta$ [Beutler et al., 1988]. The latter geometrical interpretation is rather misleading because this does not take into account the high correlation between the station height and the clock parameter. For this reason, we will consider only the first interpretation related to errors (absolute ionospheric refraction and offset in the height of the fixed station) leading to horizontal scale effects.

The results for the absolute ionospheric error are illustrated in Figures II.7b, and in Figure II.7c for the offset in the height of the fixed station (function $\cos\zeta$).

Appendix III

Integration terms

III.1 Integration over the azimuth sector

In this section, we present the integration terms J_{ij} (integration over the azimuth sector) used in the calculation of the elements of the matrix N : $(A^T P_\rho A)$ and the vector U : $(A^T P_\rho \epsilon \Delta \Phi)$.

The general form of the integrals over the azimuth sector is:

$$J_{ij} = \int_{\alpha_{\text{from}}}^{\alpha_{\text{to}}} \sin^i \alpha \cos^j \alpha \, d\alpha \quad (\text{III.1})$$

The expressions between brackets (general case, below) have to be evaluated at the upper boundary α_{to} and at the lower boundary α_{from} . The values of these terms are presented for two particular cases:

- i) where $\alpha_{\text{to}} = 2\pi - \alpha_{\text{from}}$ (column 2), and
- ii) where $\alpha_{\text{from}} = 0$ and $\alpha_{\text{to}} = 2\pi$, i.e., an all azimuth sector (column 3). In the sequel, α_{from} is abbreviated by α_f .

General case	$\alpha^{10} = 2\pi - \alpha_f$	$\alpha_f = 0$ and $\alpha^{10} = 2\pi$
$J_{00} = [\alpha]$	$2\pi - 2\alpha_f$	2π
$J_{01} = [\sin\alpha]$	$-2\sin\alpha_f$	0
$J_{02} = [2\alpha + \sin 2\alpha] / 4$	$(2\pi - 2\alpha_f - \sin 2\alpha_f) / 2$	π
$J_{03} = [3\sin\alpha - \sin^3\alpha] / 3$	$(-6\sin\alpha_f + 2\sin^3\alpha_f) / 3$	0
$J_{10} = [-\cos\alpha]$	0	0
$J_{11} = [\sin^2\alpha] / 2$	0	0
$J_{12} = [-\cos^3\alpha] / 3$	0	0
$J_{20} = [2\alpha - \sin 2\alpha] / 4$	$(2\pi - 2\alpha_f + \sin 2\alpha_f) / 2$	π
$J_{21} = [\sin^3\alpha] / 3$	$(-2\sin^3\alpha_f) / 3$	0
$J_{30} = [\cos^3\alpha - 3\cos\alpha] / 3$	0	0

III.2 Integration over the zenith angle sector

In this section, we present the integration terms I_{ijk} (integration over the zenith angle sector) used in the calculation of the elements of the matrix N: $(A^T P_\ell A)$ and the vector U:

$$(A^T P_\ell \varepsilon \Delta \Phi).$$

The general form of the integrals over the zenith angle sector is:

$$I_{ijk} = \int_{\zeta_{\min}}^{\zeta_{\max}} \sin^i \zeta \cos^j \zeta \zeta^k d\zeta \quad (\text{III.2})$$

The expressions between brackets, below, have to be evaluated at the upper boundary ζ^{\max} and at the lower boundary ζ_{\min} . Unlike the J_{ij} terms, the I_{ijk} terms will never vanish in any cases (inside the integration boundaries ζ_{\min} and ζ^{\max}).

Some of the terms have negative indices and should be interpreted as follows:

I_{1-20} means that $i = 1, j = -2$ and $k = 0$;

I_{1-100} means that $i = 1, j = -10$ and $k = 0$.

$$\begin{aligned}
 I_{010} &= [\sin\zeta] \\
 I_{030} &= [3\sin\zeta - \sin^3\zeta] / 3 \\
 I_{0-30} &= [\ln(\tan(\zeta/2 + \pi/4)) + \sin\zeta \sec^2\zeta] / 2 \\
 I_{0-50} &= [\sin\zeta \sec^4\zeta] / 4 && + 3/4 I_{0-30} \\
 I_{100} &= [-\cos\zeta] \\
 I_{110} &= [\sin^2\zeta] / 2 \\
 I_{120} &= [-\cos^3\zeta] / 3 \\
 I_{130} &= [-\cos^4\zeta] / 4 \\
 I_{1-10} &= [-\ln(\cos\zeta)] \\
 I_{1-20} &= [\sec\zeta] \\
 I_{1-40} &= [\sec^3\zeta] / 3 \\
 I_{1-60} &= [\sec^5\zeta] / 5 \\
 I_{1-80} &= [\sec^7\zeta] / 7 \\
 I_{1-100} &= [\sec^9\zeta] / 9 \\
 I_{200} &= [2\zeta - \sin 2\zeta] / 4 \\
 I_{210} &= [\sin^3\zeta] / 3 \\
 I_{220} &= [4\zeta - \sin 4\zeta] / 32 \\
 I_{2-10} &= [\ln(\tan(\zeta/2 + \pi/4)) - \sin\zeta] \\
 I_{2-20} &= [\tan\zeta - \zeta] \\
 I_{2-30} &= [\sin\zeta \sec^2\zeta] && - I_{0-30} \\
 I_{2-50} &= [\sin\zeta \sec^4\zeta] / 3 && - 1/3 I_{0-50} \\
 I_{300} &= [\cos^3\zeta - 3\cos\zeta] / 3 \\
 I_{310} &= [\sin^4\zeta] / 4 \\
 I_{3-10} &= [-\sin^2\zeta] / 2 && + I_{1-10} \\
 I_{3-20} &= [-\sin^2\zeta \sec\zeta] && + 2 I_{1-20} \\
 I_{3-30} &= [\tan^2\zeta] / 2 && - I_{1-10}
 \end{aligned}$$

$$\begin{aligned}
I_{3-40} &= [\sin^2\zeta \sec^3\zeta] & - 2 & I_{1-40} \\
I_{3-60} &= [\sin^2\zeta \sec^5\zeta] / 3 & - 2/3 & I_{1-60} \\
I_{3-80} &= [\sin^2\zeta \sec^7\zeta] / 5 & - 2/5 & I_{1-80} \\
I_{3-100} &= [\sin^2\zeta \sec^9\zeta] / 7 & - 2/7 & I_{1-100} \\
I_{4-20} &= [-\sin^3\zeta \sec\zeta] / 2 & + 3/2 & I_{2-20} \\
I_{4-30} &= [-\sin^3\zeta \sec^2\zeta] & + 3 & I_{2-30} \\
I_{4-40} &= [\tan^3\zeta] / 3 & - & I_{2-20} \\
I_{4-50} &= [\sin^3\zeta \sec^4\zeta] & - 3 & I_{2-50} \\
I_{5-30} &= [-\sin^4\zeta \sec^2\zeta] / 2 & + 2 & I_{3-30} \\
I_{5-40} &= [-\sin^4\zeta \sec^3\zeta] & + 4 & I_{3-40} \\
I_{5-50} &= [\tan^4\zeta] / 4 & - & I_{3-30} \\
I_{5-60} &= [\sin^4\zeta \sec^5\zeta] & - 4 & I_{3-60} \\
I_{5-80} &= [\sin^4\zeta \sec^7\zeta] / 3 & - 4/3 & I_{3-80} \\
I_{5-100} &= [\sin^4\zeta \sec^9\zeta] / 5 & - 4/5 & I_{3-100} \\
I_{6-40} &= [-\sin^5\zeta \sec^3\zeta] / 2 & + 5/2 & I_{4-40} \\
I_{6-50} &= [-\sin^5\zeta \sec^4\zeta] & + 5 & I_{4-50} \\
I_{7-80} &= [\sin^6\zeta \sec^7\zeta] & - 6 & I_{5-80} \\
I_{7-100} &= [\sin^6\zeta \sec^9\zeta] / 3 & - 2 & I_{5-100} \\
I_{9-100} &= [\sin^8\zeta \sec^9\zeta] & - 8 & I_{7-100} \\
I_{031} &= [3\zeta \sin\zeta - \zeta \sin^3\zeta] / 3 & + 1/3 & I_{300} & - I_{100} \\
I_{301} &= [\zeta \cos^3\zeta - 3\zeta \cos\zeta] / 3 & - 1/3 & I_{030} & + I_{010} \\
I_{212} &= [\zeta^2 \sin^3\zeta] / 3 & - 2/3 & I_{301} \\
I_{211} &= [\zeta \sin^3\zeta] / 3 & - 1/3 & I_{300} \\
I_{202} &= [4\zeta^3 + (3 - 6\zeta^2) \sin 2\zeta - 6\zeta \cos 2\zeta] / 24 \\
I_{201} &= [2\zeta^2 - 2\zeta \sin 2\zeta - \cos 2\zeta] / 8 \\
I_{122} &= [-\zeta^2 \cos^3\zeta] / 3 & + 2/3 & I_{031} \\
I_{121} &= [-\zeta \cos^3\zeta] / 3 & + 1/3 & I_{030} \\
I_{112} &= [\zeta^2 \sin^2\zeta] / 2 & - & I_{201} \\
I_{111} &= [\zeta \sin^2\zeta] / 2 & - 1/2 & I_{200} \\
I_{102} &= [2\zeta \sin\zeta + (2 - \zeta^2) \cos\zeta] \\
I_{101} &= [\sin\zeta - \zeta \cos\zeta]
\end{aligned}$$

III.3 Numerical values of matrices and vectors of normal equations

In this section, we present examples of numerical values of the elements of the matrices N and N^{-1} and the vector U (based on the J_{ij} and I_{ijk} terms) for different satellite configurations, different combination of parameters and different systematic errors.

In the following examples the observation weight matrix P_ℓ was assumed to be an identity matrix; an elevation mask angle of 15° ($\zeta^{\max}: 75^\circ$) was used; and the number of observations in the selected sector (n_{sec}) was defined to 371. This means that the number of observations in the observer's hemisphere (n) was equal to 500, 667, 828 and 1508 for the equatorial site (Eq.), the mid-latitude site (Mid.), the polar site (Pol.) and the CERN satellite configuration (CERN), respectively. See Appendix V for the description of the satellite configurations.

III.3.1 Normal equation matrices

Station coordinates and clock parameter (x, y, z, ct),

matrices N and N^{-1} are unitless.

$$\text{Eq.:} \quad N = \begin{pmatrix} 103 & 0 & 0 & 0 \\ 0 & 103 & 0 & 0 \\ 0 & 0 & 164 & -233 \\ 0 & 0 & -233 & 371 \end{pmatrix}; \quad N^{-1} = \begin{pmatrix} .97 & 0 & 0 & 0 \\ 0 & .97 & 0 & 0 \\ 0 & 0 & 5.9 & 3.7 \\ 0 & 0 & 3.7 & 2.6 \end{pmatrix} \times 10^{-2}$$

$$\text{Pol.:} \quad N = \begin{pmatrix} 139 & 0 & 0 & 0 \\ 0 & 139 & 0 & 0 \\ 0 & 0 & 93 & -179 \\ 0 & 0 & -179 & 371 \end{pmatrix}; \quad N^{-1} = \begin{pmatrix} .72 & 0 & 0 & 0 \\ 0 & .72 & 0 & 0 \\ 0 & 0 & 16 & 7.8 \\ 0 & 0 & 7.8 & 4.0 \end{pmatrix} \times 10^{-2}$$

$$\text{Mid.:} \quad N = \begin{pmatrix} 82 & 0 & -45 & 80 \\ 0 & 125 & 0 & 0 \\ -45 & 0 & 164 & -233 \\ 80 & 0 & -233 & 371 \end{pmatrix}; \quad N^{-1} = \begin{pmatrix} 1.6 & 0 & -.46 & -.63 \\ 0 & .80 & 0 & 0 \\ -.46 & 0 & 6.0 & 3.9 \\ -.63 & 0 & 3.9 & 2.9 \end{pmatrix} \times 10^{-2}$$

$$\text{CERN: } N = \begin{pmatrix} 74 & 0 & 0 & 0 \\ 0 & 149 & 125 & -224 \\ 0 & 125 & 147 & -222 \\ 0 & -224 & -222 & 371 \end{pmatrix}; \quad N^{-1} = \begin{pmatrix} 1.4 & 0 & 0 & 0 \\ 0 & 14 & 9.2 & 14 \\ 0 & 9.2 & 13 & 13 \\ 0 & 14 & 13 & 17 \end{pmatrix} \times 10^{-2}$$

Station coordinates, clock and tropospheric zenith delay parameters (x, y, z, ct, tr),
matrices N and N⁻¹ are unitless.

$$\text{Eq.: } N = \begin{pmatrix} 103 & 0 & 0 & 0 & 0 \\ 0 & 103 & 0 & 0 & 0 \\ 0 & 0 & 164 & -233 & -369 \\ 0 & 0 & -233 & 371 & 673 \\ 0 & 0 & -369 & 673 & 1420 \end{pmatrix}; N^{-1} = \begin{pmatrix} .97 & 0 & 0 & 0 & 0 \\ 0 & .97 & 0 & 0 & 0 \\ 0 & 0 & 54 & 61 & -15 \\ 0 & 0 & 61 & 71 & -18 \\ 0 & 0 & -15 & -18 & 4.7 \end{pmatrix} \times 10^{-2}$$

$$\text{Pol.: } N = \begin{pmatrix} 139 & 0 & 0 & 0 & 0 \\ 0 & 139 & 0 & 0 & 0 \\ 0 & 0 & 93 & -179 & -369 \\ 0 & 0 & -179 & 371 & 827 \\ 0 & 0 & -369 & 827 & 2000 \end{pmatrix}; N^{-1} = \begin{pmatrix} .72 & 0 & 0 & 0 & 0 \\ 0 & .72 & 0 & 0 & 0 \\ 0 & 0 & 258 & 236 & -50 \\ 0 & 0 & 236 & 219 & -47 \\ 0 & 0 & -50 & -47 & 10 \end{pmatrix} \times 10^{-2}$$

$$\text{Mid.: } N = \begin{pmatrix} 82 & 0 & -45 & 80 & 159 \\ 0 & 125 & 0 & 0 & 0 \\ -45 & 0 & 164 & -233 & -370 \\ 80 & 0 & -233 & 371 & 673 \\ 159 & 0 & -370 & 673 & 1420 \end{pmatrix}; N^{-1} = \begin{pmatrix} 1.6 & 0 & -.81 & -1.1 & .11 \\ 0 & .80 & 0 & 0 & 0 \\ -.81 & 0 & 54 & 61 & -15 \\ -1.1 & 0 & 61 & 72 & -18 \\ .11 & 0 & -15 & -18 & 4.7 \end{pmatrix} \times 10^{-2}$$

$$\text{CERN: } N = \begin{pmatrix} 74 & 0 & 0 & 0 & 0 \\ 0 & 149 & 125 & -224 & -453 \\ 0 & 125 & 147 & -222 & -370 \\ 0 & -224 & -222 & 371 & 699 \\ 0 & -453 & -370 & 699 & 1510 \end{pmatrix}; N^{-1} = \begin{pmatrix} 1.4 & 0 & 0 & 0 & 0 \\ 0 & 14 & 16 & 22 & -1.9 \\ 0 & 16 & 87 & 100 & -20 \\ 0 & 22 & 100 & 118 & -24 \\ 0 & -1.9 & -20 & -24 & 5.5 \end{pmatrix} \times 10^{-2}$$

III.3.2 Normal equation vectors

Relative tropospheric refraction

Station coordinates and clock parameter (x, y, z, ct),

$\epsilon\Delta dtrop(0)$: 10 mm, U (in metres), δ (in millimetres).

	u^T	δx δy δz $c\delta t$
Eq.:	(0, 0, -3.69, 6.73);	(0, 0, 32, 38)
Pol.:	(0, 0, -3.69, 8.27);	(0, 0, 49, 46)
Mid.:	(1.59, 0, -3.70, 6.73);	(-.2, 0, 32, 38)
CERN:	(0, -4.53, -3.70, 6.99);	(0, 3, 37, 43)

Station coordinates, clock and tropospheric zenith delay parameters (x, y, z, ct, tr),

$\epsilon\Delta dtrop(0)$: 10 mm, U (in metres), δ (in millimetres).

	u^T	δx δy δz $c\delta t$ δtr
Eq.:	(0, 0, -3.69, 6.73, 14.2);	(0, 0, 0, 0, 10)
Pol.:	(0, 0, -3.69, 8.27, 20.0);	(0, 0, 0, 0, 10)
Mid.:	(1.59, 0, -3.70, 6.73, 14.2);	(0, 0, 0, 0, 10)
CERN:	(0, -4.53, -3.70, 6.99, 15.1);	(0, 0, 0, 0, 10)

Absolute ionospheric refraction

Station coordinates and clock parameter (x, y, z, ct),

TEC: 1×10^{17} eI/m², ℓ : 100 km, U (in metres), δ (in millimetres).

		U^T	δx	δy	δz	$c\delta t$
Eq.	(α_0 : 0°):	(-6.91, 0, 0, 0);	(-67,	0,	0,	0)
	(α_0 : 90°):	(0, -6.91, 0, 0);	(0, -67,	0,	0)	
Pol.	(α_0 : 0°):	(-10.0, 0, 0, 0);	(-72,	0,	0,	0)
	(α_0 : 90°):	(0, -10.0, 0, 0);	(0, -72,	0,	0)	
Mid.	(α_0 : 0°):	(-5.45, 0, 2.61, -5.04);	(-67,	0,	-14,	-8)
	(α_0 : 90°):	(0, -8.38, 0, 0);	(0, -67,	0,	0)	
CERN	(α_0 : 0°):	(-4.97, 0, 0, 0);	(-67,	0,	0,	0)
	(α_0 : 90°):	(0, -10.0, -7.42, 14.4);	(0, -64,	44,	27)	

Offset in the latitude of the fixed station

Station coordinates and clock parameter (x, y, z, ct),

$\Delta\phi$: 10 m, ℓ : 100 km, U (in metres), δ (in millimetres).

		U^T	δx	δy	δz	$c\delta t$
Eq.	(α_0 : 0°):	(0, 0, 8.13, -12.1);	(0, 0, 29,	-15)		
	(α_0 : 90°):	(0, 0, 0, 0);	(0, 0, 0,	0)		
Pol.	(α_0 : 0°):	(0, 0, 5.23, -10.5);	(0, 0, 22,	-18)		
	(α_0 : 90°):	(0, 0, 0, 0);	(0, 0, 0,	0)		
Mid.	(α_0 : 0°):	(-1.69, 0, 8.66, -13.1);	(16,	0,	18,	-28)
	(α_0 : 90°):	(0, .39, 0, 0);	(0, 3,	0,	0)	
CERN	(α_0 : 0°):	(0, 8.37, 8.34, -13.5);	(0, 52,	53,	27)	
	(α_0 : 90°):	(-1.83, 0, 0, 0);	(-25,	0,	0,	0)

Offset in the longitude of the fixed station

Station coordinates and clock parameter (x, y, z, ct),

$\Delta\lambda$: 10 m, ℓ : 100 km, U (in metres), δ (in millimetres).

		u^T	δx	δy	δz	$c\delta t$
Eq.	$(\alpha_0: 0^\circ):$	(0, 0, 0, 0);	(0, 0, 0, 0)			
	$(\alpha_0: 90^\circ):$	(0, 0, 8.13, -12.1);	(0, 0, 29, -15)			
Pol.	$(\alpha_0: 0^\circ):$	(0, 0, 0, 0);	(0, 0, 0, 0)			
	$(\alpha_0: 90^\circ):$	(0, 0, 5.23, -10.5);	(0, 0, 22, -18)			
Mid.	$(\alpha_0: 0^\circ):$	(0, .39, 0, 0);	(0, 3, 0, 0)			
	$(\alpha_0: 90^\circ):$	(-3.23, 0, 7.61, -11.2);	(-16, 0, 39, -2)			
CERN	$(\alpha_0: 0^\circ):$	(-1.83, 0, 0, 0);	(-25, 0, 0, 0)			
	$(\alpha_0: 90^\circ):$	(0, 5.35, 6.55, -10.1);	(0, -55, 0, -60)			

Offset in the height of the fixed station

Station coordinates and clock parameter (x, y, z, ct),

Δh : 10 m, ℓ : 100 km, U (in metres), δ (in millimetres).

		u^T	δx	δy	δz	$c\delta t$
Eq.	$(\alpha_0: 0^\circ):$	(-2.47, 0, 0, 0);	(-24, 0, 0, 0)			
	$(\alpha_0: 90^\circ):$	(0, -2.47, 0, 0);	(0, -24, 0, 0)			
Pol.	$(\alpha_0: 0^\circ):$	(-2.92, 0, 0, 0);	(-21, 0, 0, 0)			
	$(\alpha_0: 90^\circ):$	(0, -2.92, 0, 0);	(0, -21, 0, 0)			
Mid.	$(\alpha_0: 0^\circ):$	(-1.95, 0, 1.30, -2.05);	(-24, 0, 8, 4)			
	$(\alpha_0: 90^\circ):$	(0, -3.00, 0, 0);	(0, -24, 0, 0)			
CERN	$(\alpha_0: 0^\circ):$	(-1.76, 0, 0, 0);	(-24, 0, 0, 0)			
	$(\alpha_0: 90^\circ):$	(0, -3.55, -3.52, 5.68);	(0, -26, -25, -16)			

Appendix IV

Program DIPOPSIM description

IV.1 Outline of program DIPOPSIM

The automation of the upgraded Geiger's simulation technique and the generation of results have been achieved by the coding of a software program called DIPOPSIM (Differential POsitioning Program SIMulator). The program is coded in FORTRAN 77 and was originally developed on a Macintosh 512K microcomputer.

The interactively entered inputs to the program are:

- 1) the output file selection and the output file names;
- 2) the selection of the combination of solved-for unknowns among station coordinates, clock and tropospheric zenith delay parameters;
- 3) the a priori weight for the selected unknowns;
- 4) the selection of the bias and its relevant characteristics (magnitude, orientation, etc.);
- 5) the number of observations in the hemisphere;
- 6) the a priori observation weight;
- 7) the selection of the azimuth boundaries (definition of the satellite sky distribution in azimuth);
- 8) the selection of the minimum zenith angle (definition of the lower boundary of the zenith angle integration); and
- 9) the loop definition of the maximum zenith angle (loop over different elevation mask angles).

Basically, the computation consists of:

- 1) evaluation of the $[e_i e_j]$ terms of the normal equation matrix $A^T P_{\rho} A$, at the selected integration boundaries, for the selected unknowns;
- 2) evaluation of the $[e_i \epsilon \Delta \Phi]$ terms of the normal equation vector $A^T P_{\rho} \epsilon \Delta \Phi$, at the selected integration boundaries, for the selected unknowns and the selected systematic error;
- 3) inversion of the matrix $A^T P_{\rho} A$; and
- 4) the matrix multiplication: $(A^T P_{\rho} A)^{-1} A^T P_{\rho} \epsilon \Delta \Phi$.

These steps allow the presentation of the following outputs:

- 1) the biases introduced into the selected unknowns by the studied systematic error;
- 2) the standard deviations of the unknowns and the correlation coefficients among them;
- 3) the station coordinate confidence ellipsoid characteristics (magnitude and orientation of the semi-axes);
- 4) and optionally, the detailed listing of intermediary matrices and vectors used in the least squares estimation process, along with the above output.

For ease of plotting the above 4 items are written in separate files.

A modification to program DIPOPSIM has been developed to allow the selection of many sky sectors of GPS observations. This program is called DIPOPSIM2. However, this program does not allow an elevation mask angle loop and the output is stored in only one output file (the one described under item #4, above).

IV.2 Main program and subprogram documentation

The program DIPOPSIM includes 8 subroutines and 1 function with a total of 1,550 lines of code. The program DIPOPSIM2 has 1,448 lines of code, including the subprograms. Almost 50% of the code, in the main program, is dedicated to the interaction with the user and the creation of the output disk files.

The execution time is less than the time required to enter the input information.

The main program and subprogram documentation are given next.

Main program:

DIPOPSIM: performs least squares adjustment of simulated GPS single difference observations (1,026 lines, DIPOPSIM2: 924 lines)

Subroutines:

DVADD: adds together two arrays (13 lines)

DVDOT: performs dot product between two arrays (12 lines)

DVMOV: moves array elements (11 lines)

DVSMY: performs multiplication of an array by a scalar (11 lines)

EIGEN: computes eigenvalues and eigenvectors of a REAL symmetric matrix (196 lines)

ELLIPS: computes lengths, azimuths and elevations of confidence ellipsoid axes (93 lines, called subprograms: EIGEN, LOC)

SPINC: inverses a symmetric positive-definite matrix where only the elements of the lower triangular part are stored vector-like (105 lines, called subroutine: DVDOT)

ZERO: zeroes REAL matrix (21 lines, called subroutine: DVMOV)

Function:

LOC: computes a vector subscript for an element in a matrix of specified storage mode (62 lines)

Appendix V

Generic GPS satellite configurations and campaign descriptions

V.1 Generic GPS satellite configurations of the future GPS constellation

In Figure V.1 is illustrated generic satellite sky distributions for equatorial, mid-latitude and polar sites which will be generated by the future GPS constellation.

V.1.1 Equatorial site

The integration boundaries used in DIPOPSIM to define this satellite configuration (refer to Chapter 6) are: $\alpha_{\text{from}}: 0^\circ$, $\alpha^{\text{to}}: 360^\circ$ and $\zeta_{\text{min}}: 0^\circ$, $\zeta^{\text{max}} < 90^\circ$.

V.1.2 Mid-latitude site

The integration boundaries used in DIPOPSIM to define this satellite configuration (refer to Chapter 6) are: $\alpha_{\text{from}}: 45^\circ$, $\alpha^{\text{to}}: 315^\circ$ and $\zeta_{\text{min}}: 0^\circ$, $\zeta^{\text{max}} < 90^\circ$.

V.1.3 Polar site

The integration boundaries used in DIPOPSIM to define this satellite configuration (refer to Chapter 6) are: $\alpha_{\text{from}}: 0^\circ$, $\alpha^{\text{to}}: 360^\circ$ and $\zeta_{\text{min}}: 45^\circ$, $\zeta^{\text{max}} < 90^\circ$.

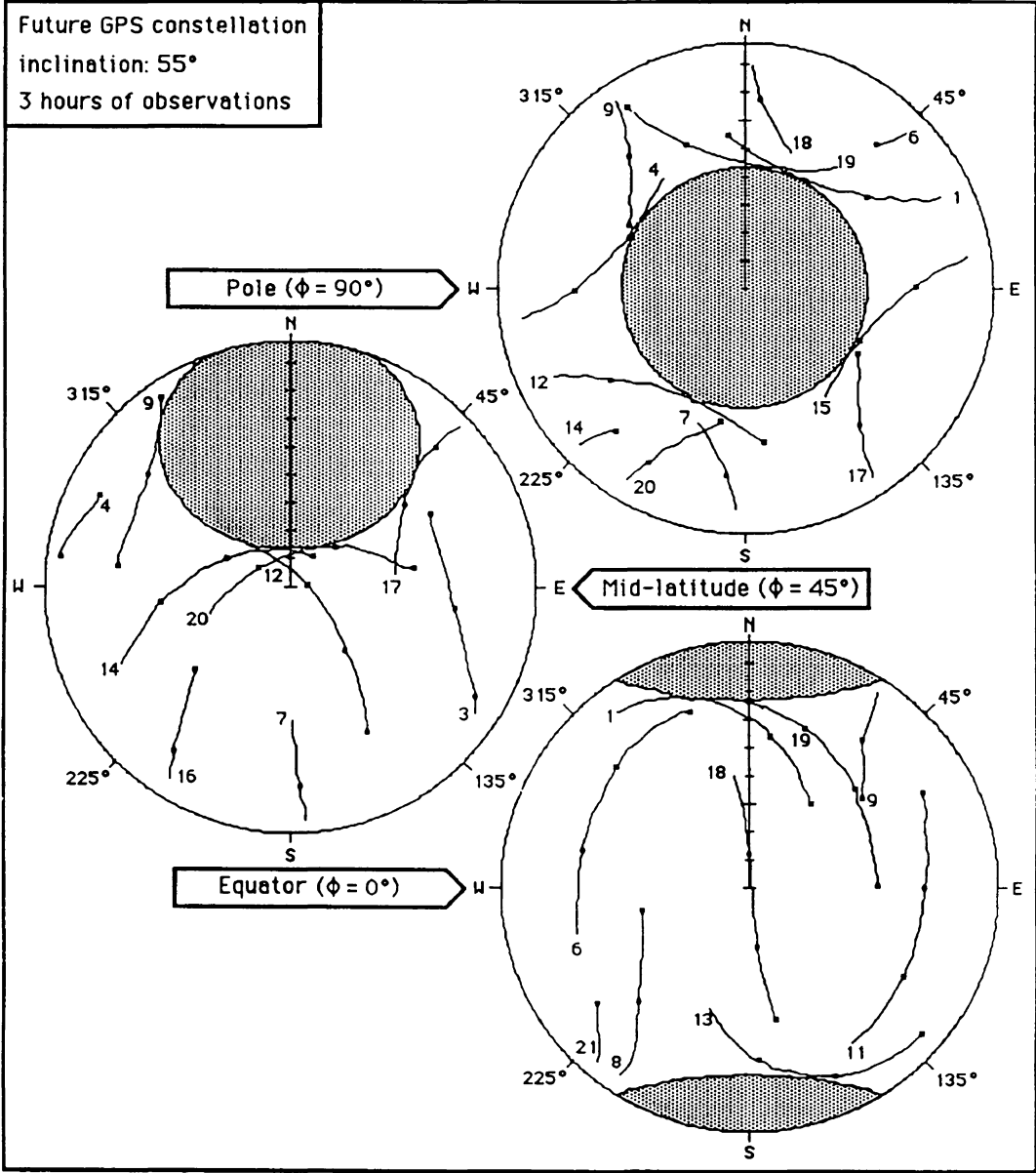


Figure V.1: Examples of satellite configurations of the future GPS constellation.

V.2 GPS campaign descriptions

V.2.1 CERN 1984 campaign [Gervaise et al., 1985; Beutler et al., 1986].

This campaign (see Figures V.2) was carried out at the France/Switzerland frontier (ϕ : 46° N, λ : 6° E). It was held from day 346 to day 348 (11 - 13 December) 1984. Three Macrometer™ V-1000 (single-frequency) receivers were operating during 3 h 20 min. (first session: 2 h, second session: 1 h 20 min.) from 0:10 to 3:50 UT (nighttime observations). Seven stations formed the network: the baseline lengths range from 3.5 km to 7.3 km and the maximum baseline height difference is 300 m. About 1,500 DD (double difference) observations (σ_{DD} : ± 6 mm, ~ 130 DD/baseline) have been processed with the Bernese software. The Macrometer receiver usually selects an elevation mask angle of 15° during the field recording. Eighteen station coordinates (station P231 fixed) have been solved for and 33 ambiguities out of 36 have been fixed. Note that each baseline has been observed twice during two different night sessions.

The actual satellite configuration has been approximated by the integration sectors defined in Figure V.2a. That is the integration sector definition which has been used to produce the prediction results reported in Chapter 5. Unfortunately, contribution of satellite 6 can only be roughly taken into account. The dotted line in the polar plot means that the satellite was not observed. Figure V.2b illustrates the station network configuration.

To simplify the analysis described in Chapter 6, we considered that the satellite configuration is described by the following integration boundaries: α_{from} : 25° , α^{to} : 155° and ζ_{min} : 20° , $\zeta^{\text{max}} < 90^\circ$. In the terminology of Chapter 6, this configuration is called the CERN satellite configuration to distinguish it from the CERN 1984 campaign satellite configuration which is used in Chapter 5 and described in the paragraph above.

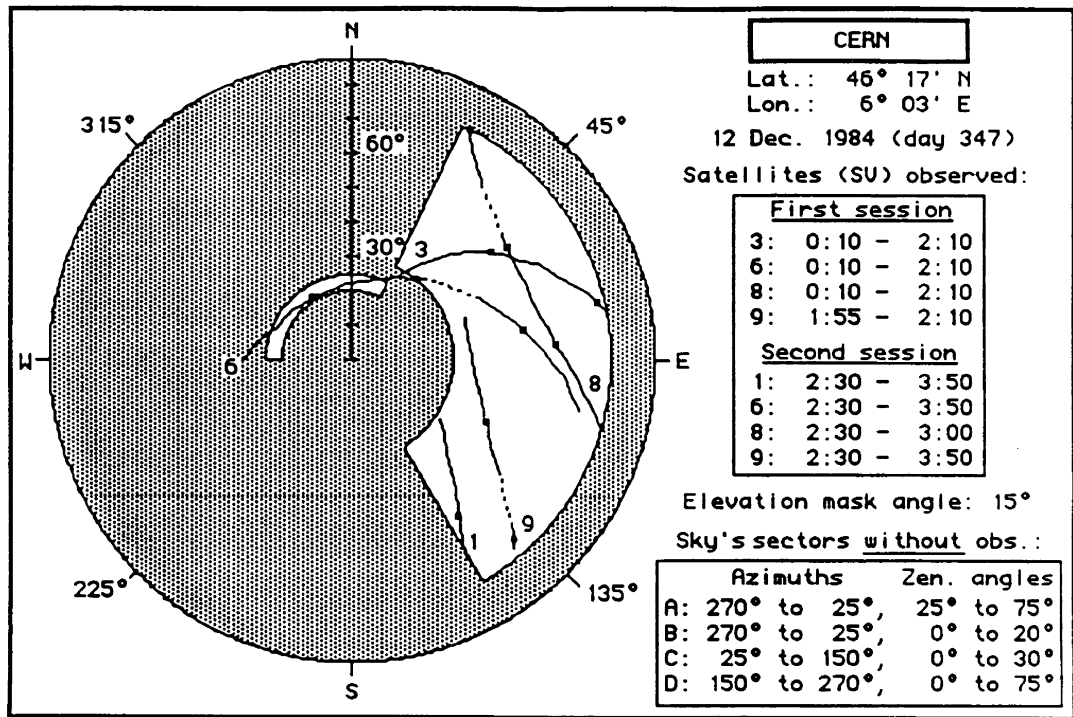


Figure V.2a: Satellite visibility CERN 1984 campaign.

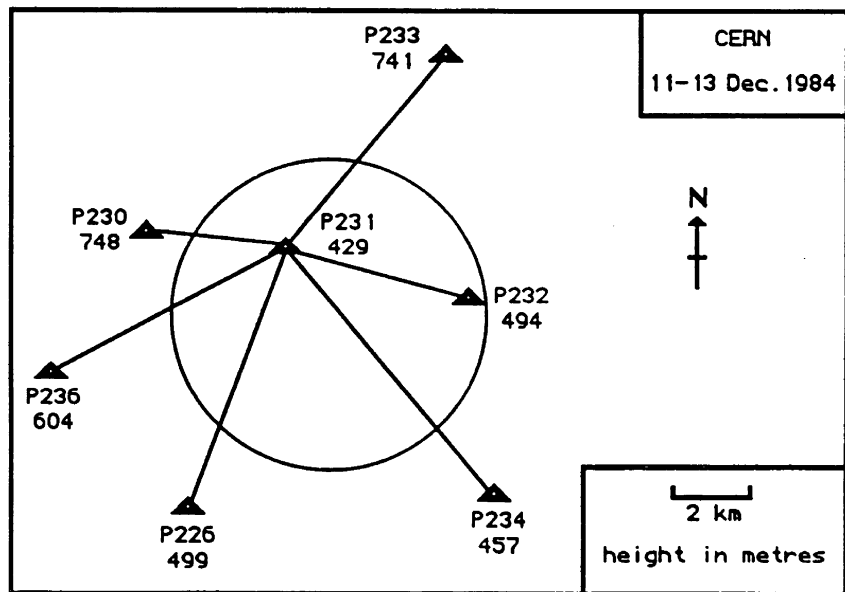


Figure V.2b: Station network CERN 1984 campaign.

V.2.2 Juan de Fuca 1986 campaign [Georgiadou and Kleusberg, 1988; Kleusberg and Wanninger, 1987] and reprocessed by Santerre.

This campaign (see Figures V.3) was carried out at the Vancouver Island/Washington State frontier (ϕ : 49° N, λ : 123° W). It lasted for many days but we have only used, in this study, the data from observing day 246 (3 September) 1986. Eight Texas Instruments TI 4100 (dual-frequency) receivers were operating during about 5 hours, from 17:00 to 21:45 UT (midday observations in local time). Eight stations were surveyed during this day. The baseline lengths range from 10 km to 30 km and the maximum baseline height difference is 224 m. About 4,800 DD observations (σ_{DD} : ± 17 mm, ~ 680 DD/baseline) have been processed with the DIPOP software. Baseline DI, DU contains about 10% fewer observations than the other observed baselines. An elevation mask angle of 20° was selected during the processing. Twenty-one station coordinates (station PG fixed) have been solved for and all ambiguities have been fixed.

The actual satellite configuration has been approximated by the integration sectors defined in Figure V.3a. That is the integration sector definition which has been used to produce the prediction results reported in Chapter 5. These sectors cover quite well the real satellite configuration but remember that the assumption of homogeneity is assumed within the integration boundaries. Figure V.3b illustrates the station network configuration.

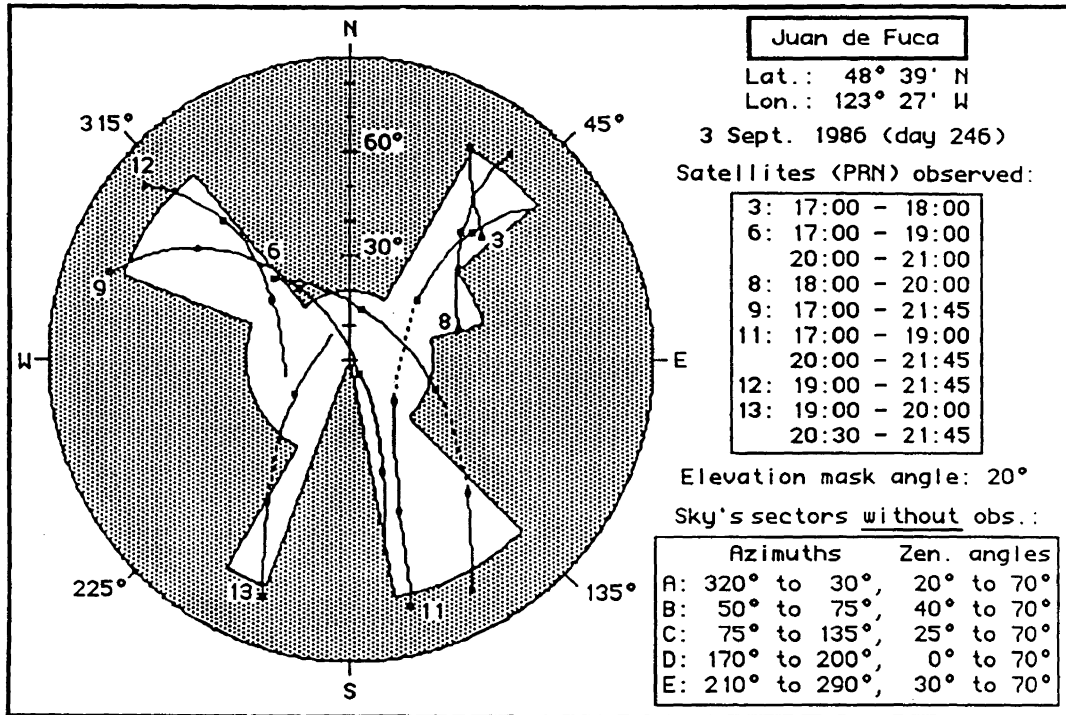


Figure V.3a: Satellite visibility Juan de Fuca 1986 campaign.

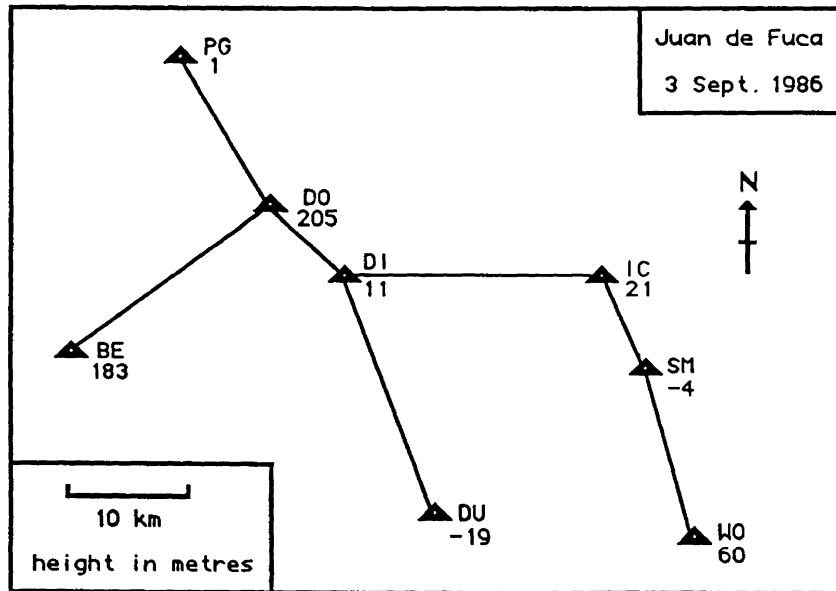


Figure V.3b: Station network Juan de Fuca 1986 campaign (3 September).

V.2.3 Ottawa 1983 campaign [Vaniček et al., 1985] and reprocessed by Santerre.

This campaign (see Figures V.4) was carried out near the city of Ottawa (ϕ : 45° N, λ : 76° W). It was held from day 200 to day 231 (19 July - 19 August) 1983. Two Macrometer™ V-1000 (single-frequency) receivers were operating during 5 hours, from 21:30 to 2:30 UT (evening observations in local time). Four stations formed the network; but we have only used 2 baselines (one session each) for this study. Baseline PA, 6A (day 206, 25 July) is 22 km long and azimuth 72°, the height difference is -77 m and 114 useful DD observations (σ_{DD} : ± 22 mm) have been recorded during the selected session. Baseline PA, MO (day 213, 1 August) is 13 km long and azimuth 335°, the height difference is -65 m and 113 useful DD observations (σ_{DD} : ± 16 mm) had been recorded during the selected session. The Macrometer receiver usually selects an elevation mask angle of 15° during the field recording. Six station coordinates (station PA fixed) have been solved for and all 8 ambiguities have been fixed. The software DIPOP has been used for this GPS data processing.

The actual satellite configuration has been approximated by the integration sectors defined in Figure V.4a. That is the integration sector definition which has been used to produce the prediction results reported in Chapter 5. Unfortunately, the contribution of satellite 4 can only be roughly taken into account. The selection of the integration sector to cover the north-east trajectory of satellite 4 has been chosen in order to be approximately in the centre of the trajectory. Figure V.4b illustrates the station network configuration.

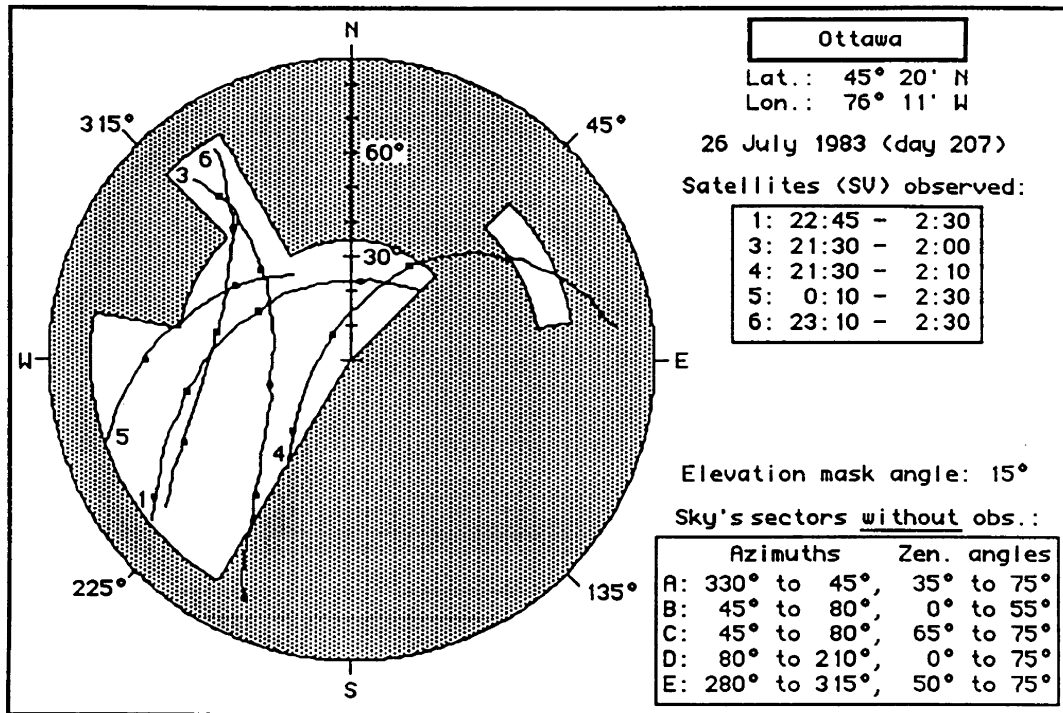


Figure V.4a: Satellite visibility Ottawa 1983 campaign.

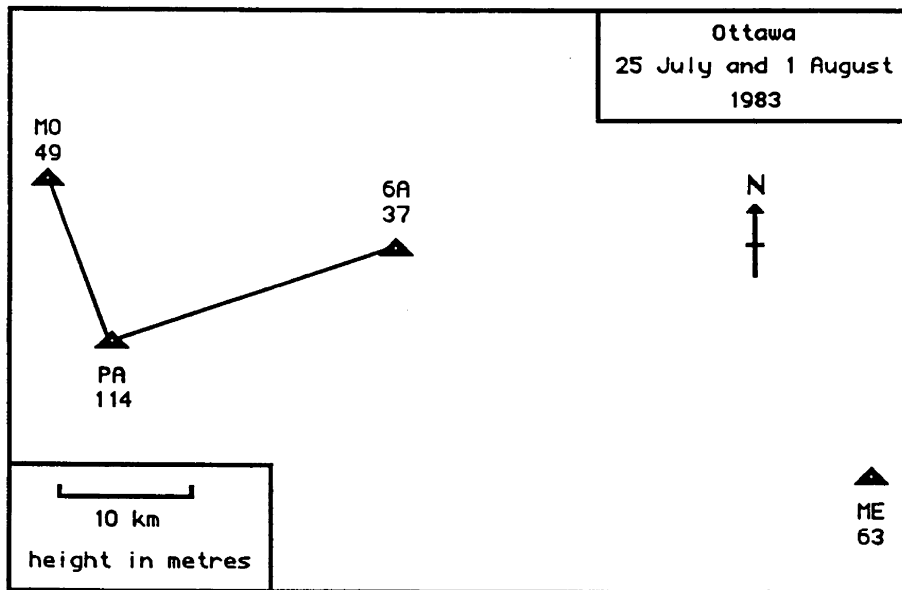


Figure V.4b: Station network Ottawa 1983 campaign.

V.2.4 Port Alberni 1986 campaign [Georgiadou, 1987] and reprocessed by Santerre.

This campaign (see Figures V.5) was carried out on Vancouver Island (ϕ : 49° N, λ : 125° W). It lasted from day 232 to day 240 (20 - 28 August) 1986. Four Texas Instruments TI 4100 (dual-frequency) receivers were operating during about 5 hours, from 17:00 to 21:45 UT (midday observations in local time). Nine stations (station RA was not used in the study performed in this thesis) formed the analysed sub-network: the baseline lengths range from 18 km to 56 km and the maximum baseline height difference is 1350 m. About 14,000 DD observations (σ_{DD} : ± 20 mm, ~ 760 DD/baseline) have been processed with the DIPOP software. Different elevation mask angles was selected during the processing. Twenty-four station coordinates (station OK fixed) have been solved for and all phase ambiguities have been fixed.

The actual satellite configuration is approximated by the integration sectors defined in Figure V.5a. That is the integration sector definition which has been used to produce the prediction results reported in Chapter 5. Figure V.5b illustrates the station network configuration. The satellite configuration is identical to the Juan de Fuca one.

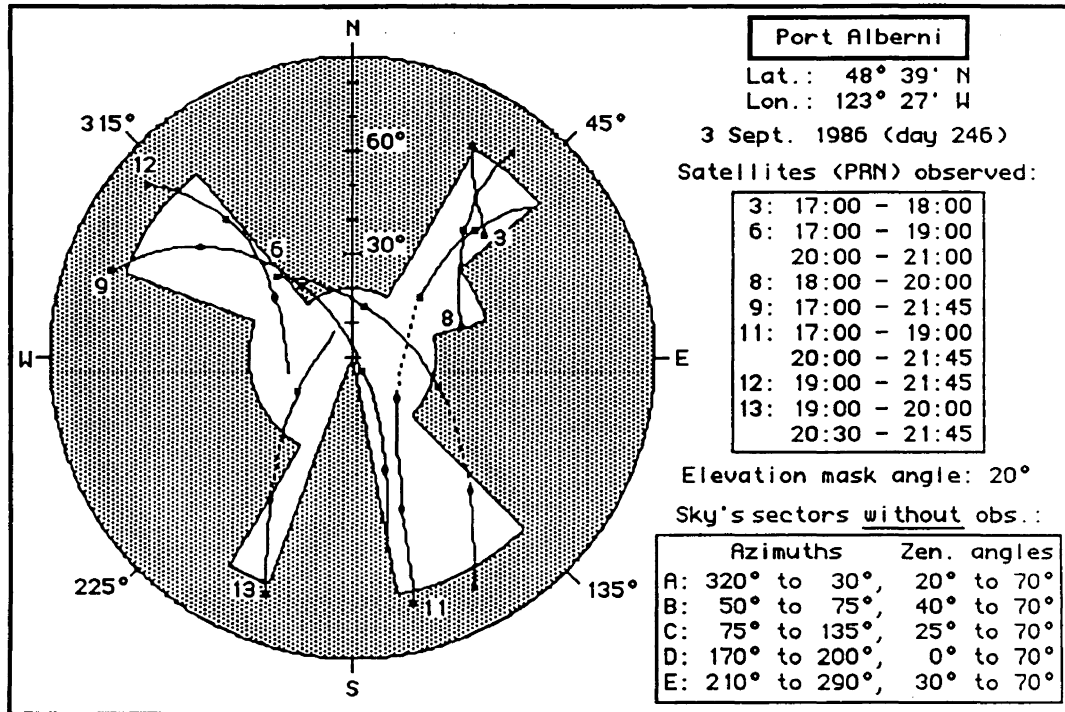


Figure V.5a: Satellite visibility Port Alberni 1986 campaign.

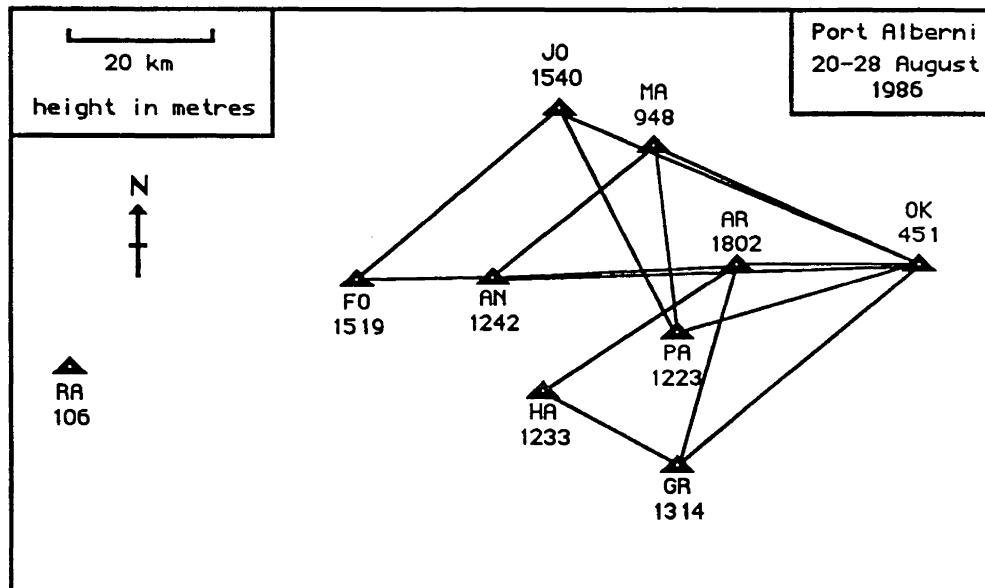


Figure V.5b: Station network Port Alberni 1986 campaign.

Appendix VI

Affine transformations

VI.1 Transformation definition and notation

The sense of the transformation has to be interpreted as the transformation we have to perform on the "true" station coordinates to get the station coordinates "biased" by the studied systematic error. In other words, the transformation parameters illustrate the station coordinate discrepancies introduced into the station network by the studied bias. The transformation involves 2 sets of station coordinates expressed in the same coordinate system, in our case the left-handed local geodetic system. These are the stations which are "moving" not the coordinate system. Figure VI.1 shows the interpretation of some affine transformation parameters.

The definition of the transformation parameters used throughout this document are:

- Rx: left-handed rotation around the x-coordinate expressed in 10^{-6} rad;
- Ry: left-handed rotation around the y-coordinate expressed in 10^{-6} rad;
- Rz: left-handed rotation around the z-coordinate expressed in 10^{-6} rad;
- Sx: shear along the x-coordinate proportional to the y-coordinate expressed in ppm;
- Sy: shear along the y-coordinate proportional to the x-coordinate expressed in ppm;
- ΔSx : remaining (differential) shear in the x-coordinate after a Rz has been applied expressed in ppm;
- ΔSy : remaining (differential) shear in the y-coordinate after a Rz has been applied expressed in ppm;
- K: horizontal scale factor expressed in ppm;
- Kx: scale factor along the x-coordinate proportional to x-coordinate expressed in ppm;
- Ky: scale factor along the y-coordinate proportional to y-coordinate expressed in ppm;
- ΔKx : remaining (differential) scale factor in the x-coordinate after a K has been applied expressed in ppm;

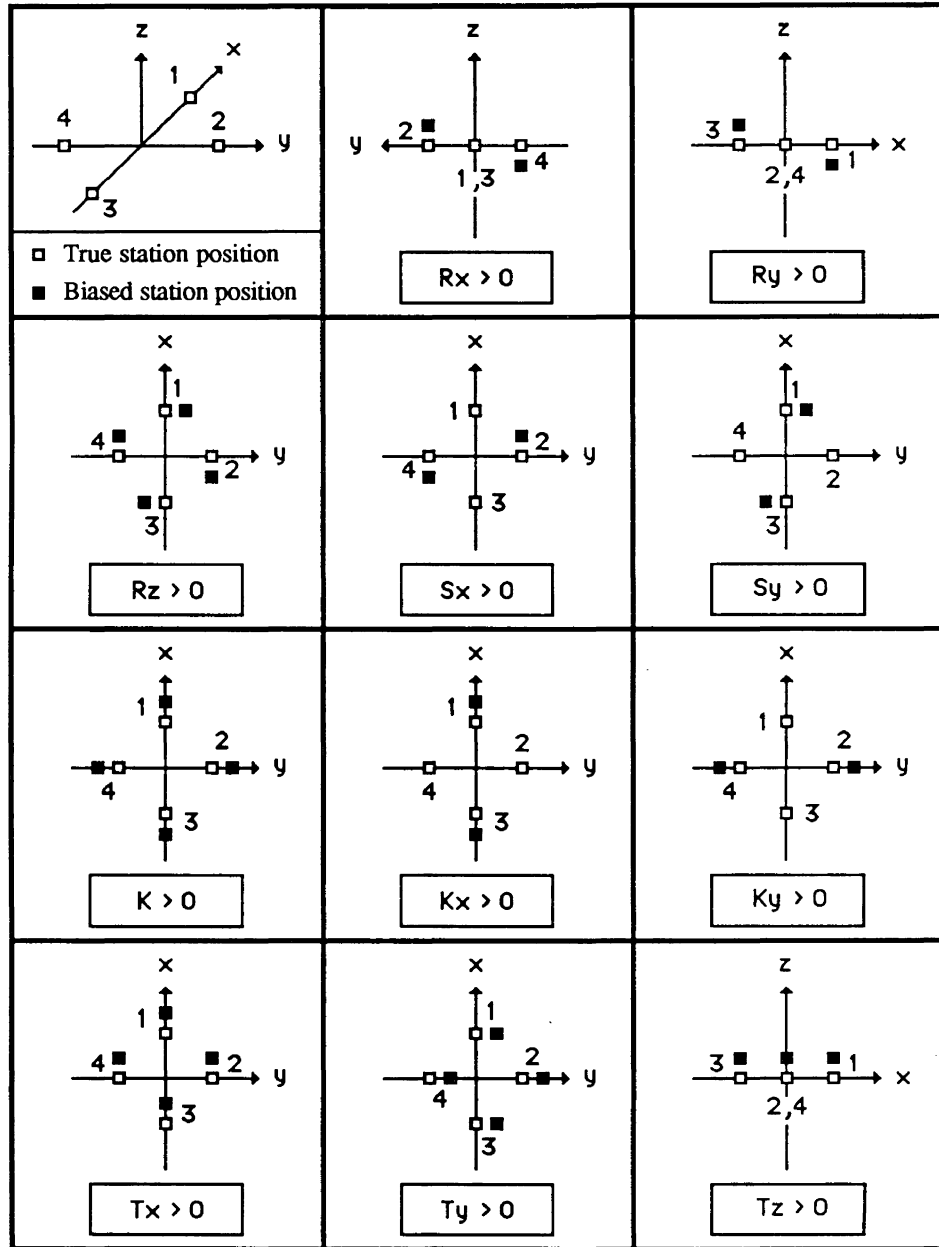


Figure VI.1: Interpretation of affine transformation parameters in a left-handed coordinate system.

ΔK_y : remaining (differential) scale factor in the y-coordinate after a K has been applied expressed in ppm;

T_x : translation along the x-coordinate expressed in mm;

T_y : translation along the y-coordinate expressed in mm;

T_z : translation along the z-coordinate expressed in mm.

With the study of the relative tropospheric zenith delay error we use the term "magnification factor". Its value is obtained by dividing the value of the translation parameter by the relative tropospheric zenith delay error expressed in millimetres.

More explicitly the transformation matrices and vector are defined as follows :

Rotation matrices (infinitesimal positive rotation in radians)

$$\mathbb{R}_x = \begin{pmatrix} 1 & 0 & 0 \\ 0 & 1 & -R_x \\ 0 & R_x & 1 \end{pmatrix}, \mathbb{R}_y = \begin{pmatrix} 1 & 0 & R_y \\ 0 & 1 & 0 \\ -R_y & 0 & 1 \end{pmatrix}, \mathbb{R}_z = \begin{pmatrix} 1 & -R_z & 0 \\ R_z & 1 & 0 \\ 0 & 0 & 1 \end{pmatrix} \quad (\text{VI.1})$$

Horizontal shear matrices

$$\mathbb{S}_x = \begin{pmatrix} 1 & S_x & 0 \\ 0 & 1 & 0 \\ 0 & 0 & 1 \end{pmatrix}, \mathbb{S}_y = \begin{pmatrix} 1 & 0 & 0 \\ S_y & 1 & 0 \\ 0 & 0 & 1 \end{pmatrix} \quad (\text{VI.2})$$

Scale factor matrices

$$\mathbb{K} = \begin{pmatrix} 1+K & 0 & 0 \\ 0 & 1+K & 0 \\ 0 & 0 & 1+K \end{pmatrix} \quad (\text{VI.3})$$

$$\mathbb{K}_x = \begin{pmatrix} 1+K_x & 0 & 0 \\ 0 & 1 & 0 \\ 0 & 0 & 1 \end{pmatrix}, \quad \mathbb{K}_y = \begin{pmatrix} 1 & 0 & 0 \\ 0 & 1+K_y & 0 \\ 0 & 0 & 1 \end{pmatrix} \quad (\text{VI.4})$$

Translation vector

$$\mathbb{T} = \begin{pmatrix} T_x \\ T_y \\ T_z \end{pmatrix} \quad (\text{VI.5})$$

VI.2 Affine and similarity transformations

The affine transformation parameters necessary to illustrate the effects of the studied systematic errors on the station network are the following:

$$\vec{x}_{\text{biased}} = \mathbb{T} + (\mathbb{R}_x \mathbb{R}_y \mathbb{S}_x \mathbb{S}_y \mathbb{K}_x \mathbb{K}_y) \vec{x}_{\text{true}} \quad (\text{VI.6a})$$

$$\begin{pmatrix} x \\ y \\ z \end{pmatrix}_{\text{biased}} = \begin{pmatrix} T_x \\ T_y \\ T_z \end{pmatrix} + \begin{pmatrix} 1+K_x & S_x & R_y \\ S_y & 1+K_y & -R_x \\ -R_y & R_x & 1 \end{pmatrix} \begin{pmatrix} x \\ y \\ z \end{pmatrix}_{\text{true}} \quad (\text{VI.6b})$$

The reason of the omission of a directional scale factor along the z-axis (K_z) in equations (VI.6) is given in the last paragraph of section VI.3.

The 7-parameter similarity transformation is obtained from the equations (VI.6), using the following identities:

$$\begin{aligned} K_x &= K_y = K \\ S_x &= -S_y \\ S_y &= R_z \text{ or } S_x = -R_z \end{aligned} \quad (\text{VI.7})$$

This means if K_x is equal to K_y , we have a horizontal (see last paragraph of section VI.3) scale factor K , which means that the horizontal displacement effect is proportional to the baseline length and directed along the baseline (horizontal) vector. And if S_x and S_y are equal in absolute value but of opposite sign, we have nothing else but a rotation around the z -axis equal to the S_y value.

$$\vec{x}_{\text{biased}} = \mathbb{T} + (1+K) (R_x R_y R_z) \vec{x}_{\text{true}} \quad (\text{VI.8a})$$

$$\begin{pmatrix} x \\ y \\ z \end{pmatrix}_{\text{biased}} = \begin{pmatrix} T_x \\ T_y \\ T_z \end{pmatrix} + (1+K) \begin{pmatrix} 1 & -R_z & R_y \\ R_z & 1 & -R_x \\ -R_y & R_x & 1 \end{pmatrix} \begin{pmatrix} x \\ y \\ z \end{pmatrix}_{\text{true}} \quad (\text{VI.8b})$$

VI.3 Design matrix and misclosure vector of the transformation

The partial derivatives pertaining to the affine transformation parameters are:

$$A = \begin{pmatrix} 1 & 0 & 0 & 0 & z & y & 0 & x & 0 \\ 0 & 1 & 0 & -z & 0 & 0 & x & 0 & y \\ 0 & 0 & 1 & y & -x & 0 & 0 & 0 & 0 \end{pmatrix} \begin{matrix} \partial x \\ \partial y \\ \partial z \\ \partial T_x \\ \partial T_y \\ \partial T_z \\ \partial R_x \\ \partial R_y \\ \partial S_x \\ \partial S_y \\ \partial K_x \\ \partial K_y \end{matrix} \quad (\text{VI.9})$$

The partial derivatives pertaining to the similarity transformation parameters are:

$$A = \begin{pmatrix} 1 & 0 & 0 & 0 & z & -y & x \\ 0 & 1 & 0 & -z & 0 & x & y \\ 0 & 0 & 1 & y & -x & 0 & z \end{pmatrix} \begin{matrix} \partial x \\ \partial y \\ \partial z \\ \partial T_x \\ \partial T_y \\ \partial T_z \\ \partial R_x \\ \partial R_y \\ \partial R_z \\ \partial K \end{matrix} \quad (\text{VI.10})$$

The misclosure vector, for both cases, is:

$$W = \vec{x}_{\text{biased}} - \vec{x}_{\text{true}} \quad (\text{VI.11})$$

In the least squares adjustment process, the a priori value of the transformation parameters were set to zero. The origin of the local geodetic system is defined at the location of the station which was considered fixed during the GPS data processing and the coordinates of this station is usually not used in the transformation least squares adjustment.

It is worthwhile to realize that for networks with small baseline height components compared to baseline length (z-coordinate small in comparison to x- and y-coordinates), the z-coordinates have practically no contribution to the transformation parameter least squares adjustments. In fact, the scale factor K, assumed equal for the 3 axes, represents in reality a horizontal scale factor. For the same reason, in the affine transformation, we do not evaluate a Kz parameter, because of the weakness of network geometry to estimate this parameter.

VI.4 Combination of the effects of latitude and longitude offsets of the fixed station

This section contains a clarification about the last statement of section 6.6 related to the analysis of the horizontal coordinate offsets of the fixed station. More explicitly, this statement can be mathematically written, as follows:

$$\delta\vec{x}_{\Delta O} = \delta\vec{x}_{\Delta\phi} \cos\alpha_1 + \delta\vec{x}_{\Delta\lambda} \sin\alpha_1 \quad (\text{VI.12})$$

where $\delta\vec{x}$ is the station coordinate discrepancies, the subscript indicates the cause for these discrepancies (ΔO : horizontal offset, $\Delta\phi$: latitude offset and $\Delta\lambda$: longitude offset; $\Delta\phi$ and $\Delta\lambda$ have magnitude ΔO), and α_1 is the azimuth of the horizontal offset. Naturally, the predictions for $\Delta\phi$ and $\Delta\lambda$ are those of the satellite sky distribution for which we want to

evaluate the effect caused by ΔO .

A generalization of the rotation parameter for any direction of the horizontal offset (ΔO) can also be drawn.

The magnitude of the rotation caused by a horizontal offset (ΔO) of azimuth α_1 is equal to:

$$R_A = [(R_{y_{\Delta\phi}} \cos\alpha_1)^2 + (R_{x_{\Delta\lambda}} \sin\alpha_1)^2]^{1/2} \quad (\text{VI.13})$$

and the azimuth of the horizontal axis around which the rotation is performed, is equal to:

$$A = \arctan [(R_{y_{\Delta\phi}} \cos\alpha_1) / (R_{x_{\Delta\lambda}} \sin\alpha_1)] \quad (\text{VI.14})$$

where $R_{y_{\Delta\phi}}$ is the rotation around the y-axis due to a latitude offset of the fixed station, the latitude offset is of magnitude ΔO ; and $R_{x_{\Delta\lambda}}$ is the rotation around the x-axis due to a longitude offset of the fixed station; the longitude offset is of magnitude ΔO . Again we note that the values of R_x and R_y are those of the satellite sky distribution for which we want to evaluate the effect caused by ΔO .

From the affine transformation parameters related to the latitude and the longitude offsets of the fixed station (section 6.6 and equations VI.13 and VI.14), we can directly calculate the coordinate discrepancies for a baseline of azimuth α_0 and length ℓ due to a horizontal offset of the fixed station of azimuth α_1 :

$$\begin{aligned} \delta x &= \ell (K_{x_{\Delta\phi}} \cos\alpha_1 \cos\alpha_0 + S_{x_{\Delta\lambda}} \sin\alpha_1 \sin\alpha_0) \\ \delta y &= \ell (K_{y_{\Delta\phi}} \cos\alpha_1 \sin\alpha_0 + S_{y_{\Delta\lambda}} \sin\alpha_1 \cos\alpha_0) \\ \delta z &= \ell R_A \sin(\alpha_0 - A). \end{aligned} \quad (\text{VI.15})$$

Vita

- Candidate's name: Rock Santerre
- Place and date of birth: Baie-des-Sables, Québec
13 October 1957
- Permanent address: Département des sciences géodésiques et de télédétection
Pavillon Casault
Université Laval
Ste-Foy
Québec G1K 7P4
- Universities attended: Département de géodésie et de cartographie
Université Laval, Québec, 1977/81
B.Sc.A. (arpentage), 1981
- Département de géodésie et de cartographie
Université Laval, Québec, 1981/83
M.Sc. (géodésie), 1984
- Department of Surveying Engineering
University of New Brunswick, Fredericton, 1985/89
Ph.D. (Surveying Engineering), 1989
- Professional activities: Arpenteur-géomètre du Québec (Quebec Land Surveyor),
since 1981
- Research Assistant
Department of Surveying Engineering
University of New Brunswick, Fredericton, 1983/85
- Publications:
- SANTERRE, R. (1988). "The impact of the sky distribution of GPS satellites on precise positioning." Paper presented at the *American Geophysical Union Chapman Conference on GPS Measurements for Geodynamics*, Fort Lauderdale, U.S.A., 19-22 September.
- SANTERRE, R. (1988). "DIPOP 2.0: Structure, Modifications and User Guide." Department of Surveying Engineering Technical Memorandum No. 20, University of New Brunswick, Fredericton, Canada.

- SANTERRE, R., M.R. Craymer, A. Kleusberg, R.B. Langley, D. Parrot, S.H. Quek, P. Vaníček, D.E. Wells and F. Wilkins (1987). "Precise relative positioning with DIPOP 2.0." Paper presented at the International Association of Geodesy Section II Scientific Meetings: "Advanced Space Technology" at the *International Union of Geodesy and Geophysics XIX General Assembly*, Vancouver, Canada, 9-22 August.
- Langley, R.B., D. Parrot, R. SANTERRE, P. Vaníček and D.E. Wells (1986). "The Spring 1985 GPS high-precision baseline test: Preliminary analyses with DIPOP." *Proceedings of the Fourth International Geodetic Symposium on Satellite Positioning*, Austin, U.S.A., 28 April - 2 May, pp. 1073-1088.
- Langley, R.B., D. Parrot, A. Kleusberg, R. SANTERRE, P. Vaníček and D.E. Wells (1986). "The Spring 1985 GPS high-precision baseline test: Very preliminary results." Presented at the *GPS Technology Workshop, Jet Propulsion Laboratory*, Pasadena, U.S.A., March.
- Langley, R.B., A. Kleusberg, R. SANTERRE, P. Vaníček and D.E. Wells (1986). "DIPOP: An interactive software package for precise positioning with GPS." Paper presented at the *American Congress on Surveying and Mapping Conference*, Washington, U.S.A., 16-21 March.
- Mertikas, S.P., D. Delikaraoglou and R. SANTERRE (1986). "Alert program for NAVSTAR Global Positioning System, Transit, Lageos and Starlette satellites." Department of Surveying Engineering Technical Report No. 85, University of New Brunswick, Fredericton, Canada.
- Kleusberg, A., G. Beutler, R.B. Langley, R. SANTERRE, P. Vaníček and D.E. Wells (1985). "Comparison of survey results from different GPS receiver types." *Proceedings of the First International Symposium on Precise Positioning with the Global Positioning System*, Rockville, U.S.A., 15-19 April, pp. 579-592.
- Kleusberg, A., R.B. Langley, S.H. Quek, R. SANTERRE, P. Vaníček and D.E. Wells (1985). "Experience with GPS at the University of New Brunswick." Paper presented at the *12th Annual Meeting of the Canadian Geophysical Union*, Calgary, Canada, 7-10 May. Abstract published in *Geophysics*, 50(8), pp. 1382-1383.
- Langley, R.B., A. Kleusberg, D. Parrot, R. SANTERRE, P. Vaníček and D.E. Wells (1985). "DIPOP processing of observations from the Spring 1985 GPS." Invited paper for the *Fall Meeting of the American Geophysical Union*, San Francisco, U.S.A., December. Abstract published in *EOS*, 66(46), p. 844.
- Moreau, R., G. Beutler, J.-G. Leclerc, B. Labrecque, R. SANTERRE and R.B. Langley (1985). "The Quebec 1984 Macrometer test: comparison of phase-difference processing and network solution methods." *Proceedings of the First International Symposium on Precise Positioning with the Global Positioning System*, Rockville, U.S.A., 15-19 April, pp. 557-566.
- SANTERRE, R. (1985). "Le système de positionnement global GPS." *Arpenteur-Géomètre*, 2(2), pp. 10-12 and 2(3), pp. 8-9. Presented at the Département de géodésie, Université Laval, Québec, April 1984.

- SANTERRE, R., A. Kleusberg and G. Beutler (1985). "DIPOP: Software documentation." Department of Surveying Engineering Technical Memorandum No. 6, University of New Brunswick, Fredericton, Canada.
- Vaníček, P., A. Kleusberg, R.B. Langley, R. SANTERRE and D.E. Wells (1985). "On the elimination of biases in processing differential GPS observations." *Proceedings of the First International Symposium on Precise Positioning with the Global Positioning System*, Rockville, U.S.A., 15-19 April, pp. 315-324.
- Vaníček, P., G. Beutler, A. Kleusberg, R.B. Langley, R. SANTERRE and D.E. Wells (1985). "DIPOP: Differential POSitioning Program package for the Global Positioning System." Department of Surveying Engineering Technical Report No. 115, University of New Brunswick, Fredericton, Canada.
- Beutler, G., D.A. Davidson, R.B. Langley, R. SANTERRE, H. Valliant, P. Vaníček and D. E. Wells (1984). "The Ottawa Macrometer experiment: An independent analysis." Paper presented at the *11th Annual Meeting of the Canadian Geophysical Union*, Halifax, Canada, June.
- Beutler, G., D.A. Davidson, R.B. Langley, R. SANTERRE, P. Vaníček and D.E. Wells (1984). "Some theoretical and practical aspects of geodetic positioning using carrier phase difference observations of GPS satellites." Department of Surveying Engineering Technical Report No. 109, University of New Brunswick, Fredericton, Canada.
- Beutler, G., D.A. Davidson, R.B. Langley, R. SANTERRE, P. Vaníček and D.E. Wells (1984). "Some theoretical and practical aspects of geodetic positioning using carrier phase difference observations of GPS satellites." *Mitteilungen der Satellitenbeobachtungsstation Zimmerwald*, No. 14, Astronomical Institute, University of Berne, Switzerland.
- Kleusberg, A., G. Beutler, D. Delikaraoglou, R.B. Langley, R. SANTERRE, R. Steeves, H. Valliant, P. Vaníček and D.E. Wells (1984). "Comparison of Macrometer V-1000 and Texas Instruments 4100 GPS survey results." Invited paper for the *Fall Meeting of the American Geophysical Union*, San Francisco, U.S.A., December. Abstract published in *EOS*, 65(45), p. 853.
- Langley, R.B., G. Beutler, D. Delikaraoglou, B. Nickerson, R. SANTERRE, P. Vaníček and D.E. Wells (1984). "Studies in the application of the Global Positioning System to differential positioning." Department of Surveying Engineering Technical Report No. 108, University of New Brunswick, Fredericton, Canada.
- Sanchez, R.N. and R. SANTERRE (1984). "Analyse de certaines déterminations astronomiques appliquées au contrôle d'orientation." *The Canadian Surveyor*, 37(2), pp. 71-78.
- SANTERRE, R. (1984). "Réfraction atmosphérique: ses effets sur les mesures du nivellement géométrique." Thèse de maîtrise en sciences, Rapport 84-5. Département de géodésie et de cartographie, Université Laval, Québec.